THESE

en vue de l'obtention du grade de Docteur, délivré par

l'ECOLE NORMALE SUPERIEURE DE LYON

Ecole Doctorale N° 340
Biologie Moléculaire Intégrative et Cellulaire

Discipline : Sciences de la vie et de la santé

Soutenue publiquement le 03/07/2023, par :

Ronald Lafayette ALCALÁ VILLARREAL

The role of a cryptic furin-like cleavage site on Ebola virus replication

---

Devant le jury composé de :

Stéphane BIACCHESI	Directeur de recherche, Université Paris-Saclay	Rapporteur
Marc JAMIN	Professeur des universités, Université Grenoble Alpes	Rapporteur
Aurélie ALBERTINI	Chargée de recherche, Université Paris-Saclay	Examinatrice
Sylvain BAIZE	Directeur de recherche, ENS de Lyon	Examinateur
Évelyne MANET	Directrice de recherche, ENS de Lyon	Examinatrice
Viktor VOLCHKOV	Professeur des universités, ENS de Lyon	Directeur de thèse

Acknowledgements

First and foremost, I would like to express my gratitude to Viktor Volchkov, my thesis director, for not only welcoming me into his BMPV team but also generously sharing his invaluable insights and guidance, which have ultimately honed my critical thinking abilities. Over the course of the past four years, this experience has proven to be truly life-changing, allowing me to pursue one of my greatest professional aspirations: delving into the fascinating world of virology.

Je remercie sincèrement Valentina Volchkova pour son aide, grâce à laquelle j'ai pu me former et apprendre beaucoup sur les différentes techniques en virologie. Je lui suis d'autant plus reconnaissant que les expériences qu'elle a menées ont contribué à mon travail et m'ont aidé à terminer ma thèse et à la défendre aujourd'hui. Merci aussi pour sa gentillesse à mon égard durant notre collaboration. Je tiens également à remercier Olivier Reynard pour son accueil chaleureux et pour ses multiples observations, à la fois techniques et théoriques, qui m'ont permis de progresser en tant que chercheur.

Es evidente que le estaré siempre agradecido al Consejo Nacional de Ciencia y Tecnología de México por haberme otorgado la beca que me permitió llevar a fin mi investigación de doctorado. Me es claro que sin su crucial apoyo, yo no habría podido concluir mis estudios. De même, je remercie l'École Normale Supérieure de Lyon pour la bourse complémentaire qu'elle m'a accordée, sans laquelle je n'aurais pas pu non plus finir mes études de doctorat.

Je tiens également à remercier Neil Kearney, Jeanne Rieber et Marwan Hamoudi, qui ont contribué à certains aspects de l'expérimentation de mon projet lors de leurs stages de master.

Je tiens à remercier une fois de plus les membres de mon comité de thèse d'avoir accepté d'évaluer mon travail scientifique. Je remercie M. Biacchesi et M. Jamin d'avoir accepté d'être les rapporteurs de ma thèse, Mme Albertini et M. Baize d'avoir accepté de faire partie du jury, ainsi que Mme Manet d'avoir accepté d'être la présidente du comité.

Il est évident que je voudrais également remercier toute l'équipe P4. En particulier, je tiens à remercier Stéphane Mely, Stéphanie Mundweiler et Delphine Pannetier de m'avoir formé, Christophe Leculier et Béatrice Labrosse pour leur disponibilité à me permettre de réaliser mes

expériences toujours, ou presque toujours, dans les délais requis, et Sabine Godard, Damian Thomas et Élodie Moissonnier pour leurs réponses à mes multiples questions et demandes.
Je tiens également à remercier Béatrice Renaudin et en général tous nos voisins de l'étage, l'équipe de l'Institut Pasteur, pour leur soutien moral ainsi que pour leur aide en matière d'expérimentation et de logistique lors des nombreux week-ends ou jours fériés où j'ai dû venir au laboratoire pour réaliser des expériences.

Je tiens également à remercier de manière très particulière Emeric Chan-Mine et Chantel Fitzsimmons pour leur présence, leur écoute, leurs conseils et les moments de rire partagés ensemble. Le doctorat a été une expérience exigeante à bien des égards, mais vous avez certainement contribué à la rendre plus facile.

Je suis également très reconnaissant du grand soutien moral et administratif que j'ai toujours reçu de Nathalie Alazard et François-Loïc Cosset, ainsi que de la part de l'école doctorale, Françoise Monéger, Mathias Faure, Roxane Leclaire et Mathilde Mauguière.

Je tiens également à remercier chaleureusement l'aide que j'ai reçue de la part de l'ENS et de l'INSERM, Clara Blasco, Halima Halimi, Myriam Friat, Nathalie Jacquet et Cécile Monnier. Faire un doctorat est déjà un défi en soi, et cela l'est d'autant plus lorsque je l'ai fait dans un pays étranger et que je me retrouvais souvent plongé dans des démarches bureaucratiques.

El doctorado me ha sido una experiencia formativa en áreas que incluso no habría sospechado antes. En este contexto, estoy bastante agradecido con mis amigos quienes han estado ahí a lo largo de todo este tiempo, y con quienes he podido desconectarme, desahogarme, reflexionar y encontrar soluciones. Muchas gracias, Lionel, Ricardo, Eduardo, Cecy, Ángela.

También quiero agradecer a mi familia, en especial a mis dos hermanas, Amy y Johanna, por haberme dado su apoyo moral durante los tiempos difíciles de diciembre de 2018, así como por su continuo apoyo durante todos estos años.

Merci, Michaël, d'avoir été à mes côtés tout ce temps. Tu as été mon plus grand soutien moral.

Por último, agradezco a mis papás, sin cuya formación ni valores, yo no habría llegado lejos.

Gracias a todos

Abbreviations **7**

Abstract in English **8**

Abstract en Français **9**

INTRODUCTION **10**

Filoviruses *10*

A case apart: RESTV lack of pathogenicity 11

EBOV's evolutionary rate 12

Epidemiology *13*

Ecology 15

Transmission 17

Management 18

Signs and symptoms *19*

Post Ebola syndrome 21

Diagnosis *22*

Reverse transcriptase polymerase chain reaction (RT-PCR) 23

Antigen detection via Enzyme-Linked Immunosorbent Assay (ELISA) 23

Antibody detection via Enzyme-Linked Immunosorbent Assay (ELISA) 24

Immunohistochemical staining 24

Treatments *25*

Convalescent whole blood and convalescent plasma 26

ZMapp 26

Loperamide 27

Recombinant nematode anticoagulant protein c2 (rNAPc2) 27

Other molecules 27

Vaccines *29*

VSV and the rVSVΔG-ZEBOV-GP 29

Adenovirus-based vaccines 31

Animal models *32*

Mouse 32

Hamster 33

Guinea Pig 34

Non-Human primates 35

Other animal models 35

Structure and Genomic organisation of EBOV *36*

Genomic organisation 37
NP 38
VP35 39
VP40 40
GP 41
$GP_{1,2}$ 41
RNA editing phenomenon 43
sGP and the Δ-peptide 44
ssGP 45
Shed GP 46
Mucin-like domain 46
VP30 46
VP24 47
L 48
Replication of EBOV's genome 49
Transcription of EBOV's genes 51
Infectious cycle *53*
Pathogenesis *57*
Mechanisms of tissue damage 59
Pathology 60
Immune evasion 61
Scientific Objectives **64**
Materials and Methods **67**
Results **81**
Comparative analysis of VSVEB-WT and VSVEB-$E_{304}A$ 82
Comparative analysis of the virus growth kinetics 88
Virus attachment experiments 94
Virus penetration assay 97
Proteolytic digestion by thermolysin 99
Characterisation of the cryptic furin-like cleavage site present in EBOV GP_1 subunit 101
Cloning of recombinant VSVEB plasmids with GP mutations at the furin-like cryptic site 104
Rescue of recombinant VSV bearing mutations of GP at the furin-like cryptic site 106
Comparative analysis of rescued VSV with GP mutations at the furin-like cryptic site 107
Comparative study of EBOV-WT and EBOV-$E_{304}A$ 113

Comparative study of virus growth between EBOV-WT and EBOV-$E_{304}A$ 117

Discussion and perspectives **119**

Conclusions **134**

Appendix **136**

Hamster-adapted EBOV *136*

Study of virus growth between EBOV-WT and EBOV-HA in primate cell lines 137

Study of virus growth between EBOV-WT and EBOV-HA in rodent cell lines 140

Bibliography **143**

Abbreviations

Bp	base pair
BSL	Biosafety level
cDNA	complementary DNA
CMC	Carboxymethyl cellulose
CMV	cytomegalovirus
DMEM	Dulbecco modified Eagle's medium
EBOV	Zaire ebolavirus, Ebola virus
EVD	Ebola virus disease
FCS	foetal calf serum
FL	full length
GMEM	Glasgow's minimum essential medium
GP	glycoprotein
HA	hamster adapted
IFN	interferon
MLD	Mucin like domain
MOI	multiplicity of infection
NCS	New-born calf serum
NHP	non-human primate
NPC1	Niemann-Pick C1
P1	amino acid residue at position 1 before a cleavage
P1'	amino acid residue at position 1 after a cleavage
PFU	plaque forming unit
PSS	poly(sodium 4-styrenesulphonate)
qPCR	quantitative PCR
RBD	receptor binding domain
rpm	revolutions per minute
RT-PCR	reverse transcription polymerase chain reaction
SDS-PAGE	sodium dodecyl sulphate - polyacrilamide
sGP	soluble glycoprotein
ssGP	small secreted glycoprotein
TAM	Tyro-3, Axl and Mertk families
$TCID_{50}$	50% tissue culture infective dose
Time (h)	Time in hours
TNF	tumour necrosis factor
VSV	vesicular stomatitis virus
WB	Western blot
WT	wild type

Abstract in English

The Ebola virus surface glycoprotein GP plays a crucial role in facilitating viral entry into host cells, although the mechanism underlying this process remains only partially understood. In a previous drug screening experiments, we identified an anionic compound that effectively inhibits the spread of Ebola virus. Further investigation using a recombinant vesicular stomatitis virus (VSV) expressing the Ebola virus surface GP allowed us to identify a single amino acid mutation at position 304 ($E_{304}A$) that conferred resistance to the inhibitor. In this study, we aimed to elucidate the molecular mechanisms underlying this resistance. We found that recombinant VSV carrying the $E_{304}A$ mutation exhibited a growth advantage over the wild-type virus even in the absence of the inhibitor, and this advantage was associated with an increase in virus entry efficiency. Further analysis revealed that the mutation caused a change in the cleavage pattern of the GP_1 subunit, leading to the loss of a mucin-like domain and an increase in the efficiency of virus entry. Interestingly, we also observed that both the wild-type and mutant viruses possess two forms of surface GP, a full-length GP_1 and a cleaved version, but in different ratios. This correlation between GP_1 cleavage and virus infectivity was confirmed using VSV-generated viruses with mutations disrupting the putative cleavage sites. Finally, we complemented our studies by using recombinant Ebola viruses bearing either wild-type GP or the E304A mutation. Our results showed that the mutation also led to GP_1 cleavage in live Ebola viruses, resulting in increased infectivity and larger plaque sizes. Taken together, our findings suggest a new model for Ebola virus biology that highlights the flexibility of GP and its cleavage patterns, with potential implications for drug development.

Key words: Ebola, glycoprotein

Abstract en Français

La glycoprotéine de surface GP du virus Ebola joue un rôle crucial dans la facilitation de l'entrée du virus dans les cellules hôtes, bien que le mécanisme sous-jacent à ce processus ne soit que partiellement compris. Dans des expériences précédentes de dépistage de médicaments, nous avons identifié un composé anionique qui inhibe efficacement la propagation du virus Ebola. Des investigations supplémentaires en utilisant un virus stomatite vésiculaire recombinant (VSV) exprimant la GP de surface du virus Ebola nous ont permis d'identifier une seule mutation d'acide aminé à la position 304 ($E_{304}A$) qui conférait une résistance à l'inhibiteur. Dans cette étude, nous avons cherché à élucider les mécanismes moléculaires sous-jacents à cette résistance. Nous avons découvert que le VSV recombinant portant la mutation $E_{304}A$ présentait un avantage de croissance par rapport au virus sauvage, même en l'absence de l'inhibiteur, et que cet avantage était associé à une augmentation de l'efficacité d'entrée du virus. Des analyses supplémentaires ont révélé que la mutation entraînait un changement dans le motif de clivage de la sous-unité GP_1, conduisant à la perte d'un domaine de type mucine et à une augmentation de l'efficacité d'entrée du virus. Nous avons également observé que les virus sauvages et mutants possédaient deux formes de la GP de surface, une GP_1 à longueur totale et sa version clivée, mais dans des ratios différents. Cette corrélation entre le clivage de GP_1 et l'infectivité du virus a été confirmée en utilisant des virus générés par VSV avec des mutations perturbant les sites de clivage putatifs. Enfin, nous avons complété nos études en utilisant des virus Ebola recombinants portant soit la GP sauvage, soit la mutation $E_{304}A$. Nos résultats ont montré que la mutation entraînait également le clivage de GP_1 dans les virus Ebola vivants, ce qui entraînait une infectivité accrue et des plaques de plus grande taille. Dans l'ensemble, nos découvertes suggèrent un nouveau modèle de la biologie du virus Ebola qui met en évidence la flexibilité de la GP et de ses motifs de clivage, avec des implications potentielles pour le développement de médicaments.

Mots clé : Ebola, glycoprotéine

INTRODUCTION

Filoviruses

Filoviruses belong to the family Filoviridae and are characterized by their enveloped, linear, non-segmented, negative-sense single-stranded RNA structure. They are classified within the order Mononegavirales, which also includes the Paramyxoviridae and Rhabdoviridae families (Audet & Kobinger, 2015; Martínez et al., 2008). Filoviruses have an approximate genome size of 19 kb, making them the largest known family of the Mononegavirales (Beer et al., 1999; Feldmann et al., 1993). The genomic organisation of filoviruses is characterised by the presence of major core protein genes in the 3' terminal part, while the polymerase is located in the 5' part. In between these regions, there are typically genes encoding for the envelope (Beer et al., 1999). Intergenic regions separate the genes, and gene overlapping is present in filovirus genomes (Feldmann et al., 1993).

While filoviruses can take on various shapes, they generally have long, filamentous structures that are uniform in diameter at approximately 80 nm (Feldmann et al., 1993). In fact, their name comes from their characteristic shape (Torres et al., 2015). Although the length of filoviruses can vary, their morphology is generally consistent. The virion contains a nucleocapsid at its core, which is surrounded by a lipid envelope derived from the host cell plasma membrane (Feldmann et al., 1993). The virus surface is covered in glycoprotein spikes that protrude approximately 7 nm from the surface (Feldmann et al., 1993). Filoviruses have the ability to replicate in a wide range of hosts, including humans, non-human primates (NHPs), pigs, and even fish (Holmes et al., 2016; Hume & Mühlberger, 2019) Given that several members of this viral family cause severe haemorrhagic fever diseases in humans, they are classified as Risk Group 4 pathogens by the World Health Organization and require Biosafety Level 4 containment (Noda, 2017).

As depicted in Figure 1, the filovirus family consists of six genera. The first two, Ebolavirus and Marburgvirus, are well-known for containing highly pathogenic human viruses (St Claire et al., 2017). The remaining four genera, Cuevavirus, Dianlovirus, Striavirus, and Thamnovirus, are less well-known and each contain only one virus (Martínez et al., 2015; Yu et al., 2017).

Since none of these four viruses has been isolated from either animal hosts or human patients, their pathogenic potential remains unknown (Hume & Mühlberger, 2019). The Marburg genus includes two viruses, the Marburg virus (MARV) and Ravn virus (RAVV) (Feldmann et al., 2020; E. Nakayama & Saijo, 2013), which are responsible for causing the Marburg virus disease (Guito et al., 2017). The Ebolavirus genus comprises 6 known viruses: Bombali virus (BOMV), Bundibugyo virus (BDBV), Reston virus (RESTV), Sudan virus (SUDV), Taï Forest virus (TAFV) and Ebola virus (EBOV) (Dixit et al., 2021; Goldstein & Simon J Anthony, 2018).

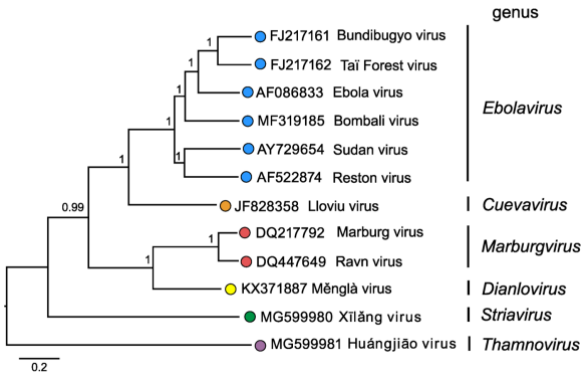

Figure 1 Phylogenetic relationships of filoviruses

From https://ictv.global/report/chapter/filoviridae/filoviridae

Ebola virus (EBOV) is the most virulent filovirus for humans due to its high case fatality rates (CFR) of 90% (Bausch, 2011) and its association with large human outbreaks, such as the West African Ebola outbreak of 2013-2016 (Bale et al., 2011; Park et al., 2015). Sudan virus (SUDV) and Bundibugyo virus (BDBV) are also pathogenic for humans, with reported CFRs of 50% and 25%, respectively (Escudero-Pérez et al., 2019).

A case apart: RESTV lack of pathogenicity

It is worth noting that the pathogenicity of TAFV and RESTV in humans remains unclear, as there is limited information available. There has only been one confirmed case of TAFV infection in a human, which occurred in the Ivory Coast in 1994 and resulted in mild symptoms (Formenty et al., 1999). Similarly, there have been few reported cases of RESTV infection in humans, but they have all resulted in asymptomatic seroconversion (Fletcher et al., 2014; Morikawa et al., 2007). However, infections of RESTV in non-human primates (Barrette et al. 2009) and domestic pigs (Haddock et al., 2021; Peñas et al., 2019) have been documented and should be taken into account.

The observation that RESTV infection in humans leads to seroconversion without causing symptoms has raised several hypotheses to explain its apathogenic behaviour (Malvy et al., 2019). One potential explanation is that RESTV has a less efficient replication and spread compared to EBOV (Morikawa et al., 2007), which has been demonstrated in in vitro studies showing slower and lower growth of RESTV (Boehmann et al., 2005). This is further supported by *in vivo* studies, which have shown limited replication of RESTV in the liver, unlike EBOV (Escudero-Pérez et al., 2019; Yamaoka & Ebihara, 2021). These findings suggest that differences in virus replication and spread may contribute to the distinct pathogenicity observed between RESTV and EBOV.

On a molecular level, there are several differences between RESTV and EBOV that could contribute to the former's lower pathogenicity. For example, amino acid variations between RESTV and EBOV's VP24 (Groseth et al., 2002) and VP35 (Pappalardo et al., 2016) may affect the virus's ability to block the cellular interferon response (Cantoni et al., 2016), which is a crucial immune response to viral infections. Additionally, RESTV appears to secrete more soluble glycoprotein (sGP) than EBOV, which could contribute to its reduced pathogenicity (Mahale & Patole, 2015). Another factor that may play a role is the difference in genomic arrangement between the two viruses, with RESTV having an intergenic region between its GP and VP30 genes (Sanchez, 2014). This contrast to EBOV's gene overlap between GP and VP30 could also play a role in RESTV's apparent lack of pathogenicity (Cantoni et al., 2016).

EBOV’s evolutionary rate

Given the extensive circulation of RESTV in various animal species (Morikawa et al., 2007), there is a concern about the emergence of a RESTV variant that may be pathogenic to humans (Cantoni et al., 2016). Similar concerns were raised in the media during the 2013-2016 West Africa Ebola outbreak, where it was reported that EBOV had mutated unusually rapidly (Holmes et al., 2016). While the emergence of resistance is always a risk (Fauci et al., 2019), the evolutionary rate of EBOV overlaps with that of other RNA viruses (1.2×10^{-3} substitutions per site per year)(Jacobs et al., 2016). Although there have been a few adaptive mutations in GP that enhance virus entry into human cells (Schieffelin et al., 2014), no evidence has shown that the presence of GP mutations or the accumulation of neutral substitutions has changed the clinical severity, outcome of the disease, or the transmissibility of the virus (Malvy et al., 2019).

Epidemiology

Filovirus infections have been a source of great public and scientific concern since the discovery of the Marburg virus in 1967 and EBOV in the mid-1970s (Figures 2 and 3) (Feldmann et al., 1999). The first recorded outbreak of Ebola in humans occurred in 1976 at a mission hospital in Yambuku, located in northern Zaire, which is now known as the Democratic Republic of the Congo, or DRC (Bosch, 2004; Burke et al., 1978). The initial patient was a 44-year-old individual who had travelled to the northern Equator province and was admitted to the Yambuku hospital for what was initially believed to be a case of malaria (Muyembe-Tamfum et al., 2012). Due to the systematic reuse of contaminated needles at the hospital, nosocomial transmission played a significant role in the spread of EBOV (Coltart et al., 2017; Torres et al., 2015), ultimately resulting in 318 cases of Ebola virus disease (EVD), of which 280 were fatal, resulting in an 88% case fatality rate (Burke et al., 1978). To avoid stigmatising the village, the virus was named after the nearby Ebola River, rather than the village where the outbreak originated (Henry, 2015).

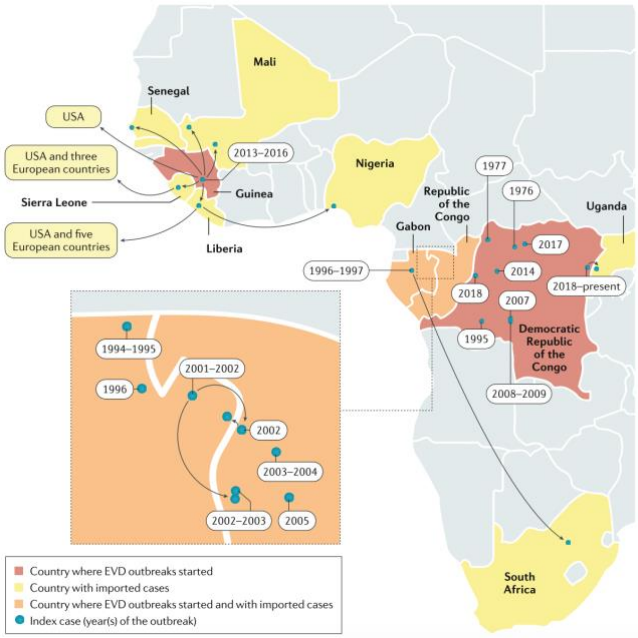

Figure 2 Ebola virus disease outbreaks

From (Jacob et al., 2020)

The Sudan outbreak of 1976 was actually the first recorded outbreak of Ebola virus disease (EVD) in humans, predating the Zaire outbreak by two months (Bosch, 2004). However, it

received much less international attention compared to the latter (Luban, 2013). The Sudan outbreak began in a cotton factory in Nzara, and nosocomial transmissions played a role in its spread as well, particularly at a hospital in Maridi (Coltart et al., 2017). A total of 284 cases were reported, with a case fatality rate of 53% (Knobloch et al., 1978). While the two outbreaks initially led some to believe that they were connected, subsequent investigation revealed that the viruses responsible for the outbreaks were actually two distinct species, Sudan ebolavirus (SUDV) and Zaire ebolavirus (EBOV), respectively (Muyembe-Tamfum et al., 2012). Between the initial outbreaks of Ebola in the 1970s and the West African epidemic in 2014, there were sporadic and minor Ebola outbreaks that occurred mostly in remote areas of central Africa (E. M. Leroy et al., 2011). Apart from the two incidents in the 1970s (Baron et al., 1983), there was a complete absence of Ebola outbreaks during the 1980s (Muyembe-Tamfum et al., 2012). While the majority of individuals afflicted with Ebola virus disease (EVD) during this time were caused by either Zaire Ebola virus (EBOV) or Sudan Ebola virus (SUDV), other cases were caused by Bundibugyo Ebola virus (BDBV) and, to a much lesser degree, Taï Forest Ebola virus (TAFV) (Audet & Kobinger, 2015).

Country (year)	Case–fatality rate (%)	Number of cases
COD (then Zaire) (1976)	88.1	318
COD (then Zaire) (1977)	100.0	1
Gabon (1994–1995)	61.5	52
COD (then Zaire) (1995)	77.3	317
Russia[a] (1996)	100.0	1
Gabon (1996)	67.7	31
Gabon, also exported to South Africa (1996–1997)	74.2	62
Gabon, COG (2001–2002)	78.2	124
COG, also exported to Gabon (2002)	90.9	11
COG (2002–2003)	89.5	143
COG (2003–2004)	82.9	35
Russia[a] (2004)	100.0	1
COG (2005)	81.8	11
COD (2007)	70.5	264
COD (2008–2009)	46.9	32
Guinea, also exported to Liberia, Mali, Senegal, Sierra Leone and USA; from Liberia, cases were exported to France, Germany, Netherlands, Nigeria, Norway, Spain and USA and, from Sierra Leone, to Italy, UK, Switzerland and USA (2013–2016)	39.5	28,652
COD (2014)	71.0	69
COD (2017)	50.0	8
COD (2018)	61.1	54
COD, also exported to Uganda (2018 to present)	66.3	3,324

Figure 3 Ebola virus disease outbreak statistics

From (Jacob et al., 2020). Country abbreviations are as used by the International Organization for Standardization (ISO). COD, Democratic Republic of the Congo; COG, Republic of the Congo.

In addition to the documented outbreaks, there have been isolated cases of individuals contracting EVD. Furthermore, three laboratory accidents have also resulted in people contracting the disease (Coltart et al., 2017). One of these cases was fatal, one was symptomatic but the individual survived, and the third case did not provide any evidence that the accident had resulted in an infection (Günther et al., 2011).

For a long time, it was believed that the threat of filovirus diseases in Africa was minor compared to existing regional health crises such as malnutrition, malaria, or HIV (Torres et al., 2015). However, this perception changed drastically in 2014 when the largest outbreak of EBOV occurred in the West African nations of Guinea, Sierra Leone, and Liberia (Gostin et al., 2014; Wong et al., 2016). This outbreak resulted in 28,616 confirmed cases and 11,310 deaths (B. W. M. Cook et al., 2016), which was several magnitudes larger than all the previous Ebola outbreaks combined (Lalle et al., 2019; Torres et al., 2015). The outbreak's magnitude was likely due to EBOV spreading to urban areas where larger chains of transmission were possible (Urbanowicz et al., 2016). Following the devastating 2013-2016 Western Africa Ebola outbreak, three subsequent Ebola outbreaks occurred in the DRC: one in 2014 and two in 2018 (Coltart et al., 2017). While the first two outbreaks were relatively contained with 66 and 54 confirmed cases respectively (Malvy et al., 2019), the 2018-2020 Kivu Ebola outbreak became the second largest with 3,470 cases and 2,280 deaths (Stoop et al., 2021). Since then, four additional Ebola outbreaks have emerged: two in the DRC in 2021, one in Guinea in 2021, and an ongoing SUDV outbreak in Uganda with the highest number of confirmed cases (140 as of now) (WHO, 2022).

Ecology

With lethality rates reaching as high as 90% (Alfson et al., 2015; Heinz Feldmann, Victoria Wahl-Jensen1, 2004), the ebolaviruses pose a serious threat to both humans and wildlife in central and western Africa (Bosch, 2004). One of the interesting aspects of EVD outbreaks is that they seem to arise suddenly from the remote wilderness (Amman et al., 2017; Bosch, 2004), last several months before subsiding, and leave behind fatal cases that, in the majority of outbreaks, number in the hundreds at most (Wong et al., 2016).

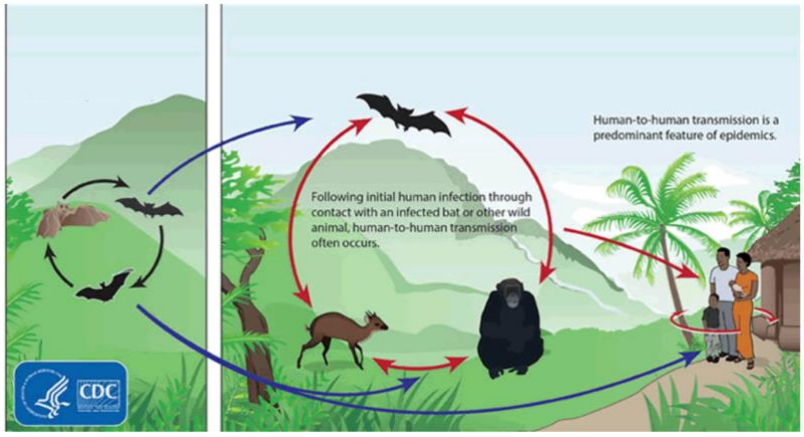

Figure 4 Life cycle of the Ebola virus

From https://www.cdc.gov/vhf/ebola/resources/virus-ecology-fr.html

Human outbreaks of EVD are believed to originate from the handling of infected animals, particularly primates and bats, either sick or dead (Malvy et al., 2019) (figure 4). Once the virus infects a person, it can spread to others through direct person-to-person contact (E. Nakayama & Saijo, 2013). The emergence and re-emergence of ebolaviruses in Africa is closely linked to various environmental and societal factors, including deforestation, climate change, urbanization, and population migration patterns. These factors can lead to increased contact between humans and potential animal hosts, as well as changes in local ecosystems that can affect the transmission dynamics of the virus (Lalle et al., 2019). Lastly, it should also be noted that Ebolaviruses are not restricted to the African Continent (Audet & Kobinger, 2015). Reston ebolavirus (RESTV) was first described in cynomolgus monkeys (*Macaca fascicularis*) that had been imported from the Philippines to a quarantine facility in Reston, USA (Audet & Kobinger, 2015; Muyembe-Tamfum et al., 2012).

The EVD is classified as a zoonotic disease, meaning it is transmitted from animals to humans (Audet & Kobinger, 2015). The virus is believed to have a natural reservoir host, and several animals have been proposed as potential hosts (Gale, 2017; Yang et al., 2000). Recent studies suggest that fruit bats belonging to the genus Pteropus are the primary natural reservoir host for the ebolaviruses (Baseler et al., 2017; Urbanowicz et al., 2016). Intriguingly, despite the extensive efforts for identifying the vector (É. Leroy et al., 2006; St Claire et al., 2017), no ebolavirus has ever been isolated from bats in natural conditions (Lacroix et al., 2021). One can thus speculate that such failed attempts can be due to either very low prevalence of infection or transient EBOV infection in animals, or virus infection at very low titres (Baseler et al., 2017).

Transmission

EVD is primarily transmitted through direct contact with bodily fluids such as saliva, mucus, vomit, faeces, tears, breast milk, urine, and semen (B. W. M. Cook et al., 2016; Jacob et al., 2020). The disease is contracted when an individual comes into contact with contaminated bodily fluids and subsequently touches their eyes, nose, mouth, an open wound, or an abrasion (Torres et al., 2015) (Figure 5). It is important to note that the virus can persist in ocular fluid, rectal fluids, vaginal fluids, and semen even after it is no longer detectable in the blood, indicating that sexual transmission from convalescent men can and does occur (Fischer et al., 2016; Srinivas et al., 2016).

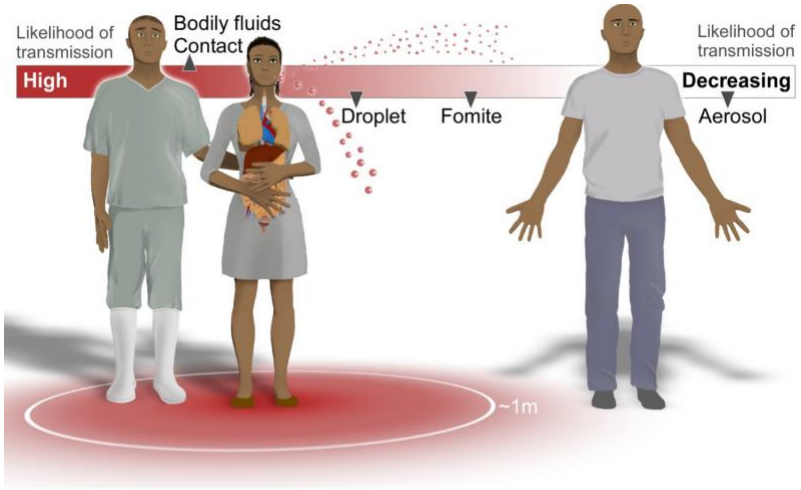

Figure 5 Potential routes of Ebola virus transmission and infection between people

From (Judson et al., 2015)

Nosocomial transmission poses a significant risk to healthcare workers (Malvy et al., 2019). While the Ebola virus is not transmitted through the air, respiratory droplets and other secretions can be infectious and could lead to an infection if they come into contact with mucous membranes (Torres et al., 2015). It is worth noting that RESTV has demonstrated the ability for aerosol transmission in cynomolgus monkeys during an outbreak that occurred in a quarantine facility in Reston from 1989-1990 (E. Nakayama & Saijo, 2013; St Claire et al., 2017). Lastly, viable virus particles can persist on the surface of bodies for more than seven days (Prescott et al., 2015), highlighting the potential for transmission of EVD through the handling of deceased individuals.

Management

Managing and controlling EVD outbreaks can be exceedingly difficult, particularly given the physical insecurity and complex political environment of affected regions in Africa (Bausch & Piot, 2020). Once an outbreak is recognised, rapid isolation of EVD cases is crucial in order to halt the chain of transmission (Malvy et al., 2019). Public health agencies should also take a series of actions, such as isolating patients, implementing barrier precautions, and identifying and tracking all contacts (Muyembe-Tamfum et al., 2012; Olupot-Olupot, 2015). Additionally, affected countries should have access to efficient national laboratories capable of rapidly and reliably detecting ebolaviruses (Malvy et al., 2019). This would help in the establishment of quarantines and provide critical information for effective outbreak management (Audet & Kobinger, 2015).

It is crucial to involve and inform community members as much as possible when managing and controlling EVD outbreaks, as cultural practices and beliefs in Central and Western African countries may create a negative perception of how EVD patients are handled and treated (Malvy et al., 2019; Raab et al., 2021). Providing education and communication on the disease and its transmission can help to build trust and encourage individuals to seek medical care, report suspected cases, and follow preventive measures (Raab et al., 2021). This includes promoting safe sex practices and encouraging convalescent men to abstain from sex or to use condoms for at least 90 days after symptom onset or until their semen has been tested negative twice (Abbate et al., 2016), as the virus can persist in semen for several months after recovery from the disease (Wong et al., 2016).

Finally, the declaration of the end of an EVD outbreak is a critical step in the management and control of the disease. According to World Health Organization guidelines (WHO, 2020), an outbreak is considered to have ended if no confirmed or probable EVD cases are detected for a period of 42 days, which is twice the maximum incubation period of EBOV, since the last potential exposure to the last case occurred. This period allows for the detection and monitoring of any new cases that may arise and ensures that there is no ongoing transmission of the virus in the community. Additionally, it is important to continue surveillance activities even after the outbreak has ended, to quickly detect and respond to any new cases that may occur, and prevent the re-emergence of the disease.

Signs and symptoms

The incubation period of the Ebola Virus Disease ranges from 2 to 21 days, as reported by various studies (Malvy et al., 2019; Muyembe-Tamfum et al., 2012). However, the average incubation period is 10 days, according to research conducted by (Torres et al., 2015). It is important to note that the incubation period may vary depending on the mode of transmission. For instance, individuals who are directly inoculated with the virus through injection with contaminated needles may experience a shorter incubation period, as reported by (Martínez et al., 2015).

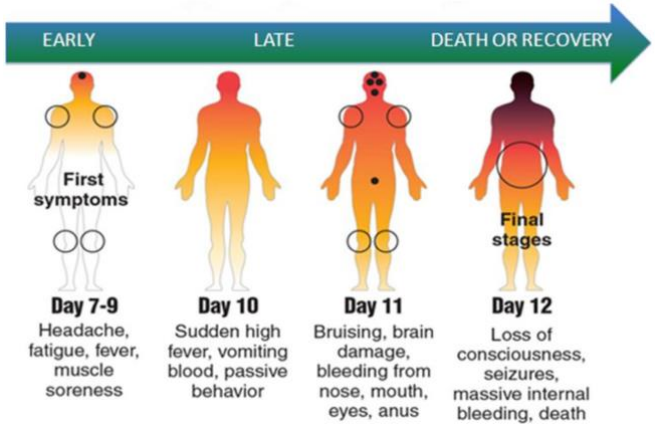

Figure 6 Course and typical symptoms of the Ebola virus disease

From https://www.emergencymedicinekenya.org/signs-and-symptoms-of-ebola/

As depicted in figure 6, after the incubation period, a sudden onset of non-specific symptoms occurs, including high fever, headache, lethargy, and myalgia (Fletcher et al., 2014; Yamaoka & Ebihara, 2021). These symptoms often overlap with those of other common tropical illnesses such as Dengue, Malaria, Typhoid fever, and other viral infections (Martínez et al., 2015; A. McElroy, 2015). Furthermore, clinical signs of Ebola virus infection, such as elevations in blood urea nitrogen and creatinine, and generalised transaminitis, are similar to those of the aforementioned diseases, making it difficult to distinguish between them (Torres et al., 2015). The acute phase of Ebola virus disease follows the initial influenza-like syndrome stage and is characterised by persistent fever and intense fatigue, often resistant to anti-malaria drugs and antibiotics, as well as gastrointestinal symptoms including diarrhoea, abdominal pain, anorexia, and vomiting (Malvy et al., 2019; A. McElroy, 2015; Muyembe-Tamfum et al., 2012). These gastrointestinal symptoms can result in massive losses of fluids, which may exceed 10 litres per

day, contributing to severe electrolyte imbalances (such as hypokalaemia, hyponatraemia, and hypocalcaemia), sepsis, multi-organ failure, hypovolemic shock, and high mortality (Chertow et al., 2015; Duraffour et al., 2017; Fletcher et al., 2014; Torres et al., 2015). It is important to highlight that the amount of diarrhea seen in Ebola outbreaks can be comparable to that observed in cholera outbreaks (Torres et al., 2015). However, unlike cholera, oral rehydration alone is often insufficient to address the severe fluid losses associated with EVD (Chertow et al., 2015). This is because EVD is a systemic viral illness that produces profound and debilitating symptoms (Chertow et al., 2015). Other symptoms that have been observed include hiccups (Torres et al., 2015) and skin manifestations such as maculopapular rash, which is more likely to be apparent in individuals with lighter skin (Malvy et al., 2019; A. McElroy, 2015).

After the acute phase, which typically lasts up to six days since the onset of symptoms, a pseudo-remission phase of one to two days occurs, during which the patient may feel better and experience an overall improvement in their health (Malvy et al., 2019). However, if the patient does not recover during this phase, they will enter a fourth phase of deterioration, during which their health status will worsen (A. McElroy, 2015). This is due to factors such as hypovolemia, an exaggerated inflammatory response, electrolyte imbalances, severe sepsis, sequential multi-organ failures, and shock (Fletcher et al., 2014; Ning et al., 2018). Although rare, some patients may also experience neurological symptoms such as confusion, delirium, and convulsions. Cases of Ebola virus disease-related encephalitis have been reported (Malvy et al., 2019). Ebola virus infection can lead to a haemorrhagic syndrome due to platelet dysfunctions, resulting in symptoms such as bloody diarrhoea, hematemesis, petaechiae, conjunctival injection, gingival bleeding, nosebleeds, and bleeding at the injection site (A. McElroy, 2015; E. Nakayama & Saijo, 2013). While haemorrhagic symptoms were more prevalent in earlier outbreaks, recent outbreaks show that haemorrhagic shock occurs in about 20% of patients, mostly due to gastrointestinal haemorrhage (Martínez et al., 2015; A. McElroy, 2015; Torres et al., 2015)

To determine the prognosis of an individual with Ebola virus disease, several factors have been identified that can aid in patient management, such as include high blood viral loads (more than 106 copies per ml), renal dysfunction, advanced age and pregnancy (Malvy et al., 2019; Martínez et al., 2015). Additionally, non-specific markers such as low serum albumin and calcium levels, and elevated levels of alanine aminotransferase and aspartate aminotransferase have been observed in patients with poor prognosis (Fletcher et al., 2014; Yamaoka & Ebihara, 2021).

Post Ebola syndrome

Finally, it is important to note that the phenomenon of post-Ebola syndrome has been observed in many survivors. Studies conducted after the 1995 outbreak in the Democratic Republic of Congo and the 2000 and 2007 outbreaks in Uganda found that up to 87% of survivors experienced ongoing symptoms even after their recovery from the disease (Abbate et al., 2016; Jacob et al., 2020). One example is the case of a British nurse who developed neurological complications more than 9 months after surviving an acute episode of Ebola virus disease (Deen et al., 2017; Rivera & Messaoudi, 2016). This highlights the need for ongoing medical care and monitoring of survivors, as the long-term effects of the disease are not fully understood.

The sequelae of the Ebola virus disease can impose significant functional limitations (Abbate et al., 2016). These long-term effects can range from persistent arthralgia, arthritis, and fatigue to vision-threatening uveitis, hearing deficits, painful swallowing and joint pain, sexual dysfunction, and mental health problems such as memory loss, confusion, and difficulty sleeping (Deen et al., 2017; Dixit et al., 2021; Jacob et al., 2020; Rivera & Messaoudi, 2016; Watson et al., 2021). In a 2016-study in Liberia, 1500 survivors were tracked for up to 5 years, and their preliminary findings evidenced that 68% of survivors had suffered from neurological complications, 60% had developed eye problems, and 53% had musculoskeletal complications (Burki, 2016).

The biological mechanisms behind the post-Ebola syndrome remain partially understood, but research suggests that antigen persistence in immunologically privileged sites of survivors may play a role (Jacob et al., 2020; Malvy et al., 2019; Rivera & Messaoudi, 2016). Up to 40% of EBOV survivors develop recurrent inflammation at certain sites, such as eyes, testis, synovium and meninges (Forrester, 2018), and isolated Ebola virus samples have been found in semen (4 months after clearance of viraemia), ocular fluid (9 weeks after clearance of viraemia), cerebrospinal fluid, placenta, and amniotic fluid from individuals who have recovered from the disease (Clark et al., 2015; Rashighi & Harris, 2017; Rivera & Messaoudi, 2016). The fact that EBOV samples can be readily cultured, not only suggests that persistent or latent infection is the cause of the recurrent inflammation (Varkey et al., 2015), but that sexually-transmitted EBOV could also represent a public health problem (Rashighi & Harris, 2017).

Diagnosis

The rapid spread of Ebola Fever Disease highlights the importance of early laboratory confirmation for suspected clinical haemorrhagic fever cases. Timely diagnosis enables appropriate sanitary measures to be implemented, such as the optimization of health resources and effective patient management (Martínez et al., 2015). By halting any potential outbreak before it becomes a full-blown epidemic (Muyembe-Tamfum et al., 2012), early detection can ultimately save countless lives. Due to the similarity of symptoms between Ebola and other endemic diseases such as Malaria, Typhoid Fever, Lassa Fever, Dengue, and Yellow Fever Disease (Torres et al., 2015), it is essential to develop reliable and differential diagnostic methods for the Ebola virus. The need for accurate diagnosis is paramount in ensuring that patients receive the appropriate treatment and preventing the spread of the disease (Muyembe-Tamfum et al., 2012). Thus, there has been a significant focus on developing diagnostic methods that can distinguish between Ebola and other similar diseases, which will be vital in containing outbreaks and saving lives.

Various laboratory techniques are available to detect an infection caused by the Ebola virus, including isolating and growing the virus, immunohistochemical staining, ELISA for detecting EBOV antigens or specific antibodies, and RT-PCR for detecting EBOV genomic material (Martínez et al., 2015; Torres et al., 2015). The choice of method for detecting the infection depends on the time point at which samples are collected, as some methods are more suitable than others at different stages of the infection (Jagga et al., 2019) (see Figure 7).

Timeline of infection of EBOV	Preferred diagnostic tests
In a few days of initial stage	•Antigen-capture ELISA •IgM ELISA •PCR including real-time quantitate (qPCR) •Virus isolation
Later in infection course or after recovery	•IgM and IgG antibodies
Retrospectively in deceased patients	•Immunohistochemistry analysis •PCR •Virus isolation

Figure 7 Diagnosis of EBOV infection

From (Jagga et al., 2019)

It is crucial to select the appropriate technique to ensure accurate and timely diagnosis, which is essential in containing outbreaks and preventing further transmission of the disease. In this section, we will discuss several of the above-mentioned methods in detail.

Reverse transcriptase polymerase chain reaction (RT-PCR)

Although the Reverse Transcriptase Polymerase Chain Reaction (RT-PCR) method was first used during the Ebola outbreaks in the Democratic Republic of Congo in 1995 and Gabon in 2000 (Perkins & Kessel, 2015), virus isolation in cell culture had been the primary method for detecting filoviruses before the 2013-16 West African Ebola virus outbreak (Malvy et al., 2019). However, during the latest and largest Ebola outbreak in West Africa, RT-PCR became the gold standard for diagnosing ebolaviruses (Martínez et al., 2015). This method enables the identification of infected individuals with the Ebola virus 24 to 48 hours earlier than antigen detection by ELISA (Torres et al., 2015) and can differentiate between different viral variants in various tissues and fluid specimens (Martínez et al., 2015). Therefore, RT-PCR is a highly sensitive and specific method for Ebola virus detection and has played a crucial role in the timely diagnosis and management of Ebola outbreaks.Sampling for EBOV RNA detection via RT-PCR can occur during the acute phase or convalescence of infection (Malvy et al., 2019). Clinical specimens that can be used for EBOV RNA detection include blood, saliva, tears, faeces, sweat, nasal blood, skin swabs, urine, cerebrospinal fluid, ocular fluid, amniotic fluid, vaginal fluid, and semen (Malvy et al., 2019; Rivera & Messaoudi, 2016; Srinivas et al., 2016).

Antigen detection via Enzyme-Linked Immunosorbent Assay (ELISA)

The antigen capture ELISA assay, which proved to be effective during the Ebola outbreaks in the Democratic Republic of Congo (1995), Gabon (1996), and Uganda (2000), utilizes a pool of monoclonal antibodies to the EBOV and SUDV, coupled with rabbit sera raised against these viruses (Saijo et al., 2006). The assay targets proteins typically including NP, VP40, and GP. Antigen detection assays are useful tools for the rapid diagnosis of Ebola virus disease in its early stages, as viral antigen is present systemically early in the course of the infection (Perkins & Kessel, 2015; Saijo et al., 2006). This type of assay is particularly helpful in detecting fatal EBOV infections, as patients often succumb to the disease before mounting an antibody response that can be detected by other means (Saijo et al., 2006). However, for individuals who

survive an EBOV infection, this assay becomes less sensitive over time as the immune system begins to clear the virus particles (Martínez et al., 2015).

Antibody detection via Enzyme-Linked Immunosorbent Assay (ELISA)

Enzyme-linked immunosorbent assays (ELISAs) can be used to detect IgM antibodies, which peak in the second week of illness and are helpful in diagnosing the disease (Martínez et al., 2015). However, unlike antigen detection, IgM and IgG antibodies are clinical markers that appear late in the progression of the disease (Torres et al., 2015). It is worth noting that while IgG and IgM antibodies develop in survivors, they may not appear in all fatal cases (Malvy et al., 2019). Therefore, it is important to consider that this method of diagnosis may be less clinically relevant for critically ill patients and the management of their disease (Martínez et al., 2015). However, if an individual is suspected of having symptomatic or asymptomatic Ebola virus infection, the detection of antibodies is the preferred method, as it can reveal extremely low viremia and the development of IgG and IgM about three weeks after infection (Malvy et al., 2019).

Immunohistochemical staining

This method of Ebola virus antigen detection has an advantage in situations where only formalin-fixed tissues are available for testing. Using specific monoclonal and polyclonal antibodies, the virus antigens can be detected in these tissues. This method is particularly useful because formalin-fixed biopsy specimens are not infectious, and can be easily transported without special precautions or refrigeration. This makes it possible to obtain and transport specimens even in the most basic field conditions. However, it is important to note that this method is not as sensitive as some of the other methods discussed above, and may not be useful for diagnosing early or mild cases of Ebola virus infection (Martínez et al., 2015).

Treatments

As of now, there are still no specific treatments for an EBOV infection (Malvy et al., 2019; Muyembe-Tamfum et al., 2012; Oestereich et al., 2014). However, the primary approach for managing patients with this disease is through supportive and critical care (Duraffour et al., 2017; Torres et al., 2015). In response to the 2013-2016 West Africa Ebola outbreak, the World Health Organization (WHO) published a guideline called Optimized Supportive Care for Ebola Virus Disease. This guideline aims to provide recommendations that can increase the chances of survival for patients (Duraffour et al., 2017). Supportive care for EBOV patients mainly involves restoring and maintaining electrolyte balance through oral or intravenous fluid rehydration, especially if the patient is too weak or in a coma. Crystalloid fluids have been shown to help restore haemodynamic stability, potentially reducing the need for blood transfusions or platelet administration. This approach can help prevent complications and increase the patient's chances of survival (Duraffour et al., 2017; Malvy et al., 2019; Torres et al., 2015). Supportive care also includes a range of strategies to restore and maintain the patient's health, such as proper nutrition, analgesics, and the use of anti-emetics and anti-diarrheal agents (Martínez et al., 2015). Antibiotics are often used in cases of secondary bacterial infections, while respiratory status is carefully monitored and coagulopathies are corrected as needed (Martínez et al., 2015; Torres et al., 2015).

The management of Ebola patients in Africa has posed significant challenges due to inadequate infrastructure, equipment, and staffing shortages (Muyembe-Tamfum et al., 2012). As a result, proper surveillance of biochemical markers such as haemoglobin or haematocrit values, electrolyte concentrations, anion gap, blood glucose, and lactate has been difficult to achieve (Chertow et al., 2015; Malvy et al., 2019). Furthermore, the lack of proper intensive care settings, including access to organ replacement strategies such as haemodialysis, artificial ventilation, or haemodynamic support, has contributed to higher mortality rates (Malvy et al., 2019). The development and commercialization of treatments for EBOV infections is hindered by the fact that these infections are rare in regions where the profitability of such research would be high (Oliphant, 2014). Nevertheless, the 2013-2016 West Africa Ebola outbreak brought increased public attention to the need for anti-viral research aimed at reducing viral replication and controlling the inflammatory response in infected patients (Malvy et al., 2019). This has resulted in an upsurge of research and development of experimental drugs that have shown

promise in lowering the case-fatality rate of the disease (Colebunders & Cannon, 2015). In this section, we will discuss some of these drugs or therapies.

Convalescent whole blood and convalescent plasma

This approach involves the collection of human convalescent blood or serum from individuals who have survived an Ebola infection, which is then administered to infected individuals to induce passive immunisation (Torres et al., 2015). The effectiveness of convalescent blood or serum therapy for Ebola treatment remains uncertain (Torres et al., 2015). While the use of convalescent blood or serum therapy for Ebola virus disease has shown some promise in small human clinical trials during the 1995 Kikwit Ebola outbreak in the Democratic Republic of Congo, subsequent outbreaks have failed to reproduce these (Muyembe-Tamfum et al., 2012). Therefore, there is currently a lack of sufficiently large studies to provide evidence supporting the effectiveness of these therapies in reducing the severity or duration of the infection (Colebunders & Cannon, 2015; Malvy et al., 2019; Martínez et al., 2015).

ZMapp

ZMapp is an experimental therapy consisting of three humanised monoclonal antibodies (c13C6, c2G4, and c4G7) designed to target the EBOV envelope transmembrane glycoprotein (Martínez et al., 2015). In preclinical studies, these antibodies demonstrated efficacy in treating rhesus monkeys with EBOV infection (Oliphant, 2014; St Claire et al., 2017). Although three healthcare volunteers from North America and Europe who contracted Ebola virus disease in Liberia in 2014 received ZMapp and experienced clinical improvement, other measures of care likely played a significant role in their recovery, and therefore the therapeutic benefit of ZMapp cannot be conclusively attributed (Martínez et al., 2015). In February 2015, a major clinical trial of ZMapp, consisting of a randomised controlled study, was conducted in Liberia, Sierra Leone, and Guinea (Martínez et al., 2015). Although the therapy showed promise by reducing the relative risk of death by 40%, the trial was conducted when the outbreak was beginning to decline, and the number of patients enrolled was insufficient to draw a definitive statistical conclusion (Duraffour et al., 2017; Malvy et al., 2019). Therefore, the efficacy of ZMapp in treating Ebola virus disease remains inconclusive and requires further investigation with larger patient populations.

Loperamide

The mechanism by which diarrhoea occurs in Ebola virus disease has not yet been fully elucidated. However, autopsy studies of patients with EVD have suggested that gastrointestinal inflammation may contribute to the pathogenesis of the disease (Chertow et al., 2015). Therefore, the use of the potent anti-diarrheal agent Loperamide may be effective in reducing diarrheal losses in Ebola virus disease. By using Loperamide, negative fluid balance and electrolyte losses can be corrected, and the risk of nosocomial transmissions can be reduced due to decreased environmental contamination (Chertow et al., 2015). However, the use of Loperamide in individuals with Ebola virus disease is not well-studied (Chertow et al., 2015).

Recombinant nematode anticoagulant protein c2 (rNAPc2)

Coagulation abnormalities are a prominent feature of filovirus infections, and it has been suggested that tissue factor is involved in triggering haemorrhagic complications (E. Nakayama & Saijo, 2013). Consequently, attention has turned to the recombinant nematode anticoagulant protein c2 (rNAPc2), which inhibits both factor VII and tissue factor (E. Nakayama & Saijo, 2013). Tissue factor overexpression is known to cause disseminated intravascular coagulation and thrombosis-related organ failure, making it a potential therapeutic target (E. Nakayama & Saijo, 2013). Studies with rhesus monkeys treated with rNAPc2 have shown an increased survival rate (E. Nakayama & Saijo, 2013; Oliphant, 2014; St Claire et al., 2017). However, there is currently no hard evidence to suggest that rNAPc2 provides therapeutic benefit beyond the 2-day post-infection period (A. McElroy, 2015; Oestereich et al., 2014).

Other molecules

Several compounds have demonstrated a level of protection against EBOV infection. For example, remdesivir, a nucleoside analogue, has been tested in non-human primates and has shown not only a good safety profile in phase I studies but also high efficacy (Malvy et al., 2019). However, subsequent clinical trials in humans between 2018 and 2019 revealed that remdesivir was less effective than monoclonal antibody treatments, leading the Congolese Health authorities to declare its reduced effectiveness (Cao et al., 2020). Nucleotide analogues such as Brincidofovir or BCX4430 have demonstrated antiviral activity (Martínez et al., 2015;

Rivera & Messaoudi, 2016), but there is no human data available to confirm these findings (Duraffour et al., 2017; Martínez et al., 2015). Phosphorodiamidate morpholino oligomers (PMOs) have also been studied as experimental drugs for Ebola infection by inhibiting gene translation of EBOV VP24, VP35, and L. This is achieved through steric blockage of ribosomal assembly (E. Nakayama & Saijo, 2013). While this drug has shown promising results in multiple animal studies, to date, there have been no clinical trials conducted in humans (E. Nakayama & Saijo, 2013).

Due to the significant role played by the EBOV GP in the internalisation of the virus, much attention has been given to the virus entry stage (Martínez et al., 2015). In this regard, chloroquine, an inhibitor of endosomal acidification, was believed to be effective against EBOV, as it would prevent mandatory GP cleavages and disrupt the viral infectious cycle. However, although *in vitro* experiments with chloroquine on pseudotype viruses bearing EBOV GP showed promising results, *in vivo* studies with guinea pigs revealed no protective effects (Dowall et al., 2015). Compound 7, a benzodiazepine derivative, is another example of a compound that has been identified as having anti-EBOV activity by preventing the virus from entering the host cell. However, no animal or human trials have been conducted on this compound (Martínez et al., 2015). Lastly, efforts to find a drug against EBOV infection have led researchers to examine the endo-lysosomal Niemann-Pick C1 (NPC1) cholesterol transporter protein more closely, as it is known to play a critical role in interacting with the EBOV GP and triggering several events that lead to virus internalization. Therefore, NPC1 inhibitors, such as the Benzylpiperazine adamantane diamides or amiodarone, may have the potential to halt virus infection (Martínez et al., 2015).

Vaccines

Since its discovery in 1976, the Ebola virus has caused several devastating outbreaks in Africa, with a fatality rate that can reach up to 90% (Kilgore et al., 2015; Reynolds & Marzi, 2017). Unfortunately, the lack of approved treatments (Piot & Spencer, 2018; Thi et al., 2015) has led to the perception that this disease has been neglected, particularly when compared to other infectious diseases such as AIDS or Malaria (Reynolds & Marzi, 2017).. Until 2014, the disease mainly affected remote and sparsely populated areas, making it less attractive to both the pharmaceutical industry and the public sector (Martínez et al., 2015; Piot & Spencer, 2018). However, the 2013-2016 West Africa Ebola outbreak had a global impact, prompting research efforts into vaccine development (Martínez et al., 2015). While there are several vaccine projects and approaches, they all share the common goal of being safe and effective, as well as addressing other practical considerations such as the ability to be transported and stored without requiring a cold chain, and providing immunity against multiple ebolaviruses (Torres et al., 2015; Walldorf et al., 2019). This section provides information on the sole 2 approved vaccines.

VSV and the rVSVΔG-ZEBOV-GP

The vesicular stomatitis virus (VSV) is a single-stranded negative sense RNA virus that primarily infects rodents, cattle, swine, and horses, but can also infect humans and other species (Lichty et al., 2004). Its 11-kb genome encodes for five proteins (figure 8), which include the nucleoprotein (N), the phosphoprotein (P), the large polymerase (L), the VSV glycoprotein (G), and the matrix protein (M) (Dietzgen et al., 2018). The N, P, and L proteins form the ribonucleoprotein, which is responsible for viral transcription and replication. The G and M proteins, on the other hand, are involved in virus internalisation and assembly, respectively, with the M protein also playing a role in virus budding (Barr et al., 2002).

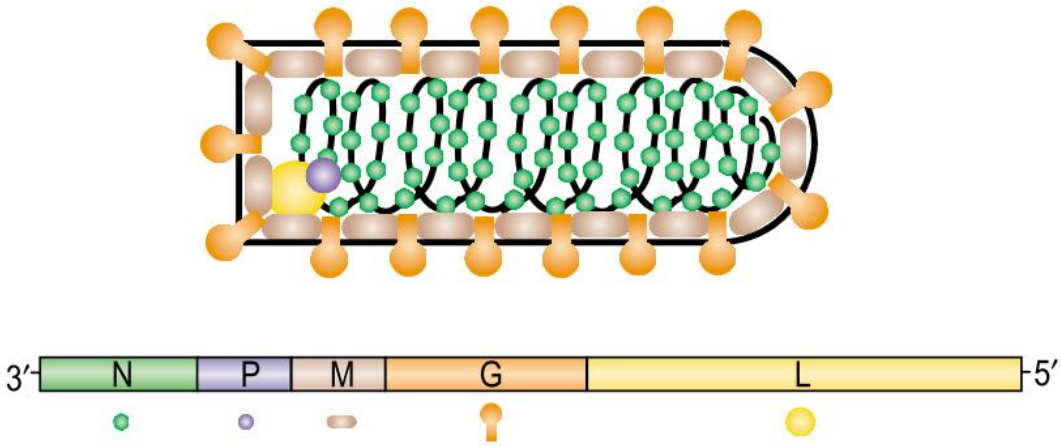

Figure 8 Vesicular stomatitis virus genome and particle structure

From (Lichty et al., 2004). VSV genome encodes for five proteins: nucleoprotein (N), phosphoprotein (P), matrix protein (M), glycoprotein (G), and the large polymerase (L).

A recombinant vaccine approach based on the vesicular stomatitis virus (VSV) has been developed to address the issue of pre-existing immunity, which can decrease the efficiency of the immune response (E. Nakayama & Saijo, 2013). The VSV glycoprotein gene is deleted and replaced with an EBOV GP (Santoro et al., 2021), creating a chimeric virus vaccine that expresses the EBOV GPz (Zaire strain). This approach allows for an immune response to be elicited while using the replication machinery of the less pathogenic VSV (Santoro et al., 2021). As a live-attenuated replicating virus, rVSV-ZEBOV-GP was initially a subject of safety concerns (Rivera & Messaoudi, 2016). However, several studies in non-human primates have concluded that this vaccine is safe and effective, with 100% protection conferred even at low doses (Lundstrom, 2020; E. Nakayama & Saijo, 2013; Santoro et al., 2021; Torres et al., 2015).

As a result of the promising findings from non-human primate studies, multiple human clinical trials were conducted to assess the efficacy and safety of rVSV-ZEBOV-GP, with individuals being monitored for at least 2 years after receiving a dose. The results of these trials showed that the vaccine induced a sustained antibody response (Santoro et al., 2021) and had only minor and occasional side effects (Rivera & Messaoudi, 2016). Based on these findings, the US FDA (United States Food and Drug Administration) approved the vaccine in December 2019, making it the first approved vaccine against Ebola. Although rVSV-ZEBOV-GP has demonstrated efficacy in clinical trials, the precise immunological mechanisms behind its protective effects are not yet fully understood (Santoro et al., 2021). However, transcriptomic data from a Phase

I/II randomised clinical trial revealed a transcriptional signature of the adaptive immune response that was correlated with anti-GP antibody titres (Santoro et al., 2021).

Adenovirus-based vaccines

Adenoviruses (Ad) are commonly used for developing recombinant viruses that express a protein antigen of a targeted pathogen. Specifically, Adenovirus serotype 5 (Ad5) is frequently used for this purpose, and a vaccine was developed that utilises the EBOV GP from the Zaire strain (Rivera & Messaoudi, 2016). Non-human primate studies demonstrated that this vaccine provided complete protection against an EBOV challenge (Geisbert & Young, 2003). However, despite the success of Ad5-based vaccines in animal studies, their efficacy in humans has been limited due to pre-existing immunity against Ad5 in a large portion of the population, especially in regions where EBOV outbreaks are most prevalent. Studies have shown that up to 85% of individuals in Africa have pre-existing immunity to Ad5, leading to reduced vaccine efficacy (Rivera & Messaoudi, 2016). As a result, alternative adenovirus serotypes such as 26 and 35 have been explored for the development of EBOV vaccines (E. Nakayama & Saijo, 2013; Rivera & Messaoudi, 2016). In non-human primate studies, these alternative adenovirus-based vaccines have demonstrated complete protection against EBOV challenges after only two vaccinations (Rivera & Messaoudi, 2016). In 2020, the European Union approved a vaccine scheme consisting of two doses, utilising Ad26.ZEBOV and a modified vaccinia virus Ankara bearing Bavarian Nordic filovector (Bausch & Piot, 2020). This vaccine was developed by Johnson and Johnson and has shown promising results in animal studies, though its efficacy in humans is yet to be fully determined.

Animal models

Due to ethical considerations, human experimentation is not possible in studying the Ebola virus (EBOV), and therefore animal models have been used for research purposes (Niemuth et al., 2021). However, the extrapolation of EBOV data from animal models to humans remains a challenge, and requires the use of validated animal models that can accurately recapitulate the human disease (Wahl-Jensen et al., 2012). Efforts have been made to develop alternative animal models for studying filovirus infections, including mice, marmosets, guinea pigs, ferrets, and hamsters (Ebihara et al., 2013; E. Nakayama & Saijo, 2013; St Claire et al., 2017; Wahl-Jensen et al., 2012; Yamaoka & Ebihara, 2021) (figure 9).

	Mouse	Guinea pig	Hamster	NHP	Human
Virus adaptation	Adapted	Adapted	Adapted	Wild-type	Wild-type
Viremia	High	High	High	High	High
Virulence	High	High	High	High	High
Weight loss	Severe	Severe	No	Severe	Severe
Rash	No	No	No	Yes	Yes
Thrombocytpenia	Yes	Yes	Yes	Yes	Yes
Lymphocyte apoptosis	Yes	Limited	Yes	Yes	Yes
Cytokine response	Yes	Yes	Yes	Yes	Yes
PT	Remained	Increased	Increased	Increased	Increased
PTT/aPTT	Remained	Increased	Increased	Increased	Increased
TT	ND	ND	Increased	Increased	ND
Fibrin deposition in organs	Little	Moderate	Little	Abundant	Observed
Protein C activity	ND	ND	Decreased	Decreased	ND

Figure 9 Comparison of EBOV pathological features amongst different animal models

From (E. Nakayama & Saijo, 2013). Abbreviations: PT, prothrombin time; PTT, partial thromboplastin time; APTT, activated partial thromboplastin time; TT, thrombin time ; ND, no data.

Mouse

Handling non-human primates (NHPs) can be challenging, which is one of the main drawbacks of using them as animal models for filovirus research. To address this issue, mouse models have been proposed as an alternative due to their small size, which helps alleviate space constraints in high containment facilities, and their relatively lower cost (E. Nakayama & Saijo, 2013). Furthermore, the availability of large numbers of mice and a wide range of reagents for biochemical and immunological assays have made them one of the preferred animal models for filovirus research (St Claire et al., 2017). It is important to note that adult immunocompetent mice are naturally resistant to wild-type EBOV infections and would not exhibit clinical symptoms (E. Nakayama & Saijo, 2013). However, immunocompromised mice have been shown to be susceptible to EBOV infections (Spengler et al., 2017). To overcome this limitation

and develop a reliable mouse model for EBOV infection, researchers have used serial passage of wild-type EBOV in new-born mice via intraperitoneal injections of liver homogenate to generate mouse-adapted EBOV (Rivera & Messaoudi, 2016; St Claire et al., 2017). This approach enables the virus to gain the ability to cause uniformly lethal infections in adult immunocompetent mice (E. Nakayama & Saijo, 2013; Yamaoka & Ebihara, 2021). Although the mouse-adapted EBOV does not cause significant coagulation disorders, which are the hallmark of EVD (E. Nakayama & Saijo, 2013; Rivera & Messaoudi, 2016), it has been shown to reliably replicate the key features of EBOV infection. This includes the dissemination of the virus throughout the body, leading to viremia, weight loss, reduced activity, and increased inflammatory cytokines. Additionally, infected mice exhibit kidney dysfunction and liver damage, and death typically occurs within 5 to 7 days post-infection (E. Nakayama & Saijo, 2013; Rivera & Messaoudi, 2016; St Claire et al., 2017).

The mouse model, however, presents a significant concern due to the discrepancies between the mouse and human immune systems, particularly in immune-mediated diseases such as EVD (Spengler et al., 2017). To address this issue, researchers have attempted to "humanise" mice by reconstituting the human immune system with functional lymphoid and myeloid cells to varying degrees (Spengler et al., 2017; St Claire et al., 2017). Despite their limitations, mouse models remain useful tools for studying fundamental aspects of replication, pathogenesis, and immune responses in EVD (E. Nakayama & Saijo, 2013).

Hamster

Syrian golden hamsters (*Mesocricetus auratus*) are commonly used as animal models for infectious disease research due to their convenient size, short life cycle, and ease of breeding in captivity (St Claire et al., 2017). However, similar to the mouse model, wild-type EBOV infection in Syrian hamsters does not cause clinical signs, and only a low level of viral replication can occur. Therefore, a hamster-adapted EBOV strain must be generated through serial passages in young animals to induce virulence (Ebihara et al., 2013; E. Nakayama & Saijo, 2013). Interestingly, when infected with the hamster-adapted EBOV, these animals display clinical and pathological features similar to those observed in humans and NHPs, making them a valuable tool for studying EVD pathogenesis and evaluating potential vaccines and therapeutics (Ebihara et al., 2013; E. Nakayama & Saijo, 2013). In addition to macrophages and dendritic cells being the primary targets of hamster-adapted EBOV (E. Nakayama & Saijo,

2013), the resulting clinical symptoms also closely resemble those seen in humans (Ebihara et al., 2013; Wahl-Jensen et al., 2012). These symptoms include cytokine dysregulation, severe coagulopathy, lymphocyte apoptosis, and organ necrosis or apoptosis in the spleen, lymph nodes, and liver, often leading to death (St Claire et al., 2017; Wahl-Jensen et al., 2012).

The suppression or non-induction of the type-I interferon response, coupled with an uncontrolled host immune response, are deemed as key pathogenic processes for these hamster-adapted EBOV (Ebihara et al., 2013; St Claire et al., 2017). This is further evidenced by an early activation of type-I IFN, mild inflammatory responses, induction of less-prominent apoptosis, and minimal pathological changes when hamsters are inoculated with wild-type EBOV (St Claire et al., 2017; Wahl-Jensen et al., 2012). The Syrian hamster model displays severe coagulopathy that is similar to that seen in NHPs infected with WT EBOV (St Claire et al., 2017). This unique feature makes the Syrian hamster model valuable not only for studying EBOV but also for investigating other viral haemorrhagic fevers (St Claire et al., 2017).

Guinea Pig

Guinea pigs have been utilised as EBOV animal models to evaluate pathogenesis, vaccines, and therapeutic agents (E. Nakayama & Saijo, 2013; St Claire et al., 2017). Despite their larger size compared to most rodent models, guinea pigs offer the advantage of a greater circulating blood volume, which allows for more flexibility in experimental designs involving blood sampling and adjustment of doses (St Claire et al., 2017). Similar to previous rodent models, when inoculated with wild-type EBOV, guinea pigs develop a short-lived, non-lethal febrile illness (E. Nakayama & Saijo, 2013; St Claire et al., 2017). The lack of virulence of WT EBOV in guinea pigs is attributed to the virus' inability to efficiently replicate in and/or be released from hepatocytes and macrophages (Mateo et al., 2011). Thus, serial passages of EBOV are necessary for the virus to acquire a lethal phenotype in guinea pigs (E. Nakayama & Saijo, 2013; St Claire et al., 2017).

(Volchkov et al., 2000) successfully generated an adapted strain of guinea pig-EBOV through serial passaging of wild-type EBOV in these animals. Detailed analysis of the nucleotide sequence revealed specific mutations in GP, NP, and VP24, leading to corresponding amino acid changes. Notably, the presence of four mutations in VP24 strongly indicates the pivotal role of this protein in the adaptation process. When infected with a Guinea pig-adapted strain

of EBOV, these animals show similar symptoms ranging from fever, anorexia, and dehydration (St Claire et al., 2017) to those observed in NHPs infected with wild-type EBOV, such as viremia and high replication in the spleen, liver, adrenal gland, and lung. Death usually occurs between the 7th and 9th day post-infection (E. Nakayama & Saijo, 2013). Guinea pigs also exhibit histopathologic lesions and serum chemistry changes during EBOV infection that are similar to those observed in mice, NHPs, and humans (E. Nakayama & Saijo, 2013; St Claire et al., 2017).

Non-Human primates

Non-human primates (NHPs) have been the preferred animal model for studying Ebola virus (EBOV) for two main reasons. Firstly, since WT EBOV can already induce disease in NHPs, there is no need to generate an adapted EBOV (Wahl-Jensen et al., 2012). Secondly, NHPs exhibit a complete recapitulation of the clinical manifestations observed in humans, including systemic viral replication, vascular leakage, coagulopathy, heightened immune responses, and an almost 100% lethality rate (Ebihara et al., 2013; E. Nakayama & Saijo, 2013; St Claire et al., 2017). Additionally, EBOV's main targets in NHPs are immune cells such as monocytes, macrophages, and dendritic cells, which is consistent with what is observed in humans (E. Nakayama & Saijo, 2013; St Claire et al., 2017). The most commonly used NHP species for EBOV research include African green monkeys (*Chlorocebus aethiops*), hamadryad baboons (*Papio hamadryas*), cynomolgus macaques (*Macaca fascicularis*), and rhesus macaques (*Macaca mulatta*) (Rivera & Messaoudi, 2016; St Claire et al., 2017).

Other animal models

Ferrets are the only small, non-primate animal model that is susceptible to wild-type EBOV infection, making them a valuable and lethal model for studying EBOV (Watson et al., 2021). Given that EBOV has been detected in the eyes of infected animals, (Watson et al., 2021) suggest that the ferret model could be used to develop treatments aimed at reducing the persistent virus observed in humans. Another animal model proposed for studying EBOV is the marmoset. While these small New World primates are susceptible to WT EBOV infection, there are few readily available immunological tools, and the small size of these animals limits the quantity of blood that can be collected (St Claire et al., 2017).

Structure and Genomic organisation of EBOV

As shown in figure 10, EBOV exhibits a filamentous appearance, but it can also take on various shapes such as branched, circular, U- or 6-shaped, or long and straight (Feldmann & Klenk, 1996). Furthermore, while EBOV virions have a uniform diameter of approximately 80nm, they can vary significantly in length (Noda et al., 2002).

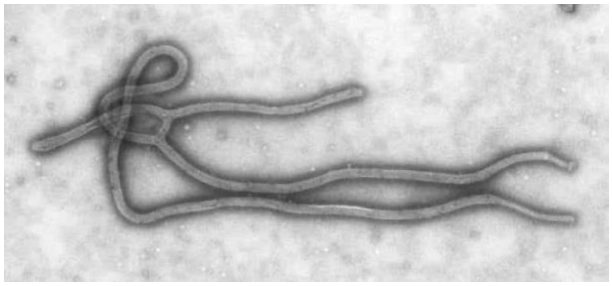

Figure 10 EBOV transmission electron microscopic image

Taken from: https://phil.cdc.gov/details.aspx?pid=1832

Structurally, EBOV particles consist of an outer envelope that is derived from the host cell and contains the sole surface glycoproteins (GP) arranged as trimers (Beniac & Timothy, 2017). These GP form spikes of approximately 7nm and are spaced at intervals ranging from 5 to 10nm (Feldmann & Klenk, 1996). Additionally, this outer layer is lined with the matrix protein VP40, which drives viral budding and particle formation (Stahelin, 2014). As depicted in Figure 11, there is also an inner core known as the ribonucleoprotein complex, which comprises the viral RNA genome and other associated nucleocapsid proteins (Davey et al., 2011).

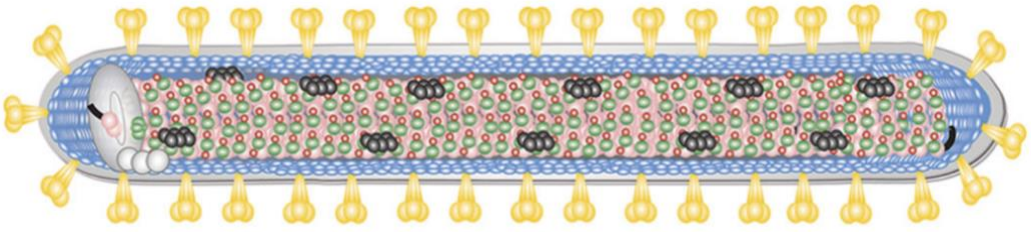

Figure 11 EBOV's structure arrangement

From (Hume & Mühlberger, 2019). The cell membrane-derived envelope (outer grey oval) is coated with viral glycoprotein trimers (yellow). The assembly of the matrix protein VP40 (blue) is the reason behind which EBOV has its characteristic filamentous shape. The viral nucleocapsid is made of the negative sense RNA (black line), enwrapped in the nucleoprotein NP (pink), coupled with polymerase cofactor VP35 (green), transcription factor VP30 (dark grey), nucleocapsid protein VP24 (red) and the catalytic polymerase subunit L (light grey ring). The representation of the L protein is based on the structure of the vesicular stomatitis virus L protein.

Genomic organisation

EBOV is an enveloped, non-segmented, single-stranded negative-sense RNA virus consisting of approximately 19,000 bases (Volchkova et al., 2011). As shown in figure 12, the EBOV genome encodes seven linearly arranged genes that express seven structural and one non-structural protein (Reynard & Volchkov, 2015). These include the nucleoprotein (NP), viral protein 35 (VP35), matrix protein VP40, glycoprotein (GP) and its derived proteins (sGP, Δ-peptide, $GP_{1,2}$ and ssGP), transcription factor VP30, protein VP24, and the L large protein (Audet & Kobinger, 2015).

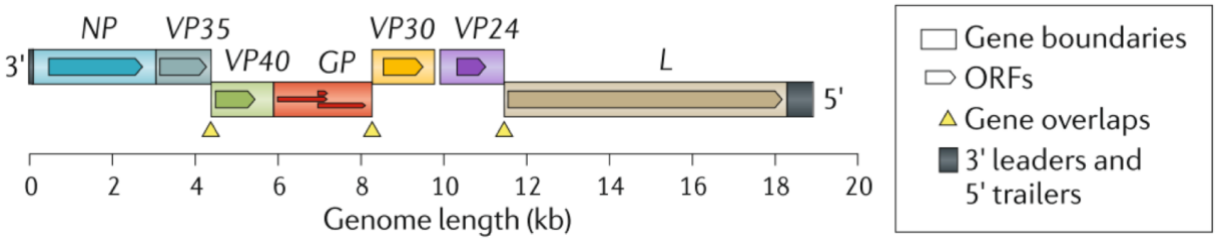

Figure 12 EBOV's genome organisation

From (Jacob et al., 2020). The triangles indicate GS and GE transcription overlapping signals.

Each EBOV gene is flanked by conserved gene start (GS) and gene end (GE) signals, which can either overlap or be separated by short intergenic regions (Hume & Mühlberger, 2019). At each end of the genome, there are also highly conserved 3' leader and 5' trailer sequences. The 3' leader sequence is located upstream of the GS signal of the first gene (NP), while the 5' trailer sequence is located downstream of the GE signal of the last gene (L) (P. et al., 1999).

The Ebola virus is composed of seven genes that encode for the following viral proteins: nucleoprotein (NP), viral protein 35 (VP35), VP40, glycoprotein GP, soluble GP (sGP), Δ-peptide, ssGP, VP30, VP24 and polymerase (L) (J. E. Lee & Saphire, 2009; Ning et al., 2017; Yu et al., 2017), as depicted in figure 13. The role of these viral proteins during the virus infectious cycle has been largely studied and elucidated (Yu et al., 2017). In this section, we will discuss each of these proteins in detail.

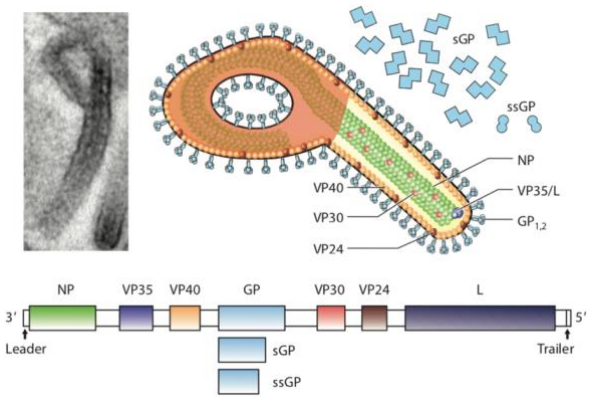

Figure 13 Ebolavirus structure and genome organisation

From (Baseler et al., 2017). Ebolavirus structure indicating the various proteins and genes that code for them. The genome displays the following structure: 3' leader, nucleoprotein (NP) gene, viral protein (VP) 35 gene, VP40 gene, glycoprotein (GP) gene, VP30 gene, VP24 gene, polymerase (L) gene and the 5' trailer.

NP

The nucleoprotein, with its molecular weight of 83 kDa and 739 amino acids, plays a crucial role in the virus infectious cycle (Sanchez et al., 1992). It is the primary constituent of the ribonucleocapsid complex (Dong et al., 2015), which also comprises VP30, VP35, and RNA-dependent RNA polymerase (L) (Watanabe et al., 2006) (figure 14). The nucleoprotein forms left-handed filament-like helical coils (Noda et al., 2006), which protect the viral genome from nucleases and the cellular innate immune response by surrounding it. Moreover, the RNA cleft is situated on the outer side of the NP helix (Kirchdoerfer et al., 2016), allowing interactions with other viral proteins during replication and transcription. The nucleoprotein is composed of a hydrophobic N-terminal and a hydrophilic C-terminal half (Watanabe et al., 2006). The N-terminal half is crucial for RNA binding (Licata et al., 2004), while the C-terminal half is responsible for incorporating more NP into the virion by interacting with VP40 (Huang et al., 2002). Additionally, the C-terminal domain has been found to play a role in the formation of inclusion bodies and virus-like particle (VLP) production (Miyake et al., 2020).

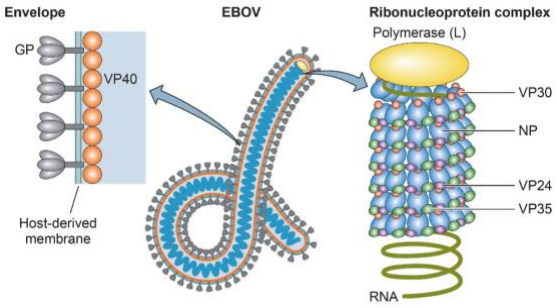

Figure 14 Envelope and ribonucleoprotein complex

Adapted from (Yamaoka & Ebihara, 2021)

The nucleoprotein undergoes sialylation and O-glycosylation, with the latter modification being required for protein-protein interactions with VP35 or VP24 (Huang et al., 2002). The NP-VP24 interaction is crucial for nucleocapsid assembly and genome packaging (Banadyga et al., 2017), while the NP-VP35 interaction plays a role in regulating viral RNA synthesis. When NP is in a monomeric state, it can bind to single-stranded RNA, but coupling with VP35 prevents this binding (Leung et al., 2016). There are several amino acid motifs within NP, such as LxxIxE (Kruse et al., 2018) and PPxPxY and SxPxLE (Kirchdoerfer et al., 2016), that are important for interactions between NP and other viral proteins, particularly VP30. Additionally, the SET and MYND domain containing protein 3 (SMYD3) (Chen et al., 2019), the nuclear RNA export factor 1 (NXF1) (Wendt et al., 2020), the HSP70 (García-Dorival et al., 2016) and the RUVBL (RuvB-like) 1 and RUVBL2 (Morwitzer et al., 2019). These interactions serve various functions, ranging from facilitating viral mRNA transcription and increasing NP stability to even being required for capsid assembly.

VP35

VP35 is a multifunctional protein consisting of 340 amino acids, playing a critical role in viral transcription and replication (Mühlberger et al., 1999). Additionally, VP35 plays a crucial role in genome packaging (Johnson et al., 2006) and nucleocapsid assembly (Kirchdoerfer et al., 2016). It has been previously mentioned that VP35 achieves the latter by binding to monomeric NP, preventing premature and non-specific encapsidation of viral RNA (Jain et al., 2021). In addition, VP35 interacts with other viral proteins to achieve multiple purposes (Jain et al., 2021). For instance, it acts as a non-enzymatic co-factor for the L protein (Leung et al., 2016), and together with NP, the complex regulates viral RNA synthesis (Prins et al., 2009).

VP35 plays a critical role in host immune evasion (Nelson & Schmidt, 2017) by blocking the recognition of viral double stranded RNA (dsRNA) by host immune receptors (Jain et al., 2021). VP35 possesses an interferon inhibitory domain (IID) (Leung et al., 2016) that binds viral dsRNA (Kimberlina et al., 2010) and prevents its recognition by retinoic acid-inducible gene I (RIG-I) and melanoma differentiation-associated protein 5 (MDA5) (Leung et al., 2016; Luthra et al., 2014). Similarly, VP35 enables host immune evasion by employing various strategies. Firstly, it obstructs the dimerisation, phosphorylation, and nuclear localisation of interferon regulatory factor 3 (IRF-3), thus hindering its normal function (Basler et al., 2003). This is achieved by VP35's ability to interfere with the interaction between IRF-3 and TANK-binding kinase 1 (TBK-1) and IB kinase epsilon (IKK) kinases (Prins et al., 2009). Additionally, VP35 can suppress the transcription of interferon (IFN) by increasing the SUMOylation of IRF-7 through interaction with the protein inhibitors of activated STATs 1 (PIAS1) (Prins et al., 2009). Lastly, VP35 can inactivate protein kinase R (PKR), which is an antiviral protein, leading to sustained viral protein synthesis (Schümann et al., 2009).

VP40

This viral protein comprises 326 amino acids and is the most abundant protein in the virions (Madara et al., 2015). It plays a crucial role in virus assembly and budding (Feldmann & Klenk, 1996), without which these processes cannot take place. VP40 interacts with several host factors, including SUMO, which significantly stabilises the viral protein (Valerdi et al., 2021). Additionally, VP40 contains two late budding domains, namely PTAP and PPEY , which interact with host proteins (J.M. et al., 2003). The PTAP domain forms a complex with the tumour susceptibility gene 101 protein (tsg101) (Juan Martín-Serrano, Trinity Zang, 2001), aiding the recruitment of VP40 into lipid raft domains on the plasma membrane, while the PPEY domain binds to ubiquitin ligase, neuronal precursor cell-expressed developmentally downregulated 4 (Nedd4) (Harty et al., 2010) and ITCH E3 ubiquitin ligase (J.M. et al., 2003), both of which are necessary for virus budding. VP40 is a transformer protein that can adopt multiple conformational states, including dimers, hexamers, filaments, and octamers (B. GC et al., 2016). The dimeric form of VP40 is crucial for its proper trafficking to the plasma membrane (Yamayoshi et al., 2008). Dimeric VP40 can assemble into filaments, which play an important role in matrix assembly and virus budding (Bornholdt et al., 2013). Additionally, octameric ring configurations of VP40 are necessary for its binding to single-stranded RNA

(ssRNA) (Hoenen et al., 2005), which in turn plays a role in the negative regulation of transcription (Hoenen et al., 2010).

GP

EBOV's glycoprotein (GP) is a transmembrane class I fusion protein consisting of 676 amino acids (Bale et al., 2011). As the sole protein on the viral surface, GP is fully responsible for attachment and virus internalisation (Kaletsky et al., 2007). GP can bind to multiple cell surface molecules, including integrin α5β1, TAM receptors, TIM-1, lectins, and glycosaminoglycans, as shown in figure 15 (Brindley et al., 2011; Jemielity et al., 2013; Martinez et al., 2011). EBOV can infect a wide range of cell types, including immune cells such as macrophages and dendritic cells, as well as hepatocytes, epithelial cells, and endothelial cells (Geisbert & Hensley, 2004).

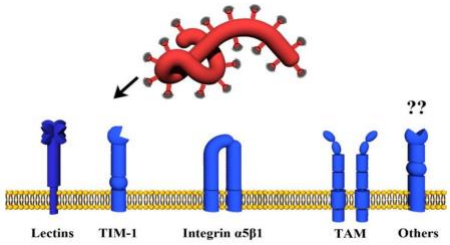

Figure 15 Attachment and signalling factors

Adapted from (Hofmann-winkler et al., 2012).

$GP_{1,2}$

The EBOV glycoprotein, GP, is initially expressed as a single polypeptide precursor ($GP_{1,2}$) which is transported to the Golgi apparatus for post-translational (Volchkov et al., 1998), including glycosylation (Simmons et al., 2002). Interestingly, the high level of glycosylation contributes to nearly half of the molecular mass of GP (Feldmann & Geisbert, 2011). Additionally, $GP_{1,2}$ undergoes cleavage by the cellular protease furin at amino acid 501, resulting in the two subunits, an N-terminal 140 kDa GP_1 and a C-terminal 26 kDa GP_2, which are linked by a disulphide bond (Volchkov et al., 1998) (figure 16). GP_1 contains a receptor-binding domain (Ning et al., 2017) and is responsible for attaching to the target cell (Wool-Lewis & Bates, 1998), whereas GP_2 facilitates fusion between the viral and host cell membranes (Kaletsky et al., 2007).



Figure 16 EBOV's glycoprotein main domains

Adapted from (Pallesen et al., 2016)

Once processed, these $GP_{1,2}$ heterodimers form trimeric functional ~7nm GP spikes (Feldmann & Klenk, 1996). $GP_{1,2}$ can induce adherent cell rounding and detachment, leading to cell death (Zampieri et al., 2007). Additionally, GP can trigger apoptosis (Bwaka et al., 1999) in B and T cells that are not targeted for infection by the virus (bystander apoptosis) through mechanisms that are still unknown (De La Vega et al., 2015). Moreover, GP can cause endothelial cell injury and loss, compromising thus the vascular integrity (Baskerville et al., 1985).

GP also contributes to viral budding by actively participating in the assembly process (Yang et al., 2000) and by antagonising tetherin, an interferon-induced antiviral factor that restricts the release of ebolaviruses by anchoring them to the cell surface (Vande Burgt et al., 2015). The mechanism behind this antagonism is not completely defined (Ning et al., 2017), but studies suggest that an appropriate processing of N-glycans and an intact receptor binding domain are required for tetherin counteraction (Brinkmann et al., 2016). After entering the cell, EBOV undergoes a process where GP is cleaved by cellular cathepsins B and L at amino acids 190-213 within the phagosome (Dube et al., 2009). This cleavage removes the mucin-like domain (Kaletsky et al., 2007) and exposes the receptor binding domain of GP_1, allowing it to bind to the cellular receptor NPC1 (Beniac & Timothy, 2017), which is also found inside the phagosome (figure 17). The resulting interaction between GP_1 and NPC1 most likely triggers membrane fusion, which is carried out by the fusion peptide of GP_2, a sequence of 16 uncharged and hydrophobic amino acids (Volchkov et al., 1998).

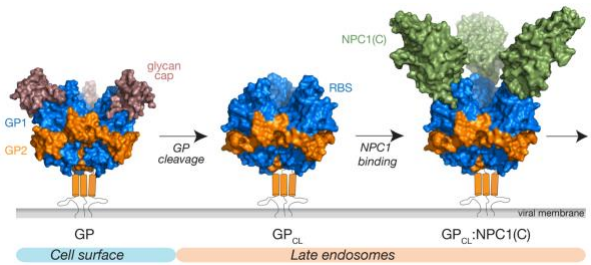

Figure 17 Interaction of EBOV's GP1,2 with the NPC1 receptor

From https://www.chandranlab.org RBS: receptor binding site; NPC1(C): domain C of the NPC1 receptor

RNA editing phenomenon

The GP gene's open reading frame contains seven consecutive uracils at positions 1021-1027, as noted by (Sanchez et al., 1996). This sequence is significant because the GP gene encodes three different proteins, and the transcription complex's editing function at the 7U GP editing site determines which protein is produced (Audet & Kobinger, 2015) (figure 18).

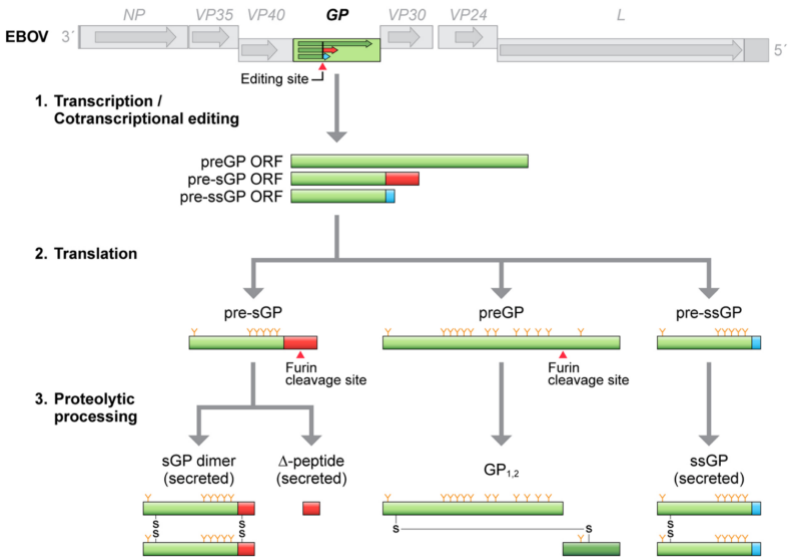

Figure 18 Schematic of EBOV's GP gene expression strategy

From (Clarke et al., 2017). Primary (unedited) transcription of the GP gene results in an mRNA leading to the expression of pre-sGP. pre-sGP is proteolytically cleaved by furin into mature and homodimerised secreted glycoprotein (sGP) and secreted Δ-peptide. EBOV RNA-dependent RNA polymerase (L) stuttering at a 7U-editing site within the GP gene infrequently results in the addition or subtraction of cognate A residues into nascent mRNAs, thereby disrupting the sGP open reading frame (ORF) and joining the sGP ORF upstream of the editing site with overlapping ORFs downstream. mRNAs with an 8A editing site result in the expression of preGP. preGP is proteolytically cleaved by furin into subunits GP_1 and GP_2, which remain connected through a disulphide bond in the form of a heterodimer ($GP_{1,2}$). mRNAs with a 6A or 9A editing site result in expression of pre-ssGP, which is proteolytically matured into homodimeric secondary secreted glycoprotein (ssGP). Orange-coloured Y's signify glycosylations.

The presence of seven adenines in the mRNA of the GP gene results in the formation of the non-structural soluble glycoprotein (Yang et al., 2000). If eight adenines are present, then $GP_{1,2}$, is formed instead (Weir & Weir, 2002). Conversely, the presence of either six or nine adenines in the transcript leads to the production of a small sGP (ssGP) (Yu et al., 2017). In Vero E6 cells, the ratios of production for sGP, $GP_{1,2}$, and ssGP were found to be 71:24:5, respectively (Zhu et al., 2019). RNA editing is a crucial factor in the pathogenicity of EBOV, as the elimination of the editing site leads to *in vivo* attenuation (Volchkova et al., 2015). High expression levels of $GP_{1,2}$ have been shown to be extremely cytotoxic, as they overload and

exhaust the cellular endoplasmic reticulum with highly glycosylated proteins. This results in an increased ability of the host defence system to recognize and eliminate virus-infected cells (Volchkova et al., 2015). Consequently, the downregulation of $GP_{1,2}$ plays an essential role in the high pathogenicity of EBOV. This is supported by evidence showing that $GP_{1,2}$ causes steric hindrance and masking of the cellular surface, thus impairing their normal functions (Reynard et al., 2009b; Sullivan et al., 2005).

sGP and the Δ-peptide

The soluble GP (sGP) is the main product of the GP gene and is initially synthesised as pre-sGP (Volchkova et al., 1999). The pre-sGP shares 295 N-terminal amino acids with the full-length GP (Volchkov et al., 1998) (figure 19). After proteolytic cleavage at its C-terminus (amino acid position 324 at R-X-R-R site) by furin, the pre-sGP yields the mature sGP and a Δ-peptide (Volchkov et al., 1998). sGP undergoes six N-glycosylations at amino acids 40, 204, 228, 238, 257, and 268 (Falzarano et al., 2006), and one C-mannosylation site at amino acid 288 (Falzarano et al., 2007). Two disulphide bonds form between residues Cys53 and Cys306, allowing sGP monomers to form 110-kDa homodimers (J. E. Lee & Saphire, 2009). Both sGP and the Δ-peptide lack the transmembrane anchor, so they are secreted extracellularly, but the Δ-peptide is retained inside the cell for a longer period (Volchkova et al., 1999).

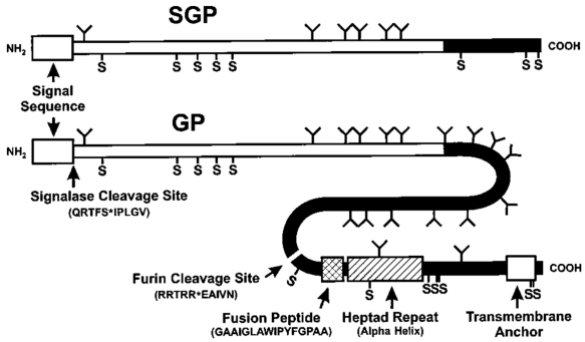

Figure 19 Diagrammatic representation of sGP and GP molecules of EBOV

From (Sanchez et al., 1998)

The function of sGP remains incompletely understood (Audet & Kobinger, 2015), but it is known to contribute to immune evasion by acting as a decoy for anti-GP antibodies (Mohan et al., 2012). In high quantities, sGP can dominate the host humoral response, diverting the production of antibodies away from $GP_{1,2}$ (De La Vega et al., 2015; Mohan et al., 2012).

Additionally, sGP appears to play a role in promoting viral dissemination by inhibiting pro-inflammatory cytokine production in non-infected macrophages and impairing chemotaxis of activated macrophages (Bradley et al., 2017). Interestingly, sGP also exhibits anti-inflammatory properties, such as the inactivation of neutrophils and partial restoration of TNF-α-induced endothelial cell barrier dysfunction (Sui & Marasco, 2002).

In addition to being secreted extracellularly, sGP can also play a structural role by forming a complex with GP_2 and substituting the GP_1 subunit (Iwasa et al., 2011). According to (Zhu et al., 2019), this may limit the cytotoxicity of $GP_{1,2}$ by removing the mucin-like domain of GP_1, allowing for more efficient replication of EBOV and promoting infectivity. Conversely, the absence of sGP and the sole presence of $GP_{1,2}$ would result in rapid clearance of infected cells by the innate immune system and early adaptive responses (Audet & Kobinger, 2015). There is a strong selective pressure in favour of sGP, which is particularly evident in animal infections (Kugelman et al., 2012).. This is highlighted by the fact that the 8U variant of the virus, which produces higher levels of sGP, can revert to its wild-type sequence after just one passage in guinea pigs, while the 7U variant requires five passages in Vero E6 cells for its editing site to become predominantly 8U (Audet & Kobinger, 2015).

Although the functions of the Δ-peptide remain unknown (He et al., 2017), this viral protein has been shown to inhibit the interaction between $GP_{1,2}$ and cellular attachment factors, potentially preventing virus superinfection and promoting systemic infection (Radoshitzky et al., 2011). Notably, while the Δ-peptide of several pathogenic ebolaviruses such as EBOV, SUDV, and TAFV can efficiently bind to permissive cells, the Δ-peptide of RESTV exhibits less efficient binding (Radoshitzky et al., 2011). Therefore, the Δ-peptide may be a determinant factor in viral virulence (Ning et al., 2017).

ssGP

The soluble small secreted glycoprotein (ssGP) is expressed when the Ebola virus transcript contains either 6U or 9U at the editing site (Mehedi et al., 2011). ssGP is a non-structural protein composed of 298 amino acids, with the 295 N-terminal amino acids identical to those of sGP and GP (Mehedi et al., 2011). Despite these similarities, ssGP does not exhibit the anti-inflammatory properties of sGP, which can reverse the loss of endothelial barrier function

induced by TNF-α (Ning et al., 2017). Mature ssGP is extensively N-glycosylated and is secreted as a homodimer, with disulphide bonds formed at amino acid 55 (Mehedi et al., 2011). However, the functions of ssGP are still unknown (Jain et al., 2021).

Shed GP

In addition to the previously mentioned GP-derived proteins, shed GP is also produced through the cleavage of $GP_{1,2}$ by the cellular metalloprotease TNFα-converting enzyme (TACE) (J. D. Cook & Lee, 2013). Shed GP shares structural similarities with $GP_{1,2}$, and can bind and sequester virus-neutralising antibodies against the surface GP, making them ineffective (Dolnik et al., 2004). Shed GP may also play a role in modulating the abundance of $GP_{1,2}$, and thus, achieve optimal virus infectivity and spread (Ning et al., 2017). This is especially important since $GP_{1,2}$ can be cytotoxic. Shed GP can activate non-infected dendritic cells and macrophages, causing a massive cytokine production and increased vascular permeability, which could contribute to viral pathogenicity (Escudero-Pérez et al., 2014).

Mucin-like domain

GP_1 contains a mucin-like domain (MLD), which is heavily N- and O-glycosylated and spans amino acids 309-489 (Ning et al., 2018; Ortega et al., 2019). This domain is rich in proline, serine, and threonine residues and is believed to act as a shield that protects GP from neutralisation by the host immune response (Dowling et al., 2007; Ou et al., 2012). The MLD's abundant glycosylation has also been shown to contribute to steric occlusion of human leukocyte antigen class I and II (HLA-1 and HLA-II) (Bale et al., 2011) and MCH class I polypeptide-related sequence A (MICA), which helps the virus evade the host immune response (Iraqi et al., 2020). The MLD has been linked to the induction of cell rounding and vascular cell cytopathogenicity (Yang et al., 2000), likely due to its ability to reduce the presence of cell surface molecules important for cellular processes such as adhesion, signalling, and immune evasion (Zampieri et al., 2007). In addition, research suggests that the MLD enhances viral infection of target cells through its contribution to the binding of hMGL, a human macrophage C-type lectin that is specific for galactose and N-acetylglucosamine (Takada et al., 2004).

VP30

VP30 is a structural phosphoprotein consisting of 288 amino acids that is an integral part of the nucleocapsid (Munjita & Kwenda, 2015). It performs multiple functions and is indispensable for RNA transcription initiation, as well as for reinitiating the process at gene junctions (Martínez et al., 2008). VP30 contains zinc-binding and RNA-binding sites in its N-terminal portion, which facilitate these functions (Modrof et al., 2002). Moreover, VP30 can interact with other nucleocapsid components such as L and NP through its C-terminal domain (Hartlieb et al., 2007; Schlereth et al., 2016). These interactions are critical for overcoming the RNA hairpin structure at the first gene start signal (Hume & Mühlberger, 2019).

VP30 can undergo phosphorylation at two serine clusters, namely amino acids 29-31 and 42-46 (Modrof et al., 2002). Its transcriptional activity is highly dependent on its phosphorylation state, where hypo or non-phosphorylated VP30 enhances transcription, whereas fully phosphorylated VP30 halts the process. This phenomenon occurs because phosphorylated VP30 is unable to interact with NP, VP35, and RNA (Biedenkopf et al., 2013). The inability to transcribe, in turn, enhances replication. This regulatory mechanism highlights the critical role of VP30 phosphorylation in balancing transcription and replication during viral infection (Deflubé et al., 2019). It is worth noting that NP has the ability to recruit the cellular phosphatase PP2A-B56, which dephosphorylates VP30 and activates transcription (Kruse et al., 2018). However, the phosphorylation state of VP30 is constantly changing, and maintaining an overall balance is crucial for a successful infection throughout the virus life cycle (Jain et al., 2021).

VP24

VP24 is a 251-amino-acid protein that plays a crucial role in the formation of the nucleocapsid, serving as an essential component of the structure (Hume & Mühlberger, 2019). Along with NP and VP35, VP24 participates in the assembly and packaging of nucleocapsids into virions (Banadyga et al., 2017). Moreover, VP24 is considered essential for the initiation of virus budding (Jain et al., 2021), making it a key player in the viral life cycle. VP24 is a multifunctional protein that can inhibit the host immune response through several mechanisms (Ilinykh et al., 2015). It has been shown to inhibit the interferon response by blocking the activation of NF-κB (nuclear factor kappa B) which is a major transcription factor in interferon-responsive genes (Guito et al., 2017). Additionally, VP24 can block the phosphorylation of p38,

thereby halting the p38 MAPK pathway (Halfmann et al., 2011). It also plays a role in inhibiting the nuclear translocation of tyrosine-phosphorylated STAT1 by binding to karyopherin-α (Mateo et al., 2010).

Interestingly, studies on adaptation in mice and guinea pigs have demonstrated that EBOV's ability to replicate in these animals is linked to mutations in VP24 (Bray et al., 1999; Mateo et al., 2011; Volchkov et al., 2000). This is because VP24 participates as a type I interferon antagonist, disrupting the interferon-mediated cellular antiviral response (E. Nakayama & Saijo, 2013). These findings highlight the crucial role of VP24 in EBOV pathogenesis, as mutations in its amino acids are sufficient to confer virulence in new host organisms (Mateo et al., 2011).

L

The L protein of EBOV is the largest, comprising 2212 amino acids, and is a multifunctional and multi-subunit protein (Ayub & Waheed, 2016). It plays a crucial role in virus replication and transcription as it contains the GDNQ motif of the catalytic subunit of RNA-dependent RNA polymerase (RdRp) and is part of the ribonucleoprotein complex (Schmidt & Hoenen, 2017). The high conservation and homology of the L protein amongst members of Mononegavirales is due to its essential function (Ogino & Green, 2019). Although L is associated with the nucleocapsid, the formation of the complex does not require L's presence, but the other nucleocapsid proteins are necessary for the functional polymerase complex to be achieved (Tchesnokov et al., 2018; Wang et al., 2011). L protein carries out several enzymatic activities essential for RNA synthesis and mRNA processing, including polyadenylation and capping activity of nascent mRNA (Liang, 2016; Volchkov et al., 1999). Lastly, L requires Mg^{+2} ions as catalytic cofactors for RNA synthesis (Hume & Mühlberger, 2019).

Replication of EBOV's genome

EBOV's genomic replication is driven by bipartite promoters composed of two promoter elements (PE), as shown in figure 20. The first PE is the 3' end sequence (Deflubé et al., 2019), which forms a hairpin loop consisting of 55 nucleotides and is illustrated in figure 21 (Crary et al., 2003). The second PE is located downstream in the 3' untranslated region of the NP gene. This promoter is composed of a stretch of eight nucleotide hexamers with every sixth nucleotides being a uridine residue, usually followed by two purine residues (NURRN2) (Hume & Mühlberger, 2019; Weik et al., 2005). The region between the two promoter elements is a short spacer sequence that consists of the gene start signal of the first gene (NP) and 12 subsequent nucleotides, which together form the second RNA hairpin loop. Interestingly, while the specific sequence of these 12 nucleotides is not important for replication, their length is critical. It must be divisible by six to allow for efficient replication, a phenomenon known as the "rule of six." (Enterlein et al., 2009; Weik et al., 2005).

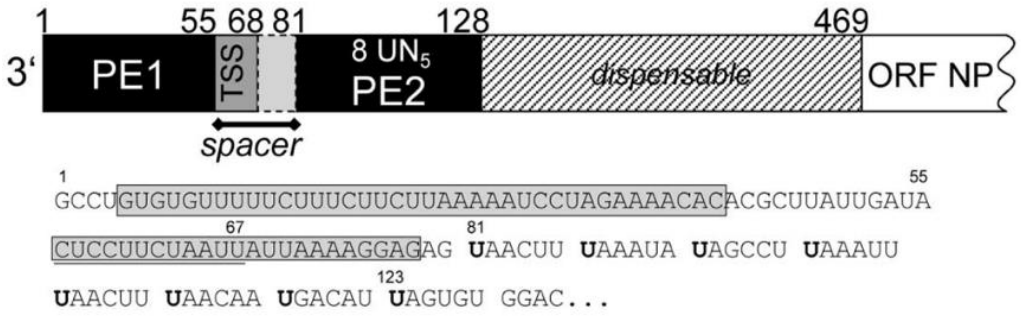

Figure 20 Promoter elements of EBOV's replication

From (Enterlein et al., 2009). Promoter elements (PE) are represented by black boxes, the transcription start signal (TSS, also known as Gene Start (GS)) of the NP gene is shown in grey, and additional sequences belonging to the spacer region are indicated in lighter grey. Unimportant regions are shown in hatching. The nucleotides that are involved in the formation of the hairpin loop structure are boxed in the sequence below the scheme. The spacer region includes the transcription start signal, as well as a downstream sequence of 12 nucleotides that are involved in the formation of the secondary structure. These said nucleotides can be extended or reduced by a multiple of 6 nucleotides. Finally, the second PE consists of eight hexamers with U residues (in bold) at positions 81, 87… until 123.

Despite the fact that the 3' leader sequence is not divisible by 6, as confirmed by its 55 nucleotides, a specific replication strategy enables the first PE to be accessible to the viral polymerase as a 54-nucleotide region (Deflubé et al., 2019). In fact, the polymerase ignores the first nucleotide, as it accurately initiates replication opposite the first C residue of a highly conserved motif (3' CCUGUG), which in the case of EBOV, is located at position number 2 of

the genome (Deflubé et al., 2019). On the other hand, it was initially thought that the hairpin structures within the leader sequence played a crucial role in facilitating efficient replication. However, experiments involving mutations that disrupted these structures revealed otherwise (Crary et al., 2003). In fact, it is now believed that while the secondary structures may contribute to replication efficiency, they are not an absolute requirement (Weik et al., 2005).

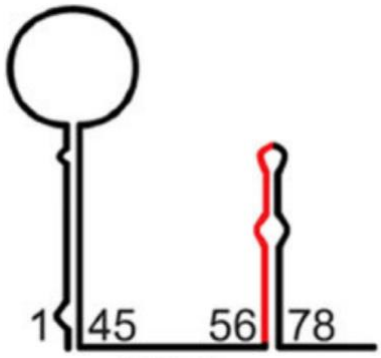

Figure 21 RNA secondary structure of the 3' end of the EBOV genome

Adapted from (Hume & Mühlberger, 2019). This predictive illustration of the negative sense RNA orientation was done by using the web serve (http://rna.tbi.univie.ac.at/cgi-bin/ RNAWebSuite/RNAfold.cgi). Numbers indicate the first and the last nucleotide of the stem-loop structures. Nucleotides 1 to 55 compose a non-transcribed region of nucleotides, followed by the GS of the NP gene (nucleotides 56 to 67, marked in red).

In addition, the formation of a panhandle structure between the 3' and 5' ends of the EBOV genome has been observed in *in vitro* transcribed negative sense minigenome experiments (Sztuba-solinska et al., 2016). Intriguingly, studies investigating mutations in the 5' trailer sequence that disrupted the panhandle structure resulted in a decrease in virus replication, highlighting the importance of nucleotides in this region for efficient viral replication (Sztuba-solinska et al., 2016). Moreover, since these mutated nucleotides are also part of the antigenomic replication promoter in the 5' trailer, which interacts with cellular host factors, it is possible that this interaction plays a role in promoting viral genome replication (Hume & Mühlberger, 2019).

Antigenomic replication promoters located at the 3' end of the antigenomes are also worth mentioning, as they are also complementary to the 5' end of the genomes. These promoters are not involved in transcription but are believed to be bipartite (Hume & Mühlberger, 2019) since they contain clusters of hexameric NURRN2 motifs downstream of the trailer sequence of the positive sense RNA (Weik et al., 2005). Interestingly, research on the replication promoters of other non-segmented negative sense (NNS) RNA viruses has shown that antigenomic

promoters are stronger than the genomic ones, resulting in a more efficient amplification of the genomic RNA during replication. This phenomenon could be due to two mechanisms: 1) differences in nucleotides within these promoter regions, and 2) competing replication and transcription activity at the genomic promoter (Mcgivern et al., 2005; Mercier et al., 2003).

Transcription of EBOV's genes

In terms of transcription, the promoter of EBOV is located within the 3' end leader, positioned upstream of the first GS signal. Due to the polymerase having only one point of entry at the 3' end of EBOV's genome, it is unable to initiate transcription elsewhere or resume transcription of a gene if it falls off the template (Trommer et al., 1996). Therefore, there is a transcription gradient, where genes closer to the transcription promoter are transcribed more frequently (Shabman et al., 2014). After accessing the NP-RNA template at the 3' end, the viral polymerase scans the genome sequence for the first gene start signal to initiate transcription of the first gene. It is worth noting that the first nucleotide of all filoviral GS signals is a cystidine residue, resulting in all filoviral mRNAs commencing with a guanosine. This characteristic plays a crucial role in mRNA capping (Das & Arnold, 2015).

Following transcription initiation and capping, the viral polymerase proceeds to elongate the mRNA by moving along the template until it encounters the first gene end signal. These signals are highly conserved across various filoviral genera and terminate with a series of 5 to 6 uridine residues. These residues cause the polymerase to stutter, leading to the addition of a poly(A) tail at the 3' end of the mRNA (Ball et al., 1981). Filovirus transcription follows the stop-start mechanism typical of non-segmented negative sense RNA viruses. When transcription concludes at the GE signal of the upstream gene, the polymerase begins scanning for the GS signal of the subsequent gene. Notably, the EBOV polymerase is capable of scanning for GS signals in both directions of the GE signal (Brauburger et al., 2016).

Additionally, as most filoviral GS and GE signals feature a conserved 3' UAAUU pentamer, three gene overlaps occur in the case of EBOV (VP35/VP40, GP/VP30, and VP24/L) (Brauburger et al., 2016). These overlaps occur because the downstream gene's GS signal and the upstream gene's GE signal share the pentamer, as illustrated in figure 22. It is worth noting that although gene overlapping signals are present in EBOV's genome, the other genes are divided by intergenic regions (IRs), of which three are short (5 or 4 nucleotides) and one is long

(144 nucleotides) (Hume & Mühlberger, 2019). Furthermore, gene overlapping signals are as effective in transcription initiation and termination as those separated by intergenic regions (Brauburger et al., 2016).

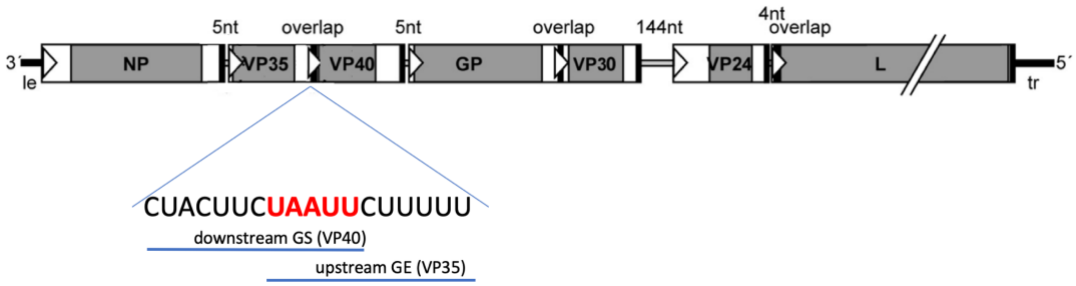

Figure 22 EBOV's transcription elements

Adapted from (Brauburger et al., 2016). EBOV genome showing the diverse gene borders. Grey boxes, ORFs (open reading frames); white boxes, UTRs (untranslated regions) flanking the ORFs; white triangles, GS signals; black bars, GE signals; le, leader; tr, trailer; grey lines, intergenic regions (with their respective lengths above). Below the genome, an example of an overlap is displayed between VP35 and VP40

Mutation experiments in these intergenic regions have revealed their involvement in transcription regulation, although not to the same extent as the untranslated regions (UTRs) of the viral genes (Neumann et al., 2009). EBOV's genes are flanked by UTRs, with upstream UTRs averaging 214 nucleotides and downstream UTRs averaging 298 nucleotides (Shabman et al., 2013). These UTRs have been suggested to play a role in mRNA stabilization and translation (Hume & Mühlberger, 2019). Finally, the sequential transcription of EBOV's genes is highly regulated. If the polymerase is unable to terminate transcription of a gene because the GE signal is destroyed, it cannot reinitiate transcription at the following gene, even if the GS signal of this gene is intact (Brauburger et al., 2016).

Infectious cycle

As described in figure 23, EBOV's infectious cycle is a complex multi-step process that encompasses virus attachment, internalisation, transcription of viral genes and translation, virus assembly and finally, its budding and egress. In this section, we will discuss each of these stages in detail.

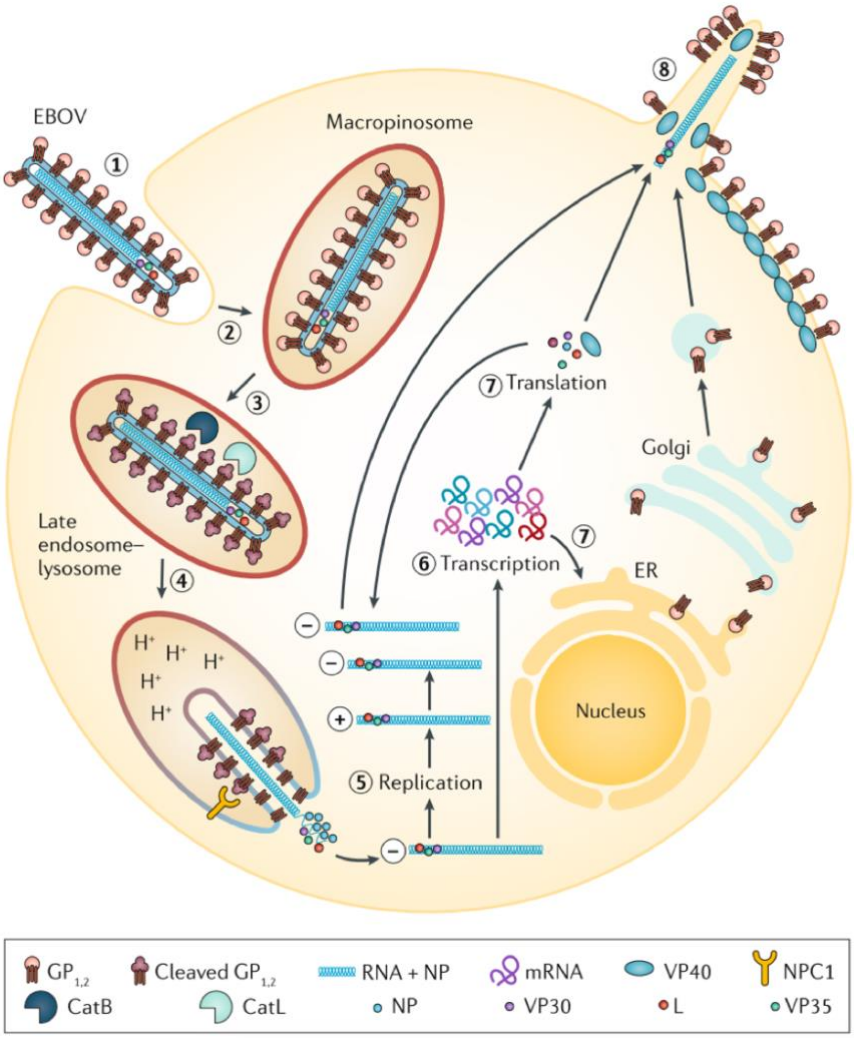

Figure 23 Infectious cycle of EBOV

Adapted from (Jacob et al., 2020). This process begins with (1) virus attachment on the surface of its target cell, which triggers (2) virus internalisation via macropinocytosis. Through a (3) series of proteolytic events performed by cellular cathepsins L (CatL) and B (CatB), EBOV $GP_{1,2}$ are cleaved. Such cleavage exposes GP_1 receptor binding domain, which then interacts with cellular receptor NPC1. It is by this interaction that EBOV particles (4) are able to trigger virus fusion with the endosomal membrane and this allows EBOV's ribonucleoprotein complex (RNA+N) to be released in the host cell cytoplasm. This is also where (5) replication of EBOV's genome, (6) transcription of viral genes and their (7) translation take place (except GP, whose transcription and translation happen in the endoplasmic reticulum). Moreover, GP experiences further cleavages in the Golgi apparatus, prior to being transported to the plasma membrane. Protein synthesis leads to an accumulation of viral proteins and viral genomes, which are assembled together and are then transported to the plasma membrane, where virus (8) budding and egress occurs.

The first step in EBOV's infectious cycle is attachment, which occurs when the virus comes into contact with its target cell (Hofmann-Winkler et al., 2015). This stage is mediated by the surface homotrimeric structural glycoprotein $GP_{1,2}$ (Chandran et al., 2005; Dahlmann et al., 2015; Furuyama et al., 2021), which enables non-specific interactions with numerous cellular attachment factors such as TAM, TIM-1, lectins, and glycosaminoglycans (Cui et al., 2021; Dahlmann et al., 2015; Jain et al., 2021; Kuroda et al., 2015; Reynard & Volchkov, 2015; Takada et al., 2004; Yu et al., 2017). However, the density and specificity of these factors result in significant differences in the kinetics of virus entry among different cell lines (Reynard & Volchkov, 2015). This situation may lead to a temporal switching of EBOV particles between the two states of attachment and detachment, resulting in a "scanning" mechanism to detect suitable target cells for infection (Reynard & Volchkov, 2015). In other words, EBOV particles may continue scanning the cell surface until they encounter a sufficient concentration of adhesion factors to enable attachment. In any case, EBOV's early replication occurs in antigen-presenting cells such as monocytes, macrophages, and dendritic cells (Fletcher et al., 2014; Geisbert & Young, 2003; Miao et al., 2016).

Following attachment, viruses are first internalised in macropinocytosis vesicles (Mulherkar et al., 2011; Saeed et al., 2010), a mechanism that has been termed apoptotic mimicry (Brunton et al., 2019), since TIM-dependant engulfment involves dead cell debris (Cui et al., 2021). The internalisation mechanism was initially debated to be clathrin- and caveolin-dependent (Moller-Tank & Maury, 2014; Sanchez, 2007), but subsequent research revealed that macropinocytosis and virus particle size were the primary factors determining EBOV entry (Aleksandrowicz et al., 2011). Once virus particles are routed to endosomal vesicles of the host cell, proteolytic events take place resulting in the cleavage of $GP_{1,2}$ (Dahlmann et al., 2015; Martin et al., 2016). Under acidic pH and reducing conditions, cellular cysteine proteases, particularly cathepsins B and L (catB and catL), cleave GP, removing the mucin-like domain and the glycan cap (Bale et al., 2011). These cleavages result in the exposure of the GP_1 receptor binding domain (RBD), which subsequently interacts with the cellular endosomal cholesterol transporter Niemann-Pick C1 (NPC1) (Kuroda et al., 2015; Miao et al., 2016; Miller et al., 2012). NPC1 is typically expressed in late endosomes or lysosomes (Miller et al., 2012; Rasmussen, 2016). Intriguingly, recent findings have suggested that not only does cholesterol in GP-containing membranes enhance fusion and facilitate EBOV cell entry (J. Lee et al., 2021), but the cellular attachment factor TIM-1 has also been implicated as a critical factor in successful interaction between NPC1 and EBOV's GP_1 RBD (Miller et al., 2012; Rasmussen, 2016). TIM-1 is not only

identified as a cellular attachment factor but also as an intracellular receptor that is proposed to play a vital role in virus fusion (Kuroda et al., 2015), leading to an increase in virus load and associated mortality (Brunton et al., 2019).

After the rearrangement in GP triggered by the binding of GP_1 RBD and NPC1, the hydrophobic fusion loop in GP_2 is exposed (J. Lee et al., 2021; Vande Burgt et al., 2015). This loop is responsible for membrane association and facilitates the fusion process (Rivera & Messaoudi, 2016; Yu et al., 2017). Calcium channel 2 (TPC2) has been identified as an important element for the fusion stage, as it regulates the pH within the endosomal vesicle, facilitating the fusion of viral and endosomal membranes (Rasmussen, 2016). Finally, the ribonucleoprotein complex, coupled with the RNA-dependent RNA L polymerase (RdRp), is released into the cytoplasm, where the virus can begin replication (Yu et al., 2017). Once this process happens, EBOV transcription begins (Rasmussen, 2016). However, since EBOV's genome is non-segmented and negative-sense RNA, the L polymerase in conjunction with the ribonucleoprotein complex (consisting of NP, VP30, and VP35) synthesises complementary positive-sense monocistronic and polyadenylated transcripts (Rasmussen, 2016; Yu et al., 2017). These transcripts are then translated into the seven structural and one non-structural EBOV protein (Jacob et al., 2020). It is worth noting that EBOV's transcriptional gradient phenomenon is an essential characteristic of the virus' replication cycle (Brauburger et al., 2016). This phenomenon results in a higher frequency of transcription for genes located proximal to the 3' promoter region (Whelan et al., 2004). As a consequence, the nucleoprotein (NP) gene is the most frequently transcribed, whereas the L gene is the least frequently transcribed (Feldmann et al., 1993).

EBOV encodes for several proteins, such as VP40, a matrix protein (Feldmann et al., 1993) that is also involved in virus budding (Noda et al., 2002; Rivera & Messaoudi, 2016). VP24 is a secondary matrix protein and also contributes to the formation of the nucleocapsid (Jain et al., 2021). NP is part of the nucleocapsid complex and it also catalyses replication and transcription of the RNA genome (Rivera & Messaoudi, 2016). VP35 serves as a polymerase cofactor and forms with L the active polymerase complex (Mühlberger et al., 1999). Lastly VP30 is a transcriptional activator (Rivera & Messaoudi, 2016), and it becomes eventually a genome replicase (Rasmussen, 2016).

In the process of infection, host factors play a crucial role in allowing EBOV to achieve a productive infection (Patrick Reid et al., 2014). For instance, DNA topoisomerase I (TOP1) directly interacts with L and is necessary for its viral polymerase activity, which is required for both transcription and replication (Takahashi et al., 2013). Similarly, the 8-kDa dynein light chain (LC8) and the double-stranded RNA-binding protein 76 (DRBP76) have also been shown to play important roles in EBOV transcriptional activity. LC8 inhibits polymerase activity (Shabman et al., 2011), while DRBP76 enhances it (Kubota et al., 2009).

Although all the proteins mentioned before are synthesised in the cytoplasm, GP is the only one that is synthesised in the endoplasmic reticulum (Jacob et al., 2020). Initially, GP is produced as the precursor $GP_{1,2}$ and requires further modifications in the Golgi apparatus, such as cleavage by the host enzyme furin, to become the mature $GP_{1,2}$ (Martin et al., 2016). These cleavages also yield other viral proteins, including Δ-peptide and ssGP (Volchkova et al., 2011). After these cleavages occur, GP products are transported via the classical secretory pathway to the plasma membrane (Yu et al., 2017). Interestingly, the endoplasmic reticulum chaperone, heat shock 70 kDa protein 5 (HSPA5), has been associated with an increase in the number of infected cells (Patrick Reid et al., 2014).

As viral proteins, particularly NP, continue to accumulate (Rasmussen, 2016; Rivera & Messaoudi, 2016), the transcription process eventually halts due to the release of VP35 from the active polymerase complex, triggering a switch to virus replication Yu et al., 2017). This switch is facilitated by the dephosphorylation of VP30 by host cell protein phosphatase 1 (PP1) (Martínez et al., 2008). Once viral proteins and genomes are synthesised, they form inclusion bodies in the cytoplasm (Yu et al., 2017), facilitating virus assembly by bringing together nucleocapsid proteins and EBOV's genetic material (Hoenen et al., 2012). These nucleocapsids are then transported along the actin cytoskeleton to the plasma membrane (Schudt et al., 2015), where particle budding occurs together with GP (Rivera & Messaoudi, 2016). The process is regulated by the presence of lipid rafts within the plasma membrane (Soni et al., 2013), where VP40 interacts with the endosomal sorting complex required for transport (ESCRT) machinery, enabling membrane fission and virus egress (Rasmussen, 2016).

Pathogenesis

The rapid and extensive replication of EBOV throughout various cell types in the body can lead to immune suppression, exacerbating the infection (Mohamadzadeh, 2009). This is further compounded by the dysregulation of certain immune responses, which is often observed in highly viraemic patients (Jacob et al., 2020). In this context, the Ebola virus disease (EVD) often leads to coagulation disorders and tissue damage (Vega et al., 2015), which can progress to multiple organ failure and death within 10 days of symptom onset without appropriate supportive care (Baseler et al., 2017). However, individuals with lower viraemia may experience a less severe course of the disease, allowing for the development of a robust immune response that can clear the virus and lead to resolution (Jacob et al., 2020).

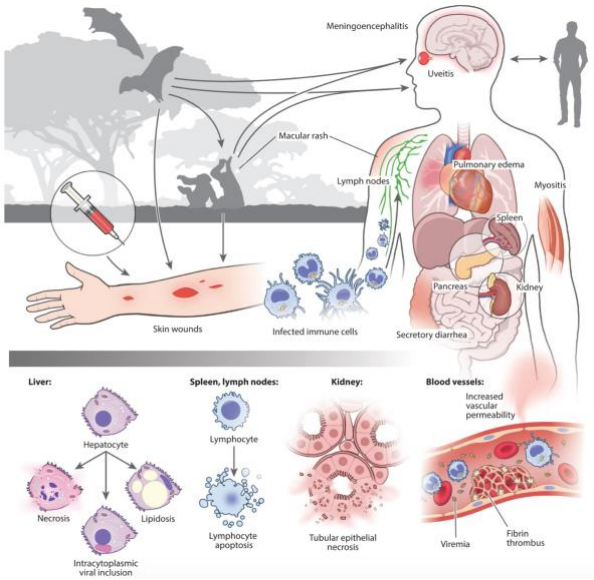

Figure 24 Transmission and pathogenesis of the ebolavirus infection

From (Baseler et al., 2017). Zoonotic, nosocomial, or person-to-person transmission of EBPOV leads to viral infection of mononuclear phagocytes, which transport the virus to regional lymph nodes. Virus replication is followed by viremia with widespread viral dissemination, leading to tissue and vascular damage.

While most human cells are susceptible to infection by EBOV (Baseler et al., 2017) following mucous membrane or skin contact (Jacob et al., 2020), EBOV primarily targets dendritic cells and other cells of the monocyte/macrophage lineage (Geisbert et al., 2003) (figure 24). These initial infections facilitate further virus dissemination (Abbet et al., 1998) as the infected cells migrate to regional lymph nodes, where virus replication occurs prior to the onset of symptoms (Jacob et al., 2020). Eventually, the infectious process involves multiple organs, particularly

the liver and spleen (Rasmussen, 2016). Binding of EBOV's $GP_{1,2}$ to macrophages activates these cells, resulting in the secretion of pro-inflammatory cytokines, chemokines, and growth factors such as interleukin 1β (IL-1β), IL-6, IL-8, IL-10 monocyte chemoattractant protein 1 (MCP-1), MCP1-1α and tumour necrosis factor α (TNFα), as well as nitric oxide (NO) and reactive oxygen species (Baize et al., 2002; Edwards et al., 1999; Rivera & Messaoudi, 2015). These signalling molecules can induce apoptosis (Simon, 2000), and may play an important role in the exacerbation of the infection by recruiting more susceptible macrophages to the site of infection (Baseler et al., 2017).

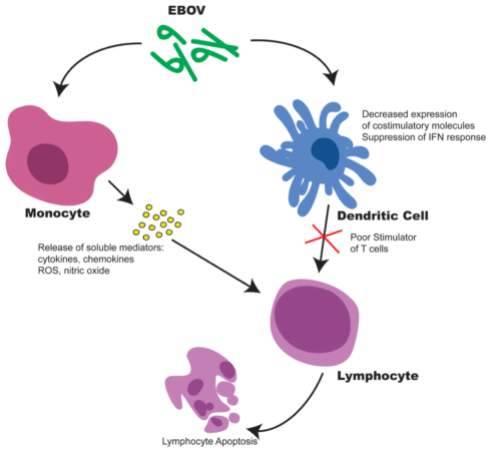

Figure 25 Dysregulation of the immune system by the Ebola virus

Modified from (Rivera & Messaoudi, 2015). Monocytes, macrophages, and dendritic cells are the preferred sites of filovirus replication. Infection of monocytes and macrophages triggers the robust expression of inflammatory mediators. Inflammatory mediators, reactive oxygen species, and nitric oxide can induce apoptosis leading to lymphocyte death. The infection of dendritic cells impairs their maturation and suppresses type I (IFN) responses, thereby preventing T cell activation.

Ebola virus (EBOV) efficiently replicates in dendritic cells (DCs), inhibiting their maturation and suppressing the type I interferon response. This, in turn, prevents T cell activation (Jin et al., 2010; Mahanty et al., 2003) (figure 25). Although lymphocytes appear to be a rare cell type that escapes EBOV infection (Martines et al., 2015), lymphopenia is a characteristic feature of EBOV infection, and it contributes to the susceptibility of patients with EVD to acquiring secondary infections and experiencing more severe forms of the disease (Bray et al., 1999; Iampietro et al., 2017; Rodriguez et al., 1995). The extensive apoptosis of lymphocytes is likely due to a combination of abortive infections, an uncontrolled cytokine response, and the expression of TNF-related apoptosis-inducing ligand (TRAIL) (Baseler et al., 2017).

Mechanisms of tissue damage

Tissue damage in EBOV infection can result from either virus-related (direct) mechanisms or host-related (indirect) mechanisms (Baseler et al., 2017). EBOV GP can cause cytopathic effects, such as cell rounding and detachment (Takada et al., 2000), and has been found to colocalise in necrotic tissue, suggesting a direct role in tissue damage (Zaki et al., 1999). On the other hand, the dysregulated inflammatory response is one of the main indirect host-related mechanisms that contribute to tissue damage and organ injury during EVD (Baseler et al., 2017). This occurs due to the excessive release of proinflammatory cytokines and chemokines, including TNFα, IL-1, IL-6, MCP-1, macrophage inflammatory protein 1α (MIP-1α) and MIP-1β (Hensley et al., 2002; Sanchez et al., 2004). This, in turn, triggers the recruitment of leukocytes to infected tissue, where they destroy virus-infected host cells, further worsening the tissue damage (Edwards et al., 1999).

One of the classic signs of EVD is the presence of conjunctival haemorrhages, bleeding from venepuncture sites, and gastrointestinal bleeding (A. McElroy, 2015). Vascular permeability is a plausible reason for these symptoms, as EBOV can infect endothelial cells and cause swelling, necrosis, and eventual loss (Martines et al., 2015). In addition, EBOV's GP has high cytotoxicity that can compromise intercellular tight junctions, leading to increased vascular permeability (Yang et al., 2000). The release of nitric oxide and TNFα also induces vasodilation and further increases vascular permeability, contributing to the depletion of intravascular volume (Feldmann et al., 1996). Another prominent manifestation of EVD is disseminated intravascular coagulation (DIC), a syndrome characterised by the activation of the coagulation system, either in a localised region or throughout the entire vascular system (Geisbert et al., 2003). This disorder leads to the generation of microthrombi in the microvasculature (Levi, 2001), which impede adequate blood supply, contribute to tissue ischemia and necrosis, and ultimately exacerbate organ dysfunction (Geisbert et al., 2003). Similarly, there is a predisposition to bleeding within tissues and from mucosal surfaces due to consumption of clotting factors (Taylor et al., 2001). Several processes could explain the development of DIC in EVD, including increased tissue factor expression on monocytes/macrophages, which triggers the extrinsic coagulation pathway and leads to the formation of fibrin thrombus (Nemerson, 1988). In addition, TNFα may decrease thrombomodulin levels (Conway & Rosenberg, 1988), while

liver injury may impair the production of proteins C and S (Mammen, 1994), resulting in decreased intravascular anticoagulant effects (Baseler et al., 2017).

Pathology

As previously mentioned, EBOV targets macrophages and dendritic cells, which upon infection, migrate to lymph nodes while producing new virions. Using its immune evasion mechanisms, EBOV can spread systemically and infect secondary target cells in almost all organs (Jacob et al., 2020), often resulting in multiple organ dysfunction (figure 26).

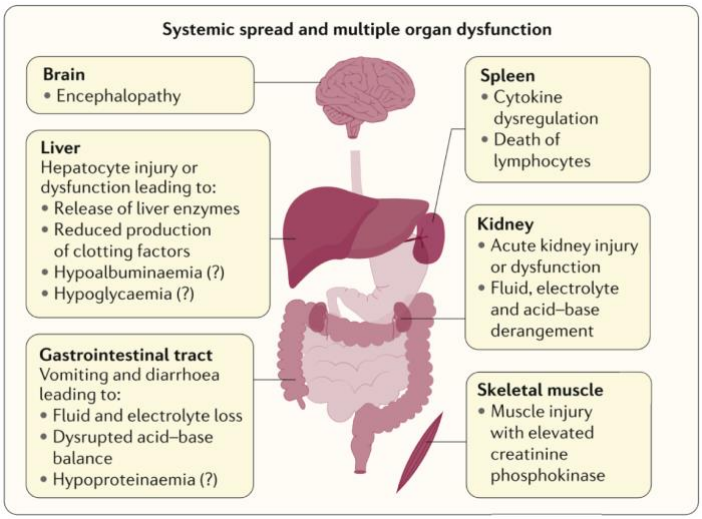

Figure 26 Systemic spread and multiple organ dysfunction

Adapted from (Jacob et al., 2020). Primary targets of infection are macrophages and dendritic cells. Infected macrophages and dendritic cells migrate to regional lymph nodes while producing progeny virions. Through suppression of intrinsic, innate and adaptive immune responses, systemic distribution of progeny virions and infection of secondary target cells occur in almost all organs.

Autopsies have revealed microscopic lesions in the spleen and lymph nodes of EBOV-infected individuals, which result from lymphocyte apoptosis and accumulation of cellular debris. These lesions contain viral antigens that have been identified in dendritic cells, fibroblasts, and macrophages (Zaki et al., 1999). Kidney damage in EBOV-infected individuals is evidenced by a low output of urine (oliguria) or even the absence of urine (anuria), as well as abnormalities in sodium and potassium electrolyte levels (Jacob et al., 2020). Pathological studies of EVD patients have revealed the presence of gastrointestinal tract haemorrhages, but only mild inflammation in the lamina propria has been reported (Martines et al., 2015). Hepatocellular damage is also a common feature of EVD (Shorten et al., 2016), and deranged liver enzymes have been documented in both animal models and human cases (Rollin et al., 2007). Although

autopsies of EVD patients have not revealed any skeletal muscle lesions, individuals with EVD often experience myalgia and exhibit elevated levels of creatine phosphokinase, indicating rhabdomyolysis, which is the breakdown of muscle tissue and subsequent release of myofibre contents into the bloodstream (Cournac et al., 2016). Lastly, dysfunction of the central nervous system is a common feature of EVD (Daniel S, 2014), with meningoencephalitis being a life-threatening complication that can appear both late in the disease and shortly after recovery (Howlett et al., 2016). Studies in non-human primates have confirmed the presence of viral antigen in glial nodules, indicating that microglial cells may serve as viral reservoirs (Larsen et al., 2007).

Immune evasion

EBOV's high pathogenicity is attributed, in part, to its efficient replication within the host, achieved through the inhibition of both innate and adaptive immune responses (Bray et al., 2001). One crucial component of innate immunity against viral infections is the interferon response. As illustrated in figure 27, interferon can be released during an RNA virus infection, such as EBOV, through the activation of membrane-bound receptors (TLR) or cytoplasmic receptors, such as the retinoic acid-inducible gene I (RIG-I) and the melanoma differentiation-associated protein 5 (MDA5). Upon activation, a series of signalling cascade events occur, ultimately resulting in the phosphorylation of IRFs 3 and 7. These phosphorylated proteins then translocate to the nucleus, where they activate interferon transcription (Khiar et al., 2015).

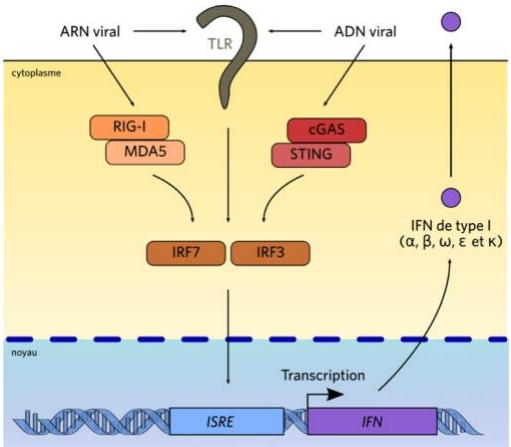

Figure 27 Production of interferon type I

From https://planet-vie.ens.fr/thematiques/animaux/systeme-immunitaire/les-interferons-de-type-i-et-iii-des-effecteurs-de-l. Both viral RNA and DNA are pathogen-associated molecular patterns that can activate several types of pattern recognition receptors, including toll-like receptors (TLRs) and other cytosolic proteins, such as

RIG-I-like receptors (RLRs), cyclic GMP-AMP synthase (cGAS), Stimulator of Interferon Genes (STING), and melanoma differentiation-associated protein 5 (MDA5). These proteins are responsible for activating IRF7 or IRF3, which, in turn, induce the production of interferons that are released into the extracellular compartment.

As depicted in figure 28, interferons released into the extracellular medium may have either an autocrine or paracrine effect by binding to the monomer interferon alpha and beta receptor subunit 1 (IFNAR1), triggering the dimerisation of IFNAR1 and activating two kinases, JAK1 and TYK2. These kinases phosphorylate cytosolic STAT proteins, allowing them to dimerise and associate with the accessory protein IRF9. The resulting complex is then transported to the nucleus via karyopherins, where it binds to the promoter region of interferon-stimulated response element (ISRE), activating the transcription of several genes collectively known as interferon-stimulated genes (ISGs) (Khiar et al., 2015).

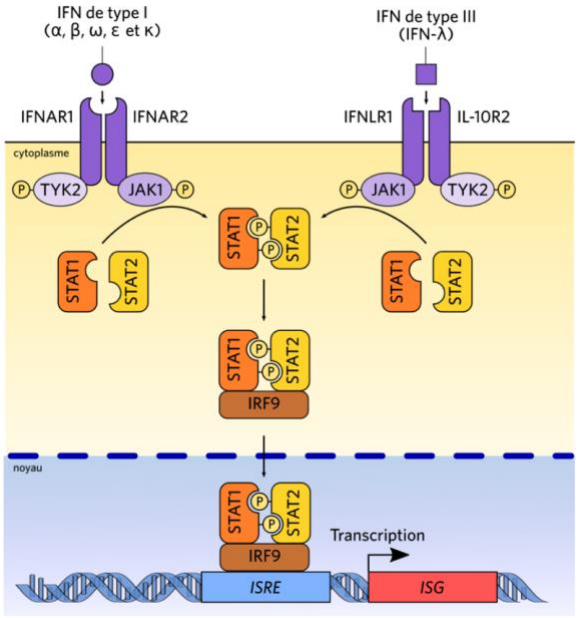

Figure 28 Transduction pathway of JAK/STAT

From https://planet-vie.ens.fr/thematiques/animaux/systeme-immunitaire/les-interferons-de-type-i-et-iii-des-effecteurs-de-l . The binding of an IFN triggers the activation of the receptor's JAKs, which phosphorylate the receptor and self-phosphorylate. Once activated, they phosphorylate STAT proteins, which dimerise and associate with the accessory protein IRF9 (thus forming the ISGF3 complex). They relocate to the nucleus, where they induce the expression of ISGs (interferon-stimulated genes).

VP24 functions as a type I interferon antagonist, disrupting the interferon-mediated cellular antiviral response (E. Nakayama & Saijo, 2013). Figure 29 shows that VP24 binds to the nuclear importer protein karyopherin α1 (KPN-α1) and prevents it from binding to phosphorylated STAT1, thereby limiting the accumulation of nuclear STAT1 and inhibiting IFN-induced gene expression (Ilinykh et al., 2015). VP35 also suppresses the production of type I interferon (Prins et al., 2009) and micro-RNA silencing (Kimberlina et al., 2010). In

addition, EBOV's $GP_{1,2}$ interferes with the function of tetherin (Audet & Kobinger, 2015). Despite the immunosuppressive effects of EBOV, cellular and humoral immune responses are generated (Mandl & Feinberg, 2015; A. K. McElroy et al., 2015). However, in the host-pathogen EVD 'arms race', the virus often gains the upper hand, resulting in severe disease (Jacob et al., 2020).

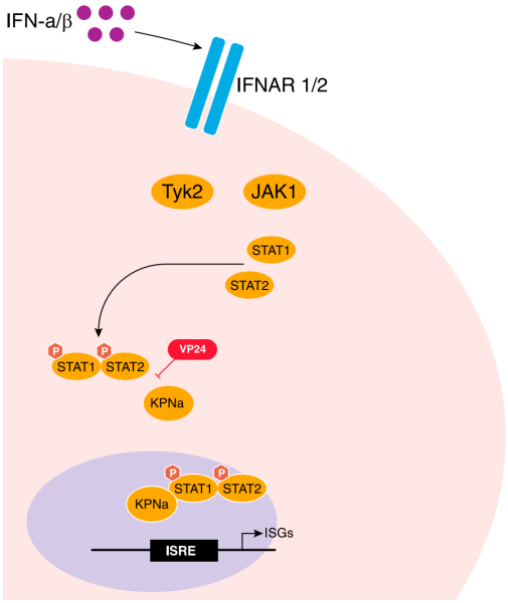

Figure 29 EBOV evades type I IFN response

Adapted from (Rivera & Messaoudi, 2016). EBOV VP24 can prevent cellular responses to IFN-α/β by binding to the nuclear importer protein karyopherin α1 (KPNα1), preventing it from binding to phosphorylated STAT1, thus limiting the accumulation of nuclear STAT1 and preventing IFN-induced gene expression. ISRE, IFN-stimulated response element.

Scientific Objectives

The GP surface glycoprotein EBOV triggers and ensures viral entry into the host cell through a complex mechanism that is only partially understood to date (Martin et al., 2016). EBOV attachment to the target cell is accomplished through interactions of the GP_1 subunit with a variety of cell surface molecules, such as TAM, TIM1, C-type lectins, and glycosaminoglycans, that have been identified (Jain et al., 2021; Takada et al., 2004). Once attached, EBOV particles are internalised by macropinocytosis (Saeed et al., 2010) and then routed by classical endosomal uptake, including fusion of initial endosomal vesicles to cellular lysosomes (Martin et al., 2016). Cellular proteases, including cathepsins B and L, digest and remove a significant portion of GP_1 in early lysosomes under acidic pH and reducing conditions (Bale et al., 2011), which leads to exposure of the GP_1 receptor binding domain and ensures its interaction with the cellular endosomal EBOV receptor, Niemann-Pick cholesterol transporter C1 (NPC1) (Kuroda et al., 2015). This interaction promotes a conformational rearrangement in the GP_2 subunit, which leads to the unfolding of the fusion peptide and fusion of the viral and endosomal membranes, resulting in the release of the viral replication complex into the cytoplasm.

In recent years, our team has been interested in shedding light on the process of EBOV entry into host cells, hoping to identify new viral or host factors that could be used to prevent EBOV infection. Analysis of drugs suspected of preventing EBOV attachment led to the identification of poly(sodium 4-styrene sulfonate) (PSS), an anionic compound that effectively inhibited EBOV cell infection at 100 μg/mL. PSS was tested for its activity against sexually transmitted diseases of viral origin, such as HIV and herpes simplex viruses (Zaneveld et al., 2002). Although its mechanism of action is not well understood, it is known that polysulphated polymers can interfere with microbial infectivity, possibly by mimicking cellular receptors such as heparan sulphate, preventing thus cell surface binding and cell entry (Herold et al., 1997).

Taking advantage of a recombinant vesicular stomatitis virus (VSVEB-WT) carrying the EBOV GP gene, a number of experiments were performed under BSL2 conditions instead of using genuine EBOV requiring BSL4 facilities. In an attempt to see if viruses with partial or complete resistance to the drug could be easily selected, experiments were also performed in which VSVEB-WT was passaged in the presence of PSS, as seen in figure 30. The genomic RNA of the obtained virus samples was subjected to sequence analysis, which revealed a

number of mutations leading to amino acid substitutions, including those in the GP EBOV gene ($E_{304}A$ and $E_{304}V$). Since the $E_{304}A$ GP mutation appeared in 94.4% as opposed to the $E_{304}V$ (5.6%), a recombinant VSVEB-$E_{304}A$ carrying a unique mutation in EBOV GP was engineered and rescued using reverse genetics for VSV. Importantly, this virus showed partial resistance to PSS and demonstrated aberrant electrophoretic mobility of the EBOV GP_1 subunit on SDS polyacrylamide gels.

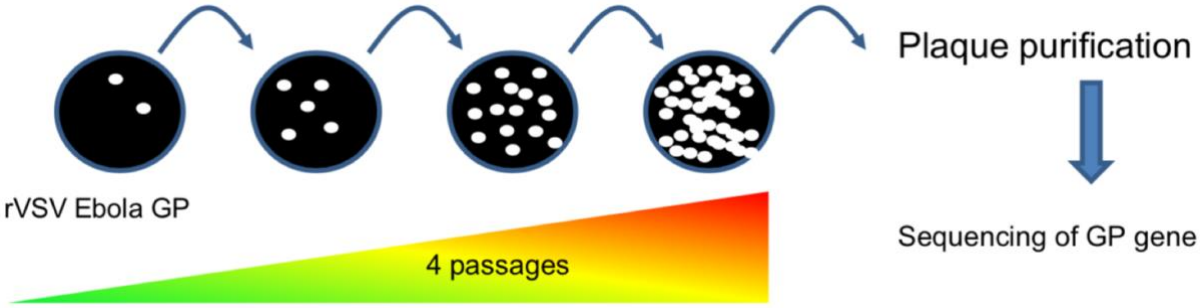

Figure 30 Generation of escape mutant in a recombinant VSV GP model

Recombinant VSV GP was cultivated during four passages (from 0.5 to 5 μg/mL) of 72 hours each with increasing concentrations of PSS. Viruses from the fourth passage were isolated via plaque purification. The GP open reading frame was amplified by RT PCR and sequenced, evidencing a $E_{304}A$ GP mutation in 17 out of 18 clones, while the $E_{304}V$ GP mutation was found in only one clone.

Therefore, the initial goal of this PhD project was to elucidate the molecular basis for the selection of a virus carrying the $E_{304}A$ mutation and possessing partial resistance to the viral attachment inhibitor PSS. The $E_{304}A$ substitution leads to a significant decrease in the molecular weight of the GP_1 EBOV subunit and, thus, may lead to important changes in the conformation of the protein as a whole. This can probably also lead to changes in the interaction of the virus with the cells, at least at some stages. Given the magnitude of the changes, we hypothesised that the difference between the viruses could be seen even without the use of PSS.

We will compare viruses expressing WT GP against the mutant GP by performing experiments on virus growth kinetics, as well as assessing virus spreading by analysing the size of viral plaques. All experiments will be performed in the absence of PSS as well as with different concentrations of PSS. All stages of virus entry into the cell, where surface GP is implicated, including virus attachment, internalisation, proteolytic digestion, and fusion, will be thoroughly studied. To address the benefits of virus growth, we are going to determine the infectivity of viruses by considering infectivity as the ratio of the number of viral particles to infectious viral titres.

To understand the origin of the western blot profile of the virus carrying the $E_{304}A$ GP mutation, we are going to elucidate the molecular mechanisms underlying this phenomenon. We hypothesise that such an abrupt decrease in molecular mass may be caused by a previously undetected cleavage event. Therefore, we will attempt to identify the protease(s) involved in GP cleavage as well as examine the role of the $E_{304}A$ mutation in protease activation. After confirming the cleavage of EBOV GP, we plan to create a set of plasmids expressing EBOV GP that would contain mutations in the cleavage site and its vicinity. These plasmids will be used to evaluate the effectiveness of GP cleavage in transient transfection experiments. It is also expected that recombinant VSVs carrying GP mutations in the putative cleavage site will be created and rescued using reverse genetics. These viruses are expected to be useful to evaluate and compare the growth, spread, and infectivity characteristics of the viruses as well as the cleavage profile of their GPs.

Finally, we will also attempt to generate and rescue a recombinant EBOV carrying the same $E_{304}A$ mutation in GP using reverse genetics for EBOV. Studying this virus and comparing it with WT EBOV will complement our previous studies using surrogate VSVs. We assume that not all VSV-based results can be easily reconstructed in an authentic system because of the significant differences between these viruses. Nevertheless, we intend to compare WT and mutated EBOV viruses using most of the experimental setups developed for VSV recombinant virus analysis, including GP cleavage profile analysis, virus growth, and differences in infectivity.

Our results are expected to propose a model that explains the molecular basis for the selection of a virus carrying the $E_{304}A$ mutation, as well as whether such an EBOV mutant can emerge and the role of cryptic furin-like cleavage in EBOV replication.

Materials and Methods

Eukaryotic cells

Vero E6 (African Green Monkey Kidney Epithelial cells), HEK 293T (Human Embryonic Kidney cells) and Raw264.7 (macrophage-like mouse cell line) cells were grown in cell culture dishes or flasks, in a humidified incubator (Thermo Fisher Scientific) at 5% CO_2 and 37 °C in DMEM (Thermo Fisher Scientific, Gibco, ref 61965-206), supplemented with 10% FCS (Eurobio ref CVFSVF00-01) with 50 U/mL of Penicillin and 50 µg/mL of Streptomycin (Thermo Fisher Scientific, Gibco, ref 15140-122). BHK T7 (Hamster kidney-derived cell line stably expressing T7 polymerase, kindly provided by K. Conzelmann, Pettenkoffer Institute, Munich, Germany) cells were grown in GMEM (Thermo Fisher Scientific, Gibco, ref 21710-025) supplemented with 10% tryptose phosphate broth (Sigma Life Sciences, ref SLCF6558), 10% FCS and 500µg/mL of G418 Geneticin (Thermo Fisher Scientific, Gibco, ref 11811-031), and adjusted to a final concentration of 2X of MEM non-essential amino acids (Thermo Fisher Scientific, Gibco, ref 11140-035). Cells were passed twice a week. Cells of confluent flasks were detached using either a cell scraper (for Raw264.7), or a 3-minute treatment with trypsin-EDTA 0.25% (Thermo Fisher Scientific, Gibco, ref 25200-056) for the other cells. Cell resuspension was centrifuged at 1000 rpm for 4 minutes. Cell pellet was resuspended in fresh medium and seeded at a 1:10 dilution.

Prokaryotic cells

Competent *Escherichia Coli* (strain XL-Gold (Stratagene cat. no. 200314)) were cultured in 2YT medium (Sigma ref Y2377-250G). For the creation of laboratory stocks, competent bacteria were cultured in 5 mL of 2YT medium during 12 hours at 37°C in agitation (Eppendorf cat. no. S2116-3051). To upscale the growth of bacteria, 100 µL of the previous 5-mL 2YT medium was used to inoculate 60 mL of fresh 2YT. When the growth of bacteria reached an optical density of 0.6 at 600 nm (Eppendorf, Biophotometer model 6131), the 60 mL were centrifuged 15 minutes at 3,000 rpm at 4°C. The pellet of bacteria was resuspended in 4 mL of TSS medium and incubated for 10 minutes on ice. For storing at -80°C, glycerol (EuroMedex ref EU3550), was added to obtain a final concentration of 20%.

TSS medium preparation: 5% DMSO (Sigma Life Science, cat. no. D2650-100ML), 10% PEG8000 (Sigma Aldrich ref P7181-5X5ML), 50mM $MgCl_2$ (USB cat. no. 18641) in LB medium (GibcoBRL cat. no. 12945-036).

Plasmids

For the generation of the two mutants of the GP gene ($RK_{299}AA$ and $R_{302}A+E_{304}A$), we used a plasmid phCMV expressing GP (Alazard-dany et al., 2006). For conducting VSV rescue experiments, we used a plasmid expressing an antigenomic copy of the VSV genome with EBOV GP instead of VSV G (Schnell et al., 1996). This plasmid (pVSV-FL) contains four VSV genes (N, P, M, and L) and EBOV GP (WT, $RK_{299}AA$, $E_{304}A$ or $R_{302}A+E_{304}A$), flanked by the bacteriophage T7 promoter, the VSV leader and trailer regions, the hepatitis delta virus ribozyme and the T7 terminator sequence. We also used helper plasmids for conducting VSV rescue, namely, pBlueScript containing the VSV genes N, P and L which are flanked by a T7 phage RNA polymerase promoter. For conducting EBOV rescue experiments, the plasmid pFL-EBOV containing EBOV's genome (including either WT GP or with the $E_{304}A$ mutation) was used, as a well as an additional pCAGGS-T7 (Novo Pro, ref. V008802) to enhance the efficiency of the rescue events. The transcription of the genomic RNA is terminated at the sequence encoding the T7 transcription termination site and its correct 3'-terminus is formed after auto cleavage by the Hepatitis Delta Virus ribozyme. Likewise, four plasmids encoding NP, VP35, VP30 and L, as well as a cDNA copy of the full-length genome were used for EBOV rescue (Volchkov et al., 2001).

Viruses

BSL2 recombinant viruses (VSVEB-WT, VSVEB-$E_{304}A$, VSVEB-$R_{302}A+E_{304}A$ and VSVEB-$RK_{299}AA$) were produced via reverse genetics, as described by (Garbutt et al., 2004). Amino acid substitution at $E_{304}A$ in EBOV GP was introduced and confirmed by sequencing this gene. BSL4 recombinant viruses (EBOV-WT, EBOV $E_{304}A$ and EBOV-HA) were produced via reverse genetics. Recombinant Zaire Ebolavirus strain Mayinga referred here as EBOV-WT was generated as described by (Volchkov et al., 2001). The amino acid substitution at $E_{304}A$ was introduced in EBOV glycoprotein of EBOV $E_{304}A$, whereas EBOV-HA had the following amino acid substitutions: GP ($S_{65}P$), VP24 ($I_{50}T$) and L ($N_{328}D$). The work with infectious

EBOV belonging to the Filoviridae family, ebolavirus genus, species EBOV was performed at INSERM's Laboratory Jean Mérieux, within biosafety level 4 containment in Lyon, France.

Production of virus stocks

For the case of **VSVEB**, subconfluent Vero E6 cells were infected at a low MOI (0.01). After the 1-hour incubation at 5% CO_2 and 37°C, virus inoculum was removed and replaced by DMEM supplemented with 2.5% FCS. Culture supernatant was harvested 44 hours post infection, clarified (3,000 rpm for 4 minutes) and aliquoted in 2ml cryogenic tubes (Sarstedt ref 72.379). These tubes were stored at -80°C prior to conducting any further experimentation.

For the case of **EBOV**, 50% confluent Vero E6 cells were infected with culture supernatant samples (diluted 1:5) from a passage zero of a successful rescue event, since we wanted to avoid an 8U GP editing site genotype from later passages. After the 1-hour incubation at 5% CO_2 and 37°C, virus inoculum was removed and replaced by DMEM supplemented with 2.5% FCS. Culture supernatant was harvested 7 days post infection, clarified (3,000 rpm for 4 minutes) and aliquoted in 2ml cryogenic tubes. These tubes were stored at -80°C prior to conducting any further experimentation.

Virus growth kinetics

Vero E6, BHK T7, HEK 293T or Raw264.7 cells were infected as described in the **production of virus stocks,** except for an MOI of either 0.001 for VSV or 0.004 for EBOV. After the 1-hour infection, virus inoculum was removed and replaced by DMEM supplemented with 2.5% FCS. Cells were kept at 5% CO_2 and 37°C for the duration of the experiment. Culture supernatants and/or cell lysate samples were collected at the indicated time points. For the case of culture supernatants, samples were collected, clarified (3,000 rpm for 4 minutes) and aliquoted in 2 mL cryogenic tubes, which were stored at -80°C prior to conducting further analysis. For the case of cell lysates, 1ml of DMEM without FCS was used for rinsing one well of a 6-well plate, and then 350 µL of RLT lysis buffer (Qiagen GmbH, Mat no. 1015762) were added per well to conduct viral RNA extraction, as detailed in the protocol of the Qiagen. The virus growth kinetics with PSS were performed as previously described, except for the use of

media supplemented with Poly(4-styrenesulphonic acid (PSS) (Aldrich ref 561223-100G) at the final concentrations of either 2, 4 or 6 μg/mL.

Virus plaque assays

For the case of **VSVEB**, subconfluent Vero E6 cells (in either 6-well plates or 100mm Petri dishes) were infected with virus serial dilutions. During the 1-hour infection at 5% CO_2 and 37°C, plates were rocked gently every 15 minutes. Virus inoculum was removed, cells were rinsed twice with DMEM, and they were overlaid with DMEM supplemented with 2.5% FCS, and an immobilising agent, either Avicel 0.8% (FMC BioPolymer ref RC.581F) or CMC 1% (Sigma Life Sciences ref C5013-500G). Plates were stored at 5% CO_2 and 37°C for 2 days.

For the case of **EBOV**, 50% confluent Vero E6, BHK T7 or HEK 293T (in either 6-well plates or 100mm Petri dishes) were infected with virus serial dilutions. During the 1-hour infection at 5% CO_2 and 37°C, plates were rocked gently every 15 minutes. Virus inoculum was removed, cells were rinsed twice with DMEM, and they were overlaid with DMEM supplemented with 2.5% FCS and Avicel 0.8%. Plates were stored at 5% CO_2 and 37°C for 7 days.

After the incubation period finished, the immobilising overlay was removed, and wells were washed with a 1X phosphate-buffered saline (PBS) solution (Thermo Fisher Scientific, Gibco, ref 20012-019). Wells were inactivated with a 20-minute treatment of 10% formalin solution (Sigma Aldrich ref HT5012-60ML).

For the case of **VSVEB**, formalin was removed and a 1X crystal violet solution was added to every well, 1ml per well (for 6-well plates) or 6ml per 100mm Petri dish. This last solution was kept for 10 minutes and then properly discarded. Wells were rinsed with water to remove any excess of crystal violet, and this residual water was disposed in special containers.

1X crystal violet preparation: 4% Paraformaldehyde (Sigma Aldrich ref 252549), 5% Ethanol and 0.1% crystal violet (Sigma ref V5265-500ML) in distilled water.

For the case of **EBOV**, formalin was removed and cells were rinsed three times with 1X tris-buffered saline (TBS) solution. TBS was used, since PBS interferes with alkaline phosphatase

signal. Cells were permeabilised with a 10-minute incubation with a TBS 0.1% Triton X-100 (Sigma ref T-8787) solution. Since EBOV virus plaques were immunologically revealed, cells were incubated for 1-hour at 5% CO_2 and 37°C in a TBS solution with 2% FCS containing anti-VP40 (1:500) (Produced by W. Weissenhorn, EMBL) and anti-NP (1:1000) monoclonal mouse antibodies (Produced by our team). Cells were rinsed three times again with 1X TBS, and were then incubated three hours at room temperature in a secondary antibody solution (1:25000 anti-mouse coupled with alkaline phosphatase) (Sigma ref A3562). Cells were rinsed 3 times with TBS and viral plaques were revealed with NBT/BCIP substrate (Thermo Scientific ref 3470).

Virus titration by $TCID_{50}$

Subconfluent Vero E6 cells in 96-well plates (Falcon®) were infected with dilutions of virus samples (100 µL per well) in DMEM without FCS. After the 1-hour incubation at 5% CO_2 and 37°C, 100 µL of DMEM supplemented with 5% FCS were added to each well, so that the final FCS concentration per well is 2.5%. The plates were kept for at least 3 days at 5% CO_2 and 37°C, until cytopathic effects were clearly observed. Plates were scored by standard light microscopy. Alternatively, plates could also be inactivated with a 10% formalin solution and stained with 1X crystal violet solution. The $TCID_{50}$ per ml titre was calculated by the Spearmean & Kärber algorithm, as described by (Killington, 1996).

Virus plaque experiments with PSS

Subconfluent Vero E6 cells were infected with approximately equal numbers of infectious units (PFU) of either VSVEB-WT or VSVEB-E_{304}A, in the absence or presence of PSS, at 2 different concentrations: 4 and 6 µg/µL. After the 1-hour incubation at 5% CO_2 and 37°C, virus inoculum was removed, cells were washed with DMEM, and fresh DMEM containing 1% CMC supplemented with 3% FCS was added. Cells were fixed with 10% formalin and stained with 0.1% crystal violet 72 hours post-infection. CMC overlay was used instead of Avicel to prevent virus spread and avoid the superposition of individual plaques, since we planned to compare a relatively large number of plaques.

Virus entry assay

Vero E6 cells in 6-well plates were either pre-treated for one hour in DMEM 3% with 100mM NH_4Cl (Sigma ref A9434-500G) or not. The pre-treatment was removed, cells were washed twice with DMEM 0% FCS and they were infected with either VSVEB-WT or VSVEB-E304A at an MOI was of 320 cDNA virus-specific copies per cell instead of an MOI based on infectious units, since these two viruses had different infectivity values. The infection took place as described in the **production of virus stocks** (page 67). After the 1-hour incubation, the virus inoculum was removed and cells were washed once with DMEM 0% FSC. Each well was incubated at 37°C and 5% CO_2 in DMEM 3% FCS supplemented with either 100 mM of NH_4Cl or not, and cell lysate samples were collected at the indicated time points. 350 µL of RLT lysis buffer (Qiagen GmbH, Mat no. 1015762) were added per well to conduct viral RNA extraction, as detailed in the protocol of the Qiagen.

Western blots

Culture supernatant samples were diluted in Laemmli buffer, heated at 96°C for 2 minutes and loaded onto a polyacrylamide precast gel (any kDa, Bio-Rad ref 4569036), where they were separated by sodium dodecyl sulphate polyacrylamide gel electrophoresis (Mini-PROTEAN Tetra Vertical Electrophoresis Cell, Bio-Rad, cat. no. 1658004). Proteins were transferred into 0.2µm PVDF membranes (Bio-Rad cat. no. 1704156) using a semi-dry transfer from Bio-Rad and the pre-saved Mixed MW programme (Trans-Blot® Turbo TM Transfer system; 1.3A, 25V for 7 minutes). Unspecific binding was blocked by incubating the membrane in a 1X PBS 10% milk solution for one hour at room temperature. Membranes were then incubated in either 1:2000 anti-VSV M (Kerafast cat. no. EB0011), 1:1500 anti-GP polyclonal (rabbit antibodies, produced by the team), 1:2000 anti-VP40 or 1:500 anti-NP diluted in a PBS supplemented with 1% milk and 0.1% Tween 20 (Sigma Life Sciences P1379-500ML) for 1 hour at room temperature. Following three washes with 1X PBS coupled with 0.1% Tween 20, the membrane was incubated for 1 hour in a 1:25000 horseradish peroxidase conjugated antibodies (Dako, anti-mouse ref P0447; anti-rabbit ref P0448). Protein detection was carried out via electrochemiluminescence with the SuperSignal® substrate (Thermo Scientific ref 34076). Membranes were read using the ImageQuantTM Las 4000 (GE, cat. no. 28-9558-10) equipped

with a CDD camera which was cooled at -25°C. Data were obtained by the ImageQuantTM Las 4000 software.

4X Laemmli buffer preparation: SDS 8% (EuroMedex ref EU0660), Glycerin 40% (EuroMedex ref EU3550), 2-mercaptoethanol 20% (Sigma ref M3148-250ML) and 0.4% bromophenol blue (Fulka Analytical ref 32712-5G).

Silver stain

Upon completion of the SDS-PAGE, the silver stain revelation was conducted by following the manufacturer's kit and instructions (ProteoSilver® Plus Silver Stain kit, Sigma Aldrich ref PROTSIL2-1KT). It is important to note that the gel is to be stained in a glass or plastic tray that has been cleaned with detergent and rinsed thoroughly. Likewise, clean, disposable gloves should be worn and changed before each step to prevent fingerprints on the gel.

RNA extraction of culture supernatant samples

Culture supernatant samples were clarified at 3,000 rpm for 4 minutes and 140 µL were taken and mixed with 560 µL of buffer solution AVL (Qiagen ref 19073) and 5.6 µL of RNA carrier (1 µg/µL) (Qiagen ref 1017647). These samples were vortexed for 15 seconds and were incubated for 10 minutes at room temperature. After the incubation, 560 µL of Ethanol 96% were added to each sample, and RNA was extracted with the kit RNeasy Qiagen (Qiagen GmbH cat 74106) following Qiagen's instructions. Samples were eluted in 40 µL and stored at -80°C.

RT-PCR

To measure genomic RNA, a two-part process was conducted. First, cDNA synthesis was peformed with the reverse transcriptase SuperScript III® (Thermofischer ref. no. 18080093). RNA samples were diluted in nuclease-free water, and were heated for 10 minutes at 65°C. Samples were then cooled down at 42°C for 1 minute, and they were incubated with the reverse transcriptase mix for 50 minutes at 42°C. Either VSV L or EBOV L forward primer (sequences in page 73) were used in the reaction. After the incubation, the reverse transcriptase was inactivated by a 10 minute-incubation at 65°C. cDNA samples were kept at -20°C until they

were used for the second part of qPCR analysis. For the second process, the quantification of virus-specific cDNA copies was performed in a two-step RTqPCR by using the kit EurobioGreen® qPCR Two-Step Lo-Rox (EuroBio, ref GAEMMXO2L-8T). Primers targeting either VSV L polymerase or EBOV L polymerase were used as follows:

Programme
95°C 2 minutes
40 cycles of (95°C for 5 seconds, 60°C for 20 seconds)

VSV F	5’	AATTCCTGAATCCCGATGAG	3’	(Position 4800)
VSV R	5’	GGGAATCGGAAGAGAATTGA	3’	(Position 4902)

EBOV F	5’	CCTAGCGTATTGAAAGCAGTGGTC	3’	(Position 17435)
EBOV R	5’	AGATCTAGCACTTGACGTTATTGGC	3’	(Position 17569)

Likewise, to quantify all either mRNA or antigenomic RNA, a one-step RTqPCR was performed by using the kit EurobioGreen® qPCR One-Step Lo-Rox (EuroBio, ref GAEMMXOS1L-8T) with the same prior primers and the following programme:

Programme
45°C 10 minutes
95°C 2 minutes
40 cycles of (95°C for 5 seconds, 60°C for 20 seconds)

The signal detection was performed by the LightCycler 96 Instrument (Roche cat. no. 05815916001) and its integrated software.

Sequencing of GP and VP24

For sequencing GP’s cryptic furin site, its editing site or the $E_{304}A$ mutation, and VP24’s $I_{50}T$ mutation, the amplification of a fragment of the VP24 and GP genes was performed with the kit Titan One tube RT-PCR system (Roche, ref 11855476001). Primers targeting either EBOV GP or EBOV VP24 were used as follows:

Programme for GP

50°C 30 minutes RT

94°C 2 minutes

40 cycles of (94°C for 15 seconds, 55°C for 30 seconds, 68°C for 2 minutes)

68°C 5 minutes

Programme for VP24

45°C 30 minutes RT

94°C 2 minutes

35 cycles of (94°C for 30 seconds, 58°C for 30 seconds, 68°C for 90 seconds)

68°C 6 minutes

EBOV GP F (position 6741)	5’	GAGGTTGACAATTTGAGACCT	3’
EBOV GP R (position 7744)	5’	AGAGCTTGAGTCGTCTCGTTG	3’
EBOV VP24 F (position 10258)	5’	GAACGTCGTTCCAACAATCGA	3’
EBOV VP24 R (position 11265)	5’	CTTGGAAGCTGGCTTACAGTG	3’

PCR products were cleaned with the NucleoSpin® Gel and PCR Clean-up kit (Machery-Nagel ref 740609.50). To confirm a correct amplification, 5 µL of the 50 µL of PCR product were run at 70 V (Bio-Rad, Power Pac 300, model 1655050) on a 1% agarose (Eurobio ref GEPAGA07-65) gel in TAE buffer (EuroMedex ref EU0201-A) supplemented with Sybr® Safe DNA gel stain (Invitrogen ref S33102). The gel observed under UV light with the device ImageQuantTM Las 4000 (GE, cat. no. 28-9558-10). Upon confirmation, samples were sent for sequencing to Eurofins Genomics in Germany.

Mutagenesis

The kit Q5® High-Fidelity DNA polymerase (NEB, ref M0491L) was used to make point mutations, and thus produce the following two VSVEB variants: $R_{302}A+E_{304}A$ and $RK_{299}AA$. For producing the $R_{302}A+E_{304}A$, the $R_{302}A$ mutagenic primers were used on phCMV plasmids that already contained GP with the $E_{304}A$ mutation. These reactions were conducted with the following mutagenic primers:

GP R_{302}A Forward	5’	TAGAAAAATTGCCAGTGAAGAGTTGTC	3’
GP R_{302}A Reverse	5’	GTGAGGTTTTTTTTAGTTTCC	3’
GP RK_{299}AA Forward	5’	ATTGCCAGTGAAGAGTTGTCTTTC	3’
GP RK_{299}AA Reverse	5’	TGCTGCAGTGAGGTTTTTTTTAGTTTC	3’

PCR

The amplification of the PCR product of a fragment of the GP gene containing the two previous GP mutations was performed with the kit Q5® High-Fidelity DNA polymerase. This reaction also created *XhoI* (in Forward) and *NheI* (in reverse) restriction sites (underlined in the primer sequences). Primers and programme were used as follows:

98°C 30 seconds
35 cycles of (98°C for 10 seconds, 63°C for 30 seconds, 72°C for 2 minutes)
72°C 5 minutes

VSV GP F: 5’ ATCCTACTCGAGCAACACAATGGGCGTTACAGGAATATTGC 3’
VSV GP R:5’ TAGGATCGCTAGCCTAAAAGACAAATTTGCATATACAGAATAAAGC 3’

Molecular cloning protocol

In a final volume of 100 µL, 6µg of either vector plasmid (pVSV-FL encoding GP), as well as the prior amplified PCR fragments were digested with *XhoI* (Ro146S) and *NheI* (R0131) (NEB). After the 2-hour incubation at 37°C, both enzymes were inactivated by a 10-minute incubation at 65°C. Samples were cleaned with the NucleoSpin® Gel and PCR Clean-up kit.

To avoid recirculation of the vector plasmid during ligation, and thus to reduce the background of non-recombinant plasmids, vector plasmid pVSV-FL encoding GP underwent an additional dephosphorylation reaction with the calf intestinal alkaline phosphatase (NEB ref M0290) of 1 hour at 37°C. Samples were incubated for 15 minutes at 75°C to inactivate the enzyme, and they were cleaned with the NucleoSpin® Gel and PCR Clean-up kit.

For quality control, 5 μL of either vector or PCR fragment samples were loaded on a 1% agarose gel in TAE buffer supplemented with Sybr® Safe DNA gel stain (1 μL for every 10 mL). The gel was run at 70 V (Bio-Rad, Power Pac 300, model 1655050), and was observed under UV light with the Invitrogen's Safe Imager transilluminator (ref G6600EU). Upon confirmation of a successful digestion reaction, appropriate samples were cut from the gel and cleaned with the NucleoSpin® Gel and PCR Clean-up kit.

Ligation

The ligation reactions were conducted in a 1:3 molar ratio of vector to insert by using NEB T4 DNA ligase (cat. no. M0202S). Considering that the vector plasmid (pVSV-FL encoding GP) has 12kb, while the insert is 2.4kb, the ligation reactions were performed by using 200 ng of vector and 900 ng of insert. They had a final volume of 20 μL and were incubated for 5 hours at 16°C. Negative controls (1. Vector only and 2. Insert only) were also included. Concentration measures were performed by Nanodrop® One (Thermo Scientific cat. no. 840274200). These reactions were used for transforming competent *Escherichia Coli* (strain XL-Gold (Stratagene cat. no. 200314)).

Bacterial transformation

100 μL of competent bacteria and 10 μL of ligation reaction were incubated 30 minutes on ice and underwent a heat shock for 45 seconds at 42°C. Bacteria were placed again on ice for two minutes. 800 μL of SOC medium (ThermoFischer ref 15544034) were added to the bacteria, and the combination was incubated for one hour at 37°C. Bacteria were used for inoculating 2YT petri dishes (1.5 g of agar (Invitrogen ref 30391-023) per litre of 2YT medium) complemented with antibiotics (ampicillin 100 μg per mL (Roche ref10835269001) or kanamycine 50 μg per mL (Gibco ref 11815024)), resulting in the selection of transformed bacteria. Plasmid DNA was purified via mini (ref 740588.250), midi (ref 740420.50) or maxi (ref 740424.50) preparations by following the manufacturer Machery-Nagel's instructions.

Recombinant VSV rescue

30% confluent BHK-T7 cells were used on the day of transfection. Cells were washed and starved for 20 minutes in DMEM without FCS before being transfected. Fugene6 (Promega, cat. no. E2691) was used with a plasmid reagent ratio of 1:3. For every T25 flask, 800 µL of GMEM without antibiotics were put in a tube, followed by the addition of 25 µL of the transfecting reagent (at room temperature). There was a subsequent inversion of tubes to guarantee that the content was as homogenised as possible. For the preparation of the helper plasmids, for every T25 flask, 100 µL of DMEM 0% FCS without antibiotic were first put in one tube, and then following plasmids were added: 1.3 µg of pBS-N, 2.2 µg of pBS-P, 0.9 µg of pBS-L, 0.3 µg of T7 and 4.5 µg of pVSV-FL encoding GP.

In addition to having a negative control (no VSV-L), 0.5µg of pVSVG was used as a positive control. Once the plasmid tube and the Fugene6 tube were respectively homogenised and ready, the plasmids were added to the Fugene6. The mix was incubated for 15 minutes at room temperature, and it was then added by small drops over the surface of the T25 flask. Six hours later, the medium was replaced with fresh GMEM supplemented with 3% NCS and antibiotics. Cells were monitored up to three days for signs of cytopathic effects. If no CPE was observed, culture supernatant was used as an inoculum (in a 1:3 dilution with DMEM) for a 1-hour infection in subconfluent Vero E6 cells. The rescue event was successful upon observing cytopathic effects either in the original transfected BHK T7 cells, or in Vero E6 cells. Culture supernatant was then collected and stored at -80°C (these aliquots are named Passage 0). Rescued viruses were amplified in Vero E6 cells. For this purpose, 10µl of Passage 0 samples were used for an infection in subconfluent Vero E6 cells. These stocks were sequenced and characterised (titrations of infectious units and viral genome copies) as described before.

Ultracentrifugation

Subconfluent Vero E6 cells were infected with VSV at an MOI of 0.001 as described in the **production of virus stocks**. Culture supernatant was collected 44 hours post infection. To remove cellular debris, culture supernatants samples were clarified at 3,000 rpm for 4 minutes. Clarified supernatants were loaded on a 5-mL 20% sucrose (Fluka BioChemika ref 84097) gradient and viruses were pelleted by ultracentrifugation using a Beckman SW-32 Ti rotor

(28,000 rpm, 1 hour at 4°C) (ref 331186) in a Beckman Optima L-70K ultracentrifuge (SKU 8043-30-1187). Pelleted virions were dissolved in 1 mL of PBS and loaded on a sucrose gradient solution (20% to 50%). For further purifying the virions, a second ultracentrifugation took place in a Beckman SW-60 Ti rotor (58,000 rpm, 1 hour at 4°C) (ref 331313). Once the tubes were taken out, a needle was inserted into the interface of the sucrose gradient to retrieve 500 µL of a ring-like single fraction containing the concentrated viruses. These samples were aliquoted and stored at -80°C until further analysis.

For the case of EBOV, 50% confluent Vero E6 cells were infected at an MOI of 0.004 as described in the **production of virus stocks**. Culture supernatant was collected 7 days post infection. To remove cellular debris, culture supernatants samples were clarified at 3,000 rpm for 4 minutes. Clarified supernatants were loaded on a 5-mL 20% sucrose cushion and viruses were pelleted by ultracentrifugation using a Beckman SW-32 Ti rotor (28,000 rpm, 1 hour at 4°C) in a Beckman Optima L-70K ultracentrifuge. Culture supernatant samples after ultracentrifugation were collected, and pelleted virion was resuspended in 1 mL of PBS, samples were aliquoted. These samples were stored at -80°C until further analysis.

Enzymatic digestion by thermolysin

This procedure was performed as described in the published protocol by (Carette et al., 2011). Purified virus was obtained via ultracentrifugation rounds. 20 µg of purified VSVEB-WT or VSVEB-E_{304}A were incubated with 0.5 mg/mL of thermolysin (Promega cat. no. V4001) in a solution of Tris 50 mM pH 8.8, $CaCl_2$ 0.5 mM at 37°C. The digestion was stopped at the right interval by adding EDTA (final concentration 0.1 M). The efficacy of the digestion was visualised by western blot analysis with 1:1,500 anti-GP polyclonal (rabbit antibodies, produced by the team) and 1:25,000 horseradish peroxidase conjugated antibodies (Dako, anti-mouse ref P0447; anti-rabbit ref P0448).

Inactivation of BSL4 samples

After inactivation following strict biosecurity protocols which include the inactivation of samples in front of a witness, culture supernatants or cell lysates were taken out from the Jean Mérieux BSL4 facilities.

Statistical analysis

Mean and standard deviations, represented as error bars in figures, as well as unpaired Welch's t-tests were calculated using Prism 8.2.0 (GraphPad software, La Jolla, California, USA). All experiments were performed three times. For some results, a graph summarising the data is presented, whereas for some other results, a representative experiment is chosen and displayed.

Results

This research project was launched in response to the Ebola disease outbreak that occurred in West Africa between 2014 and 2016. The swift transmission of the virus in three countries that had not previously experienced an Ebola outbreak prompted the exploration of whether antiviral compounds that had been utilised to treat other viral infections could be repurposed to combat EBOV and serve as emergency drugs. As a result of this research endeavour, poly(sodium 4-styrenesulphonate) (PSS) was identified as a potent inhibitor of EBOV replication. Further experiments were conducted to examine whether the use of PSS could result in the emergence of drug-resistant variants. The detection of mutations that lead to diminished drug effectiveness can offer valuable insights into the mechanisms behind PSS's action and the molecular dynamics of the interaction between the virus and the host during the selection of drug-resistant variants.

Subsequent experiments were carried out using a surrogate system of recombinant vesicular stomatitis virus (VSV) in which the genuine VSV G gene was substituted by the EBOV GP gene, allowing for the expression of EBOV's full-length surface glycoprotein (VSVEB). As VSV is not a human pathogen, all experiments involving VSVEB could be conducted under BSL2 conditions. The continuous passaging of VSVEB in the presence of PSS led to the emergence of variants of the virus that exhibited heightened drug resistance. Upon sequencing the cloned virus variants, it was found that mutations had occurred in the virus genome. However, only one mutation was observed in the GP EBOV gene, where a glutamic acid residue at position 304 was substituted with an alanine. As a result, a recombinant VSVEB containing this specific mutation, VSVEB-$E_{304}A$, was created and subsequently generated using reverse genetics for VSV.

The initial objective of this study was to produce and characterise stock samples of two recombinant viruses: one containing the wild-type EBOV GP sequence (VSVEB-WT) and the other containing the EBOV GP $E_{304}A$ mutation (VSVEB-$E_{304}A$), and then to compare them in terms of their growth and plaque size under the presence or absence of the inhibitor PSS.

Comparative analysis of VSVEB-WT and VSVEB-$E_{304}A$

The first step of this study involved the production and characterisation of virus stocks for both recombinant VSVEB-WT and VSVEB-$E_{304}A$. Vero E6 cells were infected with either VSVEB-WT or VSVEB-$E_{304}A$ at a MOI of 0.01, and the culture supernatants were harvested 44 hours post-infection. The infectious titres of the virus stocks were determined using a $TCID_{50}$ titration assay. Interestingly, the virus with the $E_{304}A$ mutation (1×10^9 $TCID_{50}$/mL) exhibited 7.5 times higher titres than VSVEB-WT (1.33×10^8 $TCID_{50}$/mL).

We also conducted a plaque forming unit assay to determine the viral titres of VSVEB-WT and VSVEB-$E_{304}A$. In this assay, Vero E6 cells were infected with virus serial dilutions of either VSVEB-WT or VSVEB-$E_{304}A$, which were then overlaid with DMEM containing 3% FCS and 0.8% Avicel. The cells were incubated until the formation of viral plaques. The results of this method of virus titration indicated that the VSVEB-$E_{304}A$ mutation led to a 4-fold increase in titres as compared to VSVEB-WT. Specifically, VSVEB-$E_{304}A$ exhibited titres of 1.65×10^8 PFU/mL, while VSVEB-WT displayed titres of 4.14×10^7 PFU/mL. Moreover, during our assessment of virus titres by plaque analysis, we observed a difference in plaque size between the two viruses. To quantify these differences, we infected Vero E6 cells with virus dilutions containing comparable quantities of infectious units, as previously described. After the plates were fixed and stained with crystal violet, the surface of each plaque (measured in pixels) was calculated using ImageJ software and used for statistical analysis (see figure 31).

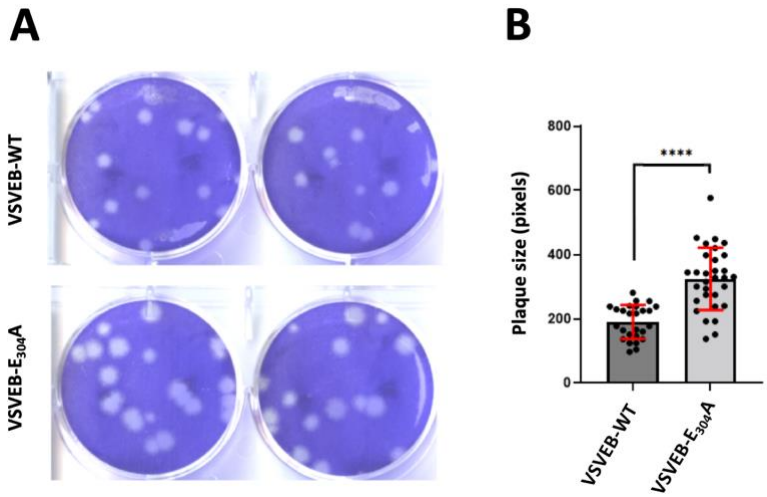

Figure 31. VSVEB-$E_{304}A$ showed growth advantages over VSVEB-WT

Vero E6 cells were infected with either VSVEB-WT or VSVEB-$E_{304}A$, and incubated with an overlay of DMEM 3% FCS supplemented with 0.8% Avicel. After 72 hours, cells were fixed and stained. A representative image of

the plaques for each virus is shown in panel A. ImageJ software was used to compare the size of plaques. Data are representative of three independent experiments, and error bars on the graph represent the standard deviation of the measured values. Approximately 30 plaques for each virus were randomly selected for analysis (see panel B). The statistical significance was determined using a two-tailed t-test. In this case, the result was highly significant with a p-value of less than 0.0001 (****p<0.0001).

Overall, VSVEB-E_{304}A produced larger plaques than VSVEB-WT, with an average pixel value of 364.38 compared to 163.11. However, we observed the presence of small plaques with both viruses. Since our two recombinant viruses were different only by their surface glycoprotein: EBOV WT vs EBOV GP E_{304}A, we decided to assess the composition of these virions by Western blot analysis with anti-GP_2 and anti-GP_1 antibodies, as seen in figure 32.

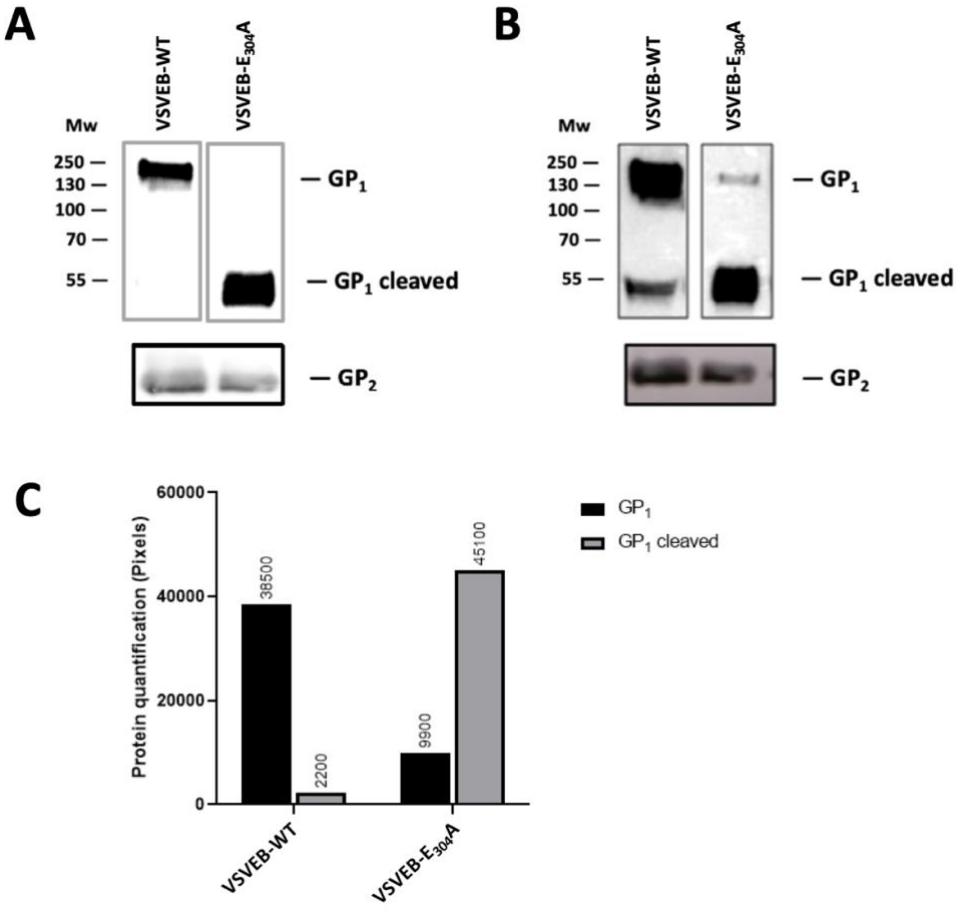

Figure 32. VSVEB showed striking differences in GP_1 migration pattern in SDS-PAGE

Samples of culture supernatant of the two recombinant viruses were analysed by WB using anti-GP_1 and anti- GP_2 antibodies. Panels A and B represent the same WB membrane with two different exposure times. Panel B: A longer exposure allowed visualisation of minor protein bands in both viruses. Panel C plots the quantification (in pixels) of the GP-recognised protein bands of panel B. Presented data are representative of a series of independent experiments.

As previously stated, the surface glycoprotein of EBOV consists of two subunits, GP_1 (130-160 kDa) and GP_2 (~26 kDa). In the samples of VSVEB-WT, both proteins were detected as

expected (Panel A of figure 32). However, in the case of VSVEB-$E_{304}A$, a protein band of approximately 55 to 60 kDa was observed instead of GP_1. Subsequent analysis revealed that, after a longer gel exposure (Panel B of figure 32), GP_1 appears in VSVEB-$E_{304}A$ as well as a lower molecular weight protein for VSVEB-WT. These findings suggest that the GP_1 subunit in VSVEB-$E_{304}A$ undergoes proteolytic processing, resulting in the detection of only one cleaved part by anti-GP1 antibodies. Importantly, our anti-GP_1 antibodies specifically target the N-terminal part of GP_1, and considering that the cysteines connecting the two GP subunits are situated at positions 53 and 609, this study revealed a new cleaved product of the GP gene, designated as GP_1 cleaved, which is located in the N-terminal part of GP_1. The gel quantification results (Panel C of figure 32) confirmed that the main GP_1-specific protein in VSVEB-$E_{304}A$ is GP_1 cleaved, in contrast to VSVEB-WT where GP_1 is the main protein with smaller amounts of GP_1 cleaved. Interestingly, both viruses contain full-length GP_1 and GP_1 cleaved, but in different proportions. Since the only difference between the two viruses is the mutation at position 304 (as shown in figure 33), it is reasonable to assume that the cleavage site is located in close proximity to this mutation.

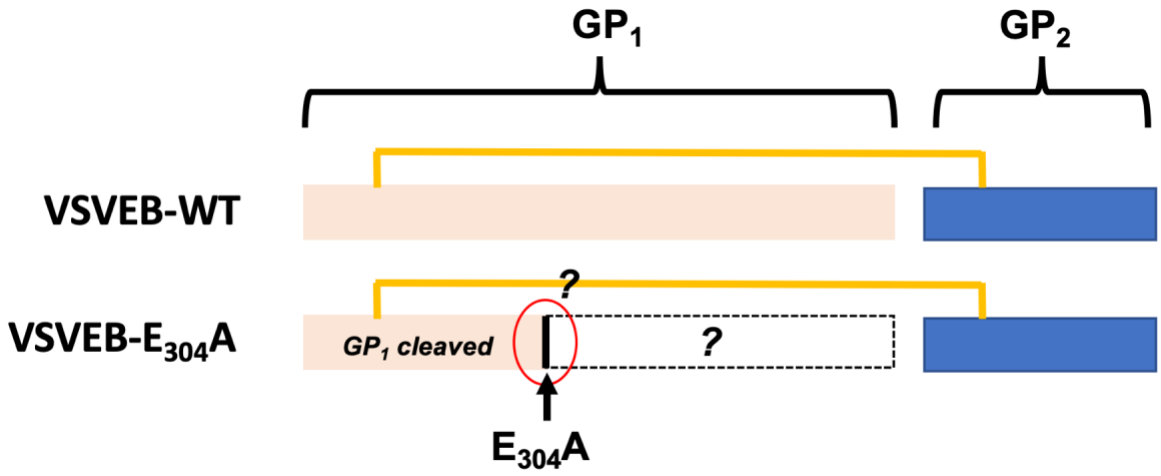

Figure 33. Schematic presentation of the surface GP of the two recombinant VSVEB

After the cleavage of the EBOV GP precursor by cellular furin at a multibasic amino acid motif located at positions 497 to 501 of the open reading frame, GP_1 and GP_2 remain bound by a cysteine bridge. In the case of VSVEB-$E_{304}A$, WB analysis revealed a GP_1-specific product with a lower molecular weight than GP_1, suggesting that GP_1 cleavage occurs in close proximity to position 304, which distinguishes VSVEB-$E_{304}A$ from VSVEB-WT. This product was named GP_1 cleaved, while the second part of GP_1, which was not visible on the WB, is marked with a question mark (?). The exact location of the cleavage is also uncertain and marked with a question mark.

Computer analysis of GP_1 sequence for presence of proteolytic cleavage sites in proximity to the 304-position revealed three potential proteases: sk1, nardylisine and furin (figure 34).

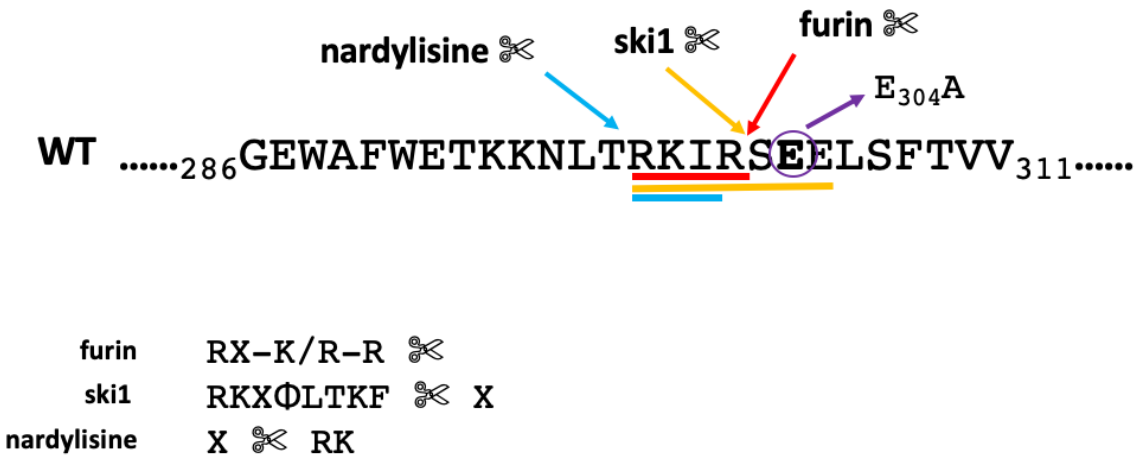

Figure 34. Putative proteases and their cleavage sites near position 304

Following a computer-based analysis, we identified Furin, Ski1, and Nardylisine as potential proteases capable of cleaving GP_1 in proximity to the position 304. The top panel of the figure displays the sites that could be theoretically recognised by these proteases. The bottom panel displays the sequences recognised by each protease, along with the position of the cleavage. In the sequence, a hydrophobic amino acid is represented by Φ, and an undetermined amino acid is represented by "X."

Based on the size of GP_1 and GP_1 cleaved, a simple calculation predicts that the second cleavage product could have a molecular weight ranging from 75 to 100 kDa. However, it is concerning that anti-GP_1 antibodies did not detect this product in either VSVEB-E_{304}A or VSVEB-WT virions. This could indicate that either our antibodies cannot visualise this additional product, or that it is not present in virions and has been removed from the surface GP structure after cleavage. Interestingly, this mysterious product contains multiple N- and O-glycosylation sites and partially corresponds to the mucin-like domain (MLD) in the EBOV GP_1 subunit.

In attempt to solve this mystery, we conducted a 2-step ultracentrifugation-based concentration and purification process for both viruses. First, we concentrated the viruses by pelleting the virions through a 20% sucrose cushion, and subsequently, we purified them by sedimentation in a sucrose gradient (20%-50%). The opalescent band containing the virus was collected, the proteins were separated using SDS-PAGE and visualised via silver staining. As depicted in figure 35, this approach enabled us to detect all virion proteins, including VSV-specific ones, as well as the processed products of EBOV GP: GP_1, GP_1 cleaved, and GP_2.

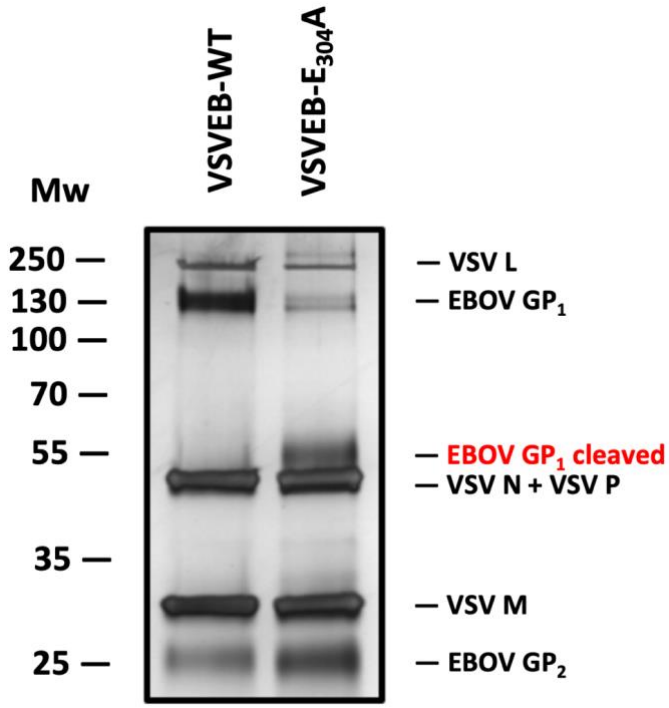

Figure 35. VSVEB-E_{304}A virions contain a single GP_1 cleavage product

Vero E6 cells were infected with VSVEB-WT or VSVEB-E_{304}A at an equal MOI (0.001), and culture supernatant samples were collected 72 hours post infection and clarified at 3000 rpm for 4 minutes. These samples were then subjected to ultracentrifugation twice, once using a 20% sucrose cushion and a second time using a sucrose gradient. Opalescent bands containing the viruses were collected, the proteins were separated on an SDS-PAGE and visualised using silver staining assay. EBOV GP_1 cleavage product is shown in red. This protein band is abundantly present in VSVEB-E_{304}A when compared to GP_1. GP_1 cleaved can also been seen in VSVEB-WT, but in much lower amounts. On the contrary, most of GP present in VSVEB-WT is full-length GP_1, whereas in VSVEB-E_{304}A this latter protein is found in much lower amounts. The data presented are representative of three independent experiments.

Our data provide clear evidence of three key findings regarding the VSVEB-E_{304}A virus: First, the absence of the second GP_1-specific product, which corresponds to the mucin-like domain. Second, the major GP_1-specific protein in this virus is cleaved GP_1. And third, unprocessed GP_1 is also present in the virus, albeit in much smaller quantities than in the VSVEB-WT virions.

To further characterise the viruses, we conducted an analysis of their genomic RNAs using RTqPCR. RNA was isolated from both viruses and converted into cDNA using specific primers and reverse transcriptase. The number of cDNA copies was then quantified using qPCR with primers specific to the L gene of VSV, for determining the number of viral particles. However, it is important to note that the methodology used in this study does not allow for a direct determination of the genome copy number, as it does not account for the efficiency in RNA extraction nor the reverse transcription efficiency during the construction of cDNA. Nevertheless, this approach enabled a relative comparison between the two viruses. The data

obtained showed that the RNA samples from VSVEB-WT and VSVEB-E_{304}A yielded a similar amount of virus-specific cDNA: 2.20×10^9 and 2.86×10^9 copies, respectively.

	cDNA copies	$TCID_{50}$	Infectivity
VSVEB-WT	2.20×10^9	1.33×10^8	16.54
VSVEB-E_{304}A	2.86×10^9	1.00×10^9	2.86

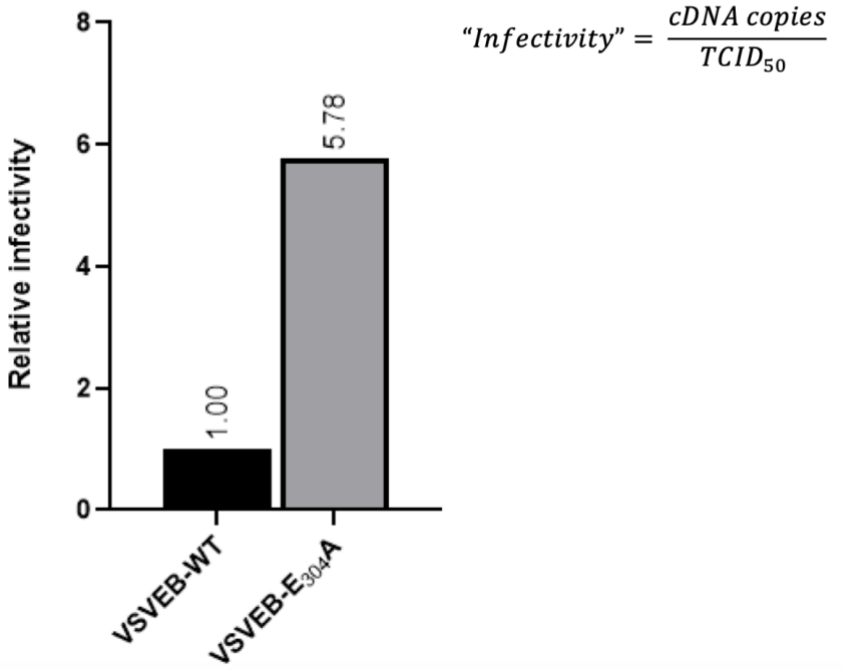

Figure 36. VSVEB-E_{304}A is more infectious than VSVEB-WT

Top panel: The infectious units were determined as $TCID_{50}$/ml, while cDNA copies per ml were determined using RT-qPCR. It is important to note that the methodology of this study cannot directly quantify viral genome copies since it does not account for the efficiency of reverse transcription during cDNA construction and RNA extraction. We put the term infectivity in quotation marks to indicate this problem. The infectivity was calculated as the ratio of the number of cDNA copies to the number of infectious units. The bottom graph shows the difference in infectivity of VSVEB-E_{304}A and VSVEB-WT, considering that the latter has an adjusted infectivity value of 1. Data are representative of three independent experiments.

Based on the data presented in figure 36, it is evident that the difference in $TCID_{50}$ titres between the two viruses is significantly higher than the difference in the quantity of genomic RNA (in a relative manner). This finding led us to hypothesise that the viruses might differ in their ability to induce viral replication or, as we will refer hereafter, differences in infectivity. The data in figure 36 also supports this hypothesis, as it shows that VSVEB-E_{304}A is 5.78 times more infectious than VSVEB-WT.

Comparative analysis of the virus growth kinetics

To investigate whether the differences in infectivity between VSVEB-E_{304}A and VSVEB-WT persist over the course of virus replication, virus growth kinetics were conducted. Vero E6 cells were inoculated with a low MOI to ensure multicycle infection, and culture supernatant samples were collected over a 48-hour period post-infection. The samples were then titrated by $TCID_{50}$ and were also used for RNA extraction and RTqPCR analysis (figure 37). Additionally, samples of culture medium were assayed by WB using anti-VSV M antibodies (figure 39). These experiments were aimed at determining whether the differences in infectivity observed between the two viruses are due to intrinsic properties or are just features of virus stocks.

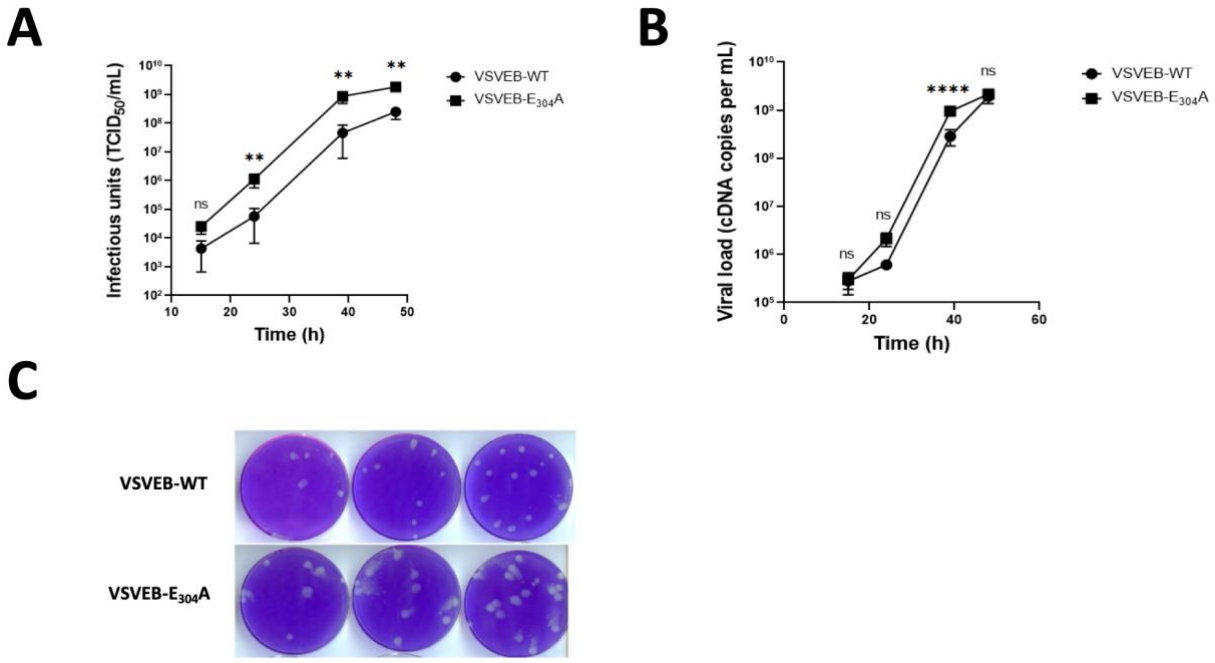

Figure 37. VSVEB-E_{304}A outperforms VSVEB-WT in growth kinetics

Vero E6 cells were infected with either VSVEB-WT or VSVEB-E_{304}A at an equal MOI (0.001). Panels A and B show the results of virus titration by $TCID_{50}$ and RTqPCR of culture medium samples collected at different time points during growth kinetics experiment. Panel C shows the results of the virus titration of the inoculum samples (dilution 1:30), indicating that the experiment started with approximately the same number of PFU for both viruses. Data are representative of three independent experiments, and error bars on the graph represent the standard deviation of the measured values. The statistical significance was determined using a two-tailed t-test.

Panel A of figure 37 demonstrates that, with an average of 12.89-fold increase, VSVEB-E_{304}A consistently outperformed VSVEB-WT in terms of infectious viral titres. RTqPCR analysis of culture medium samples collected during virus replication revealed a slight higher increment of 2.24-fold in the titres of cDNA copies of VSVEB-E_{304}A over VSVEB-WT (Panel B of figure

37). Furthermore, even though the same virus dose was used for inoculation, a difference in virus titres was observed at 15 hours post-infection. To ensure that this difference was not due to variations in the initial infectious dose, virus plaque assays were conducted on inoculum samples, confirming that comparable amounts of both viruses were used (see panel C of figure 37). However, our observations show that the difference between the viruses diminished 48 hours after infection, which can be attributed to the heightened cytotoxicity during the later stages of infection for the virus with the advantages. Evidently, VSVEB-E_{304}A reached a plateau earlier than its counterpart, while the latter continued to proliferate until all cells were infected. Remarkably, the titres of the viruses clearly differed at this time point. By utilising the proposed ratio to evaluate virus infectivity (refer to figure 38), we were able to compare the viruses and confirm that VSVEB-E_{304}A exhibited greater infectivity, averaging a 6.25-fold higher infectivity than that of the parental virus throughout the experiment.

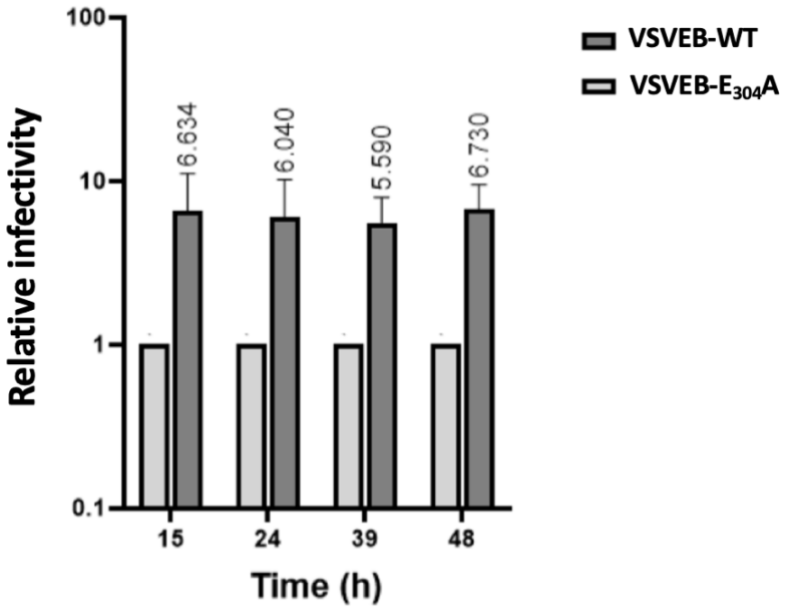

Figure 38. The increased infectivity of VSVEB-E_{304}A persists over time

The infectivity value was calculated as the ratio of cDNA copies over the virus titres. The graph plots the difference between infectivity of VSVEB-E_{304}A and VSVEB-WT, considering that the latter has an adjusted value of 1. Data are representative of three independent experiments, and error bars on the graph represent the standard deviation of the measured values.

We also conducted a comparison of virus growth using Western blot analysis with anti-VSV-M antibodies. As depicted in figure 39, the VSV matrix protein was only detected in the culture supernatants at two time points: 39 and 48 hours post-infection. The average 1.63-fold increase of the quantification of VSV-M of VSVEB-E_{304}A over the WT, supported our previous findings regarding the growth advantage of VSVEB-E_{304}A, which were also consistent with the data

obtained from the RT-qPCR assay. Since M is a structural protein of VSV, the amount of M present in the culture medium reflects in relative terms the number of virions. This enabled us to use the Western blot data and once again compare the viruses in terms of their ability to infect cells (i.e., viral infectivity). Our results using VSV-M indicate that VSVEB-$E_{304}A$ exhibited a 7.6-fold infectivity advantage over VSVEB-WT, confirming thus our previous findings.

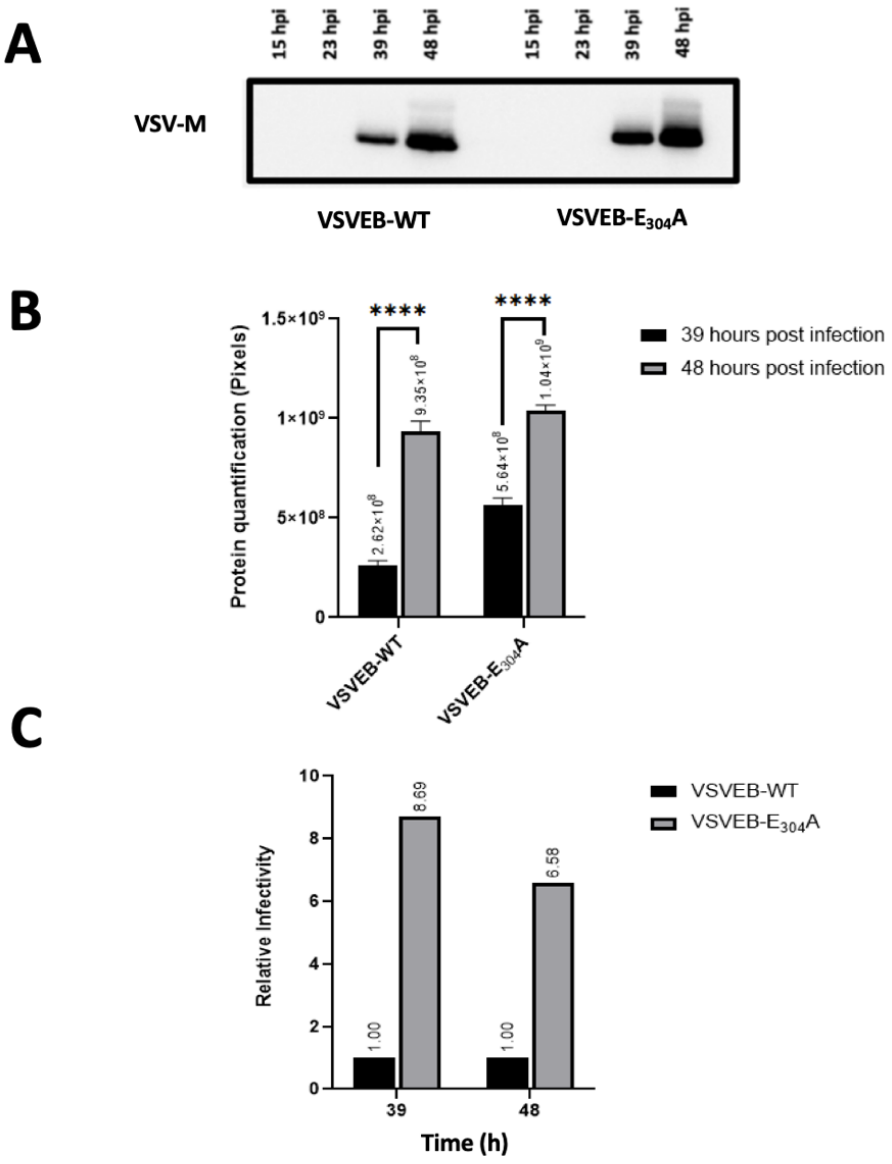

Figure 39. The higher infectivity of VSVEB-$E_{304}A$ is confirmed by WB analysis

Panel A: Culture supernatant samples from both recombinant VSV were analysed by WB using anti-VSV-M antibodies. Panel B: The protein bands from Panel A were quantified by measuring their pixel values with the ImageJ software. The infectivity values were calculated as the ratio of the VSV-M protein (pixel values of the protein bands) to the infectious units ($TCID_{50}$). Panel C: The graph shows how many times VSVEB-$E_{304}A$ is more infectious than VSVEB-WT, considering that the latter has an adjusted infectivity value of 1. Data presented are representative of three independent experiments. The statistical significance was determined using a two-tailed t-test. In this case, the result was highly significant with a p-value of less than 0.0001 (****$p<0.0001$).

It is worth noting here that the virus selected by multiple passages in the presence of PSS, in addition to the mutation in EBOV GP ($E_{304}A$), also contained an amino acid substitution in the VSV L gene. In order to exclude the influence of this latter mutation, VSVEB-$E_{304}A$ was created by reverse genetics, providing a single $E_{304}A$ mutation compared to VSVEB-WT. This virus was used in all of the above experiments. To assess whether the $E_{304}A$ substitution is responsible for the "PSS resistance" phenomenon, Vero E6 cells were infected with either VSVEB-WT or VSVEB-$E_{304}A$ at a MOI of 0.001. Infected cells were cultured in DMEM medium containing 3% FCS. Different concentrations of PSS were added to the medium or used without PSS for comparison purposes. Samples of culture medium were collected at various intervals after infection and virus titres were determined by $TCID_{50}$ assay.

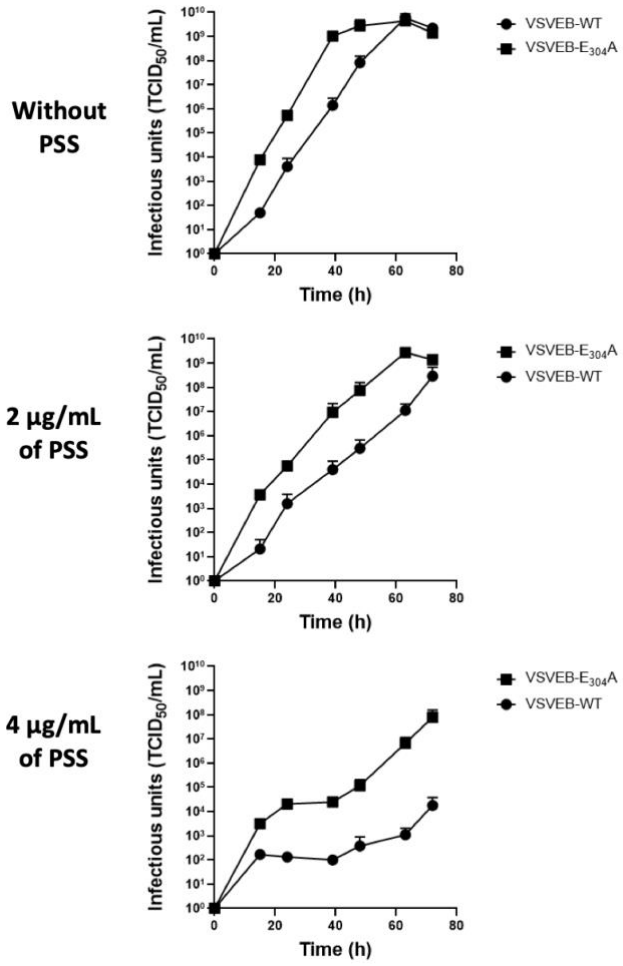

Figure 40 Dose dependant effect of PSS on the growth kinetics of viruses

Vero E6 cells were infected with either VSVEB-WT or VSVEB-$E_{304}A$ at an equal MOI (0.001). After the 1-hour infection, the inoculum was removed, and cells were incubated for 72 hours in three different conditions: considering PSS concentration 4 µg/mL, 2 µg/mL, and without PSS. Samples of culture medium were collected at different time points post infection and the virus titres were determined by $TCID_{50}$ assay. Data are representative of three independent experiments, and error bars on the graph represent the standard deviation of the measured values.

As it can be seen in figure 40, the results of the experiment performed in the absence of PSS correspond well with those presented in figure 37. Since the duration of the experiment was extended from 48 to 72 hours, both viruses reached a plateau at the end of the experiment. As expected from the previous experiments (figure 37), VSVEB-WT replicated less efficiently than VSVEB-E_{304}A and therefore reached the plateau later. At a PSS concentration of 2 µg/mL both viruses showed a reduction in growth, but VSVEB-E_{304}A again demonstrated a clear advantage with an average a 135-fold increase in titres of infectious units compared to the VSVEB-WT. An even more pronounced inhibitory effect was observed at a PSS concentration of 4 µg/mL. Specifically, the average virus titres at 72h were 2.83×10^3 for VSVEB-WT, and 1.22×10^7 for VSVEB-E_{304}A, versus an average of 10^9 at 72h for both virus without PSS. As it can be seen, VSVEB-WT growth was completely blocked during the first 40 hours after infection. VSVEB-E_{304}A replication was also significantly affected by the inhibitor. However, this virus still showed a slight increase in virus titres during the same period. It should be noted that both viruses resumed replication later, possibly indicating degradation of the inhibitor over time. The presence of virus in the culture medium early after infection in the last growth kinetics can be explained by the release of virus from initially infected cells, which took place in the absence of PSS.

Theoretically, in experiments on virus growth kinetics, an interpretation problem could arise if the doses of viruses are not equal due to, for example, pipetting error. To rule out this potential problem, we performed a viral plaque size analysis, an alternative method for characterisation of the virus growth. Vero E6 cells were infected with approximately equal doses of viruses without PSS and then the cells were covered by DMEM containing different amounts of PSS and supplemented with 3% FCS and 0.8% Avicel. Virus plaques were assayed 64 hours post infection. Since each viral plaque originates from a single infected cell, even the initial doses of viral inoculums were different, we are still able to conclude which virus has a growth advantage by comparing the size of the plaques.

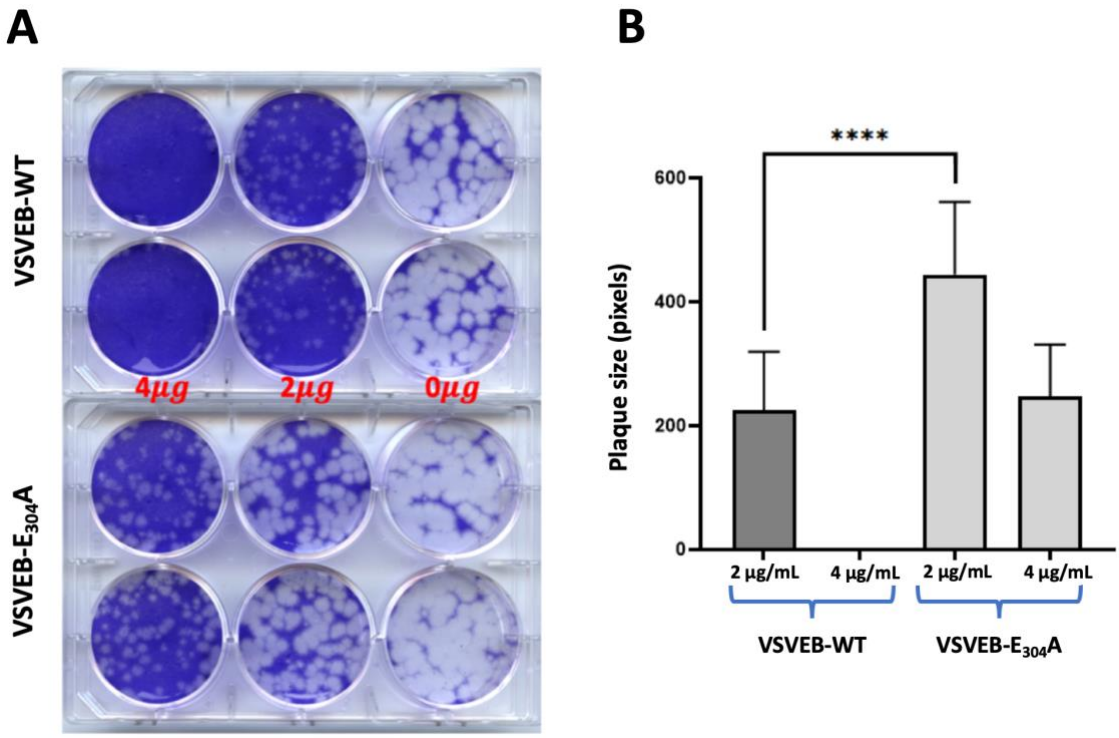

Figure 41 Dose dependant effect of PSS on the size of virus plaques

Vero E6 cells were infected with either VSVEB-WT or VSVEB-E_{304}A, and incubated with an overlay of DMEM containing different concentrations of PSS and supplemented with 3% FCS and 0.8% Avicel. Panel A: Virus plaques were observed on plates after 64 hours post infection. Cells were fixed and stained with crystal violet. Panel B: The size of the plaques was measured in pixels. Data are representative of three independent experiments, and error bars on the graph represent the standard deviation of the measured values. The statistical significance was determined using a two-tailed t-test. In this case, the result was highly significant with a p-value of less than 0.0001 (****$p<0.0001$).

As shown in figure 41, recombinant VSVEB-E_{304}A shows bigger plaques (1.98-fold increase) and thus clear growth advantages in the presence of PSS, confirming its 'PSS-resistant' status. At the same time, these results suggest that the E_{304}A mutation does not confer “true resistance” to the inhibitor. In particular, a significant effect of PSS on VSVEB-E_{304}A was observed at a concentration of 4 µg/mL, but it was very comparable to the effect induced by 2 µg/mL PSS on VSVEB-WT. Here once again, clear growth advantages of VSVEB-E_{304}A were observed with or without PSS.

Next, we performed a series of experiments aimed at elucidating the molecular basis of VSVEB-E_{304}A's growth advantages.

Virus attachment experiments

Given that the virus attachment inhibitor (PSS) was used during consecutive passages of recombinant VSV carrying EBOV GP, we first aimed to understand whether the two viruses differed indeed in their attachment stage of virus entry into cells, as the first step in identifying the mechanisms underlying increased infectivity. We decided to limit the action of PSS to only 1 hour, during which cells will be inoculated with the virus. To prevent further exposure to the inhibitor, the inoculum containing PSS should be removed and the cells washed with DMEM. Under these experimental conditions, the size of the plaques formed by the virus was supposed to be independent of the concentration of PSS (used only 1 hour). At the same time, it was expected that there would be differences in the number of plaques depending on PSS concentration. A higher concentration of PSS was expected to have a higher inhibitory effect and thus lesser quantity of plaques. We hypothesised that if two viruses did differ in attachment, then this would be reflected in the effectiveness of PSS inhibition. On the contrary, if there is no difference between the viruses, the same inhibitory effect will be observed for both viruses.

Briefly, Vero E6 cells were infected in the absence or in presence of PSS (4 and 6 µg/mL) using approximately equal PFU per well. The inoculum containing inhibitor was removed, cells were washed twice with DMEM, and fresh DMEM containing 3% FCS supplemented with 1% CMC was added. To visualise virus plaques, cells were fixed and stained with crystal violet at 72 hours post-infection (figure 42, panel A). Since a relatively large number of plaques were planned to be compared, an overlay containing CMC was used instead of Avicel in this experiment. This approach prevented the rapid spread of the virus, resulted in reduction of the plaques' size when compared to Avicel-based cover and thus avoided the overlapping of individual plaques.

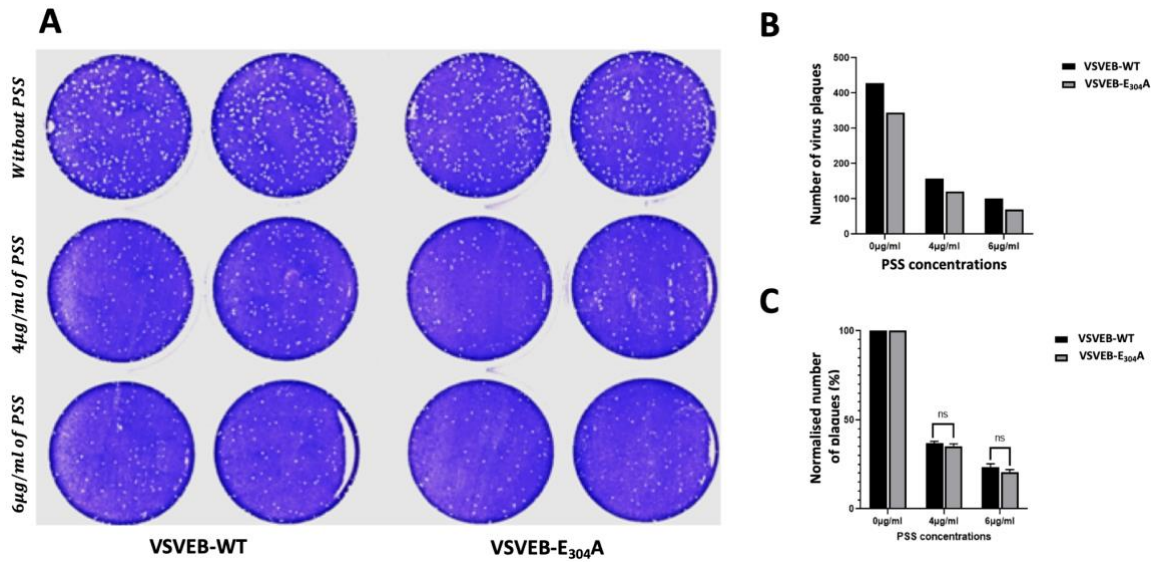

Figure 42. Attachment inhibition PSS equally blocks infection regardless of the virus

Vero E6 cells were infected with either VSVEB-WT or VSVEB-E_{304}A, and plates were incubated for 72 hours in 1% CMC coupled with DMEM containing 3% FCS. Panel A: Virus plaques were visualised by staining with crystal violet. Panel B: The number of discrete plaques was counted, and the average and standard deviation values were plotted. Panel C: The average number of plaques for PSS concentrations of 4 and 6µg/ml were normalised to the 0µg/ml condition, which is plotted as 100%. Data are representative of three independent experiments.

The results described above indirectly suggested that virus attachment is probably not critical for the growth benefits demonstrated by VSVEB-E_{304}A. To answer this tricky question, we performed 'classical' virus attachment experiments. To avoid problems related to differences in virus infectivity, cells were inoculated with equal amounts of virus-specific cDNA copies, which were assessed by RT-qPCR (~320 cDNA copies per cell). Such settings seem to be more appropriate for assessing virus attachment than using an equal MOI, as was done in previous experiments. Briefly, cells were inoculated with virus at 4°C for 1 hour, then washed three times with pre-cooled medium and finally lysed. Similarly, the experiments were also performed at 37°C. After the above procedures, cells were lysed and RNA was isolated for RT-qPCR analysis.

Inoculation of the virus at 4°C was expected to allow the virus to attach, but prevent its internalisation into the cells. On the other hand, an experiment performed at 37°C would ensure internalisation of the virus and possibly even increase the efficiency of virus attachment. As shown in figure 43, for VSVEB-WT and VSV-E_{304}A at the two temperatures used, only slight differences in the number of virions attached to the cells were observed. As expected, the number of virions attached to the cells increased at 37°C but remained very similar for both

viruses. The results indicate that other steps in virus entry process, not virus attachment, are responsible for the differences in viruses' growth.

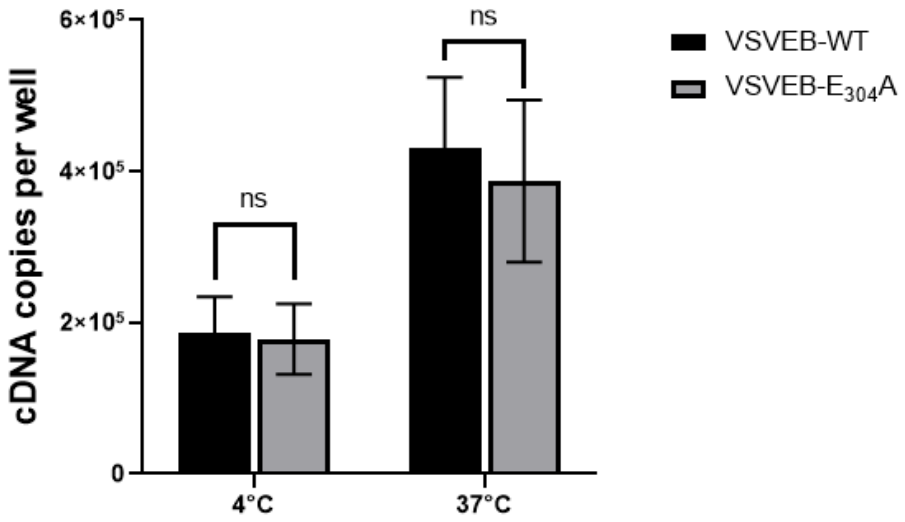

Figure 43. VSVEB-WT and VSVEB-E$_{304}$A have very similar attachment potency

Vero E6 cells were inoculated with approximately the same number of viral particles assessed by RTqPCR (~320 cDNA copies per cell). The cells were incubated at 4°C or 37°C for 1 hour, and they were then washed twice with cold PBS, lysed, viral RNA was isolated, retro transcribed into cDNA and the number of attached virions was estimated by qPCR. Error bars represent the standard deviation of these measured values. Data are representative of three independent experiments, and error bars on the graph represent the standard deviation of the measured values. We found that VSVEB-WT and VSVEB-E$_{304}$A were not statistically different (two-tailed t-test).

Therefore, what else could provide a growth advantage for VSVEB-E$_{304}$A? In trying to answer this question, we thought of another factor that may play an important role: the efficiency of infection.

Virus penetration assay

EBOV penetration is known to be a multistep process involving virus attachment to the cell, internalization, proteolytic digestion of the surface GP by cellular cathepsins, interaction with the intracellular viral receptor NPC1 and membrane fusion culminating in the release of the viral nucleocapsid into the cytoplasm. After having found that the attachment was not critical for the growth advantage of VSVEB-E_{304}A, we decided to conduct experiments where viruses will be compared in terms of efficiency of the infection. The release of viral nucleocapsids in the cell cytoplasm will initiate the synthesis of virus-specific RNA and its accumulation in cells, which can be measured by RTqPCR.

In these experiments, we used the same approach as described above in Figure 43, which allowed us to rule out the difference between viruses in infectivity. Briefly, Vero E6 cells were inoculated with the same number of virions of either virus (VSVEB-WT and VSVEB-E_{304}A). Infection dose was adjusted to approximately 320 virus specific cDNA copies per cell. After virus inoculation during 1 hour, the cells were washed thoroughly, and were either immediately lysed (1h) or incubated further at different intervals post infection and then lysed (figure 44, panel A). Cellular RNA was isolated and assayed by RT-qPCR using virus specific primers. In parallel experiments, the cells were treated for 1 hour with 100mM NH4Cl prior to infection (Figure 44, panel B). This reversible lysosomotropic agent is capable of blocking endosomal trafficking to acidified endosomes and is known to inhibit entry a number of pH-dependent viruses. RNA from the inoculum samples was also isolated and quantified by RTqPCR in order to ensure equal viral load during infection (Figure 44, panel C).

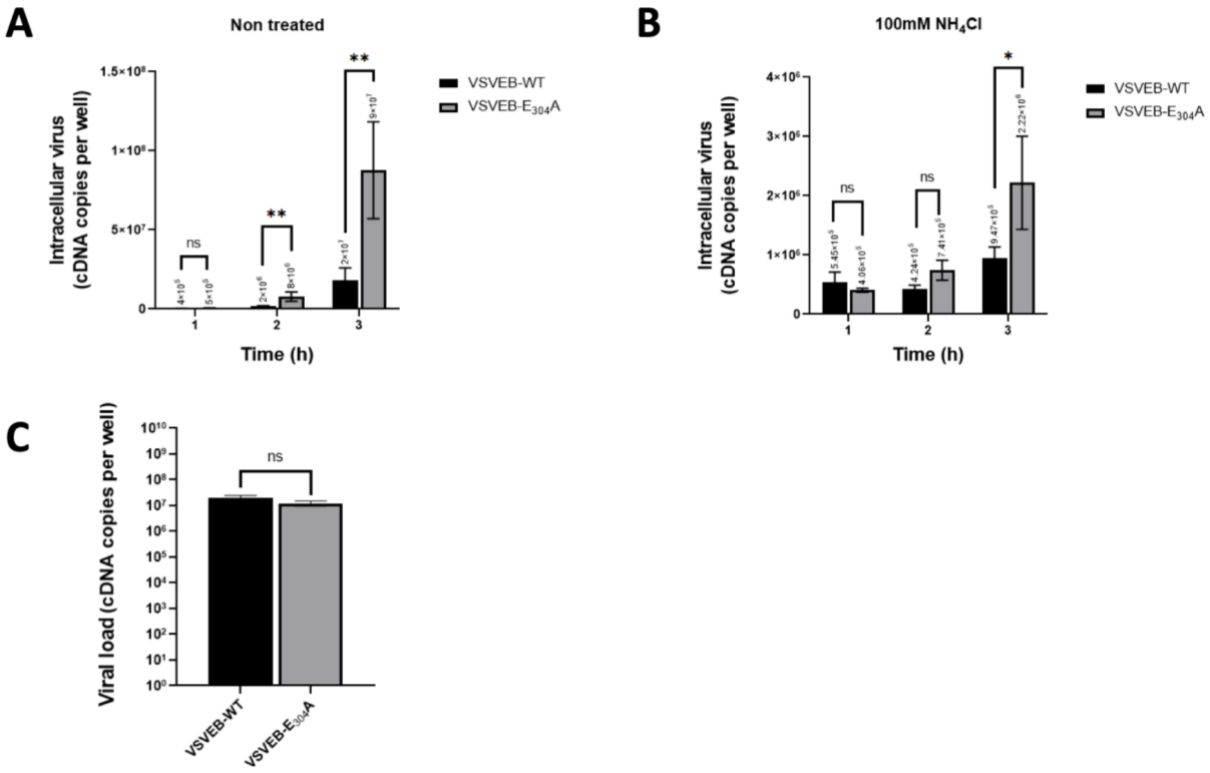

Figure 44. VSVEB-E$_{304}$A showed higher levels of virus specific RNA (genomic, antigenomic and mRNA), suggesting higher efficiency of RNA internalisation when compared to VSVEB-WT

Prior to infection, Vero E6 cells were either kept untreated or were pre-treated for one hour with 100mM NH_4Cl, DMEM, 3% FCS. The cells were washed three times with DMEM and subsequently inoculated with approximately the same quantity of viral particles, estimated by RTqPCR (~320 cDNA copies per cell), and maintained at 37°C during 1h. Panel A: The inoculum samples were assessed by RTqPCR. Panels B and C: Infected cells were kept for different time post infection as indicated and then lysed. Quantity of virus-specific RNA was estimated by RTqPCR. Data are representative of three independent experiments, and error bars on the graph represent the standard deviation of the measured values.

As shown in figure 44, significantly higher levels of virus-specific RNA were present in cells infected with VSVEB-E$_{304}$A as early as two hours after infection. Remarkably, equal amounts of viral RNA were detected one hour after infection, which is consistent with previous data from the virus attachment experiment (figure 43). As expected, pre-treatment of the cells with ammonium chloride reduced and delayed the synthesis of virus-specific RNA. No differences between viruses were observed 1 and 2 hours after infection. However, at later times after infection the viruses showed statistical significant differences (4.5 and 2.3 times more of VSVEB-E$_{304}$A over the WT, without and with NH_4Cl, respectively), which can be explained by the reversible nature of the inhibitor and the recovery of endosomal trafficking.

Proteolytic digestion by thermolysin

The proteolytic digestion of EBOV GP by cellular cathepsins L and B occurs in the endosomal/lysosomal compartment, which is a crucial event for opening up the receptor binding region in GP_1. Radical cleavage of GP_1 to approximately 19kDa molecule facilitates interaction of GP_1 with the NPC1 receptor, ultimately leading to membrane fusion and release of viral nucleocapsid into the cell cytoplasm (Beniac & Timothy, 2017). Based on the results described above, including the fact that VSVEB-E_{304}A contains an atypical proteolytically processed GP_1 subunit that has lost much of the authentic GP_1 present in VSVEB-WT, we hypothesised that this 'pre-cleaved' GP_1 probably provides a considerable advantage in terms of further proteolytic digestion and thus may be the turning point that explains the increased infectivity of VSVEB-E_{304}A compared to VSVEB-WT. To prove this, we performed experiments in which VSVEB-WT or VSVEB-E_{304}A samples were treated with thermolysin, a protease that mimics the action of cellular cathepsins and is often used in EBOV proteolytic digestion experiments. At the end of the predetermined digestion time, EDTA was added to the samples to stop the reaction. The samples obtained were analysed by Western blotting using antibodies against GP_1 (figure 45).

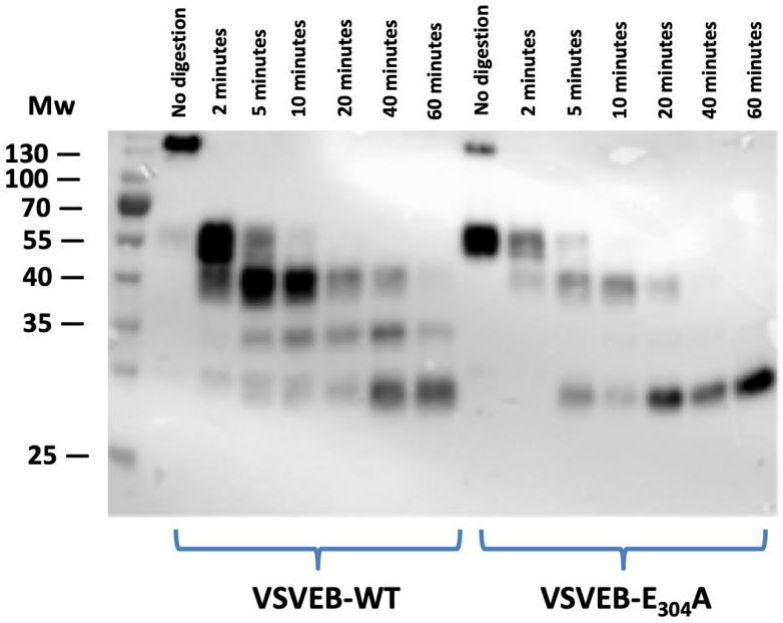

Figure 45. The efficiency of GP_1 digestion by thermolysin differs between viruses. Surface GP VSVEB-E_{304}A is prone to faster and more efficient cleavage when compared with VSVEB-WT

Vero E6 cells were infected with VSVEB-WT or VSVEB-E304A at an equal MOI (0.001), and culture supernatant samples were collected 72 hours post infection and clarified at 3000 rpm for 4 minutes. These samples were then

subjected to ultracentrifugation twice, once using a 20% sucrose cushion and a second time using a sucrose gradient. Opalescent bands containing the viruses were collected and titrated via $TCID_{50}$. An equal number of $TCID_{50}$ of virus pellet samples of VSVEB-WT and VSVEB-E_{304}A were subjected to enzymatic digestion with thermolysin for varying durations. Upon completion of the designated digestion time, the reaction was terminated using EDTA. Protein samples were subsequently analysed via Western blotting using anti-GP_1 antibodies. Data are representative of three independent experiments

The results showed that the GP_1 subunit present in VSVEB-E_{304}A is indeed digested faster and more efficiently compared to GP_1 VSVEB-WT. Very clear difference between the viruses can be seen after 2-5 min incubation with thermolysin. GP_1 of VSVEB-E_{304}A turned out to be almost completely cleaved after 20 minutes and completely later, whereas the GP_1 of VSVEB-WT was not yet completely cleaved even after 60 minutes of treatment. To conclude this part, VSVEB- E_{304}A is more readily cleaved than the WT GP, leading to a more efficient penetration into cells. It is likely that the 'pre-cleavage' of GP_1 in VSVEB-E_{304}A also helps to evade potential inactivation in lysosomes.

Characterisation of the cryptic furin-like cleavage site present in EBOV GP_1 subunit

The GP $E_{304}A$ mutation is located adjacent to the furin-like site of R-K-I-R. After observing virus growth discrepancies that we attribute to an additional furin cleavage at the furin-like site in GP_1, we aimed to generate recombinant VSV with altered furin-like motifs to investigate the correlation between different amounts of GP_1 cleaved and virus infectivity. Furin cleaves proteins downstream of the consensus amino acid sequence R-X-K/R-R (Morikawa et al., 2007). Hence, we produced the following two additional GP mutations: $R_{302}A+E_{304}A$ and $RK_{299}AA$. After constructing these plasmids, we conducted first a transfection experiment to evaluate the cleavability levels of the furin-like motif in GP_1. To do this, we also used previously created plasmids with GP mutations within or in proximity of the site, including $RK_{299}AA+R_{302}A$, $RK_{299}AA+E_{304}A$, $KI_{300}IK$ and $RK_{299}AA+R_{302}A+E_{304}A$ (figure 46).

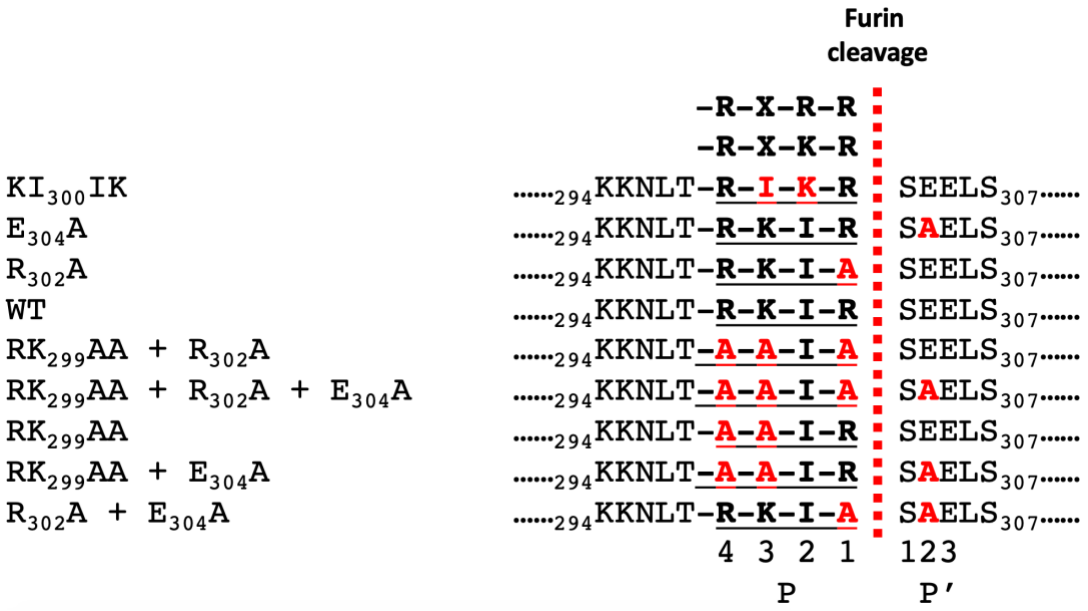

Figure 46. Set of plasmids to study the role of positively charged amino acids in cleavage of EBOV GP_1

The optimal cleavage sites for cellular protease furin (Morikawa et al., 2007) are indicated at the top of the figure. Amino acid positions within the site are labeled as P1, P2, P3 and P4, and amino acids located after cleavage are labeled as P'1, P'2 and P'3. The plasmids were based on phCMV-EBOVGP-WT (WT) and were created using site-directed mutagenesis. The location and mutations are reflected in the names of the plasmids. Furin-like cleavage sites are underlined. Amino acid changes are shown in red. Furin cleavage is shown by the vertical dotted line.

HEK 293T cells were transfected with plasmids encoding the GP mutants mentioned above. After 24 hours, the cells were harvested and the resulting pellets were used for Western blot analysis using anti-GP_1, anti-GP_2, and anti-actin antibodies (Panel A of figure 47). The protein

bands were then quantified using ImageQuant software, and the values were plotted as the ratio of GP_2 to cleaved GP_1, after normalising with their respective actin values (Panel B of figure 47).

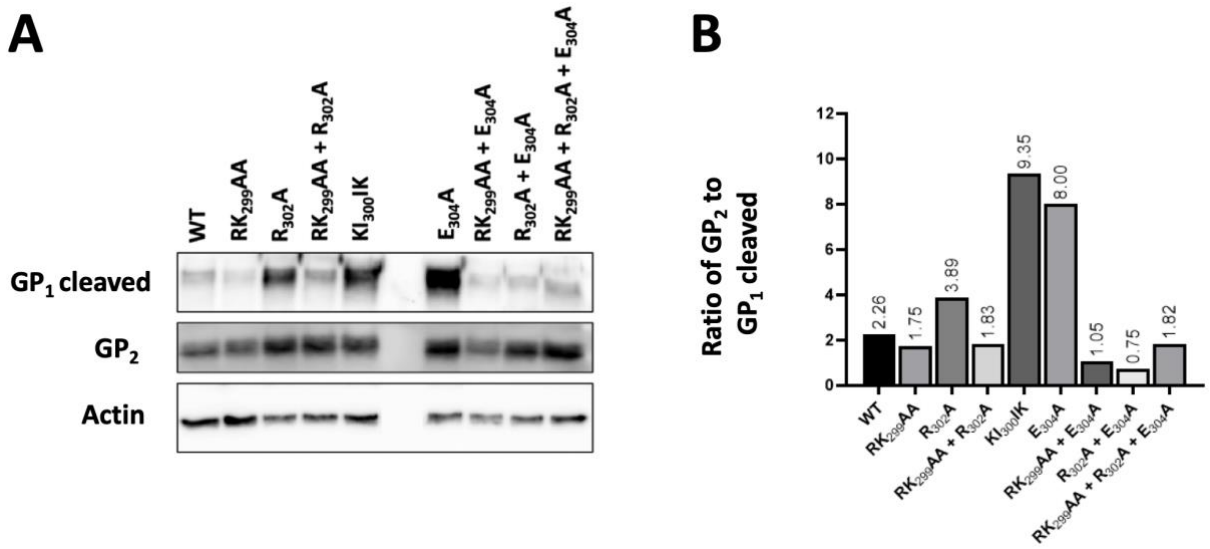

Figure 47. Most mutations that disrupt the furin-like site have a negative impact on the cleavage of EBOV GP_1

HEK 293T cells were transfected with plasmids encoding either WT EBOV GP or various mutants as indicated, including EBOVGP-E_{304}A. Cells were harvested 24 hours after transfection. Panel A: EBOV GP expression was analysed by WT using monoclonal anti-GP_1, polyclonal anti-GP_2 and anti-actin antibodies. Panel B: Protein bands were quantified using ImageQuant software. The graph shows the ratio of GP_1 cleaved to GP_2 after normalisation to the corresponding actin values. Sequence optimisation for the furin site in KI_{300}IK resulted in improved cleavage, which is comparable to the one found in the E_{304}A mutant. Most mutations that disrupt the furin-like site negatively affect the cleavage of EBOV GP_1. An arginine substitution at position 302 showed an unexpected positive effect on GP_1 cleavage. The data presented are representative of three independent experiments.

The results indicate that the KI_{300}IK (RIKR) mutant exhibited the highest degree of GP_1 cleavability, which is consistent with furin's optimal cleavage site of R-X-K/R-R. Additionally, the GP E_{304}A mutant displayed a significant level of cleavability. However, the other GP mutations exhibited considerably lower levels of furin cleavage. Notably, the R_{302}A and RK_{299}AA mutations appeared to reverse the increased GP_1 cleavability observed in E_{304}A, as demonstrated in both RK_{299}AA+E_{304}A and R_{302}A+E_{304}A as well as RK_{299}AA+R_{302}A+E_{304}A mutants.

On the other hand, we were also interested in understanding why VSVEB-WT exhibits far lower levels of cleaved GP_1 compared to VSVEB-E_{304}A, despite the presence of the furin-like cryptic site in both variants. In this regard, (Duckert et al., 2004) have developed a software (Prop method) that allows the prediction of the cleavage site of proprotein convertases, such as

furin. After having used this tool and having input the $GP_{1,2}$ amino acid sequence (figure 48), we can clearly see that both WT and $E_{304}A$ GP reach the threshold of cleavability for their classical furin cleavage site between amino acids 501 and 502. More importantly, while the GP with the $E_{304}A$ mutation reaches again the threshold of cleavability (red box figure 48) at the cryptic site (between amino acids 302 and 303), the WT GP does not.

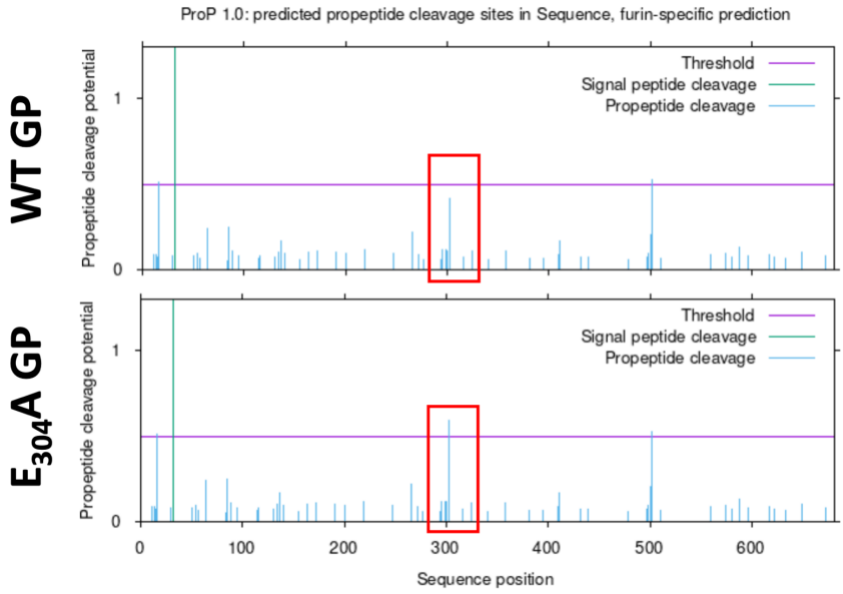

Figure 48 Prediction of furin-specific cleavage sites for the amino acid sequence of $GP_{1,2}$

The entire GP sequence of both WT and $E_{304}A$ was used for this analysis. On the one hand, we can observe that for both cases the threshold of cleavability is reached between amino acids 501 and 502, which is the canonical furin cleavage that results in the formation of the subunits GP_1 and GP_2. On the other hand, and as framed by the red boxes, while the $E_{304}A$ GP reaches again the threshold between amino acids 302 and 303, the WT GP does not. The ProP method is based on furin-specific experimental results from the literature, and a general proprotein convertase-specific network trained on data from protein databases. This method predicts cleavage sites in independent sequences with a sensitivity of 95% for the furin and 62% for the general proprotein convertases. The analysis provides scores between zero and one. For scores above 0.5, ProP method predicts a cleavage event.

Cloning of recombinant VSVEB plasmids with GP mutations at the furin-like cryptic site

To determine whether different amounts of GP_1 cleaved correlate with virus infectivity, we aimed to rescue VSV bearing the 2 following GP mutations: $R_{302}A+E_{304}A$ and $RK_{299}AA$. To accomplish this, we first proceeded with the molecular cloning to generate full-length VSV plasmids containing the targeted GP mutations.

First, to generate PCR fragments carrying each of the three desired GP mutations, we employed mutagenic primers containing *XhoI* and *NheI* enzyme restriction sites at each end. The quality of the resulting PCR products was evaluated visually by running them on a 1% agarose gel (Panel A of figure 49). After purifying the PCR fragments, we subjected both the fragments and the full-length VSV vector, which contains the complete VSV genome except for its G gene, to enzymatic digestion using the same restriction enzymes as before (Panel B of figure 49). This was done to generate sticky ends for subsequent ligation. To avoid plasmid vector recirculation and minimise the background of non-recombinant plasmids during the ligation reaction, the vector fragments underwent an additional dephosphorylation step.

After the ligation reactions were completed, competent E. coli were transformed with the presumptive recombinant plasmids, and the following day, 20 colonies were selected for large-scale growth. Plasmid DNA was extracted from these samples, and after digestion with *XhoI* and *NheI*, the products were analysed on a 1% agarose gel. Out of the 20 analysed plasmids, 6 contained the desired insertions (Panel C of figure 49). Finally, these positive plasmids were sequenced to confirm their mutations and were used to rescue three different mutant viruses.

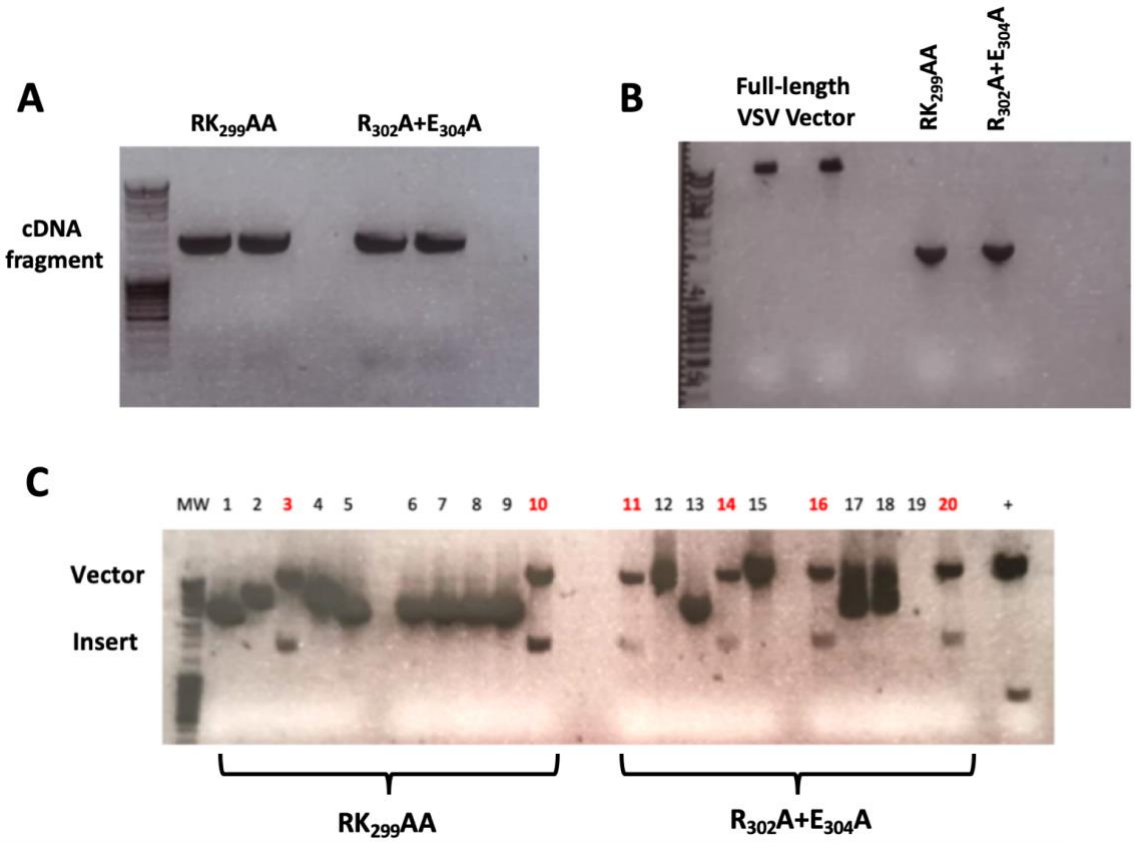

Figure 49. Construction of plasmids carrying the VSV genome in which the authentic G gene has been replaced with a gene encoding the GP of EBOV

Panel A: Electrophoretic migration in agarose gel of cDNA fragments (2400 bp) obtained by PCR. The molecular weight marker is loaded on the left. Two different plasmids containing the substitutions in the furin-like cleavage site, as indicated, were used as templates together with EBOV GP-specific primers complemented with the *XhoI* and *NheI* restriction sites. Panel B: Agarose gel shows semi-quantitative assessment of cDNA fragments and vector plasmid (12kb) after digestion with *XhoI* and *NheI*, and after additional treatment with alkaline phosphatase in case of vector. Panel C: Agarose gel shows the digestion with *XhoI* and *NheI* of recombinant plasmids obtained after ligation of cDNA fragments and vector DNA. Samples marked in red (3, 10, 11, 14, 16 and 20) showed a profile consistent with the desired recombinant plasmids.

BHK-T7 cells were used on the day of transfection. Prior to transfection, the cells were washed and starved for 20 minutes in DMEM 0% FCS. Transfection was then carried out using Fugene6 and support plasmids, including pBS-N, pBS-P, pBS-L, T7, and pVSV-FL, which encodes the entire VSV genome carrying any of the three GP mutants mentioned earlier (figure 50). Of note, we utilised an additional source of T7 RNA polymerase, specifically a support plasmid, to enhance the efficiency of the rescue event. Culture supernatant samples were collected once cytopathic effects were observed, and to confirm the recovery of infectious viruses, these samples were subsequently passed in Vero E6 cells.

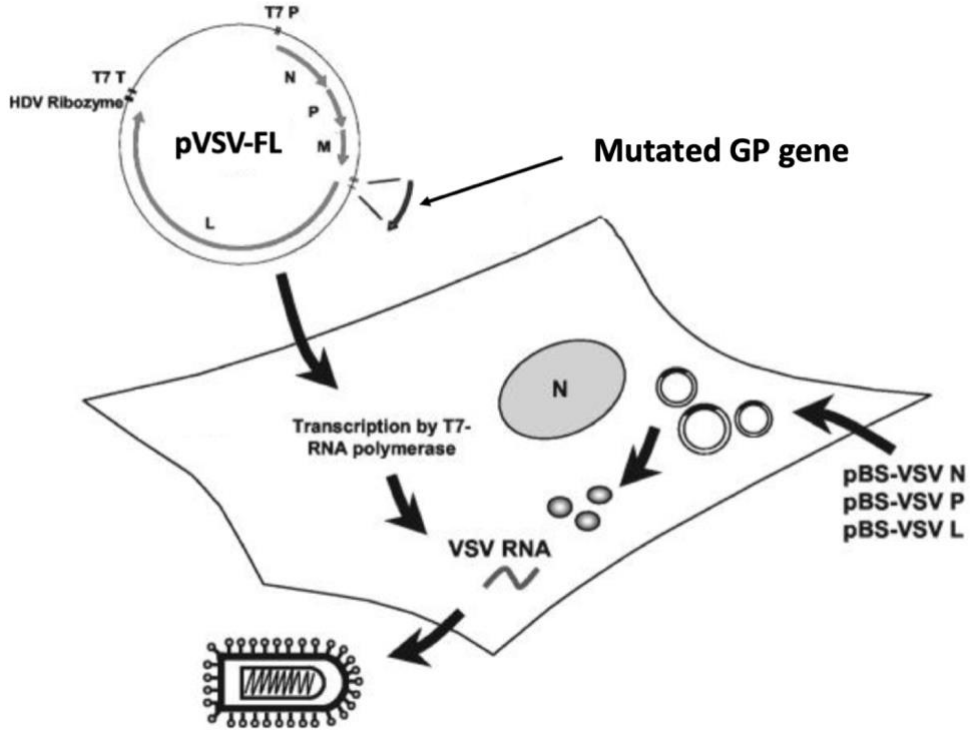

Figure 50. Schematic representation of the generation of recombinant VSV using a reverse genetics system

BHK T7 cells, stably expressing T7 polymerase, were co-transfected with a plasmid carrying the VSV genome and three plasmids expressing the VSV viral proteins N, P and L. All plasmids contain bacteriophage T7 promoter which allows RNA synthesis from DNA template. In the case of pVSV-FL, the transcription of the genomic RNA is terminated at the sequence encoding the T7 transcription termination site and its correct 3'-terminus is formed after auto cleavage by the Hepatitis Delta Virus ribozyme. Reproduced from (Garbutt et al., 2004).

Comparative analysis of rescued VSV with GP mutations at the furin-like cryptic site

Once the viruses were successfully rescued, virus stocks were produced in Vero E6 cells. The GP gene of each virus was then sequenced to confirm the presence of the respective mutations (figure 51). Furthermore, a comprehensive sequence analysis of the GP gene of these four viruses was carried out to rule out the existence of any additional mutations.

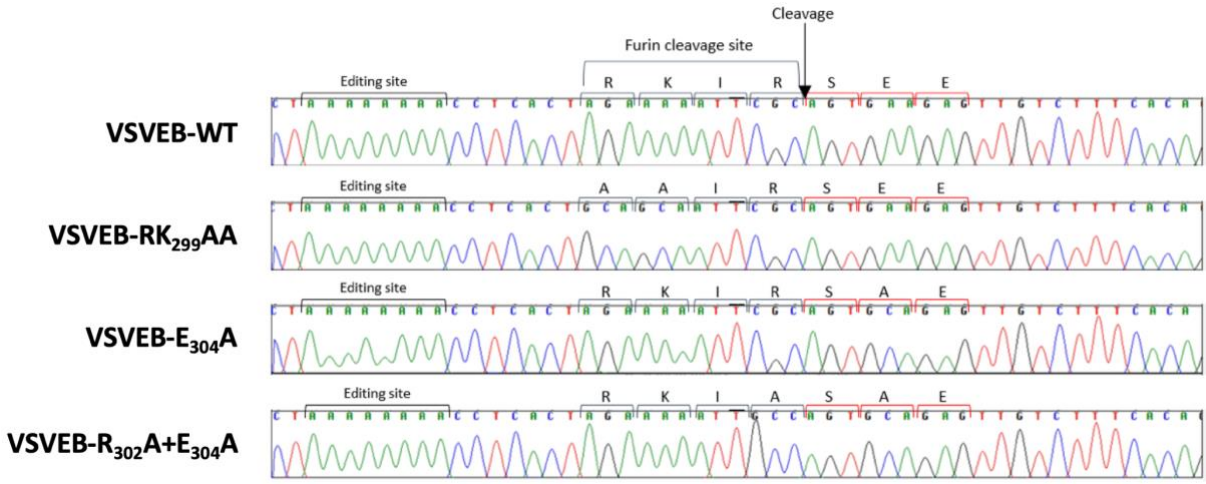

Figure 51. Confirmation of GP mutations present in rescued recombinant VSV

Viral RNA was isolated from virus stocks obtained after two passages in Vero E6 cells. The cDNA fragments were generated by RT-PCR on viral RNA using VSV-specific primers flanking the EBOV GP gene. The cDNA fragments were sequenced and the data obtained were analysed using Sequencher software. Mutations introduced into the furin-like site and amino acid substitutions are shown for each mutant compared to the EBOV WT sequence. The GP editing site of EBOV is also shown. In all cases it contains 8 adenosine residues and thus encodes a full-length GP without the need for editing.

Titration of these four viruses was performed using $TCID_{50}$ assays, which yielded the following titres in $TCID_{50}$ per mL: VSVEB-WT (7.5×10^6), VSVEB-$E_{304}A$ (5×10^7), VSVEB-$R_{302}A$+$E_{304}A$ (1.2×10^7), and VSVEB-$RK_{299}AA$ (7.5×10^6). Additionally, the virus-specific cDNA copies per mL were determined using 2-step RT-qPCR and the following titres were obtained: VSVEB-WT (7.8×10^7), VSVEB-$E_{304}A$ (5.7×10^7), VSVEB-$R_{302}A$+$E_{304}A$ (1.3×10^8), and VSVEB-$RK_{299}AA$ (9.3×10^7). Using these values, we calculated the infectivity as the ratio of cDNA copies per mL to $TCID_{50}$ per mL, and obtained the following values: 10.4 (VSVEB-WT), 1.13 (VSVEB-$E_{304}A$), 10.2 (VSVEB-$R_{302}A$+$E_{304}A$), and 12.4 (VSVEB-$RK_{299}AA$). Remarkably, when the infectivity value of VSVEB-WT is set to 1, the relative infectivity of VSVEB-$E_{304}A$ increases by a factor of 10.86. However, the differences in relative infectivity are marginal for VSVEB-$R_{302}A$+$E_{304}A$ and VSVEB-$RK_{299}AA$, with values of 0.98 and 1.19, respectively.

To confirm if the viruses displayed the same cleavability differences observed in transfected cells (see figure 47), we infected Vero E6 cells with VSV-derived recombinant viruses at an equal MOI of 0.05. After 48 hours, we collected culture supernatant samples and performed Western blot assay using anti-GP_1 and anti-VSV-M monoclonal antibodies (Panel A of figure 52). We used ImageQuant software to quantify the protein bands, and the values for GP_1 and GP_1 cleaved were normalised by the corresponding VSV-M values. After adding the values together to calculate 100% GP_1 expression, we plotted the percentage of GP_1 cleaved for each virus (see Panel B of figure 52). Our findings revealed that VSVEB-E_{304}A had the highest percentage of cleaved protein, followed by VSVEB-R_{302}A+E_{304}A, which was significantly lower. Notably, the R_{302}A mutation resulted in a significant loss of GP_1 cleavability. In contrast, VSVEB-WT and VSVEB-RK_{299}AA showed only marginal differences. Interestingly, these results are consistent with the infectivity values of the virus stocks.

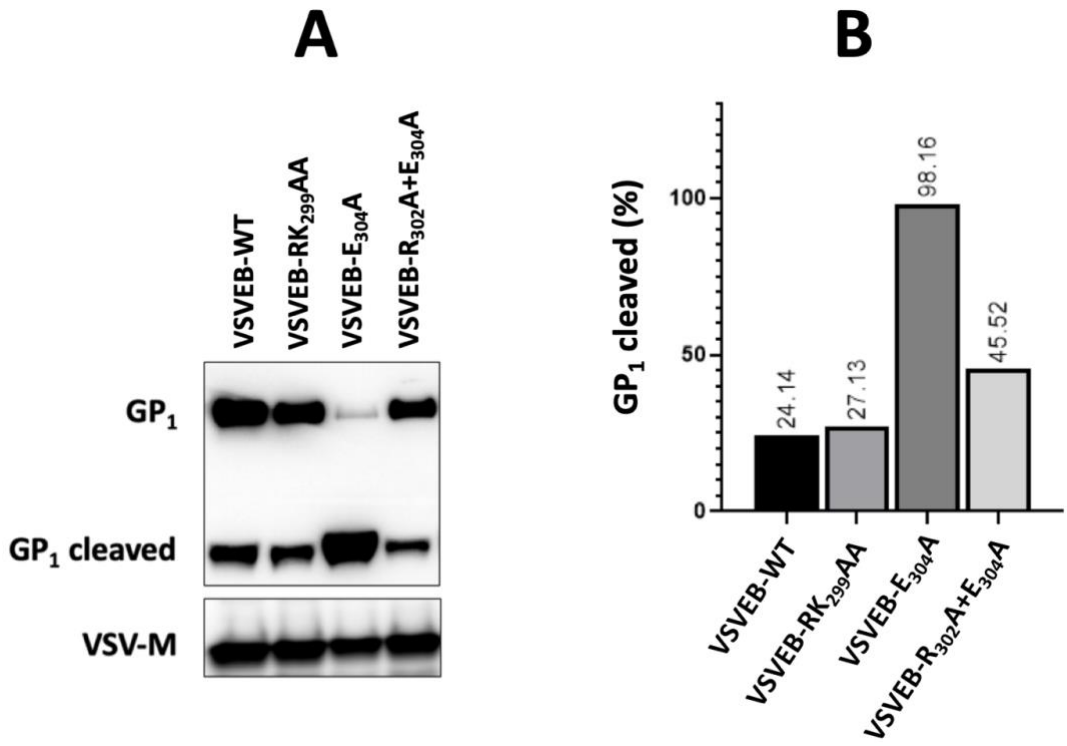

Figure 52. An arginine substitution at position 302 disrupts the sequence of furin-like site and dramatically reduces the cleavage of GP_1 in VSVEB-R_{302}A+E_{304}A

Panel A: Vero E6 cells were infected with VSV-derived recombinant viruses at an equal MOI of 0.05. Culture supernatant samples were collected 48 hours after infection and analysed by WB using anti-GP_1 and anti-VSV-M monoclonal antibodies. The specificity of the protein bands is indicated. Panel B: Protein bands were quantified using ImageQuant software, and the values obtained for GP_1 and GP_1 cleaved were normalised by the corresponding VSV-M values and then summed to calculate 100% GP_1 expression. The graph shows the percentage of GP_1 cleaved in relation to the total number of GP_1-related proteins present in virions. The data presented are representative of three independent experiments.

To further confirm our findings, we performed virus plaque assays using the VSV-derived recombinant viruses. Vero E6 cells were infected with virus dilutions containing roughly equal quantities of PFU, as previously described. After the plates were fixed and stained with crystal violet, the surface area of each plaque was calculated using ImageJ software and these data were used for statistical analysis (figure 53).

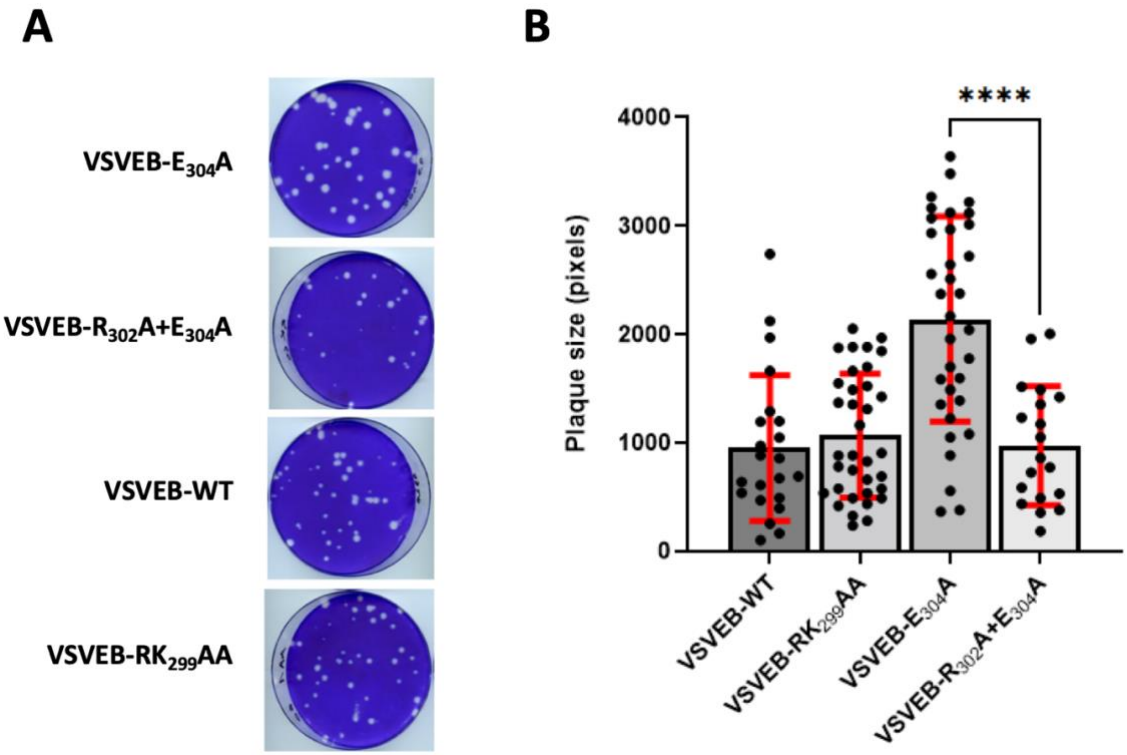

Figure 53. Mutation disrupting the furin-like site leads to a reduction in the virus plaque size

Panel A: Vero E6 cells were infected with the indicated viruses. After infection, cells were washed once and then covered with DMEM 3% FSC supplemented with 0.8% Avicel. The cells were fixed and stained with crystal violet 72 hours after infection. Panel B: Viral plaques were measured using ImageJ software. The graph shows the values obtained for approximately 25 number of plaques of each virus, and the error bars on the graph represent the standard deviation of the measured values. Mutation disrupting the consensus sequence of the furin-like site in VSVEB-$RK_{299}AA$ has no significant effect on virus plaque size when compared to VSVEB-WT. However, there is a high statistical significance between VSVEB-$E_{304}A$ and VSVEB-$R_{302}A+E_{304}A$, as accounted by a two-tailed t-test, with a p-value of less than 0.0001 (****$p<0.0001$).

This virus plaque assay provides evidence that the $E_{304}A$ mutation in the GP of VSVEB is associated with larger virus plaques, while disruptions in the furin-like cleavage site (RKIR) lead to a similar plaque size compared to VSVEB-WT. In this regard, the virus plaque size of VSVEB-$R_{302}A+E_{304}A$, despite possessing the $E_{304}A$ mutation, shows only a slight difference

compared to those of VSVEB-RK$_{299}$AA and VSVEB-WT. Furthermore, when comparing VSVEB-R$_{302}$A+E$_{304}$A to VSVEB-E$_{304}$A, our data reveal a very high significant statistical difference in the size of virus plaques.

Finally, since our evaluation of infectivity of these rescued recombinant VSV was based on a single time point collection (production of stocks at 44 hours post infection), we sought to examine the performance of these viruses over a longer period of time. To this end, we conducted a low MOI (0.0004) infection and collected culture supernatant samples at various time points to determine TCID$_{50}$ titres and the number of cDNA copies (figure 54).

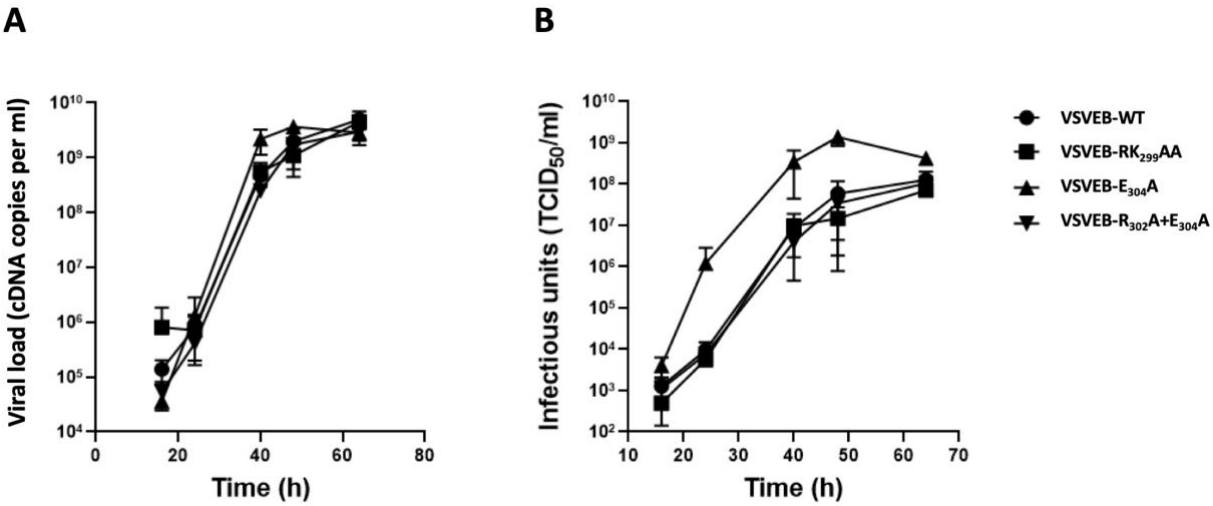

Figure 54. Mutation that disrupts the furin-like site in VSVEB-R$_{302}$A+E$_{304}$A eliminates the growth benefits provided by the E$_{304}$A substitution in VSVEB-E$_{304}$A

Vero E6 cells were infected with indicated viruses at an equal MOI (0.0004). Panels A and B display the results of virus titration of culture medium samples by RTqPCR and TCID$_{50}$ respectively. A mutation that disrupts the consensus sequence of furin-like site in VSVEB-R$_{302}$A+E$_{304}$A eliminates the growth benefits provided by the substitution E$_{304}$A in VSVEB-E$_{304}$A. On the contrary, mutation disrupting the consensus sequence of the furin-like site in VSVEB-RK$_{299}$AA has no significant effect on virus growth compared to VSVEB-WT. Presented data are representative of three independent experiments, and error bars on the graph represent the standard deviation of the measured values.

Our TCID$_{50}$ titre results confirm the clear growth advantages of VSVEB-E$_{304}$A, which distinguishes it from the other three recombinant VSV. In addition, our results provide further support for the idea that the growth advantages resulting from the E$_{304}$A mutation are lost by the R$_{302}$A GP mutation, as demonstrated by the nearly identical TCID$_{50}$ and cDNA values observed for VSVEB-R$_{302}$A+E$_{304}$A and both VSVEB-WT and VSVEB-RK$_{299}$AA. Furthermore, we calculated the infectivity parameter by dividing the cDNA per mL by the TCID$_{50}$ per mL titres, and to more accurately present the differences between the viruses, we

normalised the values obtained for all viruses by using the VSVEB-WT values as a reference (Panel A of figure 55). Our infectivity analysis confirmed that VSVEB-E_{304}A has a sustained and superior infectivity compared to the other rescued viruses. VSVEB-R_{302}A+E_{304}A comes in second place, but its infectivity value is marginally different from the other two recombinant VSV. This reinforces the notion that the R_{302}A mutation reverts the effects of the E_{304}A mutation. Panel B of figure 55 shows that the same trend in infectivity can be observed on Western blot analysis, where an equal number of infectious units (1.5E+05 $TCID_{50}$) were loaded per lane. Since VSV-M provides a relative comparison of viral particles, the differences in the amount amongst these recombinant VSV can confirm the notion of increased infectivity of VSVEB-E_{304}A, in that there are fewer viral particles of the latter for the same $TCID_{50}$ titre. Similarly, the deleterious effect of the R_{302}A GP mutation on infectivity can also be observed since there is an equal amount of VSV-M for both the mutant and the other two viruses: VSVEB-WT and VSVEB-RK_{299}AA.

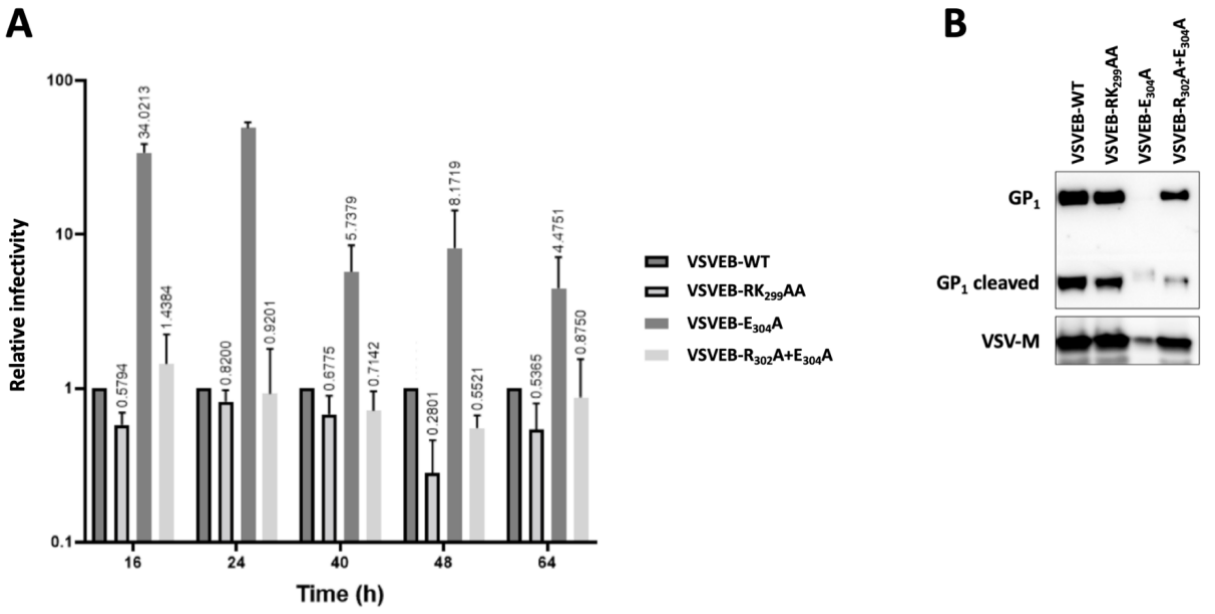

Figure 55. Mutations that disrupt the consensus sequence of the furin-like site result in reduced infectivity of the virus

Panel A: The infectivity of the viruses during the course of experiment (see figure 54) was calculated as the ratio of the number of cDNA copies to the number of infectious units and then normalised to the values obtained for VSVEB-WT. The graph plots the difference in infectivity between the viruses. Data are representative of three independent experiments, and error bars on the graph represent the standard deviation of the measured values. Panel B: Vero E6 cells were infected with indicated recombinant VSV viruses at an equal MOI of 0.05. Samples of the culture supernatant were collected 48 hours after infection and analysed by WB using anti-GP_1 and anti-VSV-M monoclonal antibodies. The specificity of the protein bands was shown. Equal numbers of infectious units (1.5E+05) measured in $TCID_{50}$ were loaded onto each lane for each virus. VSVEB-E_{304}A showed the lowest number of viral proteins, indicating its highest infectivity. The data presented are representative of three independent experiments.

To minimise biological risks and accelerate the pace of our research, we first opted to use the recombinant VSV surrogate system instead of Ebola viruses. However, having obtained sufficient data to confirm the effects of the $E_{304}A$ GP mutation on virus growth, infectivity, and larger size of virus plaques, we decided to conduct research on Ebola Zaire viruses in BSL4 settings to validate these observations. Thus, recombinant Ebola viruses with either the WT GP or the $E_{304}A$ GP mutation were created, as described in figure 56.

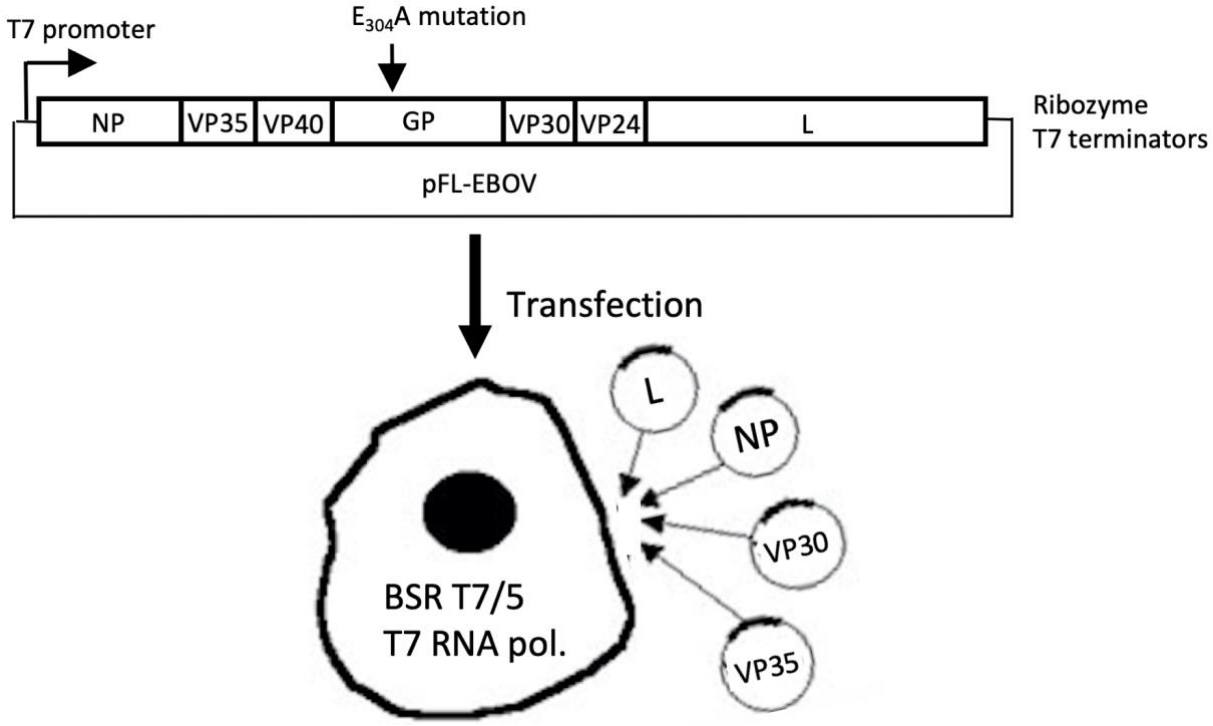

Figure 56 Schematic representation of the generation of recombinant EBOV using a reverse genetics system

BSR T7 /5 cells, stably expressing T7 polymerase, were co-transfected with a plasmid carrying the EBOV genome and four plasmids expressing the EBOV viral proteins L, NP, VP30 and VP35. All plasmids contain bacteriophage T7 promoter which allows RNA synthesis from DNA template. In the case of pFL-EBOV, the transcription of the genomic RNA is terminated at the sequence encoding the T7 transcription termination site and its correct 3'-terminus is formed after auto cleavage by the Hepatitis Delta Virus ribozyme. Adapted from (Volchkov et al., 2001).

Comparative study of EBOV-WT and EBOV-$E_{304}A$

We began therefore by growing and characterising the recombinant EBOV bearing either WT GP (EBOV-WT) or the $E_{304}A$ GP mutation (EBOV-$E_{304}A$). For this purpose, we first quantified cDNA copies per mL via RTqPCR and titrated these stocks to determine the number of PFU per mL. Using these values, we calculated the infectivity of each virus as previously defined. Our results, summarised in Figure 57, confirmed that EBOV-$E_{304}A$ is 9.52 times more infectious than EBOV-WT.

	cDNA copies	PFU	Infectivity
EBOV-WT	1.20×10^8	1.20×10^5	1000
EBOV-$E_{304}A$	2.10×10^7	2.00×10^5	105

$$\text{“}Infectivity\text{”} = \frac{cDNA\ copies}{PFU}$$

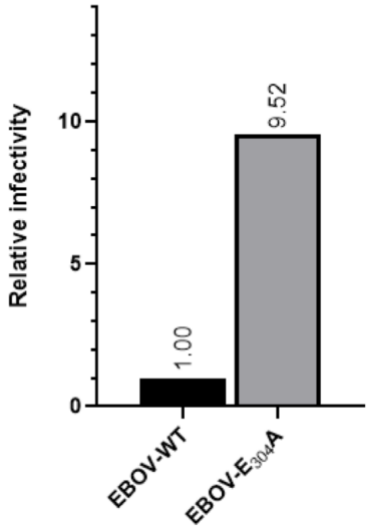

Figure 57. EBOV-$E_{304}A$ is more infectious than EBOV-WT

Virus infectious titres were estimated by virus plaque assay and indicated as PFU/ml. The virus titres (as physical particles) were assessed via RTqPCR and indicated as cDNA copies/mL. It should be noted that the methodology used in this study does not allow the direct quantification of viral genome copies, since it does not reflect the efficiency of the reverse transcription during cDNA construction nor the efficiency of RNA extraction. For that reason, we labelled and defined “infectivity” as the ratio of cDNA copies over the infectious units. The bottom graph plots the difference between EBOV-$E_{304}A$ and EBOV-WT in “infectivity”, considering that the EBOV-WT has an adjusted value of 1. Data shown are representative of three independent experiments.

After confirming the higher infectivity of EBOV-$E_{304}A$, we were interested in examining the protein profiles of GP for both viruses. Although at first glance, Panel A of figure 58 indicated that there was similar GP_1 cleavage in both EBOV-WT and EBOV-$E_{304}A$, the 55kDa band was an accumulation of EBOV sGP and GP_1 cleaved. In this regard, as previously discussed in the GP editing section, EBOV has a GP expression ratio of 71:24:5 for sGP, GP_1, and ssGP, respectively (De La Vega et al., 2015). Additionally, the molecular weight of monomeric sGP

is very similar to that of the GP_1 cleaved product, which is 55 kDa (Zhu et al., 2019). In this context, we resorted therefore to concentrating and purifying these two viruses. To achieve this, we employed a single round of ultracentrifugation with a 20% sucrose cushion. Our aim was to isolate the soluble GP in the culture supernatant after ultracentrifugation, while simultaneously verifying the presence of the GP_1 cleaved product in the resuspended virus pellets, as shown in Panels B and C of figure 58.

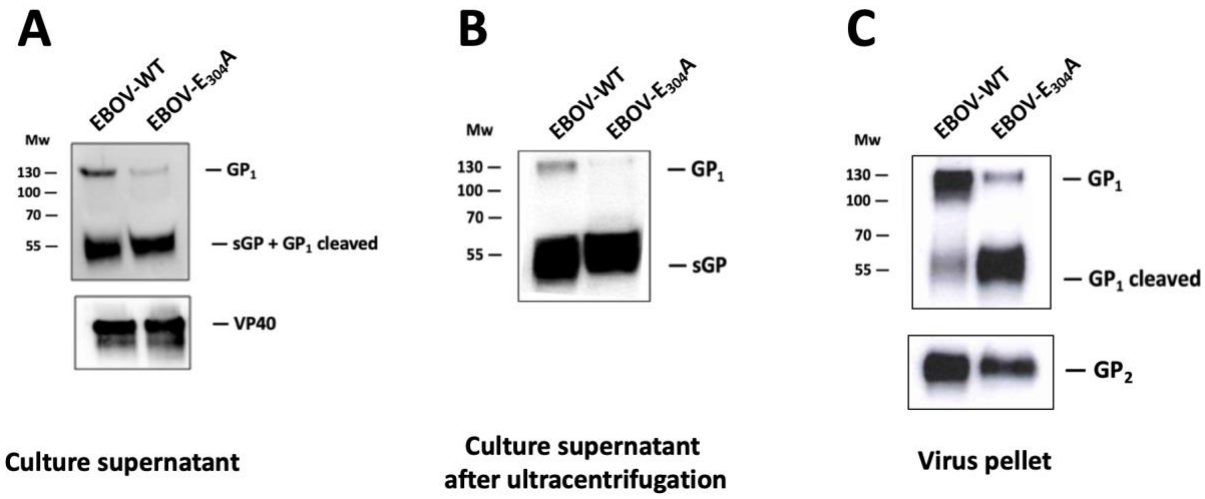

Figure 58. The recombinant EBOV carrying the $E_{304}A$ mutation showed the same GP_1 cleavage profile as did the recombinant VSVEB- $E_{304}A$

Vero E6 cells were infected with either EBOV-WT or EBOV-$E_{304}A$ at equal MOI of 0.01. Culture supernatants were collected 7 days post infection, and then subjected to ultracentrifugation through 20% sucrose cushion. Samples of culture supernatants (Panel A), ultrasupernatants (Panel B) and virus pellet (Panel C) were analysed by WB using polyclonal anti-GP_1, anti-VP40 and anti GP_2 antibodies. It is worth noting that the molecular weight of cleaved GP_1 is very similar to that of sGP secreted in high quantities into the culture medium of EBOV-infected cells (~ 55 kDa). After sedimentation of the virus by ultracentrifugation soluble sGP was separated from virions fraction. Virions of recombinant EBOV carrying the $E_{304}A$ mutation showed the same GP_1 cleavage profile as did the recombinant VSVEB- $E_{304}A$ (Panel B of figure 32). Approximately the same amounts of GP_2 were found in samples of virus pellets. Quantification was performed using ImageQuant software. Data shown are representative of two independent experiments.

By excluding sGP from the culture supernatant following ultracentrifugation (Panel B of figure 58), we were able to exclusively observe the cleaved product of GP_1 (as depicted in panel C of figure 58) in the virus pellet samples. Our results confirmed that there is indeed an inverted ratio of GP protein profile between EBOV-WT and EBOV-$E_{304}A$. Additionally, our findings suggest that the mucin-like domain is not present in the virus particles of EBOV-$E_{304}A$, given that the cleavage at the cryptic furin-like site is confirmed in EBOV GP.

We also sought to investigate whether there were differences in virus plaque size between EBOV-WT and EBOV-$E_{304}A$. As previously mentioned in the introduction, continuous passage

of EBOV in cell culture (for at least 5 passages in Vero E6 cells) results in the 7U GP editing site being predominantly converted to 8U. This shift in editing site leads to increased production of $GP_{1,2}$ and decreased production of sGP, resulting in higher cytotoxicity and larger virus plaques than those produced by the wild type EBOV 7U variant (Hume & Mühlberger, 2019; Reynard & Volchkov, 2015). To confirm the absence of 8U in the GP editing site, we first sequenced EBOV-WT and EBOV-E_{304}A (Panel A of figure 59). With that possibility excluded, we conducted virus plaque assays to compare the size of viral plaques between the recombinant EBOV. Vero E6 cells were infected with virus dilutions containing roughly equal quantities of PFU, and the resulting plaques were fixed and immunostained with anti-VP40 and anti-NP antibodies (Panel B of figure 59). The surface area of each plaque was calculated using ImageJ software and these data used for statistical analysis (Panel B of figure 59).

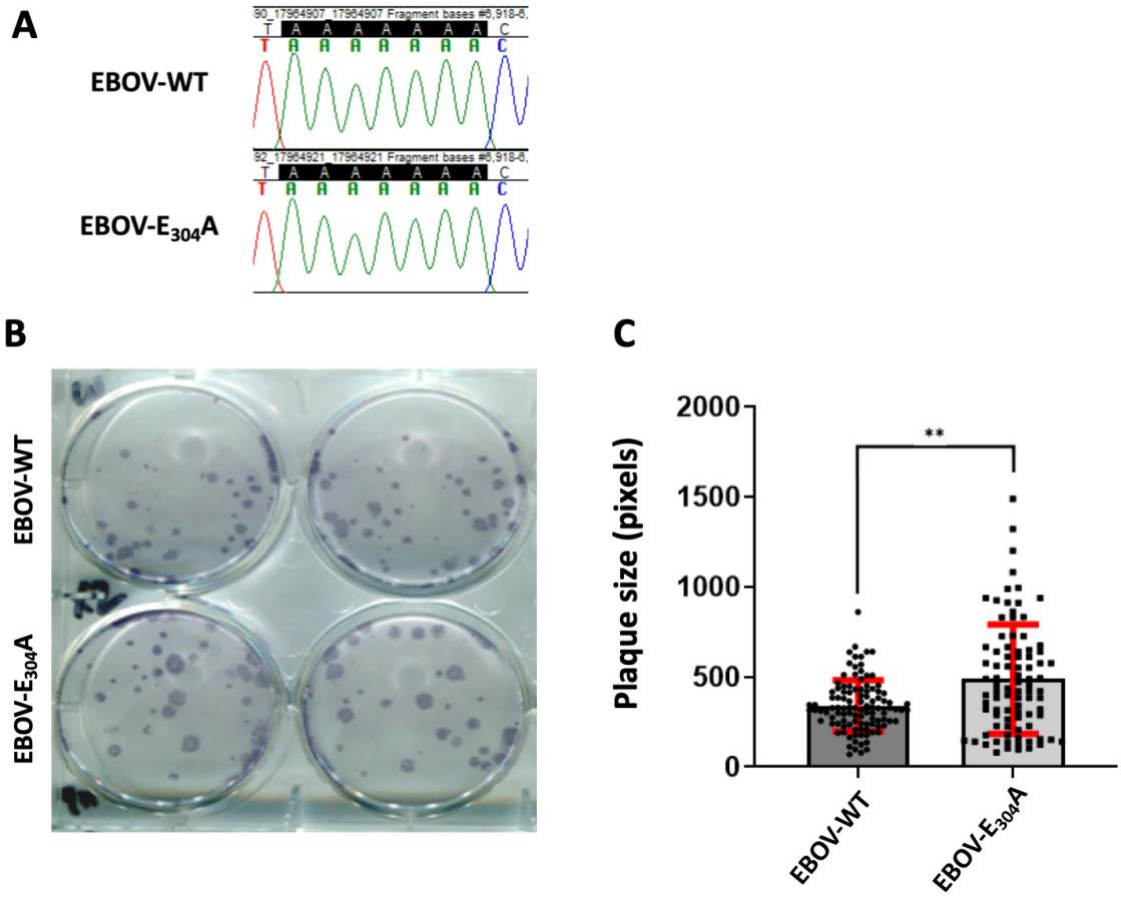

Figure 59. Both recombinant EBOVs showed heterogeneity in the size of the viral plaques. Compared with EBOV-WT, the plaques created by EBOV-E_{304}A are larger

Vero E6 cells were infected with either EBOV-WT or EBOV-E_{304}A, and then overplayed with DMEM 3% FCS supplemented with 0.8% Avicel. After seven days, cells were fixed and immunostained with anti-NP and anti-VP40 antibodies. A representative image of the plaques for each virus is shown in panel A. Panel B: ImageJ software was used to measure and compare the size of plaques. Data are representative of three independent experiments, and error bars on the graph represent the standard deviation of the measured values. Approximately

40 plaques for each virus were randomly taken for analysis. The statistical significance was determined using a two-tailed t-test. In this case, the difference between EBOV-E_{304}A and EBOV-WT was found to be statistically significant, with a p-value of less than 0.01 (**$p<0.01$). Panel C: cDNA fragments were generated by RT-PCR on viral RNA using primers flanking the EBOV GP gene. The cDNA fragments were sequenced and the data obtained were analysed using Sequencher software. The GP editing site of both EBOV-WT and EBOV-E_{304}A are shown and they contain 7 adenosine residues.

Our results demonstrate that although viral plaques vary in size, those produced by the EBOV-E_{304}A virus are, on average, 1.6 times larger than those produced by the EBOV-WT virus. This supports previous experiments indicating that the E_{304}A GP mutation makes the virus more infectious.

Comparative study of virus growth between EBOV-WT and EBOV-$E_{304}A$

Given the EBOV-$E_{304}A$'s demonstrated higher infectivity, larger virus plaques, and different GP cleavage pattern, we sought to determine if this mutant would also sustain its increased infectivity over time, as observed in the VSV surrogate system. To this end, we conducted a virus growth kinetics experiment (figure 60) whereby Vero E6 cells were infected with either EBOV-WT or EBOV-$E_{304}A$ at a low MOI of 0.004. We sampled culture supernatant to determine PFU titres and viral cDNA copies per mL via RTqPCR. Additionally, we titrated inoculum samples of both viruses within the same hour in which this experiment began to attempt to ensure that it started with an equal dose of infectious units.

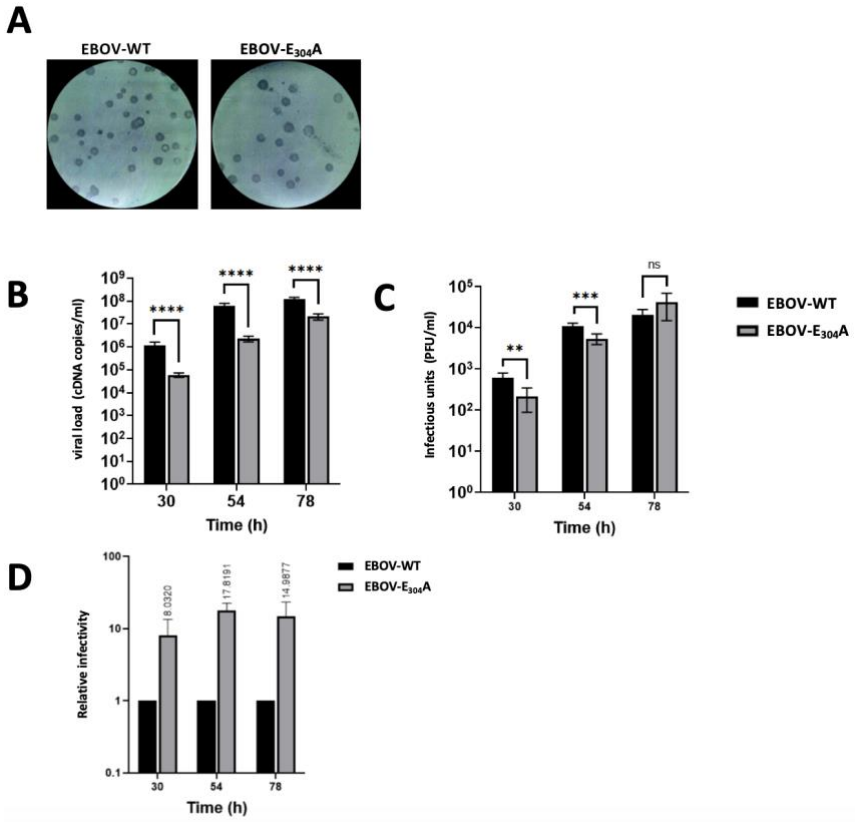

Figure 60. Despite higher infectivity, EBOV-$E_{304}A$ showed no growth advantages over EBOV-WT

Vero E6 cells were infected with either EBOV- WT or EBOV-$E_{304}A$ at an equal MOI (0.004). Samples of culture medium were collected at different intervals post infection and the virus titres were determined by plaque assay and RTqPCR analysis. Panel A: The results of the inoculum titration by plaque assay. Inoculum samples were diluted 1:100. Panels B and C: The figures show the results of virus titration by RTqPCR and plaque assay in samples collected during virus growth experiment. Panel D: The graph plots the relative infectivity of EBOV-$E_{304}A$ compared to EBOV- WT, considering the adjusted infectivity value of the latter as 1. The infectivity value was calculated as the ratio of cDNA copies over the infectious units. Data are representative of three independent experiments, and error bars on the graph represent the standard deviation of the measured values. The statistical significance was determined using a two-tailed t-test.

While viruses with the $E_{304}A$ GP mutation exhibited growth advantages in recombinant VSV growth kinetics, such as an average of 12.89-fold increase in virus titres and a 6.25-fold higher infectivity, our results with recombinant EBOV growth kinetics were less conclusive. Specifically, EBOV-WT produced more PFU per mL at 30 and 54 hours post-infection, but was surpassed by EBOV-$E_{304}A$ at 78 hours post-infection. On the other hand, EBOV-WT showed superior titres of viral cDNA copies per ml at all times. Interestingly, our infectivity values revealed that EBOV-$E_{304}A$ was still significantly more infectious than EBOV-WT, exhibiting infectivity values 13.6 times higher than the latter. Lastly, it is important to note that our inoculum titrations revealed a slightly more than a 2-fold difference in their PFU/mL titres (EBOV-WT: 5.8×10^3, EBOV-$E_{304}A$: 2.7×10^3). In this regard, although EBOV-$E_{304}A$ started the growth kinetics with less infectious units, its infectivity is consistently higher through the experiment.

Discussion and perspectives

The EBOV surface glycoprotein GP triggers and enables virus entry into the host cell via a complex mechanism that, as of now, is only partially understood (Martin et al., 2016). The attachment is the first step that happens upon EBOV first contact with its target cell. This stage is mediated by GP_1, and so far numerous cellular attachment factors have been identified, such as TAM, TIM1, lectins and glycosaminoglycans (Jain et al., 2021; Takada et al., 2004). Following attachment, EBOV is first internalised by macropinocytosis vesicles (Saeed et al., 2010), which are then routed to endosomal vesicles of the host cell, where proteolytic events occur to cleave $GP_{1,2}$ (Chandran et al., 2005). Under acidic pH and reducing conditions cellular cathepsins B and L remove a part of GP_1 (Bale et al., 2011), which leads to exposing GP_1 receptor binding domain that interacts with the cellular endosomal cholesterol transporter Niemann-Pick C1 (NPC1) (Kuroda et al., 2015). The binding of these two structures facilitate membrane fusion by reducing steric barriers to GP_2 rearrangement and membrane association, culminating thus in the release of the replication complex to the cytoplasm.

After drug screen work, our team identified Poly(sodium 4-styrenesulphonate) (PSS), as a poly-anionic compound that blocked drastically EBOV infection in cells. Further experiments with serial passages of PSS revealed viruses that bore a single mutation in their GP gene (GP Zaire $E_{304}A$ mutation), resulting in a partial resistance towards said inhibitor drug. Having thus two distinct viruses: VSVEB-WT and VSVEB-$E_{304}A$, we first assessed differences in their replication in the absence of PSS. Interestingly, we found that VSVEB-$E_{304}A$ has in average 7.5 times more $TCID_{50}$ titres than the VSVEB-WT. While the growth advantages of the $E_{304}A$ GP mutation-carrying virus in the absence of PSS were unexpected, it is not unheard of for viruses to gain infectivity following single amino acid mutation(s). For instance, a single point mutation ($I_{414}T$) in the viral protein E2 of the Hepatitis C virus has been shown to enhance the production of infectious viral particles by a factor of 5 (Tao et al., 2009). Similarly, studies on the Human metapneumovirus (hMPV) have revealed that a single-point mutation ($S_{101}P$) in the putative cleavage site of the viral fusion protein, resulted in the capacity of this virus to grow in Vero cells without the addition of trypsin, as otherwise hMPV would grow very poorly and with minimal cytopathic effects (Biacchesi et al., 2006; Schickli et al., 2005).

In terms of single-point mutations in viral glycoproteins, a 2021 study addressing SARS-CoV-2 variants of concern demonstrated that a substitution $S_{655}Y$, represented in the gamma and omicron strains, increased furin cleavage by more than 50% (compared to WT), and enhanced viral replication (Escalera et al., 2022). Likewise, a study on the hemagglutinin protein of Avian Influenza A viruses of the H7 subtype (Dreier et al., 2019) revealed that mutations in this viral protein increased the pathogenicity in mice in at least three times more than the parental virus. Of note, these last two viruses are particular in that they require a cleavage of their surface viral proteins to proceed with their infectious cycle. Similar cleavage-dependent viruses include Paramyxoviruses (Diederich et al., 2009) and the Ebola virus. In this context, we decided to address therefore GP protein profiles, as it could be plausible that a single-point mutation could either create a new cleavage site or affect one that already exists, and this could thus have either a detrimental or incremental effect on the proteolytic event, ultimately affecting the virus' ability to infect host cells.

As previously mentioned, during the synthesis of the EBOV GP, $GP_{1,2}$ is translated in the Golgi apparatus, where it is subjected to a proteolytic cleavage by the cellular protease furin. This cleavage process results in the formation of two GP subunits, namely GP_1 and GP_2, which are held together by a disulphide bond (Jain et al., 2021). This proteolytic cleavage by furin is an essential step in EBOV's infectious cycle because it transforms GP into its trimeric mature form, known as the spike protein $GP_{1,2}$, located on the surface of the virus (Bale et al., 2011). However, in addition to this canonical furin cleavage, we found evidence of a secondary furin-like cleavage site that is extensively cleaved in the case of VSVEB-E_{304}A, while it is only marginally cleaved by VSVEB-WT. We observed that the secondary furin-like cleavage in the GP_1 subunit not only resulted in the production of a GP_1 cleaved fragment, but also of a 75-100 kDa fragment corresponding to the Mucin-like domain (MLD). Once cleaved, the GP_1 cleaved fragment remains bound to the GP_2 by the disulphide bond, while the MLD appears to be lost into the supernatant after cleavage, as it is not part of the virus particle.

It is important to note that the MLD is a highly glycosylated region spanning EBOV GP_1 residues 313 to 501 (Tran et al., 2014). When EBOV viral particles internalise into cells, they are enclosed in endosomal vesicles where proteolytic events occur (Martin et al., 2016), leading to the removal of the MLD (Bale et al., 2011) (figure 61). This step is important because it exposes the receptor binding domain (RBD), which interacts with the cellular endosomal cholesterol transporter Niemann-Pick C1 (NPC1) (Kuroda et al., 2015), allowing membrane

fusion and the release of the replication complex to the cytoplasm. In this regard, the presence of this additional cleavage and the resulting loss of the Mucin-like domain can have implications for viral pathogenesis and could potentially affect the virus-host interactions. For instance, although the mucin-like domain is not directly implicated in virus entry, it does occlude the receptor-binding region that triggers the virus fusion stage (Martinez et al., 2011), potentially serving as a protection from antibody recognition (Lennemann et al., 2014).

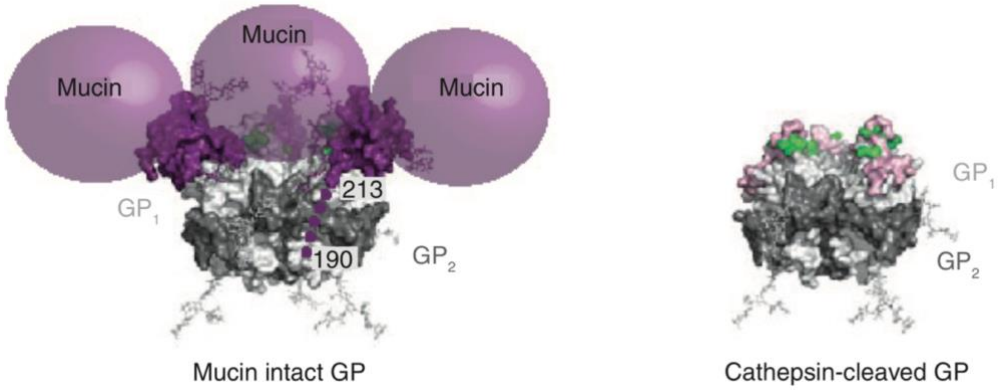

Figure 61 Zaire Ebolavirus GP cathepsin cleavage

Adapted from (J. E. Lee & Saphire, 2009). Left picture displays the trimeric GP spike before the cathepsin cleavage (and thus with the MLD), while the right picture illustrates the GP structure after this proteolytic event.

Moreover, the MLD has been implicated as a major determinant of vascular injury (Yang et al., 2000), and its presence has been shown to obstruct the access of crucial surface-cell molecules. For instance, the recognition of β1 integrins and MHC-1 by CD8 T cells is obstructed due to steric hindrance caused by the MLD. As a consequence of obstructing surface-cell molecules, the presence of the MLD can result in a reduction of the immune response against cells expressing GP that bear this domain (Reynard et al., 2009a). Moreover, the MLD has been shown to induce cell rounding and loss of adhesion (Francica et al., 2009). In addition to its other roles, the MLD has been linked as an element of viral attachment (Tran et al., 2014). For example, the MLD is important in the interaction of GP with human macrophage galactose-specific and N-acetylgalactosamine-specific C-type lectin (hMGL), which promotes EBOV infection in these primary and early cell targets (Takada et al., 2004). Lastly, the presence of this domain has also been correlated with an ability to alter cellular signalling (Zampieri et al., 2007), such as cytokine secretion from stimulated dendritic cells (Martinez et al., 2007). Although the loss of the MLD in an immunocompetent organism may initially seem

disadvantageous to the virus, our findings at the cellular level suggest that VSVEB lacking this domain (mostly with the GP E_{304}A mutation) exhibit growth advantages over the VSVEB-WT. We decided to confirm the growth differences through the calculation of infectivity, as we had defined it: the ratio of virus-specific cDNA copies per mL over the titre of infectious unit (be them in $TCID_{50}$ or PFU). In the case of the $TCID_{50}$ titre, its value describes the dilution of a virus that is required to infect 50% of a given cell culture (Lei et al., 2021), whereas the value of the PFU titres offers an direct quantification of infectious viral particles, since one can actually count discrete plaques in cell culture (Baer & Kehn-Hall, 2014). On the other hand, in order to quantify virus particles in a given volume, there are several approaches encompassing direct methods (electron or confocal microscopy) (Bhattacharya et al., 2004) and indirect ones, like immunochemical detection of viral proteins (Kimpton & Emerman, 1992). Likewise, the quantification of virus particles can also be performed via RTqPCR (Weidmann et al., 2011), as one could potentially ascribe one viral genome copy to one virus particle. For the purposes of our study, we decided to quantify a relative value of viral particles, namely, virus-specific cDNA, since we acknowledge that our methodology does not allow for a direct determination of the genome copy number, as it does not account for the efficiency in RNA extraction nor the reverse transcription efficiency during the construction of cDNA. We calculated therefore the infectivity value as the ratio of virus-specific cDNA copies per mL to the $TCID_{50}$ per mL.

One of our earlier findings indicated that VSVEB-WT and VSVEB-E_{304}A had respective values of 16.54 and 2.86. In other words, VSVEB-E_{304}A had a relative and sustained superior infectivity of 5.78 times over the VSVEB-WT. Our calculation of infectivity derives from the approach of measuring the value of "particles to infectious units". This latter parameter is a widely-used method for comparing the efficiency by which a virus infects cultured cells (Alfson et al., 2015). For instance, through this ratio, one can determine whether a virus has become attenuated (Carpenter et al., 2009), or whether it has become more infectious. Likewise, since this value is a measure of the fraction of virus particles in a given sample that can complete an infectious cycle, 1 is the lowest theoretical value that the ratio can ever have. Studies on the ratio of viral particles to PFU have shown that these values depend on both the assay system and the viruses (Coffey & Vignuzzi, 2011). Additionally, this ratio may range from values that are as low as almost 1, for the case of bacteriophages (Luria & Anderson, 1942), up to values of several thousand for varicella-zoster virus (Buckingham et al., 2016). One study aimed at vaccine manufacturing of VSV-GPz in human embryonic kidney HEK 293A cells, offered much insight in virus titration values. Having conducted infection and titration (Wong & Qiu,

2016) in a similar manner to ours, they found an average $TCID_{50}$ per mL of 3.13×10^7, and 7.24×10^9 genome copies per ml (Gélinas et al., 2020). In this regards, our virus-specific cDNA copy titres of VSVEB-WT from Vero E6 cells were similar. If anything, the $TCID_{50}$ titre of the VSVEB-E_{304}A is the sole parameter that distances considerably (7.5-fold difference, 1.00×10^9 $TCID_{50}$ for VSVEB-E_{304}A versus 1.33×10^8 $TCID_{50}$ for VSVEB-WT), rendering therefore its ratio of cDNA copies to $TCID_{50}$ 5.78 times more than that of the VSVEB-WT. While we did not obtain our values in HEK 293A cell lines, another study on the optimisation of production of VSV, compared its $TCID_{50}$ titration results in Vero E6 with those of HEK293A, and found no significant differences in virus titres (Elahi et al., 2019). Moreover, since it is known that there is a strong correlation between the number of viral particles and infectious units (Brandolini et al., 2021; Jonsson et al., 2008), we addressed the estimation of former through protein quantification assays of the VSV matrix protein. Following the infectivity calculations with these data, we confirmed a superior infectivity value (in average, it is 7.6 times more infectious) of VSVEB-E_{304}A over the WT.

Lastly, both VSV and EBOV are negative-sense RNA viruses, which means that at one point antigenomes are synthesised by their RNA dependant RNA polymerase, as a step towards replicating the viral genome. In this regard, a study on the ratios of genomes and antigenomes in VSV observed that there was 50 times more of the former than the latter in both VSV-infected cells and in virions that had been harvested at the peak of the infection (Irie et al., 2014). It is thus important to say that we decided to perform the RT (change from genomes to cDNA) and the qPCR processes as two independent stages (as opposed to using a commercial kit of a one-step qPCR assays: RT + qPCR), since we wanted to run longer RT reactions (50 minutes, instead of 10 minutes of the commercial kit) to truly measure genomic RNA levels that would be more reflective of the number of viral genome copies in the sample.

Considering thus, on the one hand the differences in virus growth as well as in the ratios of particles to infectious units, and on the other hand, the physical differences between the virus particles (majority of GP_1 cleaved vs full GP_1), we could not but suspect that this mucin-like domain was behind rVSV-GPz E_{304}A increase in infectivity, and that its presence or lack thereof, played an important role in at least one stage of virus entry. Though as of now the mechanisms through which EBOV's GP triggers virus entry into its host cell are only partially understood (Martin et al., 2016), we can differentiate nonetheless several stages within this process: attachment, uptake/internalisation and fusion. As it has already been mentioned, the

team's initial drug screen experiments demonstrated that the polymeric PSS compound was found to efficiently hamper EBOV infection *in vitro*. Moreover, VSVEB-WT experiments led to the identification of resistant variants bearing the GPz $E_{304}A$ mutation after consecutive passages in this drug. PSS had been tested against sexually transmitted diseases of viral origin, such as HIV and herpes simplex viruses (Zaneveld et al., 2002). Although its mechanism of action is not well understood, it is known that polysulphated polymers can interfere with microbial infectivity, possibly by mimicking cellular receptors such as heparan sulphate, preventing thus cell surface binding and cell entry (Herold et al., 1997). Thus, considering that PSS is likely to be an attachment inhibitor, and that the $E_{304}A$ GP mutation was first detected as viruses were grown under its selective pressure, we first addressed whether such growth advantages could be due to a difference in attachment, especially since GP is the sole protein that mediates virus entry to host cells (Reynard & Volchkov, 2015).

However, our first results ruled out a difference in attachment between these two viruses, as they were equally affected to the action of PSS. Although this was already an indication that an increased attachment could not explain the growth advantages of VSVEB- $E_{304}A$, we addressed virus attachment with a different experimental setting. Since virus entry into the host cell is normally facilitated at 37 °C, but it is typically precluded at 4 °C (Tai et al., 2015), we proceeded with an analysis of virus binding by means of conducting the infections under different temperatures. Interestingly, the results of these binding assays confirmed that the differences in virus attachment were marginal, and that therefore, another factor that was yet to be identified, was responsible of the differences between VSVEB-WT and VSVEB-$E_{304}A$.

After attachment, EBOV particles are internalised in macropinocytosis vesicles (Saeed et al., 2010). Once the proteolytic events take place, and the RBD of GP_1 interacts with NPC1, viruses are ready for their fusion with the endolysosomal membrane, which culminates in the release of the replication complex to the cytoplasm. Thus, in an attempt of addressing whether the viruses bearing the $E_{304}A$ mutation could have an enhanced internalisation, we designed a set of experiments whereby viral mRNA was measured in cell lysates at different time points post infection. Likewise, these experiments were performed in parallel with the lysosomotropic agent ammonium chloride, since this compound has demonstrated a capacity of inhibition of viral replication by accumulating within the acidic intracellular compartments, notably lysosomes, elevating pH and ultimately interfering with the proteolytic events that lead to the viral fusion stage (Mizzen et al., 1985). Not only were the results of both conditions consistent,

but they also evidenced that there was indeed an enhanced virus internalisation into the cytoplasm of VSVEB-E_{304}A over VSVEB-WT, as manifested by the statistically significant differences of 4.5 and 2.3 times more of VSVEB-E_{304}A over the WT, without and with NH_4Cl, respectively at the last collection point. However, since the virus internalisation is a rather multi-step process, we decided to explore in more depth an important event that happens just before the EBOV's GP interaction with its cellular endosomal receptor: The GP processing by cellular proteases.

The cleavage of GP by cathepsins B and L in the endosome (Bale et al., 2011), coupled with the activity of TPC2 calcium channel (Penny et al., 2019), is crucial for the exposure of the receptor binding region in GP_1, as it removes the mucin-like domain, and allows the interaction with the cellular endosomal cholesterol transporter NPC-1 receptor (Kuroda et al., 2015), culminating with the virus fusion (Beniac & Timothy, 2017). Since most of VSVEB-E_{304}A do not have the MLD, we could conceive a model whereby these viruses, being already more cleaved than VSVEB-WT, would have an advantage at the proteolysis event because they would not have to undergo all the cleavages that the viruses bearing the WT GP would. We devised therefore an experimental design wherein thermolysin, a protease of bacterial origin, cleaves GP into its active form, just like cathepsins B do (Markosyan et al., 2016). Interestingly, our results on this proteolytic assays with thermolysin revealed that, in comparison to the WT GP, the GP bearing the E_{304}A mutation is indeed processed faster (with clear differences starting at 2 and 5 minutes), reaching its 19-kDa active form with the exposed RBD and potentially evading virus degradation and inactivation by cellular lysosomes when virions remain long enough inside endosomes (Kuroda et al., 2015).

With these data, we explained the gained virus growth advantages of VSVEB-E_{304}A as a result of two events: on the one hand, the GP of these viruses is more cleaved than that of the VSVEB-WT, requiring thus fewer proteolytic cleavages to proceed with the fusion stage and carry on with the infectious cycle; and on the other hand, VSVEB-E_{304}A virus particles are also more likely to escape the later stages of endosomes that lead to full proteolysis and virus inactivation. Thus, knowing that both VSVEB-WT and VSVEB-E_{304}A share the same ribonucleprotein complex, and that their protein synthesis, assembly and budding should therefore be identical, we attempted to confirm our proposal of model via virus release kinetics, in that VSVEB-E_{304}A should release virus particles into the supernatant much earlier than VSVEB-WT.

The furin-like cleavage site

Furin has been extensively studied, and there are general amino acid rules for furin specificity, such as two essential arginine residues at position 1 and 4 (P1 and P4, see figure 62), while a basic amino acid (such as lysine or arginine) at the P2 is not, but it can greatly enhance the efficiency of furin processing (Gary, 2007; K. Nakayama, 1997).

Given that our results indicated that viruses bearing the $E_{304}A$ GP mutation had growth advantages due to being more cleaved by furin, we produced two plasmids bearing the GP gene with mutations that technically impeded the cleavage of the furin-like cryptic site of R-K-I-R, namely, $RK_{299}AA$ and $R_{302}A+E_{304}A$. We then used these plasmids for conducting the rescue of recombinant VSV with those GP mutations. After having compared the 4 recombinant viruses: VSVEB-WT, VSVEB-$RK_{299}AA$, VSVEB-$E_{304}A$ and VSVEB-$R_{302}A+E_{304}A$, we found that VSVEB-$E_{304}A$ had the highest GP_1 cleavability, the highest virus growth, the largest size of virus plaques and the highest infectivity value. On the other hand, the other three recombinant viruses were marginally different. The fact that VSVEB-$R_{302}A+E_{304}A$ displayed a similar GP_1 cleavability and infectivity as VSVEB-WT, allowed us to conclude that it does not only suffice to have the $E_{304}A$ GP mutation, so that the VSVEB in question presents growth advantages over the parental virus. In fact, it is the furin cleavage at the cryptic site that promotes the growth advantages of VSVEB-$E_{304}A$, or in this case, the lack thereof, that renders VSVEB-$R_{302}A+E_{304}A$ as infectious as the viruses bearing WT GP or VSVEB-$RK_{299}AA$.

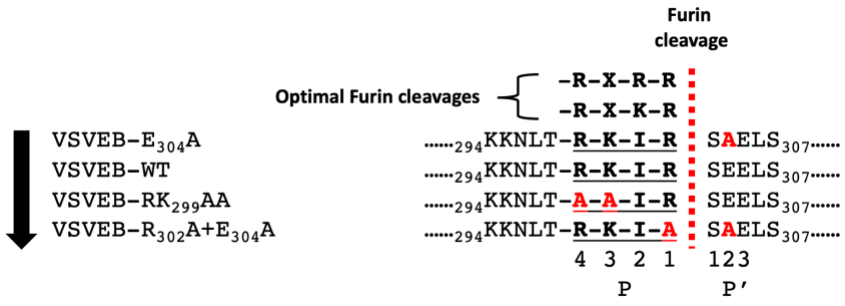

Figure 62 Comparison of the 4 rescued recombinant VSV with GP mutations in or near the cryptic furin-like site

The four rescued recombinant VSV with GP mutations in or near the cryptic furin-like site are ordered in descending manner (from top to bottom) of their theoretical levels of GP_1 cleaved. In all these sequences, the furin-like cleavage site is underlined, while effective amino acid mutations are highlighted in red. These mutations are to be compared with the two-possible optimal furin cleavages: RXRR and RXKR. Amino acid sequences are separated by the furin cleavage. Prior to this point, amino acid residues are labelled from right to left as P1, P2 (position 1, position 2) etc., while after the cleavage, amino acid residues are labelled from left to right as P1', P2' etc.

Interestingly, despite the theoretical disruption at the furin cryptic site of VSVEB-$RK_{299}AA$ and VSVEB-$R_{302}A+E_{304}A$, our results indicate that these two viruses present as much GP_1 cleaved as VSVEB-WT. With our results being inconsistent with a full furin impairment at the cryptic site, one could potentially argue that this cleavage takes place even without the essential arginines. In their work on the prediction of furin cleavage sites, (Duckert et al., 2004) found that although one could always reach consensus amino acid sequences, and build from them rules that would be thus consistent with most of the furin cleavage sites, there will still be exceptions. For instance, they found that the cleavage of the human insulin-like growth factor IA precursor and the shiga toxin A-chain precursors did not follow the previous rules from Nakayama, and they observed that for these two cases, lysine residues at P7 or two histidines at P8 and P9 could have compensatory effects. Likewise, it is also important to mention that (K. Nakayama, 1997) himself stated that not all furin cleavage sites contain the furin consensus sequence, in the same manner that not all sites containing the consensus sequence are cleavage sites for furin. Indeed, we certainly cannot exclude that the cleavage of the cryptic site is not only performed by furin, but it is also done in conjunction with another protease(s), such as ski1 or nardylisine, as proposed in figure 34.

Based on the amino acid sequence of the RKIR furin cryptic site, we can infer that the $E_{304}A$ mutation should not interfere with this proteolytic processing. If the mutation had affected the cleavage site, it would have led to reduced or abolished cleavage, which would have explained our findings. However, since the $E_{304}A$ mutation is shown to enhance cleavage and that the cryptic site is present in both viruses, we propose that the spatial configuration of the GP_1 subunit may hinder furin and/or other proteases from accessing the cryptic site, resulting in reduced cleavage. Conversely, the $E_{304}A$ mutation - which replaces a glutamic acid with an alanine - could alter the spatial arrangement, making the cryptic site more easily accessible and cleavable.

In this regard, the notion of steric hindrance is not new. For instance, in their work with the macrophage colony-stimulating factor (M-CSF), (Deng et al., 1996) proposed a mechanism of steric hindrance, wherein the deletion of a 7-amino acid region likely resulted in an interference with protease accessibility and a decrease in the cleavage efficiency of certain M-CSF mutants. Similarly, the loss of a carbohydrate side chain of the HA1 subunit of the hemagglutinin of an H5N2 avian influenza virus, due to a single point mutation ($T_{13}K$) was shown to be responsible for the appearance of high virulence in chickens. This mutation led to a loss of an N-

glycosylation consensus motif (asparagine) at position 11 (Kawaoka et al., 1984). Interestingly, wild-type low-pathogenic isolates had the normal oligosaccharide of HA1, which was demonstrated to interfere with cleavage of HA by steric hindrance (Böttcher-Friebertshäuser et al., 2013). In the case of the GP_1 subunit, its amino acids 296, 297 and 298 are NLT respectively (see figure 62), and they are a known N-glycosylation site (Falzarano et al., 2006). Although this glycosylation takes place for both VSVEB-WT and VSVEB-E_{304}A, we cannot rule out a that the alanine of the E_{304}A mutation allows a better spatial conformation of this glycan.

EBOV-WT and EBOV-E_{304}A

The choice of developing the initial part of the characterisation of the E_{304}A GP mutation with a recombinant VSV GPz surrogate system, rather than with the real EBOV, was mainly so for three reasons: 1. VSV poses far lesser biological risks (BSL2 working conditions), 2. allowing thus work to be performed at a faster peace; moreover, 3. considering that EBOV GP is the sole responsible of attachment, internalisation and virus fusion, our results from the VSV system expressing GP can technically be extrapolated to EBOV. However, after having generated enough data that correlate the presence of the E_{304}A GP mutation with growth advantages, we decided to proceed with experimentation with real EBOV in BSL4 settings to assess whether we would find consistencies.

While our initial GP profile assessments appeared to indicate that there was as much GP_1 cleaved in the EBOV-WT as there was in EBOV-E_{304}A, we determined that the 55-kDa protein band was an accumulation of EBOV sGP and GP_1 cleaved. Indeed, unlike VSV, EBOV GP presents an editing phenomenon whereby EBOV L protein adds extra adenine(s) to the mRNA as it passes through the "7A" GP editing site (De La Vega et al., 2015), resulting in the generation of several transcripts of the GP gene (Mehedi et al., 2011). However, after a subsequent sGP separation via ultracentrifugation, we confirmed that the E_{304}A GP mutation enhanced the cleavage of the second cryptic furin site and that there is indeed an inverted ratio in the GP protein profile, being EBOV-GPz E_{304}A the virus that has far more GP_1 cleaved (85.4%) than EBOV-WT (37.2%). Considering these findings, we also confirmed that the MLD is not part of the virus particles presenting the GP_1 cleaved instead of the full GP_1. While we do not evaluate the effect of MLD-deficiency in EBOV particles, on the course or outcome of the disease, it is certainly interesting to note that amongst the presumed functions of this domain, we may find: 1. the protection of conserved regions of GP from antibody recognition,

2. the masking of immune regulatory molecules on infected cell surfaces, 3. the promotion/enhancement of virus infection, and 4. its ability to alter cellular signalling (Martinez et al., 2007; Takada et al., 2004; Tran et al., 2014; Zampieri et al., 2007). In this regards, although it was not the scope of our project to ever delve into animal experimentation, we could conceive a handicap of the EBOV-E_{304}A in triggering a disease state in an immunocompetent organism by means of a humoral neutralisation, which could be potentially overcome through virus selection resulting in the reversion of the E_{304}A GP mutation into the wild-type GP.

As stated before, the normal EBOV GP editing site contains 7 uridines (7U), which lead to three different transcripts and the ultimate production of three different proteins, being sGP the most abundant. However, it has also been noted that if EBOV is continuously passed in cell culture (at least 5 passages in Vero E6 cells), its 7U GP editing site eventually becomes predominantly 8U, probably due to the loss of an original and very strong selective pressure in favour of the production of sGP, as it plays an important role in immune evasion (Audet & Kobinger, 2015). Not only does this 8U cell culture adaptation variant shift the production from sGP to a predominant $GP_{1,2}$, but it also increases EBOV cytotoxicity (Hume & Mühlberger, 2019). Moreover, there are also clear differences in virus plaque phenotype between a 7U and an 8U genotype, being EBOV 8U bigger than those of the original wild type EBOV 7U (Reynard & Volchkov, 2015). Likewise, EBOV 8U variant is also known to have significant growth advantages over EBOV 7U in cell cultures (Reynard & Volchkov, 2015). Thus, since an 8U genotype displays already bigger size plaques than a 7U, and that in regardless of any other GP mutation, after having sequenced the GP gene of both EBOV-WT and EBOV-E_{304}A. After having excluded the 8U genotype, we concluded that the EBOV-E_{304}A had larger virus plaques than the EBOV-WT.

It is also interesting to note that although the difference in plaque size was statistically significant, both recombinant viruses displayed heterogeneity in the size of their plaques. In this regard, we consider that differences in size could be explained by either an early or late virus internalisation, following the attachment. As stated by (Reynard & Volchkov, 2015), EBOV has a natural asynchronous entry process, as it could remain in a cell-bound state for even up to 6 hours prior to being internalised. This was further supported by an experiment in which (Reynard & Volchkov, 2015) isolated several EBOV clones from plaques displaying either small or large diameter sizes. They grew these clones in plaque assays and demonstrated

that a second passage exhibited a similar diversity in size as the first passage, regardless of whether the clone originated from a large or small plaque.

Since EBOV-E_{304}A displayed a superior infectivity over EBOV-WT, we were interested in determining whether it would also present growth advantages. However, surprisingly, while EBOV-E_{304}A superior infectivity was confirmed throughout the entire growth kinetics experiments, we did not see growth advantages of this virus over EBOV-WT. In fact, we even determined the contrary, in that EBOV-E_{304}A released a lesser number of virus-specific cDNA copies into the culture supernatant. In this regard, it is known that GP contributes to viral budding, not only by actively participating in the assembly (Ning et al., 2017), but also by antagonising tetherin, an IFN-induced antiviral factor that restricts the release of ebolaviruses from infected cells by anchoring them to the cell surface (Vande Burgt et al., 2015). In fact, in their studies using virus-like particles bearing GPz without the glycan cap (that is, a full removal of the MLD), (Vande Burgt et al., 2015) demonstrated that there is no antagonistic activity against tetherin. Therefore, since we suspected of a potential virus release problem that EBOV-E_{304}A could be experiencing, in a further experiment we attempted to address this issue by sampling cell lysate samples. Although we did observe preliminary differences between the ratios of culture supernatant to cell lysates of virus-specific cDNA, we do acknowledge that such differences were minimal and that more BSL4 experiments should be conducted to evaluate this hypothesis.

Considering therefore our findings, we propose a model of the biology of EBOV, whereby WT viruses present both GP_1 forms (full and cleaved) in a heterogenic state. However, unlike EBOV-E_{304}A, the GP_1 cleaved is far rare in the EBOV-WT, since this virus does not have the E_{304}A mutation that renders the furin-like cleavage site more accessible to furin (figure 63).

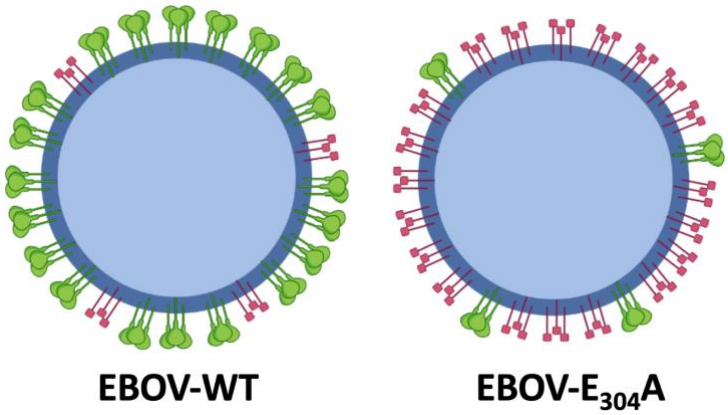

Figure 63 Comparison of the ratios of GP_1 to GP_1 cleaved in EBOV-WT and EBOV-$E_{304}A$

The picture illustrates a transversal cut of the filamentous EBOV. The GP of EBOV-$E_{304}A$ undergoes two furin cleavages. Firstly, the classical cleavage between the amino acids 501 and 502, which produces the GP_1 and GP_2 subunits; and secondly, the cleavage at the cryptic furin-like site (RKIR) in GP_1 between the amino acids 302 and 303. Of note, the WT GP has this cryptic furin-like site and thus EBOV-WT possesses as well both forms of GP1: Full GP_1 (marked in green) and GP_1 cleaved (marked in red). However, the $E_{304}A$ GP mutation enhances the furin cleavage at this cryptic site, resulting in an inverted pattern of more GP_1 cleaved than full GP_1. Picture created with BioRender.com.

Interestingly, we cannot exclude the possibility that the E_{304A} GP mutation could result in the cleavage of one, two or the three GP_1 subunits of the trimeric GP structure, as seen in figure 64. For instance, (Zhou et al., 2020) discusses that in the case of the spike protein of SARS-CoV-2, which is also a trimeric structure, the mandatory proteolytic cleavage so that the virus can fuse, appears not to take place extensively resulting thus in the majority of these spike trimers being only partially cleaved (i.e., cleavage occurring in only one or two of the three units of the trimer). In this regard, (Rey, 2021) proposes that these partial cleaved forms of the spike protein could even have functional consequences, such as giving more stability to the virus during its fusion with the membrane.

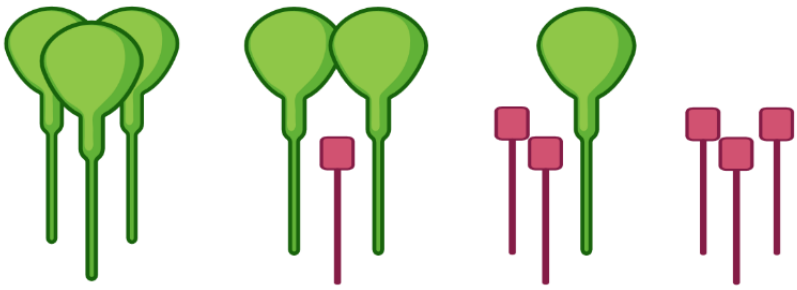

Figure 64 Potentially different degrees of GP_1 cleavability

Picture created with BioRender.com

Moreover, it is important to note that all our work with either VSV or EBOV was performed at the cellular level, specifically using Vero E6 cells, which leaves room for the possibility of testing these viruses in other cell lines, such as macrophages, dendritic cells or hepatocytes. While we propose the existence of both GP_1 forms (full GP_1 and GP_1 cleaved) in EBOV-WT, the scope of our research never delved into understanding whether the $E_{304}A$ GP mutation would have an effect, if any, on the course of the disease in an organism. However, considering the importance of the MLD in the immune evasion, we could anticipate that an infection with EBOV- $E_{304}A$ of an organism would result in a better virus neutralisation by the humoral response. It is also true that perhaps this additional stress that EBOV would face (a better antibody recognition) might also induce a virus selection that could potentially result in the reversion of the $E_{304}A$ mutation into the WT GP. If so, this would be an example of EBOV's genetic plasticity.

Finally, considering our results, we propose that on the one hand, by being more cleaved, the GP_1 of EBOV-$E_{304}A$ is either already sufficiently cleaved so that is RBD is already exposed, or it must undergo less cleavage events so that this domain can interact with the endosomal NPC1 receptor (figure 65). This translates into a more efficient release of EBOV-$E_{304}A$'s genetic material into the cytoplasm, and by extension, a lesser probability of being inactivated by the lysosomes (figure 66).

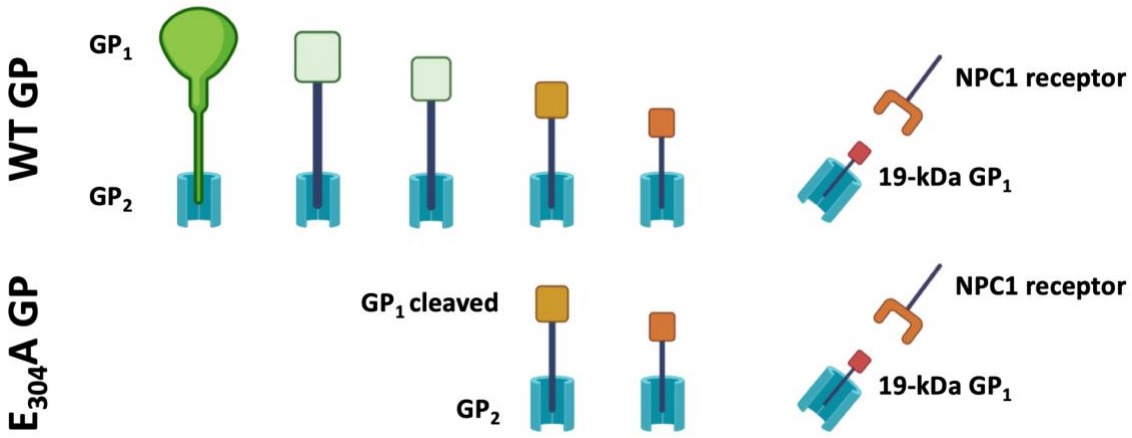

Figure 65 Proposal of our model: EBOV-$E_{304}A$ requires lesser cleavage events

This picture illustrates the difference in cleavability of the GP1 between WT GP and the GP with the $E_{304}A$ mutation. Since the $E_{304}A$ GP is already more cleaved, it needs lesser proteolytic events to reach its 19-kDa active form. Once GP_1 has reached this active form, its receptor binding domain can interact with the NPC1 receptor. Picture created with BioRender.com.

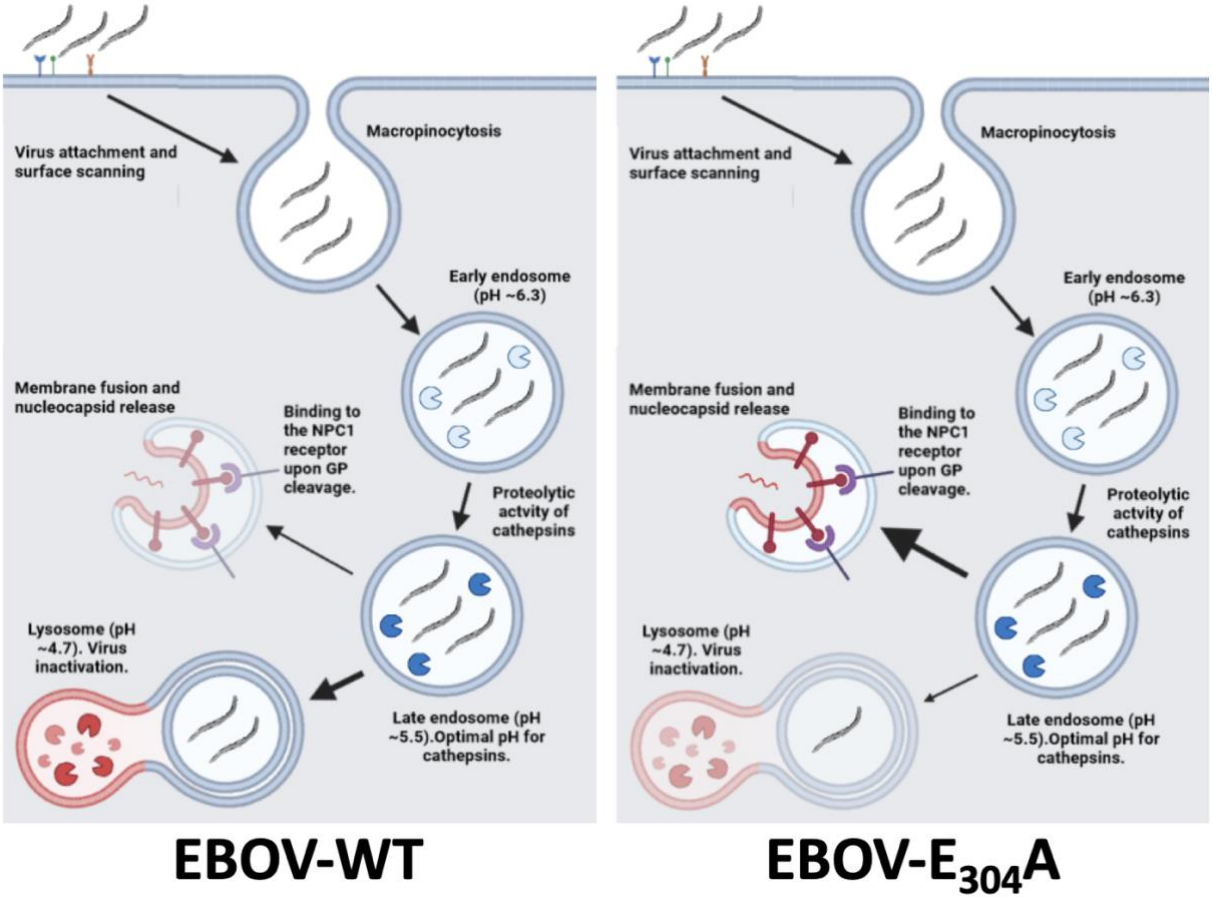

Figure 66 Proposal of our model: Comparison of the outcome of EBOV infection between EBOV-WT and EBOV-$E_{304}A$

The internalisation of EBOV begins through unspecific interactions between the viral GP and several attachment molecules such as TIM1, TAM, lectins and glycosaminoglycans. Once these interactions reach a sufficient threshold, viral particles are internalised via macropinocytosis. This is turn leads to the formation of an early endosome where the viruses are enclosed. As time passes, there is a gradual acidification of the endosome (later stages), which allows the cleavage of cathepsins B and L. Is it in this stage where such cleavages remove the MLD of the GP_1 subunit and reduce this structure to a 19-kDa protein that exposes its receptor binding site. If this receptor binding site interacts with the endosomal NPC1 receptor, then the GP_2 subunit exposes its hydrophobic domain that allows the membrane fusion and subsequent dissemination of the viral genome into the cytoplasm. It is important to note that the macropinocytosis normally ends with the fusion of a lysosome that fully proteolyses all the contents of the late endosome, which results in virus inactivation. Thus, since EBOV-$E_{304}A$ already more cleaved, by the time it is in the endosome, it is either already sufficiently cleaved so that its RBD is already exposed, or it must undergo less cleavage events so that its GP_1 exposes this domain. This translates into a more efficient release of the EBOV-$E_{304}A$'s genetic material into the cytoplasm, and by extension a lesser probability of these viruses being inactivated by the lysosomes. Picture created with BioRender.com.

Conclusions

EBOV is a highly pathogenic virus that causes a severe haemorrhagic fever in both human and nonhuman primates. EBOV uses its GP to enter the host cell through a complex mechanism that is only partially understood to date.

We ascertained that the GP_1 subunit of VSVEB-$E_{304}A$ undergoes a proteolytic processing performed by the cellular protease furin at a previously unnoticed cryptic furin-like site found in the GP_1 subunit. This second furin cleavage was demonstrated by the presence of a highly abundant GP_1 cleaved fragment, which remained a constituent of the VSVEB-$E_{304}A$. On the other hand, despite our efforts, we were unable to detect the second theoretical fragment that corresponds to the Mucin-like domain, leading us to conclude that it is no longer associated with the VSVEB-$E_{304}A$ virion. Moreover, our findings revealed that VSVEB-WT demonstrated a comparable second proteolytic cleavage, although to a significantly lesser degree. This confirms that the $E_{304}A$ mutation did not create a new cleavage site in the GP_1 subunit. Instead, it augmented the existing furin cleavage at the furin-like site.

We also confirmed that VSVEB-$E_{304}A$ displayed partial resistance to PSS, as evidenced by the dose-dependent effect on virus growth kinetics. Notably, we showed that even in the absence of the PSS inhibitor, VSVEB-$E_{304}A$ displayed significant growth advantages over VSVEB-WT. Specifically, we observed higher production of infectious units, greater virus infectivity, and larger surface area of virus plaques in VSVEB-$E_{304}A$, compared to VSVEB-WT.

In order to elucidate the molecular basis of selection, we first addressed virus attachment and concluded that both VSVEB-WT and VSVEB-$E_{304}A$ exhibited similar levels of attachment to the host cell. Our follow-up studies revealed that the difference in virus growth were due to a more efficient internalisation of VSVEB-$E_{304}A$ into the cytoplasm. Our *in vitro* experiments with thermolysin, which is often used to mimic the action of cellular cathepsins, showed that GP with the $E_{304}A$ mutation was digested to its "final" form more efficiently and significantly faster than in the case of WT GP. This finding supports VSVEB-$E_{304}A$'s increased entry efficiency, since it is already pre-cleaved compared with VSVEB-WT and requires therefore fewer cleavage events to achieve its receptor binding active form.

Moreover, by generating recombinant VSV with GP mutations that altered the furin cryptic cleavage site, we were able to confirm the correlation between the amount of GP_1 cleaved and virus infectivity as evidenced by the size of virus plaques, titres of infectious units and virus infectivity. Furthermore, our findings suggest that, besides furin, other proteases may also be involved in the cleavage process at the furin-like cryptic site.

Lastly, after successfully rescuing recombinant Ebola viruses (EBOV-WT and EBOV-$E_{304}A$), we conducted BSL4 experiments to determine whether the results would be consistent with those seen in the VSV surrogate system. Our findings confirmed the existence of additional furin cleavage at the cryptic furin-like site in EBOV-$E_{304}A$, and we also demonstrated that most of virus particles lacked the mucin-like domain. Although our findings showed that the virus carrying the $E_{304}A$ mutation had a larger surface area of viral plaques, higher rate of production of infectious particles and higher infectivity than EBOV-WT, our virus growth kinetics revealed that EBOV-$E_{304}A$ did not have growth advantages over the EBOV-WT.

We propose a model in which the $E_{304}A$ GP mutation enhances the entry efficiency of viruses, resulting in growth advantages. This is due to two factors: Firstly, most of the viruses carrying the $E_{304}A$ mutation lack the mucin-like domain, and their GP_1 is already more cleaved. As a result, the receptor binding domain of their GP_1 is already exposed, or they require fewer cleavage events to proceed with the fusion stage. Secondly, these cleaved viruses are more likely to evade the later stages of endosomes that result in complete proteolysis and virus inactivation. Moreover, we also propose a model of the biology of EBOV, whereby viruses with wild type GP express both forms of the protein (GP_1 and GP_1 cleaved) in a heterogeneous manner (although GP_1 is more prevalent than GP_1 cleaved). Indeed, as evidenced by our results, while the $E_{304}A$ GP mutation enhances the second furin cleavage, its absence does not fully preclude this process.

In the proposed model, we assume that the sequence organization surrounding the cryptic furin-like cleavage site is aimed at limiting the probability of cleavage. However, the fact that all Zairean Ebolaviruses retain the same configuration suggests that it plays an important role in virus replication.

Appendix

Hamster-adapted EBOV

Nonhuman primates have traditionally been the primary animal models for studying filovirus infections, but other models have been developed, including mice, guinea pigs, and hamsters (E. Nakayama & Saijo, 2013). However, adult immunocompetent animals have shown resistance to the virus in its natural form in several cases, making it necessary to pass the virus sequentially to achieve comparable levels of lethality to those seen in nonhuman primate infections (Audet & Kobinger, 2015).

Our team has always been interested in elucidating the molecular basis underlying the transition from an apathogenic EBOV to a pathogenic EBOV. To explore this phenomenon, our team has previously conducted experiments involving the generation of a guinea pig-adapted strain of EBOV (Volchkov et al., 2000) through serial passaging of WT EBOV in these animals. Their results evidenced amino acid changes in GP, NP and VP24, and highlighted particularly the pivotal role of the latter viral protein in the virus adaptation process. Additionally, (Ebihara et al., 2013) used a mouse-adapted EBOV in Syrian Hamsters with specific amino acid mutations in NP and VP24 (originally generated by (Bray et al., 1999)), and they were able to describe a lethal Syrian Hamster model of EVD.

In this context, our team conducted research on the generation of EBOV adapted to Golden Syrian Hamsters. After 7 consecutive passages in these animals, there was the identification of an adapted Ebola virus that induced a consistent pattern of infection in hamsters. It is worth highlighting that the hamster-adapted virus exhibited three non-synonymous mutations in VP24 ($I_{50}T$), L ($N_{328}D$), and GP ($S_{65}P$), which emerged during the second passage for the first two mutations and by the fourth passage for the GP mutation. Considering that previous studies had established a clear association between EBOV replication in mice and guinea pigs with mutations in VP24 (Mateo et al., 2011; E. Nakayama & Saijo, 2013; Volchkov et al., 2000), our team rescued recombinant EBOV with only the VP24 $I_{50}T$ mutation, which we will refer hereafter as EBOV-HA (hamster adapted EBOV). The rescued EBOV-HA was amplified in

Vero E6 cells and these virus stocks will be used for conducting virus growth kinetics using different cell lines.

Since we are interested in assessing whether EBOV-HA's growth advantages over EBOV-WT are either host-dependant or interferon-dependant, we will first conduct virus growth kinetics in primate interferon non-competent Vero E6 (kidney epithelial Green Monkey cells) and primate interferon competent HEK 293T (human embryonic kidney cells). Similarly, we will complement our studies with virus growth kinetics in rodent interferon non-competent BHK T7 (hamster kidney-derived cell line stably expressing T7 polymerase) and rodent interferon competent Raw264.7 (macrophage-like mouse cells). Furthermore, the GP editing site of both EBOV-WT and EBOV-HA will be sequenced for confirming exclusively 7U populations, since we will also evaluate growth advantages by means of virus plaque assays in Vero E6 and BHK T7 cells.

Study of virus growth between EBOV-WT and EBOV-HA in primate cell lines

To investigate whether EBOV-HA growth advantages were host-dependant or interferon-dependant, virus growth kinetics were conducted in Vero E6 cells. Cells were inoculated with a low MOI of 0.01 to ensure multicycle infection, and culture supernatant samples were collected over a 96-hour period post-infection. The samples were titrated by PFU and were also used for RNA extraction and RTqPCR analysis (figure 67). Additionally, samples of culture medium were assayed by WB using anti-VP40 antibodies and HRP-conjugated anti-mouse IgG (figure 67).

Interestingly, not only did we observe virus growth from EBOV-WT and EBOV-HA, but we also observed a slight difference between them, being 3.2, 3.15 and 3.83 times more of infectious units of EBOV-HA over the WT. Due to the relatively modest disparity in infectious units, with EBOV-HA displaying an average of 3.36 times more PFU than EBOV-WT, we decided to conduct plaque forming unit assays for the exclusive purpose of evaluating the plaque sizes, as it is another method of assessing virus growth. In this assay, Vero E6 cells were infected with virus serial dilutions of either EBOV-WT or EBOV-HA, which were then overlaid with DMEM containing 3% FCS and 0.8% Avicel. After the plates were fixed and immunostained with anti-VP40 and anti-NP monoclonal antibodies, the surface area of each plaque was calculated using ImageJ software and used for statistical analysis (see bottom and

top graphs of Panel A figure 68). Likewise, we also confirmed the absence of 8U in the GP editing site of both EBOV-WT and EBOV-HA, as seen in Panel B of figure 68.

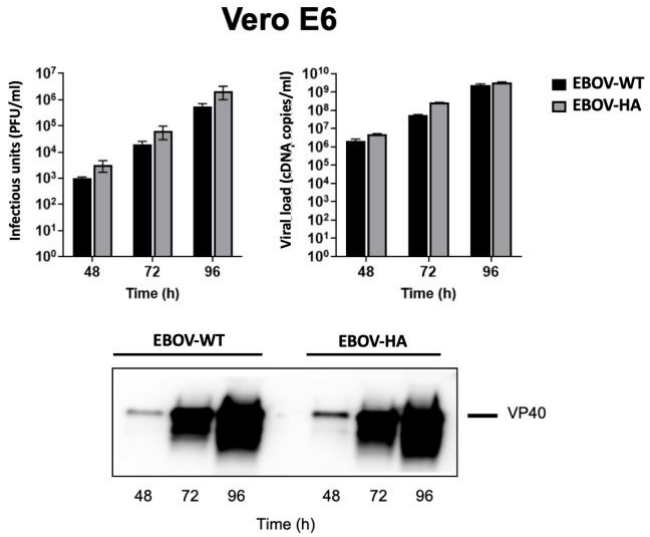

Figure 67 Analysis of EBOV-WT and EBOV-HA in Vero E6

Vero E6 cells were infected with either EBOV-WT or EBOV-HA at an MOI of 0.01. Culture supernatants were collected at the indicated time post infection, virus titres were determined via PFU and virus-specific cDNA copies were assessed by RTqPCR. Error bars represent the standard deviation of the measured values. Western blot analysis was performed via anti-VP40 antibodies and HRP-conjugated anti-mouse IgG.

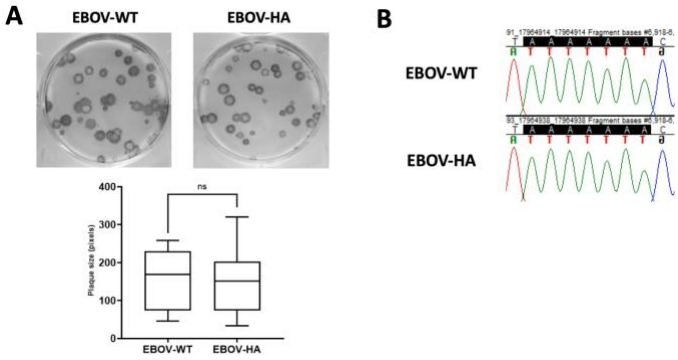

Figure 68 plaque assay and surface comparison between EBOV-WT and EBOV-HA

Panel A Top picture: Vero E6 cells were infected with virus dilutions of either EBOV-WT or EBOV-HA. They were fixed 7 days post infection, followed by immunostaining (anti-VP40 and anti-NP monoclonal antibodies) and HRP-conjugated anti-mouse IgG. Panel A Bottom graph: Plaque surface size was measured in pixels with the software ImageJ. Box shows median ± second and third quartiles. Panel B: cDNA fragments were generated by RT-PCR on viral RNA using primers flanking the EBOV GP gene. The cDNA fragments were sequenced and the data obtained were analysed using Sequencher software. The GP editing site of both EBOV-WT and EBOV-HA are shown and they contain 7 adenosine residues.

Overall, EBOV-HA exhibited virus plaques of comparable size to those generated by EBOV-WT. This observation is substantiated by the absence of a statistically significant difference

between the two datasets, further reinforcing the similarity in their growth capacities in Vero E6 cells.

Given that Vero E6 cells are primate interferon non-competent, we made a deliberate choice to employ primate interferon-competent cells to investigate whether the growth advantages of EBOV-HA could be attributed to an interferon-related mechanism. Thus, we conducted virus growth kinetics in HEK 293T human kidney-derived cells at the same MOI of the Vero E6 cell experiments, and culture supernatant samples were collected over a 96-hour period post-infection. The samples were titrated by PFU and were used for RNA extraction and RTqPCR analysis (figure 69). Additionally, samples of culture medium were assayed by WB using anti-VP40 antibodies and HRP-conjugated anti-mouse IgG (figure 69).

Our findings with the HEK 293T virus growth kinetics revealed that EBOV-WT and EBOV-HA replicate well in these primate cells, irrespective of the presence of the interferon response, as demonstrated by WT analysis, PFU titres and virus-specific cDNA levels. Based on our findings, which suggest that the growth advantages of EBOV-HA are not dependant on the interferon response, we proceeded to conduct virus growth kinetics in rodent cell lines to explore potential host-dependent growth advantages.

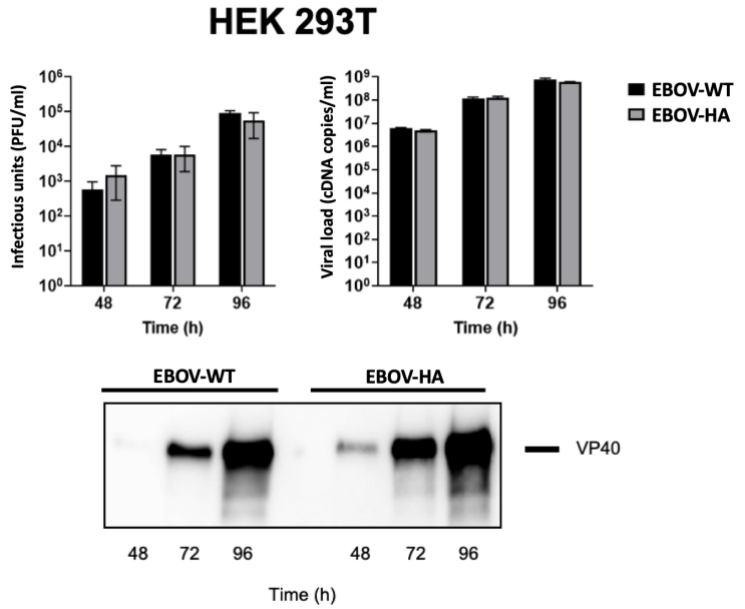

Figure 69 Analysis of EBOV-WT and EBOV-HA in HEK 293T

HEK 293T cells were infected with either EBOV-WT or EBOV-HA at an MOI of 0.01. Culture supernatants were collected at the indicated time post infection, virus titres were determined via PFU and virus-specific cDNA copies were assessed by RTqPCR. Error bars represent the standard deviation of the measured values. Western blot analysis was performed via anti-VP40 antibodies and HRP-conjugated anti-mouse IgG.

Study of virus growth between EBOV-WT and EBOV-HA in rodent cell lines

To confirm whether EBOV-HA growth advantages were host-dependant, virus growth kinetics were conducted in BHK T7 mouse-derived cells. Cells were inoculated with the same low MOI as the other growth kinetics, and culture supernatant samples were collected over a 108-hour period post-infection. The samples were titrated by PFU and were used for RNA extraction and RTqPCR analysis (figure 70). Additionally, samples of culture medium were assayed by WB using anti-VP40 antibodies and HRP-conjugated anti-mouse IgG (figure 70).

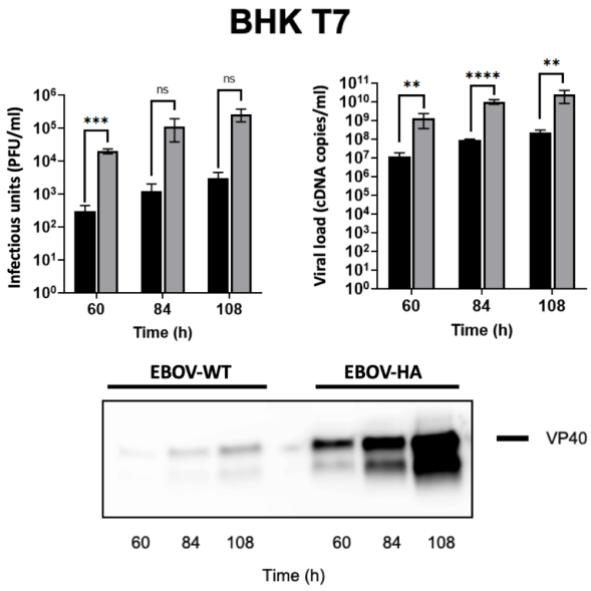

Figure 70 Analysis of EBOV-WT and EBOV-HA in BHK T7

BHK T7 cells were infected with either EBOV-WT or EBOV-HA at an MOI of 0.01. Culture supernatants were collected at the indicated time post infection, virus titres were determined via PFU and virus-specific cDNA copies were assessed by RTqPCR. Error bars represent the standard deviation of the measured values. Western blot analysis was performed via anti-VP40 antibodies and HRP-conjugated anti-mouse IgG. The statistical significance was determined using a two-tailed t-test

Interestingly, we observed a significant growth advantage of EBOV-HA in the BHK T7 cell line. Consistently throughout the experiment, we detected a roughly 100-fold increase in both PFU per mL and cDNA copies per mL of EBOV-HA over the EBOV-WT. The growth disparities are also evident in the WB samples analysis showing a faster production of VP40 protein in cells infected with EBOV-HA.

Since we were interested in confirming these growth advantages with a different method, we conducted plaque forming unit assays for the specific purpose of evaluating differences in

plaque size. BHK T7 cells were infected with virus serial dilutions of either EBOV-WT or EBOV-HA, which were then overlaid with DMEM containing 3% FCS and 0.8% Avicel. After the plates were fixed and immunostained with anti-VP40 and anti-NP monoclonal antibodies, the surface area of each plaque was calculated using ImageJ software and used for statistical analysis (see figure 71).

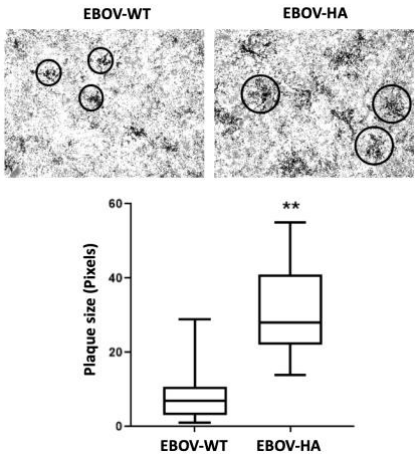

Figure 71 Plaque analysis and surface comparison of EBOV-WT and EBOV-HA

Top figure: BHK T7 cells were infected with virus dilutions of EBOV-WT or EBOV-HA. They were fixed 7 days post infection, followed by immunostaining (anti-VP40 and anti-NP monoclonal antibodies) and HRP-conjugated anti-mouse IgG. Bottom graph: Plaque surface size was measured in pixels with the software ImageJ. Box shows median ± second and third quartiles. P-values were calculated using a two-tailed t-test; ** indicates $p<0.01$

Overall, our results demonstrate a statistically significant ($p< 0.01$) difference, with the EBOV-HA producing virus plaques 3.39 times larger than those of the EBOV-WT, as reflected by the average pixel values of 8.1 compared to 27.44, respectively.

Lastly, we decided to complement this study by infecting interferon-competent Raw264.7 hamster-derived cells. Cells were inoculated with the same low MOI as the other growth kinetics, and culture supernatant samples were collected over a 96-hour period post-infection. The samples were titrated by PFU and were used for RNA extraction and RTqPCR analysis (figure 72). Additionally, samples of culture medium were assayed by WB using anti-VP40 antibodies and HRP-conjugated anti-mouse IgG (figure 72).

Our findings evidenced clear growth advantages of EBOV-HA over EBOV-WT in this hamster cell line. For instance, there is an approximately 100-fold increase in PFU at 96 hours post-infection of EBOV-HA over EBOV-WT. This observation was supported by western blot analysis and quantification of virus-specific cDNA copies, which showed that EBOV-HA

produced approximately 10 times more virus particles than EBOV-WT. Similarly, our results showed that EBOV-WT did not grow in this hamster cell line, as opposed to what happened in the other previous three cell lines.

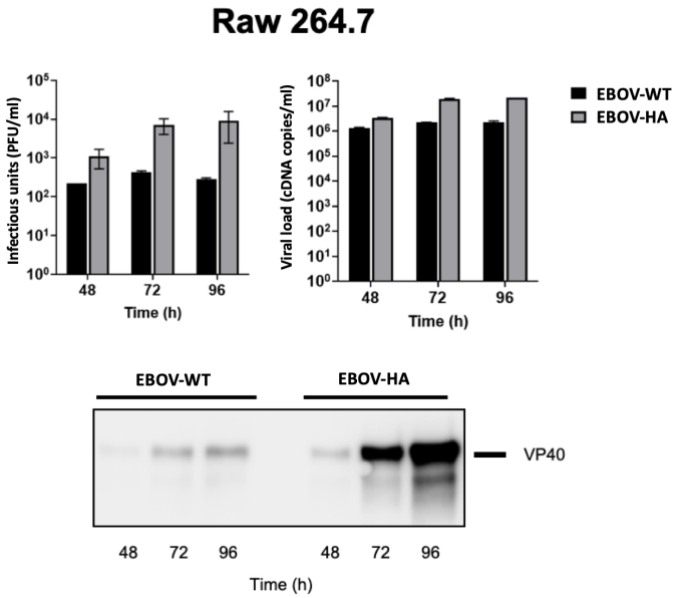

Figure 72 EBOV-HA presents growth advantages over EBOV-WT in Raw264.7

Raw264.7 cells were infected with either EBOV-WT or EBOV-HA at an MOI of 0.01. Culture supernatants were collected at the indicated time post infection, virus titres were determined via PFU and virus-specific cDNA copies were assessed by RTqPCR. Error bars represent the standard deviation of the measured values. Western blot analysis was performed via anti-VP40 antibodies and HRP-conjugated anti-mouse IgG.

Based on the absence of growth disparities between interferon-competent and interferon non-competent cell lines, coupled with the observed differences in growth between primate and rodent cell lines, we are prone to conclude that the growth advantages of EBOV-HA are host-dependent rather than being influenced by the interferon response. In this regard, while mutations in VP24 have been linked to multiple successful EBOV animal adaptations, the interferon response is not always the key element. For instance, in their work with guinea pig-EBOV adapted, (Mateo et al., 2011) associated the increase of virulence of the adapted virus with changes in the structural protein VP24, rather than with an antagonistic function towards the interferon response. Furthermore, (Mateo et al., 2011) made a significant observation: the presence of inclusion bodies exclusively in macrophages infected with the adapted EBOV, while such inclusion bodies were absent in cells infected with EBOV-WT. This led them to propose that the enhanced growth capabilities of the adapted virus could be attributed to EBOV-WT's inability to properly bud due to VP24's failure in regulating the assembly of viral nucleocapsids.

Bibliography

Abbate, J. L., Murall, C. L., Richner, H., & Althaus, C. L. (2016). Potential Impact of Sexual Transmission on Ebola Virus Epidemiology: Sierra Leone as a Case Study. *PLoS Neglected Tropical Diseases*, *10*(5). https://doi.org/10.1371/journal.pntd.0004676

Abbet, P., Procopiou, M., Genne, D., Defabiani, N., & Auckenthaler, R. (1998). *Marburg and Ebola Hemorrhagic Fevers : Does the UC : CID*. *27*, 404–406.

Alazard-dany, N., Volchkova, V., Reynard, O., Carbonnelle, C., Dolnik, O., Khromykh, A., & Volchkov, V. E. (2006). *Ebola virus glycoprotein GP is not cytotoxic when expressed constitutively at a moderate level Printed in Great Britain*. 1247–1257. https://doi.org/10.1099/vir.0.81361-0

Aleksandrowicz, P., Marzi, A., Biedenkopf, N., Beimforde, N., Becker, S., Hoenen, T., Feldmann, H., & Schnittler, H. J. (2011). Ebola virus enters host cells by macropinocytosis and clathrin-mediated endocytosis. *Journal of Infectious Diseases*, *204*(SUPPL. 3), 957–967. https://doi.org/10.1093/infdis/jir326

Alfson, K. J., Avena, L. E., Beadles, M. W., Staples, H., Nunneley, J. W., Ticer, A., Dick, E. J., Owston, M. A., Reed, C., Patterson, J. L., Carrion, R., & Griffiths, A. (2015). Particle-to-PFU Ratio of Ebola Virus Influences Disease Course and Survival in Cynomolgus Macaques. *Journal of Virology*, *89*(13), 6773–6781. https://doi.org/10.1128/jvi.00649-15

Amman, B. R., Schuh, A. J., & Towner, J. S. (2017). Ebola virus field sample collection. In *Methods in Molecular Biology* (Vol. 1628, pp. 373–393). Humana Press Inc. https://doi.org/10.1007/978-1-4939-7116-9_30

Audet, J., & Kobinger, G. P. (2015). Immune evasion in ebolavirus infections. In *Viral Immunology* (Vol. 28, Issue 1, pp. 10–18). Mary Ann Liebert Inc. https://doi.org/10.1089/vim.2014.0066

Ayub, G., & Waheed, Y. (2016). Sequence analysis of the L protein of the Ebola 2014 outbreak: Insight into conserved regions and mutations. *Molecular Medicine Reports*, *13*(6), 4821–4826. https://doi.org/10.3892/mmr.2016.5145

B. GC, J., Johnson, K. A., Husby, M. L., Frick, C. T., & Gerstman, B. S. (2016). Interdomain salt-bridges in the Ebola virus protein VP40 and their role in domain association and plasma membrane localization. *Protein Science*, *25*, 1648–1658. https://doi.org/10.1002/pro.2969

Baer, A., & Kehn-Hall, K. (2014). Viral concentration determination through plaque assays: Using traditional and novel overlay systems. *Journal of Visualized Experiments*, *93*, 1–10. https://doi.org/10.3791/52065

Baize, S., Leroy, E. M., Georges, A. J., Capron, M., & Bedjabaga, I. (2002). *Inflammatory responses in Ebola virus-infected patients*. 163–168.

Bale, S., Liu, T., Li, S., Wang, Y., Abelson, D., Fusco, M., Woods, V. L., & Saphire, E. (2011). Ebola virus glycoprotein needs an additional trigger, beyond proteolytic priming for membrane fusion. *PLoS Neglected Tropical Diseases*, *5*(11). https://doi.org/10.1371/journal.pntd.0001395

Ball, L. A., Wertz, G. W., Hill, C., & Carolina, N. (1981). *VSV RNA Synthesis : How Can You Be Positive ? 26*(October), 143–144.

Banadyga, L., Hoenen, T., Ambroggio, X., Dunham, E., Groseth, A., & Ebihara, H. (2017). Ebola virus VP24 interacts with NP to facilitate nucleocapsid assembly and genome packaging. *Scientific Reports*, *7*(1), 1–14. https://doi.org/10.1038/s41598-017-08167-8

Baron, R. C., McCormick, J. B., & Zubeir, O. A. (1983). Ebola virus disease in southern Sudan: Hospital dissemination and intrafamilial spread. *Bulletin of the World Health Organization*, *61*(6), 997–1003.

Barr, J. N., Whelan, S. P. J., & Wertz, G. W. (2002). Transcriptional control of the RNA-dependent RNA polymerase of vesicular stomatitis virus. *Biochimica et Biophysica Acta - Gene Structure and Expression*, *1577*(2), 337–353. https://doi.org/10.1016/S0167-4781(02)00462-1

Baseler, L., Chertow, D. S., Johnson, K. M., Feldmann, H., & Morens, D. M. (2017). The Pathogenesis of Ebola Virus Disease∗. In *Annual Review of Pathology: Mechanisms of Disease* (Vol. 12, pp. 387–418). Annual Reviews Inc. https://doi.org/10.1146/annurev-pathol-052016-100506

Baskerville, A., Fisher-Hoch, S. P., Neild, G. H., & Dowsett, A. B. (1985). Ultrastructural pathology of experimental ebola haemorrhagic fever virus infection. *The Journal of Pathology*, *147*(3), 199–209. https://doi.org/10.1002/path.1711470308

Basler, C. F., Mikulasova, A., Martinez-Sobrido, L., Paragas, J., Mühlberger, E., Bray, M., Klenk, H.-D., Palese, P., & García-Sastre, A. (2003). The Ebola Virus VP35 Protein Inhibits Activation of Interferon Regulatory Factor 3. *Journal of Virology*, *77*(14), 7945–7956. https://doi.org/10.1128/jvi.77.14.7945-7956.2003

Bausch, D. G. (2011). Ebola virus as a foodborne pathogen? Cause for consideration, but not panic. In *Journal of Infectious Diseases* (Vol. 204, Issue 2, pp. 179–181). https://doi.org/10.1093/infdis/jir201

Bausch, D. G., & Piot, P. (2020). Ebola vaccines: Biomedical advances, human rights challenges: Commentary on: A randomized, blinded, dose-ranging trial of an ebola virus glycoprotein (EBOVGP) nanoparticle vaccine with Matrix-M adjuvant in healthy adults. In *Journal of Infectious Diseases* (Vol. 222, Issue 4, pp. 521–524). Oxford University Press. https://doi.org/10.1093/infdis/jiz520

Beer, B., Kurth, R., & Bukreyev, A. (1999). Characteristics of Filoviridae: Marburg and Ebola Viruses. In *Naturwissenschaften* (Vol. 86). Springer-Verlag.

Beniac, D. R., & Timothy, B. F. (2017). Structure of the Ebola virus glycoprotein spike within the virion envelope at 11 Å resolution. *Scientific Reports*, *7*. https://doi.org/10.1038/srep46374

Bhattacharya, B., Weiss, R. A., Davis, C., Holmes, H., Hockley, D., & Fassati, A. (2004). Detection and quantitation of human immunodeficiency virus type-1 particles by confocal microscopy. *Journal of Virological Methods*, *120*(1), 13–21. https://doi.org/10.1016/j.jviromet.2004.03.019

Biacchesi, S., Pham, Q. N., Skiadopoulos, M. H., Murphy, B. R., Collins, P. L., & Buchholz, U. J. (2006). Modification of the Trypsin-Dependent Cleavage Activation Site of the Human Metapneumovirus Fusion Protein To Be Trypsin Independent Does Not Increase Replication or Spread in Rodents or Nonhuman Primates. *Journal of Virology*, *80*(12), 5798–5806. https://doi.org/10.1128/jvi.00294-06

Biedenkopf, N., Hartlieb, B., Hoenen, T., & Becker, S. (2013). Phosphorylation of ebola virus VP30 influences the composition of the viral nucleocapsid complex: Impact on viral transcription and replication. *Journal of Biological Chemistry*, *288*(16), 11165–11174. https://doi.org/10.1074/jbc.M113.461285

Boehmann, Y., Enterlein, S., Randolf, A., & Mühlberger, E. (2005). A reconstituted replication and transcription system for Ebola virus Reston and comparison with Ebola virus Zaire. *Virology*, *332*(1), 406–417. https://doi.org/10.1016/j.virol.2004.11.018

Bornholdt, Z. A., Noda, T., Abelson, D. M., Halfmann, P., Wood, M. R., Kawaoka, Y., & Saphire, E. O. (2013). Structural rearrangement of ebola virus vp40 begets multiple functions in the virus life cycle. *Cell*, *154*(4), 763–774. https://doi.org/10.1016/j.cell.2013.07.015

Bosch, X. (2004). Sudan Ebola outbreak of known strain. *The Lancet Infectious Diseases*, *4*(7), 388. https://doi.org/10.1016/S1473-3099(04)01071-0

Böttcher-Friebertshäuser, E., Klenk, H. D., & Garten, W. (2013). Activation of influenza viruses by proteases from host cells and bacteria in the human airway epithelium. *Pathogens and Disease*, *69*(2), 87–100. https://doi.org/10.1111/2049-632X.12053

Bradley, J. H., Harrison, A., Corey, A., Gentry, N., & Gregg, R. K. (2017). *Ebola virus secreted glycoprotein decreases the anti-viral immunity of macrophages in early in fl ammatory responses*. *November*.

Brandolini, M., Taddei, F., Marino, M. M., Grumiro, L., Scalcione, A., Turba, M. E., Gentilini, F., Fantini, M., Zannoli, S., Dirani, G., & Sambri, V. (2021). Correlating qrt-pcr, dpcr and viral titration for the identification and quantification of sars-cov-2: A new approach for infection management. *Viruses*, *13*(6), 1–13. https://doi.org/10.3390/v13061022

Brauburger, K., Boehmann, Y., Krähling, V., & Mühlberger, E. (2016). Transcriptional Regulation in Ebola Virus: Effects of Gene Border Structure and Regulatory Elements on Gene Expression and Polymerase Scanning Behavior. *Journal of Virology*, *90*(4), 1898–1909. https://doi.org/10.1128/jvi.02341-15

Bray, M., Davis, K., Geisbert, T., Schmaljohn, C., & Huggins, J. (1999). A mouse model for evaluation of prophylaxis and therapy of Ebola hemorrhagic fever. *Journal of Infectious Diseases*,

179(SUPPL. 1), 651–661. https://doi.org/10.1086/514292

Bray, M., Hatfill, S., Hensley, L., & Huggins, J. W. (2001). Haematological, biochemical and coagulation changes in mice, guinea-pigs and monkeys infected with a mouse-adapted variant of Ebola Zaire virus. *Journal of Comparative Pathology*, *125*(4), 243–253. https://doi.org/10.1053/jcpa.2001.0503

Brindley, M. A., Hunt, C. L., Kondratowicz, A. S., Bowman, J., Sinn, P. L., McCray, P. B., Quinn, K., Weller, M. L., Chiorini, J. A., & Maury, W. (2011). Tyrosine kinase receptor Axl enhances entry of Zaire ebolavirus without direct interactions with the viral glycoprotein. *Virology*, *415*(2), 83–94. https://doi.org/10.1016/j.virol.2011.04.002

Brinkmann, C., Nehlmeier, I., Nehls, J., Hoffmann, M., Qiu, X., Takada, A., & Schindler, M. (2016). *The Tetherin Antagonism of the Ebola Virus Glycoprotein Requires an Intact Receptor-Binding Domain and Can Be Blocked by GP1- Specific Antibodies*. *90*(24), 11075–11086. https://doi.org/10.1128/JVI.01563-16.Editor

Brunton, B., Rogers, K., Phillips, E. K., Brouillette, R. B., Bouls, R., Butler, N. S., & Maury, W. (2019). TIM-1 serves as a receptor for ebola virus in vivo, enhancing viremia and pathogenesis. *PLoS Neglected Tropical Diseases*, *13*(6). https://doi.org/10.1371/journal.pntd.0006983

Buckingham, E. M., Jarosinski, K. W., Jackson, W., Carpenter, J. E., & Grose, C. (2016). Exocytosis of Varicella-Zoster Virus Virions Involves a Convergence of Endosomal and Autophagy Pathways. *Journal of Virology*, *90*(19), 8673–8685. https://doi.org/10.1128/jvi.00915-16

Burke, J., Declerq, R., & Ghysebrechts, G. (1978). Ebola haemorrhagic fever in Zaire, 1976. Report of an international commission. *Bulletin of the World Health Organization*, *56*(2), 271–293.

Burki, T. K. (2016). Post-Ebola syndrome. *The Lancet. Infectious Diseases*, *16*(7), 780–781. https://doi.org/10.1016/S1473-3099(15)00259-5

Bwaka, M. A., Bonnet, M. J., Calain, P., Colebunders, R., De Ann, R., Guimard, Y., Katwiki, K. R., Kibadi, K., Kipasa, M. A., Kuvula, K. J., Mapanda, B. B., Massamba, M., Mupapa, K. D., Muyembe-Tamfum, J. J., Ndaberey, E., Peters, C. J., Rollin, P. E., & Van Den Enden, E. (1999). Ebola hemorrhagic fever in Kikwit, Democratic Republic of the Congo: Clinical observations in 103 patients. *Journal of Infectious Diseases*, *179*(SUPPL. 1), 1–7. https://doi.org/10.1086/514308

Cantoni, D., Hamlet, A., Michaelis, M., Wass, M. N., & Rossman, J. S. (2016). Risks Posed by Reston, the Forgotten Ebolavirus. *MSphere*, *1*(6). https://doi.org/10.1128/msphere.00322-16

Cao, Y. chen, Deng, Q. xin, & Dai, S. xue. (2020). Remdesivir for severe acute respiratory syndrome coronavirus 2 causing COVID-19: An evaluation of the evidence. *Travel Medicine and Infectious Disease*, *35*(March). https://doi.org/10.1016/j.tmaid.2020.101647

Carette, J. E., Raaben, M., Wong, A. C., Herbert, A. S., Obernosterer, G., Mulherkar, N., Kuehne, A. I., Kranzusch, P. J., Griffin, A. M., Ruthel, G., Cin, P. D., Dye, J. M., & Whelan, S. P. (2011). Ebola virus entry requires the cholesterol transporter Niemann-Pick C1. *Nature*, 0–6. https://doi.org/10.1038/nature10348

Carpenter, J. E., Henderson, E. P., & Grose, C. (2009). Enumeration of an Extremely High Particle-to-PFU Ratio for Varicella-Zoster Virus. *Journal of Virology*, *83*(13), 6917–6921. https://doi.org/10.1128/jvi.00081-09

Chandran, K., Sullivan, N. J., Felbor, U., Whelan, S. P., & Cunningham, J. M. (2005). Virology: Endosomal proteolysis of the ebola virus glycoprotein is necessary for infection. *Science*, *308*(5728), 1643–1645. https://doi.org/10.1126/science.1110656

Chen, J., He, Z., Yuan, Y., Huang, F., Luo, B., Zhang, J., Pan, T., Zhang, H., & Zhang, J. (2019). Host factor SMYD3 is recruited by Ebola virus nucleoprotein to facilitate viral mRNA transcription. *Emerging Microbes and Infections*, *8*(1), 1347–1360. https://doi.org/10.1080/22221751.2019.1662736

Chertow, D. S., Uyeki, T. M., & Dupont, H. L. (2015). Loperamide therapy for voluminous diarrhea in ebola virus disease. In *Journal of Infectious Diseases* (Vol. 211, Issue 7, pp. 1036–1037). Oxford University Press. https://doi.org/10.1093/infdis/jiv001

Clark, D. V., Kibuuka, H., Millard, M., Wakabi, S., Lukwago, L., Taylor, A., Eller, M. A., Eller, L. A., Michael, N. L., Honko, A. N., Olinger, G. G., Schoepp, R. J., Hepburn, M. J., Hensley, L. E., & Robb, M. L. (2015). Long-term sequelae after Ebola virus disease in Bundibugyo, Uganda: A retrospective cohort study. *The Lancet Infectious Diseases*, *15*(8), 905–912. https://doi.org/10.1016/S1473-3099(15)70152-0

Clarke, E. C., Collar, A. L., Ye, C., Caì, Y., Anaya, E., Rinaldi, D., Martinez, B., Yarborough, S., Merle, C., Theisen, M., Wada, J., Kuhn, J. H., & Bradfute, S. B. (2017). *Production and Purification of Filovirus Glycoproteins in Insect and Mammalian Cell Lines*. *April*, 1–12. https://doi.org/10.1038/s41598-017-15416-3

Coffey, L. L., & Vignuzzi, M. (2011). Host Alternation of Chikungunya Virus Increases Fitness while Restricting Population Diversity and Adaptability to Novel Selective Pressures. *Journal of Virology*, *85*(2), 1025–1035. https://doi.org/10.1128/jvi.01918-10

Colebunders, R. L., & Cannon, R. O. (2015). Large-scale convalescent blood and plasma transfusion therapy for ebola virus disease. In *Journal of Infectious Diseases* (Vol. 211, Issue 8, pp. 1208–1210). Oxford University Press. https://doi.org/10.1093/infdis/jiv043

Coltart, C. E. M., Lindsey, B., Ghinai, I., Johnson, A. M., & Heymann, D. L. (2017). The Ebola outbreak, 2013–2016: Old lessons for new epidemics. In *Philosophical Transactions of the Royal Society B: Biological Sciences* (Vol. 372, Issue 1721). Royal Society. https://doi.org/10.1098/rstb.2016.0297

Conway, E. M., & Rosenberg, R. D. (1988). *2854203.pdf* (Vol. 8, Issue 12, pp. 5588–5592).

Cook, B. W. M., Cutts, T. A., Nikiforuk, A. M., Leung, A., Kobasa, D., & Theriault, S. S. (2016). The Disinfection Characteristics of Ebola Virus Outbreak Variants. *Scientific Reports*, *6*. https://doi.org/10.1038/srep38293

Cook, J. D., & Lee, J. E. (2013). The Secret Life of Viral Entry Glycoproteins: Moonlighting in Immune Evasion. *PLoS Pathogens*, *9*(5). https://doi.org/10.1371/journal.ppat.1003258

Cournac, J. M., Karkowski, L., Bordes, J., Aletti, M., Duron, S., Janvier, F., Foissaud, V., Savini, H., De Greslan, T., Rousseau, C., Billhot, M., Gagnon, N., Mac Nab, C., Dubrous, P., Moroge, S., Broto, H., Cotte, J., Maugey, N., Cordier, P. Y., … Cellarier, G. (2016). Rhabdomyolysis in Ebola Virus Disease. Results of an Observational Study in a Treatment Center in Guinea. *Clinical Infectious Diseases*, *62*(1), 19–23. https://doi.org/10.1093/cid/civ779

Crary, S. M., Towner, J. S., Honig, J. E., Shoemaker, T. R., & Nichol, S. T. (2003). *Analysis of the role of predicted RNA secondary structures in Ebola virus replication*. *306*, 210–218. https://doi.org/10.1016/S0042-6822(02)00014-4

Cui, X., Lapinski, N., Zhang, X. (Frank), & Jagota, A. (2021). Length of mucin-like domains enhances cell-Ebola virus adhesion by increasing binding probability. *Biophysical Journal*, *120*(5), 781–790. https://doi.org/10.1016/j.bpj.2021.01.025

Dahlmann, F., Biedenkopf, N., Babler, A., Jahnen-Dechent, W., Karsten, C. B., Gnirß, K., Schneider, H., Wrensch, F., O'Callaghan, C. A., Bertram, S., Herrler, G., Becker, S., Pöhlmann, S., & Hofmann-Winkler, H. (2015). Analysis of Ebola Virus Entry into Macrophages. *Journal of Infectious Diseases*, *212*, S247–S257. https://doi.org/10.1093/infdis/jiv140

Daniel S. (2014). Ebola Virus Disease in West Africa — Clinical Manifestations and Management. *New England Journal of Medicine*, *371*(22), 2052–2054. https://doi.org/10.1056/nejmp1411794

Das, K., & Arnold, E. (2015). *Previews Negative-Strand RNA Virus L Proteins : One Machine , Many Activities*. 239–241. https://doi.org/10.1016/j.cell.2015.06.063

Davey, N., Parsy, M., Becker, S., & Briggs, J. A. G. (2011). *Cryo-Electron Tomography of Marburg Virus Particles and Their Morphogenesis within Infected Cells*. *9*(11). https://doi.org/10.1371/journal.pbio.1001196

De La Vega, M. A., Wong, G., Kobinger, G. P., & Qiu, X. (2015). The multiple roles of sGP in Ebola pathogenesis. In *Viral Immunology* (Vol. 28, Issue 1, pp. 3–9). Mary Ann Liebert Inc. https://doi.org/10.1089/vim.2014.0068

Deen, G. F., Broutet, N., Xu, W., Knust, B., Sesay, F. R., McDonald, S. L. R., Ervin, E., Marrinan, J. E., Gaillard, P., Habib, N., Liu, H., Liu, W., Thorson, A. E., Yamba, F., Massaquoi, T. A., James, F., Ariyarajah, A., Ross, C., Bernstein, K., … Sahr, F. (2017). Ebola RNA Persistence in Semen of Ebola Virus Disease Survivors — Final Report. *New England Journal of Medicine*, *377*(15), 1428–1437. https://doi.org/10.1056/nejmoa1511410

Deflubé, L. R., Cressey, T. N., Hume, A. J., Olejnik, J., Haddock, E., Feldmann, F., Ebihara, H., Fearns, R., & Mühlberger, E. (2019). Ebolavirus polymerase uses an unconventional genome replication mechanism. *Proceedings of the National Academy of Sciences of the United States of America*, *116*(17), 8535–8543. https://doi.org/10.1073/pnas.1815745116

Deng, P., Rettenmier, C. W., & Pattengale, P. K. (1996). Structural requirements for the ectodomain cleavage of human cell surface macrophage colony-stimulating factor. *Journal of Biological*

Chemistry, *271*(27), 16338–16343. https://doi.org/10.1074/jbc.271.27.16338
Diederich, S., Dietzel, E., & Maisner, A. (2009). Nipah virus fusion protein: Influence of cleavage site mutations on the cleavability by cathepsin L, trypsin and furin. *Virus Research*, *145*(2), 300–306. https://doi.org/10.1016/j.virusres.2009.07.020
Dietzgen, R. G., Hideki, K., Goodinc, M. M., Kurathd, G., & Vasilakis, N. (2018). The family Rhabdoviridae: mono- and bipartite negative-sense RNA viruses with diverse genome organization and common evolutionary origins. *Physiology & Behavior*, *176*(1), 139–148. https://doi.org/10.1016/j.virusres.2016.10.010.The
Dixit, D., Masumbuko Claude, K., Kjaldgaard, L., & Hawkes, M. T. (2021). Review of Ebola virus disease in children–how far have we come? In *Paediatrics and International Child Health* (Vol. 41, Issue 1, pp. 12–27). Taylor and Francis Ltd. https://doi.org/10.1080/20469047.2020.1805260
Dolnik, O., Volchkova, V., Garten, W., Carbonnelle, C., & Becker, S. (2004). *Ectodomain shedding of the glycoprotein GP of Ebola virus*. *23*(10), 2175–2184. https://doi.org/10.1038/sj.emboj.7600219
Dong, S., Yang, P., Li, G., Liu, B., Wang, W., Liu, X., Xia, B., Yang, C., Lou, Z., Guo, Y., & Rao, Z. (2015). Insight into the Ebola virus nucleocapsid assembly mechanism : crystal structure of Ebola virus nucleoprotein core domain at 1 . 8 Å resolution. *Protein & Cell*, *6*(5), 351–362. https://doi.org/10.1007/s13238-015-0163-3
Dowall, S. D., Bosworth, A., Watson, R., Bewley, K., Taylor, I., Rayner, E., Hunter, L., Pearson, G., Easterbrook, L., Pitman, J., Hewson, R., & Carroll, M. W. (2015). Chloroquine inhibited ebola virus replication in vitro but failed to protect against infection and disease in the in vivo guinea pig model. *Journal of General Virology*, *96*(12), 3484–3492. https://doi.org/10.1099/jgv.0.000309
Dowling, W., Thompson, E., Badger, C., Mellquist, J. L., Garrison, A. R., Smith, J. M., Paragas, J., Hogan, R. J., & Schmaljohn, C. (2007). Influences of Glycosylation on Antigenicity, Immunogenicity, and Protective Efficacy of Ebola Virus GP DNA Vaccines. *Journal of Virology*, *81*(4), 1821–1837. https://doi.org/10.1128/jvi.02098-06
Dreier, C., Resa-Infante, P., Thiele, S., Stanelle-Bertram, S., Walendy-Gnirß, K., Speiseder, T., Preuss, A., Müller, Z., Klenk, H. D., Stech, J., & Gabriel, G. (2019). Mutations in the H7 HA and PB1 genes of avian influenza a viruses increase viral pathogenicity and contact transmission in guinea pigs. *Emerging Microbes and Infections*, *8*(1), 1324–1336. https://doi.org/10.1080/22221751.2019.1663131
Dube, D., Brecher, M. B., Delos, S. E., Rose, S. C., Park, E. W., Schornberg, K. L., Kuhn, J. H., & White, J. M. (2009). The Primed Ebolavirus Glycoprotein (19-Kilodalton GP 1,2): Sequence and Residues Critical for Host Cell Binding . *Journal of Virology*, *83*(7), 2883–2891. https://doi.org/10.1128/jvi.01956-08
Duckert, P., Brunak, S., & Blom, N. (2004). Prediction of proprotein convertase cleavage sites. *Protein Engineering, Design and Selection*, *17*(1), 107–112. https://doi.org/10.1093/protein/gzh013
Duraffour, S., Malvy, D., & Sissoko, D. (2017). How to treat Ebola virus infections? A lesson from the field. In *Current Opinion in Virology* (Vol. 24, pp. 9–15). Elsevier B.V. https://doi.org/10.1016/j.coviro.2017.03.003
Ebihara, H., Zivcec, M., Gardner, D., Falzarano, D., Lacasse, R., Rosenke, R., Long, D., Haddock, E., Fischer, E., Kawaoka, Y., & Feldmann, H. (2013). A syrian golden hamster model recapitulating ebola hemorrhagic fever. *Journal of Infectious Diseases*, *207*(2), 306–318. https://doi.org/10.1093/infdis/jis626
Edwards, K. M., Davis, J. E., Browne, K. A., Sutton, V. R., & Trapani, J. A. (1999). Anti-viral strategies of cytotoxic T lymphocytes are manifested through a variety of granule-bound pathways of apoptosis induction. In *Immunology and Cell Biology* (Vol. 77, Issue 1, pp. 76–89). https://doi.org/10.1046/j.1440-1711.1999.00799.x
Elahi, S. M., Shen, C. F., & Gilbert, R. (2019). Optimization of production of vesicular stomatitis virus (VSV) in suspension serum-free culture medium at high cell density. *Journal of Biotechnology*, *289*, 144–149. https://doi.org/10.1016/j.jbiotec.2018.11.023
Enterlein, S., Schmidt, K. M., Schümann, M., Conrad, D., Krähling, V., Olejnik, J., & Mühlberger, E. (2009). The Marburg Virus 3′ Noncoding Region Structurally and Functionally Differs from That of Ebola Virus. *Journal of Virology*, *83*(9), 4508–4519. https://doi.org/10.1128/jvi.02429-08
Escalera, A., Gonzalez-Reiche, A. S., Aslam, S., Mena, I., Laporte, M., Pearl, R. L., Fossati, A., Rathnasinghe, R., Alshammary, H., van de Guchte, A., Farrugia, K., Qin, Y., Bouhaddou, M.,

Kehrer, T., Zuliani-Alvarez, L., Meekins, D. A., Balaraman, V., McDowell, C., Richt, J. A., … Aydillo, T. (2022). Mutations in SARS-CoV-2 variants of concern link to increased spike cleavage and virus transmission. *Cell Host and Microbe*, *30*(3), 373-387.e7. https://doi.org/10.1016/j.chom.2022.01.006

Escudero-Pérez, B., Ruibal, P., Rottstegge, M., Lödtke, A., Port, J. R., Hartmann, K., Gómez-Medina, S., Möller-Guhl, J., Nelson, E. V., Krasemann, S., Rodríguez, E., & Munoz-Fontela, C. (2019). Comparative pathogenesis of Ebola virus and Reston virus infection in humanized mice. *JCI Insight*, *4*(21). https://doi.org/10.1172/jci.insight.126070

Escudero-Pérez, B., Volchkova, V. A., Dolnik, O., Lawrence, P., & Volchkov, V. E. (2014). Shed GP of Ebola Virus Triggers Immune Activation and Increased Vascular Permeability. *PLoS Pathogens*, *10*(11). https://doi.org/10.1371/journal.ppat.1004509

Falzarano, D., Krokhin, O., Domselaar, G. Van, Wolf, K., Seebach, J., Schnittler, H., & Feldmann, H. (2007). *Ebola sGP — The first viral glycoprotein shown to be C-mannosylated*. *368*, 83–90. https://doi.org/10.1016/j.virol.2007.06.015

Falzarano, D., Krokhin, O., Wahl-Jensen, V., Seebach, J., Wolf, K., Schnittler, H. J., & Feldmann, H. (2006). Structure-function analysis of the soluble glycoprotein, sGP, of ebola virus. *ChemBioChem*, *7*(10), 1605–1611. https://doi.org/10.1002/cbic.200600223

Fauci, A. S., Saphire, E. O., & Sabeti, P. (2019). *Voices Ending Ebola Partners in Ebola Research Navigate Remaining Obstacles Let the 10th Be the Last*.

Feldmann, H., Bugany, H., Mahner, F., Klenk, H., Drenckhahn, D., Schnittler, H., & Universita, J. (1996). *Filovirus-Induced Endothelial Leakage Triggered by Infected Monocytes / Macrophages*. *70*(4), 2208–2214.

Feldmann, H., & Geisbert, T. W. (2011). Ebola haemorrhagic fever. *The Lancet*, *377*(9768), 849–862. https://doi.org/10.1016/S0140-6736(10)60667-8

Feldmann, H., & Klenk, H. (1996). *Marburg and ebola viruses*. *47*.

Feldmann, H., Klenkl, H.-D., & Sanchez, A. (1993). Molecular biology and evolution of filoviruses. In *Arch Virol* (Vol. 7).

Feldmann, H., Sprecher, A., & Geisbert, T. W. (2020). Ebola. *New England Journal of Medicine*, *382*(19), 1832–1842. https://doi.org/10.1056/NEJMra1901594

Feldmann, H., Volchkov, V. E., Volchkova, V. A., & Klenk, H. D. (1999). The glycoproteins of Marburg and Ebola virus and their potential roles in pathogenesis. *Archives of Virology, Supplement*, *15*, 159–169. https://doi.org/10.1007/978-3-7091-6425-9_11

Fischer, R. J., Judson, S., Miazgowicz, K., Bushmaker, T., & Munster, V. J. (2016). Ebola virus persistence in semen ex vivo. *Emerging Infectious Diseases*, *22*(2), 289–291. https://doi.org/10.3201/eid2202.151278

Fletcher, T. E., Fowler, R. A., & Beeching, N. J. (2014). Understanding organ dysfunction in Ebola virus disease. *Intensive Care Medicine*, *40*(12), 1936–1939. https://doi.org/10.1007/s00134-014-3515-1

Formenty, P., Hatz, C., Le Guenno, B., Stoll, A., Rogenmoser, P., & Widmer, A. (1999). Human infection due to Ebola virus, subtype Cote d'Ivoire: Clinical and biologic presentation. *Journal of Infectious Diseases*, *179*(SUPPL. 1), 48–53. https://doi.org/10.1086/514285

Forrester, J. V. (2018). Ebola virus and persistent chronic infection: when does replication cease? *Annals of Translational Medicine*, *6*(S1), S39–S39. https://doi.org/10.21037/atm.2018.09.60

Francica, J. R., Matukonis, M. K., & Bates, P. (2009). Requirements for cell rounding and surface protein down-regulation by Ebola virus glycoprotein. *Virology*, *383*(2), 237–247. https://doi.org/10.1016/j.virol.2008.10.029

Furuyama, W., Shifflett, K., Feldmann, H., & Marzi, A. (2021). The Ebola virus soluble glycoprotein contributes to viral pathogenesis by activating the MAP kinase signaling pathway. *PLoS Pathogens*, *17*(9). https://doi.org/10.1371/journal.ppat.1009937

Gale, P. (2017). Could Bat Cell Temperature and Filovirus Filament Length Explain the Emergence of Ebola Virus in Mammals? Predictions of a Thermodynamic Model. In *Transboundary and Emerging Diseases* (Vol. 64, Issue 6, pp. 1676–1693). Blackwell Publishing Ltd. https://doi.org/10.1111/tbed.12580

Garbutt, M., Liebscher, R., Wahl-jensen, V., Jones, S., Wagner, R., Volchkov, V., Klenk, H., Feldmann, H., & Stro, U. (2004). *Properties of Replication-Competent Vesicular Stomatitis Virus Vectors*

Expressing Glycoproteins of Filoviruses and Arenaviruses. *78*(10), 5458–5465. https://doi.org/10.1128/JVI.78.10.5458

García-Dorival, I., Wu, W., Armstrong, S. D., Barr, J. N., Carroll, M. W., Hewson, R., & Hiscox, J. A. (2016). Elucidation of the Cellular Interactome of Ebola Virus Nucleoprotein and Identification of Therapeutic Targets. *Journal of Proteome Research*, *15*(12), 4290–4303. https://doi.org/10.1021/acs.jproteome.6b00337

Gary, T. (2007). Furin at the cutting edge: from protein traffic to embryogenesis and disease. *Molecular Cell*, *3*(10), 753–766.

Geisbert, T. W., & Hensley, L. E. (2004). Ebola virus: New insights into disease aetiopathology and possible therapeutic interventions. *Expert Reviews in Molecular Medicine*, *6*(20), 1–23. https://doi.org/10.1017/S1462399404008300

Geisbert, T. W., Hensley, L. E., Larsen, T., Young, H. A., Reed, D. S., Geisbert, J. B., Scott, D. P., Kagan, E., Jahrling, P. B., & Davis, K. J. (2003). *Pathogenesis of Ebola Hemorrhagic Fever in Cynomolgus Macaques Evidence that Dendritic Cells Are Early and Sustained Targets of Infection*. *163*(6), 2347–2370.

Geisbert, T. W., & Young, H. A. (2003). Pathogenesis of Ebola Hemorrhagic Fever in Primate Models: Evidence that Hemorrhage Is Not a Direct Effect of Virus-Induced Cytolysis of Endothelial Cells. *American Journal of Pathology*, *163*(6), 2371–2382. https://doi.org/10.1016/S0002-9440(10)63592-4

Gélinas, J. F., Kiesslich, S., Gilbert, R., & Kamen, A. A. (2020). Titration methods for rVSV-based vaccine manufacturing. *MethodsX*, *7*, 100806. https://doi.org/10.1016/j.mex.2020.100806

Goldstein, T., & Simon J Anthony. (2018). Discovery of a new ebolavirus (Bombali virus) in molossid bats in Sierra Leone. *Physiology & Behavior*, *176*(1), 139–148. https://doi.org/10.1038/s41564-018-0227-2.Discovery

Gostin, L. O., Hodge, J. G., & Burris, S. (2014). Is the United States prepared for Ebola? In *JAMA - Journal of the American Medical Association* (Vol. 312, Issue 23, pp. 2497–2498). American Medical Association. https://doi.org/10.1001/jama.2014.15041

Groseth, A., Ströher, U., Theriault, S., & Feldmann, H. (2002). Molecular characterization of an isolate from the 1989/90 epizootic of Ebola virus Reston among macaques imported into the United States. *Virus Research*, *87*(2), 155–163. https://doi.org/10.1016/S0168-1702(02)00087-4

Guito, J. C., Albariño, C. G., Chakrabarti, A. K., & Towner, J. S. (2017). Novel activities by ebolavirus and marburgvirus interferon antagonists revealed using a standardized in vitro reporter system. *Virology*, *501*(September 2016), 147–165. https://doi.org/10.1016/j.virol.2016.11.015

Günther, S., Feldmann, H., Geisbert, T. W., Hensley, L. E., Rollin, P. E., Nichol, S. T., Ströher, U., Artsob, H., Peters, C. J., Ksiazek, T. G., Becker, S., Ter Meulen, J., Ölschläger, S., Schmidt-Chanasit, J., Sudeck, H., Burchard, G. D., & Schmiedel, S. (2011). Management of accidental exposure to Ebola virus in the biosafety Level 4 Laboratory, Hamburg, Germany. *Journal of Infectious Diseases*, *204*(SUPPL. 3). https://doi.org/10.1093/infdis/jir298

Haddock, E., Saturday, G., Feldmann, F., Hanley, P. W., Okumura, A., & Lovaglio, J. (2021). *Reston virus causes severe respiratory disease in young domestic pigs*. *118*(2), 1–7. https://doi.org/10.1073/pnas.2015657118

Halfmann, P., Neumann, G., & Kawaoka, Y. (2011). The Ebolavirus VP24 protein blocks phosphorylation of p38 mitogen-activated protein kinase. *Journal of Infectious Diseases*, *204*(SUPPL. 3), 953–956. https://doi.org/10.1093/infdis/jir325

Hartlieb, B., Muziol, T., Weissenhorn, W., & Becker, S. (2007). Crystal structure of the C-terminal domain of Ebola virus VP30 reveals a role in transcription and nucleocapsid association. *Proceedings of the National Academy of Sciences of the United States of America*, *104*(2), 624–629. https://doi.org/10.1073/pnas.0606730104

Harty, R. N., Brown, M. E., Wang, G., Huibregtse, J., & Hayes, F. P. (2010). A PPxY motif within the VP40 protein of Ebola virus interacts physically and functionally with a ubiquitin ligase: Implications for filovirus budding. *Proceedings of the National Academy of Sciences of the United States of America*, *107*(41), 17733–17738. https://doi.org/10.1073/pnas.1006098107

He, J., Melnik, L. I., Komin, A., Wiedman, G., Fuselier, T., Morris, C. F., Starr, C. G., Searson, P. C., Gallaher, W. R., Hristova, K., Garry, R. F., & Wimley, W. C. (2017). Ebola Virus Delta Peptide Is a Viroporin. *Journal of Virology*, *91*(16), 1–14. https://doi.org/10.1128/jvi.00438-17

Heinz Feldmann, Victoria Wahl-Jensen1, S. M. J. and U. S. (2004). Ebola virus ecology: a continuing mystery. In *Trends in Microbiology* (Vol. 12, Issue 10, pp. 433–437). https://doi.org/10.1016/j.tim.2004.08.007

Henry, R. (2015). Ebola [eb′o-lə]. *Emerging Infectious Diseases*, *21*(11), 1905.

Hensley, L. E., Young, H. A., Jahrling, P. B., & Geisbert, T. W. (2002). Proinflammatory response during Ebola virus infection of primate models: Possible involvement of the tumor necrosis factor receptor superfamily. *Immunology Letters*, *80*(3), 169–179. https://doi.org/10.1016/S0165-2478(01)00327-3

Herold, B. C., Siston, A., Bremer, J., Kirkpatrick, R., Wilbanks, G., Fugedi, P., Peto, C., & Cooper, M. (1997). Sulfated carbohydrate compounds prevent microbial adherence by sexually transmitted disease pathogens. *Antimicrobial Agents and Chemotherapy*, *41*(12), 2776–2780. https://doi.org/10.1128/aac.41.12.2776

Hoenen, T., Biedenkopf, N., Zielecki, F., Jung, S., Groseth, A., Feldmann, H., & Becker, S. (2010). Oligomerization of Ebola Virus VP40 Is Essential for Particle Morphogenesis and Regulation of Viral Transcription. *Journal of Virology*, *84*(14), 7053–7063. https://doi.org/10.1128/jvi.00737-10

Hoenen, T., Shabman, R. S., Groseth, A., Herwig, A., Weber, M., Schudt, G., Dolnik, O., Basler, C. F., Becker, S., & Feldmann, H. (2012). Inclusion Bodies Are a Site of Ebolavirus Replication. *Journal of Virology*, *86*(21), 11779–11788. https://doi.org/10.1128/jvi.01525-12

Hoenen, T., Volchkov, V., Kolesnikova, L., Mittler, E., Timmins, J., Ottmann, M., Reynard, O., Becker, S., & Weissenhorn, W. (2005). VP40 Octamers Are Essential for Ebola Virus Replication. *Journal of Virology*, *79*(3), 1898–1905. https://doi.org/10.1128/jvi.79.3.1898-1905.2005

Hofmann-Winkler, H., Gnirß, K., Wrensch, F., & Pöhlmann, S. (2015). Comparative Analysis of Host Cell Entry of Ebola Virus from Sierra Leone, 2014, and Zaire, 1976. *Journal of Infectious Diseases*, *212*, S172–S180. https://doi.org/10.1093/infdis/jiv101

Hofmann-winkler, H., Kaup, F., & Pöhlmann, S. (2012). *Host Cell Factors in Filovirus Entry: Novel Players, New Insights*. 3336–3362. https://doi.org/10.3390/v4123336

Holmes, E. C., Dudas, G., Rambaut, A., & Andersen, K. G. (2016). The evolution of Ebola virus: Insights from the 2013-2016 epidemic. In *Nature* (Vol. 538, Issue 7624, pp. 193–200). Nature Publishing Group. https://doi.org/10.1038/nature19790

Howlett, P., Brown, C., Helderman, T., Brooks, T., Lisk, D., Deen, G., Solbrig, M., & Lado, M. (2016). Ebola virus disease complicated by late-onset encephalitis and polyarthritis, sierra leone. In *Emerging Infectious Diseases* (Vol. 22, Issue 1, pp. 150–152). https://doi.org/10.3201/eid2201.151212

Huang, Y., Xu, L., Sun, Y., & Nabel, G. J. (2002). The assembly of Ebola virus nucleocapsid requires virion-associated proteins 35 and 24 and posttranslational modification of nucleoprotein. *Molecular Cell*, *10*(2), 307–316. https://doi.org/10.1016/S1097-2765(02)00588-9

Hume, A. J., & Mühlberger, E. (2019). Distinct Genome Replication and Transcription Strategies within the Growing Filovirus Family. In *Journal of Molecular Biology* (Vol. 431, Issue 21, pp. 4290–4320). Academic Press. https://doi.org/10.1016/j.jmb.2019.06.029

Iampietro, M., Younan, P., Nishida, A., Dutta, M., Lubaki, N. M., Santos, R. I., Koup, R. A., Katze, M. G., & Bukreyev, A. (2017). Ebola virus glycoprotein directly triggers T lymphocyte death despite of the lack of infection. *PLoS Pathogens*, *13*(5). https://doi.org/10.1371/journal.ppat.1006397

Ilinykh, P. A., Lubaki, N. M., Widen, S. G., Renn, L. A., Theisen, T. C., Rabin, R. L., Wood, T. G., & Bukreyev, A. (2015). Different Temporal Effects of Ebola Virus VP35 and VP24 Proteins on Global Gene Expression in Human Dendritic Cells. *Journal of Virology*, *89*(15), 7567–7583. https://doi.org/10.1128/jvi.00924-15

Iraqi, M., Edri, A., Greenshpan, Y., Kundu, K., Bolel, P., Cahana, A., Ottolenghi, A., Gazit, R., Lobel, L., Braiman, A., & Porgador, A. (2020). N-Glycans Mediate the Ebola Virus-GP1 Shielding of Ligands to Immune Receptors and Immune Evasion. *Frontiers in Cellular and Infection Microbiology*, *10*. https://doi.org/10.3389/fcimb.2020.00048

Irie, T., Okamoto, I., Yoshida, A., Nagai, Y., & Sakaguchi, T. (2014). Sendai Virus C Proteins Regulate Viral Genome and Antigenome Synthesis To Dictate the Negative Genome Polarity. *Journal of Virology*, *88*(1), 690–698. https://doi.org/10.1128/jvi.02798-13

Iwasa, A., Shimojima, M., & Kawaoka, Y. (2011). *sGP Serves as a Structural Protein in Ebola Virus Infection*. *204*(Suppl 3), 897–903. https://doi.org/10.1093/infdis/jir313

J.M., L., M., S.-H., N.T., W., Z., H., J., P., & R.N., H. (2003). Overlapping motifs (PTAP and PPEY) within the Ebola virus VP40 protein function independently as late budding domains: involvement of host proteins TSG101 and VPS-4. *Journal of Virology*, *77*(3), 1812–1819. https://doi.org/10.1128/JVI.77.3.1812

Jacob, S. T., Crozier, I., Fischer, W. A., Hewlett, A., Kraft, C. S., Vega, M. A. de La, Soka, M. J., Wahl, V., Griffiths, A., Bollinger, L., & Kuhn, J. H. (2020). Ebola virus disease. In *Nature Reviews Disease Primers* (Vol. 6, Issue 1). Nature Research. https://doi.org/10.1038/s41572-020-0147-3

Jacobs, M., Rodger, A., Bell, D. J., Bhagani, S., Cropley, I., Filipe, A., Gifford, R. J., Hopkins, S., Hughes, J., Jabeen, F., Johannessen, I., Karageorgopoulos, D., Lackenby, A., Lester, R., Liu, R. S. N., MacConnachie, A., Mahungu, T., Martin, D., Marshall, N., … Thomson, E. C. (2016). Late Ebola virus relapse causing meningoencephalitis: a case report. *The Lancet*, *388*(10043), 498–503. https://doi.org/10.1016/S0140-6736(16)30386-5

Jagga, S., Sharma, A. R., Chakraborty, C., & Lee, S. S. (2019). Ebola virus disease: Recent advancs in diagnostics and therapeutics. *Asian Pacific Journal of Tropical Medicine*, *12*(9), 385–395. https://doi.org/10.4103/1995-7645.267581

Jain, S., Martynova, E., Rizvanov, A., Khaiboullina, S., & Baranwal, M. (2021). Structural and functional aspects of ebola virus proteins. In *Pathogens* (Vol. 10, Issue 10). MDPI. https://doi.org/10.3390/pathogens10101330

Jemielity, S., Wang, J. J., Chan, Y. K., Ahmed, A. A., Li, W., Monahan, S., Bu, X., Farzan, M., Freeman, G. J., Umetsu, D. T., DeKruyff, R. H., & Choe, H. (2013). TIM-family Proteins Promote Infection of Multiple Enveloped Viruses through Virion-associated Phosphatidylserine. *PLoS Pathogens*, *9*(3). https://doi.org/10.1371/journal.ppat.1003232

Jin, H., Yan, Z., Prabhakar, B. S., Feng, Z., Ma, Y., Verpooten, D., Ganesh, B., & He, B. (2010). *The VP35 protein of Ebola virus impairs dendritic cell maturation induced by virus and lipopolysaccharide*. 352–361. https://doi.org/10.1099/vir.0.017343-0

Johnson, R. F., McCarthy, S. E., Godlewski, P. J., & Harty, R. N. (2006). Ebola Virus VP35-VP40 Interaction Is Sufficient for Packaging 3E-5E Minigenome RNA into Virus-Like Particles. *Journal of Virology*, *80*(11), 5135–5144. https://doi.org/10.1128/jvi.01857-05

Jonsson, N., Gullberg, M., & Lindberg, A. M. (2008). Real-time polymerase chain reaction as a rapid and efficient alternative to estimation of picornavirus titers by tissue culture infectious dose 50% or plaque forming units. *Microbiology and Immunology*, *53*(3), 149–154. https://doi.org/10.1111/j.1348-0421.2008.00107.x

Juan Martín-Serrano, Trinity Zang, P. D. B. (2001). *HIV-1 and Ebola virus encode small peptide motifs that recruit Tsg101 to sites of particle assembly to facilitate egress*.

Judson, S., Prescott, J., & Munster, V. (2015). Understanding Ebola virus transmission. In *Viruses* (Vol. 7, Issue 2, pp. 511–521). MDPI AG. https://doi.org/10.3390/v7020511

Kaletsky, R. L., Simmons, G., & Bates, P. (2007). Proteolysis of the Ebola Virus Glycoproteins Enhances Virus Binding and Infectivity. *Journal of Virology*, *81*(24), 13378–13384. https://doi.org/10.1128/jvi.01170-07

Kawaoka, Y., Naeve, C. W., & Webster, R. G. (1984). Is virulence of H5N2 influenza viruses in chickens associated with loss of carbohydrate from the hemagglutinin? *Virology*, *139*(2), 303–316. https://doi.org/10.1016/0042-6822(84)90376-3

Khiar, S., Pietrancosta, N., & Vidalain, P. O. (2015). Stimuler la réponse interféron de type I avec des petites molécules: le renouveau d'une vieille idée. *Biologie Aujourd'hui*, *209*(2), 145–159. https://doi.org/10.1051/jbio/2015015

Kilgore, P. E., Grabenstein, J. D., Salim, A. M., & Rybak, M. (2015). Treatment of Ebola virus disease. *Pharmacotherapy*, *35*(1), 43–53. https://doi.org/10.1002/phar.1545

Killington, R. A. (1996). *Virus isolation and quantitation*.

Kimberlina, C. R., Bornholdta, Z. A., Lib, S., Woods, V. L., MacRae, I. J., & Saphire, E. O. (2010). Ebolavirus VP35 uses a bimodal strategy to bind dsRNA for innate immune suppression. *Proceedings of the National Academy of Sciences of the United States of America*, *107*(1), 314–319. https://doi.org/10.1073/pnas.0910547107

Kimpton, J., & Emerman, M. (1992). Detection of replication-competent and pseudotyped human immunodeficiency virus with a sensitive cell line on the basis of activation of an integrated beta-galactosidase gene. *Journal of Virology*, *66*(4), 2232–2239. https://doi.org/10.1128/jvi.66.4.2232-

2239.1992
Kirchdoerfer, R. N., Abelson, D. M., Li, S., Wood, M. R., Saphire, O., Sciences, M., Jolla, L., Diego, S., Jolla, L., Facility, M., Jolla, L., & Jolla, L. (2016). *Assembly of the Ebola virus nucleoprotein from a chaperoned VP35 complex*. *12*(1), 140–149. https://doi.org/10.1016/j.celrep.2015.06.003.Assembly
Knobloch, J., Cornet, M., & Baskerville, A. (1978). Ebola haemorrhagic fever in Sudan, 1976. *Bulletin of the World Health Organization*, *56*(2), 247–270. https://doi.org/10.1021/ie000475z
Kruse, T., Biedenkopf, N., Hertz, E. P. T., Dietzel, E., Stalmann, G., López-Méndez, B., Davey, N. E., Nilsson, J., & Becker, S. (2018). The Ebola Virus Nucleoprotein Recruits the Host PP2A-B56 Phosphatase to Activate Transcriptional Support Activity of VP30. *Molecular Cell*, *69*(1), 136-145.e6. https://doi.org/10.1016/j.molcel.2017.11.034
Kubota, T., Matsuoka, M., Chang, T.-H., Bray, M., Jones, S., Tashiro, M., Kato, A., & Ozato, K. (2009). Ebolavirus VP35 Interacts with the Cytoplasmic Dynein Light Chain 8. *Journal of Virology*, *83*(13), 6952–6956. https://doi.org/10.1128/jvi.00480-09
Kugelman, J. R., Lee, M. S., Rossi, C. A., Mccarthy, S. E., Radoshitzky, S. R., Dye, J. M., Hensley, L. E., Honko, A., Kuhn, J. H., Jahrling, P. B., Warren, T. K., Whitehouse, C. A., Bavari, S., & Palacios, G. (2012). *Ebola Virus Genome Plasticity as a Marker of Its Passaging History : A Comparison of In Vitro Passaging to Non-Human Primate Infection*. *7*(11). https://doi.org/10.1371/journal.pone.0050316
Kuroda, M., Fujikura, D., Nanbo, A., Marzi, A., Noyori, O., Kajihara, M., Maruyama, J., Matsuno, K., Miyamoto, H., Yoshida, R., Feldmann, H., & Takada, A. (2015). Interaction between TIM-1 and NPC1 Is Important for Cellular Entry of Ebola Virus. *Journal of Virology*, *89*(12), 6481–6493. https://doi.org/10.1128/jvi.03156-14
Lacroix, A., Kingebeni, P. M., Kumugo, S. P. N., Lempu, G., Butel, C., Serrano, L., Vidal, N., Thaurignac, G., Esteban, A., Bamuleka, D. M., Likofata, J., Delaporte, E., Tamfum, J. J. M., Ayouba, A., Peeters, M., & Mundeke, S. A. (2021). Investigating the circulation of Ebola viruses in bats during the Ebola virus disease outbreaks in the Equateur and north Kivu provinces of the democratic republic of Congo from 2018. *Pathogens*, *10*(5). https://doi.org/10.3390/pathogens10050557
Lalle, E., Biava, M., Nicastri, E., Colavita, F., Di Caro, A., Vairo, F., Lanini, S., Castilletti, C., Langer, M., Zumla, A., Kobinger, G., Capobianchi, M. R., & Ippolito, G. (2019). Pulmonary involvement during the Ebola virus disease. In *Viruses* (Vol. 11, Issue 9). MDPI AG. https://doi.org/10.3390/v11090780
Larsen, T., Stevens, E. L., Davis, K. J., Geisbert, J. B., Daddario-DiCaprio, K. M., Jahrling, P. B., Hensley, L. E., & Geisbert, T. W. (2007). Pathologic findings associated with delayed death in nonhuman primates experimentally infected with Zaire Ebola virus. *Journal of Infectious Diseases*, *196*(SUPPL. 2), 323–328. https://doi.org/10.1086/520589
Lee, J. E., & Saphire, E. O. (2009). Ebolavirus glycoprotein structure and mechanism of entry. In *Future Virology* (Vol. 4, Issue 6, pp. 621–635). https://doi.org/10.2217/fvl.09.56
Lee, J., Kreutzberger, A. J. B., Odongo, L., Nelson, E. A., Nyenhuis, D. A., Kiessling, V., Liang, B., Cafiso, D. S., White, J. M., & Tamm, L. K. (2021). Ebola virus glycoprotein interacts with cholesterol to enhance membrane fusion and cell entry. *Nature Structural and Molecular Biology*, *28*(2), 181–189. https://doi.org/10.1038/s41594-020-00548-4
Lei, C., Yang, J., Hu, J., & Sun, X. (2021). On the Calculation of TCID50 for Quantitation of Virus Infectivity. *Virologica Sinica*, *36*(1), 141–144. https://doi.org/10.1007/s12250-020-00230-5
Lennemann, N. J., Rhein, B. A., Ndungo, E., Chandran, K., Qiu, X., & Maury, W. (2014). Comprehensive functional analysis of N-linked glycans on ebola virus GP1. *MBio*, *5*(1). https://doi.org/10.1128/mBio.00862-13
Leroy, E. M., Gonzalez, J. P., & Baize, S. (2011). Ebola and Marburg haemorrhagic fever viruses: Major scientific advances, but a relatively minor public health threat for Africa. *Clinical Microbiology and Infection*, *17*(7), 964–976. https://doi.org/10.1111/j.1469-0691.2011.03535.x
Leroy, É., Pourrut, X., & Gonzalez, J. P. (2006). Bats, reserves of the Ebola virus: The mystery is dissipated. In *Medecine/Sciences* (Vol. 22, Issue 1, pp. 78–79). Editions EDK. https://doi.org/10.1051/medsci/200622178
Leung, D. W., Borek, D. M., Luthra, P., Binning, J. M., Liu, G., Harvey, I. B., Su, Z., Endlich-frazier,

A., Pan, J., Shabman, R. S., Chiu, W., Davey, R., Otwinowski, Z., Christopher, F., Amarasinghe, G. K., Louis, S., States, U., States, U., States, U., … States, U. (2016). *An intrinsically disordered peptide from Ebola virus VP35 controls viral RNA synthesis by modulating nucleoprotein-RNA interactions*. *11*(3), 376–389. https://doi.org/10.1016/j.celrep.2015.03.034.An

Levi, M. (2001). Pathogenesis and treatment of disseminated intravascular coagulation in the septic patient. *Journal of Critical Care*, *16*(4), 167–177. https://doi.org/10.1053/jcrc.2001.30666

Liang, B. (2016). Structure of the L-protein of vesicular stomatitis virus from electron cryomicroscopy. *Cognition Emotion Journal*, *30*(7), 1289–1303. https://doi.org/10.1016/j.cell.2015.06.018.Structure

Licata, J. M., Johnson, R. F., Han, Z., & Harty, R. N. (2004). Contribution of Ebola Virus Glycoprotein, Nucleoprotein, and VP24 to Budding of VP40 Virus-Like Particles. *Journal of Virology*, *78*(14), 7344–7351. https://doi.org/10.1128/jvi.78.14.7344-7351.2004

Lichty, B. D., Power, A. T., Stojdl, D. F., & Bell, J. C. (2004). Vesicular stomatitis virus: Re-inventing the bullet. *Trends in Molecular Medicine*, *10*(5), 210–216. https://doi.org/10.1016/j.molmed.2004.03.003

Luban, J. (2013). No Time to Lose: A Life in Pursuit of Deadly Viruses by PeterPiot (2012) W. W. Norton & Company, Inc., New York, NY. *The FASEB Journal*, *27*(3), 853–854. https://doi.org/10.1096/fj.13-0302ufm

Lundstrom, K. (2020). Self-amplifying rna viruses as rna vaccines. In *International Journal of Molecular Sciences* (Vol. 21, Issue 14, pp. 1–29). MDPI AG. https://doi.org/10.3390/ijms21145130

Luria, S. E., & Anderson, T. F. (1942). The Identification and Characterization of Bacteriophages with the Electron Microscope. *Proceedings of the National Academy of Sciences*, *28*(4), 127. https://doi.org/10.1073/pnas.28.4.127

Luthra, P., Ramanan, P., Mire, C. E., Weisend, C., Yen, B., Liu, G., Leung, D. W., Geisbert, T. W., Ebihara, H., Amarasinghe, G. K., & Basler, C. F. (2014). *Mutual Antagonism between the Ebola Virus VP35 Protein and the RIG-I Activator PACT Determines Infection Outcome*. *14*(1), 1–23. https://doi.org/10.1016/j.chom.2013.06.010.Mutual

Madara, J. J., Han, Z., Ruthel, G., Freedman, B. D., & Harty, R. N. (2015). The multifunctional Ebola virus VP40 matrix protein is a promising therapeutic target. *Future Virology*, *10*(5), 537–546. https://doi.org/10.2217/fvl.15.6

Mahale, K. N., & Patole, M. S. (2015). The crux and crust of ebolavirus: Analysis of genome sequences and glycoprotein gene. *Biochemical and Biophysical Research Communications*, *463*(4), 756–761. https://doi.org/10.1016/j.bbrc.2015.06.008

Mahanty, S., Hutchinson, K., Agarwal, S., Mcrae, M., Rollin, P. E., & Pulendran, B. (2003). Cutting Edge: Impairment of Dendritic Cells and Adaptive Immunity by Ebola and Lassa Viruses. *The Journal of Immunology*, *170*(6), 2797–2801. https://doi.org/10.4049/jimmunol.170.6.2797

Malvy, D., McElroy, A. K., de Clerck, H., Günther, S., & van Griensven, J. (2019). Ebola virus disease. In *The Lancet* (Vol. 393, Issue 10174, pp. 936–948). Lancet Publishing Group. https://doi.org/10.1016/S0140-6736(18)33132-5

Mammen, E. F. (1994). Coagulation defects in liver disease. *Medical Clinics of North America*, *78*(3), 545–554. https://doi.org/10.1016/S0025-7125(16)30146-8

Mandl, J. N., & Feinberg, M. B. (2015). Robust and sustained immune activation in human Ebola virus infection. In *Proceedings of the National Academy of Sciences of the United States of America* (Vol. 112, Issue 15, pp. 4518–4519). https://doi.org/10.1073/pnas.1503864112

Markosyan, R. M., Miao, C., Zheng, Y. M., Melikyan, G. B., Liu, S. L., & Cohen, F. S. (2016). Induction of Cell-Cell Fusion by Ebola Virus Glycoprotein: Low pH Is Not a Trigger. *PLoS Pathogens*, *12*(1), 1–31. https://doi.org/10.1371/journal.ppat.1005373

Martin, B., Hoenen, T., Canard, B., & Decroly, E. (2016). Filovirus proteins for antiviral drug discovery: A structure/function analysis of surface glycoproteins and virus entry. *Antiviral Research*, *135*, 1–14. https://doi.org/10.1016/j.antiviral.2016.09.001

Martines, R. B., Ng, D. L., Greer, P. W., Rollin, P. E., & Zaki, S. R. (2015). Tissue and cellular tropism, pathology and pathogenesis of Ebola and Marburg viruses. *Journal of Pathology*, *235*(2), 153–174. https://doi.org/10.1002/path.4456

Martínez, M. J., Biedenkopf, N., Volchkova, V., Hartlieb, B., Alazard-Dany, N., Reynard, O., Becker,

S., & Volchkov, V. (2008). Role of Ebola Virus VP30 in Transcription Reinitiation. *Journal of Virology*, *82*(24), 12569–12573. https://doi.org/10.1128/jvi.01395-08

Martínez, M. J., Salim, A. M., Hurtado, J. C., & Kilgore, P. E. (2015). Ebola Virus Infection: Overview and Update on Prevention and Treatment. In *Infectious Diseases and Therapy* (Vol. 4, Issue 4, pp. 365–390). Springer Healthcare. https://doi.org/10.1007/s40121-015-0079-5

Martinez, O., Tantral, L., Mulherkar, N., Chandran, K., & Basler, C. F. (2011). Impact of Ebola mucin-like domain on antiglycoprotein antibody responses induced by Ebola virus-like particles. *Journal of Infectious Diseases*, *204*(SUPPL. 3), 825–832. https://doi.org/10.1093/infdis/jir295

Martinez, O., Valmas, C., & Basler, C. F. (2007). Ebola virus-like particle-induced activation of NF-κB and Erk signaling in human dendritic cells requires the glycoprotein mucin domain. *Virology*, *364*(2), 342–354. https://doi.org/10.1016/j.virol.2007.03.020

Mateo, M., Carbonnelle, C., Reynard, O., Kolesnikova, L., Nemirov, K., Page, A., Volchkova, V. A., & Volchkov, V. E. (2011). VP24 Is a molecular determinant of Ebola virus virulence in guinea pigs. *Journal of Infectious Diseases*, *204*(SUPPL. 3), 1011–1020. https://doi.org/10.1093/infdis/jir338

Mateo, M., Reid, S. P., Leung, L. W., Basler, C. F., & Volchkov, V. E. (2010). Ebolavirus VP24 Binding to Karyopherins Is Required for Inhibition of Interferon Signaling. *Journal of Virology*, *84*(2), 1169–1175. https://doi.org/10.1128/jvi.01372-09

McElroy, A. (2015). Understanding bleeding in Ebola virus disease. *Clinical Advances in Hematology and Oncology*, *13*(1), 29–31.

McElroy, A. K., Akondy, R. S., Davis, C. W., Ellebedy, A. H., Mehta, A. K., Kraft, C. S., Lyon, G. M., Ribner, B. S., Varkey, J., Sidney, J., Sette, A., Campbell, S., Ströher, U., Damon, I., Nichol, S. T., Spiropoulou, C. F., & Ahmed, R. (2015). Human Ebola virus infection results in substantial immune activation. *Proceedings of the National Academy of Sciences of the United States of America*, *112*(15), 4719–4724. https://doi.org/10.1073/pnas.1502619112

Mcgivern, D. R., Collins, P. L., & Fearns, R. (2005). *Identification of Internal Sequences in the 3 J Leader Region of Human Respiratory Syncytial Virus That Enhance Transcription and Confer Replication Processivity*. *79*(4), 2449–2460. https://doi.org/10.1128/JVI.79.4.2449

Mehedi, M., Falzarano, D., Seebach, J., Hu, X., Carpenter, M. S., Schnittler, H.-J., & Feldmann, H. (2011). A New Ebola Virus Nonstructural Glycoprotein Expressed through RNA Editing. *Journal of Virology*, *85*(11), 5406–5414. https://doi.org/10.1128/jvi.02190-10

Mercier, P. Le, Garcin, D., Garcia, E., & Kolakofsky, D. (2003). *Competition between the Sendai Virus N mRNA Start Site and the Genome 3 J -End Promoter for Viral RNA Polymerase*. *77*(17), 9147–9155. https://doi.org/10.1128/JVI.77.17.9147

Miao, C., Li, M., Zheng, Y. M., Cohen, F. S., & Liu, S. L. (2016). Cell-cell contact promotes Ebola virus GP-mediated infection. *Virology*, *488*, 202–215. https://doi.org/10.1016/j.virol.2015.11.019

Miller, E. H., Obernosterer, G., Raaben, M., Herbert, A. S., Deffieu, M. S., Krishnan, A., Ndungo, E., Sandesara, R. G., Carette, J. E., Kuehne, A. I., Ruthel, G., Pfeffer, S. R., Dye, J. M., Whelan, S. P., Brummelkamp, T. R., & Chandran, K. (2012). Ebola virus entry requires the host-programmed recognition of an intracellular receptor. *EMBO Journal*, *31*(8), 1947–1960. https://doi.org/10.1038/emboj.2012.53

Miyake, T., Farley, C. M., Neubauer, B. E., Beddow, T. P., Hoenen, T., & Engel, D. A. (2020). Ebola Virus Inclusion Body Formation and RNA Synthesis Are Controlled by a Novel Domain of Nucleoprotein Interacting with VP35. *Journal of Virology*, *94*(16), 1–18. https://doi.org/10.1128/jvi.02100-19

Mizzen, L., Hilton, A., Cheley, S., & Anderson, R. (1985). Attenuation of murine coronavirus infection by ammonium chloride. *Virology*, *142*(2), 378–388. https://doi.org/10.1016/0042-6822(85)90345-9

Modrof, J., Mühlberger, E., Klenk, H. D., & Becker, S. (2002). Phosphorylation of VP30 impairs Ebola virus transcription. *Journal of Biological Chemistry*, *277*(36), 33099–33104. https://doi.org/10.1074/jbc.M203775200

Mohamadzadeh, M. (2009). *Potential Factors Induced by Filoviruses that Lead to Immune Supression*. 174–185.

Mohan, G. S., Li, W., Ye, L., Compans, R. W., & Yang, C. (2012). *Antigenic Subversion : A Novel Mechanism of Host Immune Evasion by Ebola Virus*. *8*(12).

https://doi.org/10.1371/journal.ppat.1003065
Moller-Tank, S., & Maury, W. (2014). Phosphatidylserine receptors: Enhancers of enveloped virus entry and infection. *Virology*, *468*, 565–580. https://doi.org/10.1016/j.virol.2014.09.009
Morikawa, S., Saijo, M., & Kurane, I. (2007). Current knowledge on lower virulence of Reston Ebola virus (in French: Connaissances actuelles sur la moindre virulence du virus Ebola Reston). In *Comparative Immunology, Microbiology and Infectious Diseases* (Vol. 30, Issues 5–6, pp. 391–398). https://doi.org/10.1016/j.cimid.2007.05.005
Morwitzer, M. J., Tritsch, S. R., Cazares, L. H., Ward, M. D., Nuss, J. E., Bavari, S., & Reid, S. P. (2019). Identification of RUVBL1 and RUVBL2 as novel cellular interactors of the Ebola virus nucleoprotein. *Viruses*, *11*(4). https://doi.org/10.3390/v11040372
Mühlberger, E., Weik, M., Volchkov, V. E., Klenk, H.-D., & Becker, S. (1999). Comparison of the Transcription and Replication Strategies of Marburg Virus and Ebola Virus by Using Artificial Replication Systems. *Journal of Virology*, *73*(3), 2333–2342. https://doi.org/10.1128/jvi.73.3.2333-2342.1999
Mulherkar, N., Raaben, M., de la Torre, J. C., Whelan, S. P., & Chandran, K. (2011). The Ebola virus glycoprotein mediates entry via a non-classical dynamin-dependent macropinocytic pathway. *Virology*, *419*(2), 72–83. https://doi.org/10.1016/j.virol.2011.08.009
Munjita, S., & Kwenda, G. (2015). Descriptive Analysis of Ebola virus Proteins: Towards Development of Effective Therapeutics and Vaccines. *British Microbiology Research Journal*, *8*(3), 457–479. https://doi.org/10.9734/bmrj/2015/16297
Muyembe-Tamfum, J. J., Mulangu, S., Masumu, J., Kayembe, J. M., Kemp, A., & Paweska, J. T. (2012). Ebola virus outbreaks in Africa: Past and present. *Onderstepoort Journal of Veterinary Research*, *79*(2). https://doi.org/10.4102/ojvr.v79i2.451
Nakayama, E., & Saijo, M. (2013). Animal models for Ebola and Marburg virus infections. In *Frontiers in Microbiology* (Vol. 4, Issue SEP). Frontiers Research Foundation. https://doi.org/10.3389/fmicb.2013.00267
Nakayama, K. (1997). Furin: A mammalian subtilisin/Kex2p-like endoprotease involved in processing of a wide variety of precursor proteins. *Biochemical Journal*, *327*(3), 625–635. https://doi.org/10.1042/bj3270625
Nelson, E. V., & Schmidt, K. M. (2017). Analysis of the cellular stress response during ebola virus infection by immunofluorescence. In *Methods in Molecular Biology* (Vol. 1628, pp. 211–225). Humana Press Inc. https://doi.org/10.1007/978-1-4939-7116-9_17
Nemerson, Y. (1988). Tissue factor and hemostasis [published erratum appears in Blood 1988 Apr;71(4):1178]. *Blood*, *71*(1), 1–8. https://doi.org/10.1182/blood.v71.1.1.1
Neumann, G., Watanabe, S., & Kawaoka, Y. (2009). *Characterization of Ebolavirus regulatory genomic regions*. *144*, 1–7. https://doi.org/10.1016/j.virusres.2009.02.005
Niemuth, N. A., Fallacara, D., Triplett, C. A., Tamrakar, S. M., Rajbhandari, A., Florence, C., Ward, L., Griffiths, A., Carrion, R., Goez-Gazi, Y., Alfson, K. J., Staples, H. M., Brasel, T., Comer, J. E., Massey, S., Smith, J., Kocsis, A., Lowry, J., Johnston, S. C., … Fay, M. P. (2021). Natural history of disease in cynomolgus monkeys exposed to Ebola virus Kikwit strain demonstrates the reliability of this nonhuman primate model for Ebola virus disease. *PLoS ONE*, *16*(7 July). https://doi.org/10.1371/journal.pone.0252874
Ning, Y. J., Deng, F., Hu, Z., & Wang, H. (2017). The roles of ebolavirus glycoproteins in viral pathogenesis. In *Virologica Sinica* (Vol. 32, Issue 1, pp. 3–15). Science Press. https://doi.org/10.1007/s12250-016-3850-1
Ning, Y. J., Kang, Z., Xing, J., Min, Y. Q., Liu, D., Feng, K., Wang, M., Deng, F., Zhou, Y., Hu, Z., & Wang, H. (2018). Ebola virus mucin-like glycoprotein (Emuc) induces remarkable acute inflammation and tissue injury: evidence for Emuc pathogenicity in vivo. In *Protein and Cell* (Vol. 9, Issue 4, pp. 389–393). Higher Education Press. https://doi.org/10.1007/s13238-017-0471-x
Noda, T. (2017). Electron microscopy of ebola virus-infected cells. In *Methods in Molecular Biology* (Vol. 1628, pp. 243–250). Humana Press Inc. https://doi.org/10.1007/978-1-4939-7116-9_19
Noda, T., Ebihara, H., Muramoto, Y., Fujii, K., Takada, A., Sagara, H., Jin, H. K., Kida, H., Feldmann, H., & Kawaoka, Y. (2006). Assembly and budding of Ebolavirus. *PLoS Pathogens*, *2*(9), 0864–0872. https://doi.org/10.1371/journal.ppat.0020099
Noda, T., Sagara, H., Suzuki, E., Takada, A., Kida, H., & Kawaoka, Y. (2002). Ebola Virus VP40 Drives

the Formation of Virus-Like Filamentous Particles Along with GP. *Journal of Virology*, *76*(10), 4855–4865. https://doi.org/10.1128/jvi.76.10.4855-4865.2002

Oestereich, L., Lüdtke, A., Wurr, S., Rieger, T., Muñoz-Fontela, C., & Günther, S. (2014). Successful treatment of advanced Ebola virus infection with T-705 (favipiravir) in a small animal model. *Antiviral Research*, *105*(1), 17–21. https://doi.org/10.1016/j.antiviral.2014.02.014

Ogino, T., & Green, T. J. (2019). RNA synthesis and capping by nonsegmented negative strand RNA viral polymerases: Lessons from a prototypic virus. *Frontiers in Microbiology*, *10*(JULY), 1–28. https://doi.org/10.3389/fmicb.2019.01490

Oliphant, E. (2014). Ebola hemorrhagic fever: genetic biomarkers and vaccine development. In *Genetic testing and molecular biomarkers* (Vol. 18, Issue 11, pp. 715–716). https://doi.org/10.1089/gtmb.2014.1560

Olupot-Olupot, P. (2015). Ebola in children: Epidemiology, clinical features, diagnosis and outcomes. *Pediatric Infectious Disease Journal*, *34*(3), 314–316. https://doi.org/10.1097/INF.0000000000000638

Ortega, V., Stone, J. A., Contreras, E. M., Iorio, R. M., & Aguilar, H. C. (2019). Addicted to sugar: Roles of glycans in the order Mononegavirales. *Glycobiology*, *29*(1), 2–21. https://doi.org/10.1093/glycob/cwy053

Ou, W., Delisle, J., Jacques, J., Shih, J., Price, G., Kuhn, J. H., Wang, V., Verthelyi, D., Kaplan, G., & Wilson, C. A. (2012). Induction of ebolavirus cross-species immunity using retrovirus-like particles bearing the Ebola virus glycoprotein lacking the mucin-like domain. *Virology Journal*, *9*. https://doi.org/10.1186/1743-422X-9-32

P., C., M.C., M., & S.T., N. (1999). Ebola virus defective interfering particles and persistent infection. *Virology*, *262*(1), 114–128. http://ovidsp.ovid.com/ovidweb.cgi?T=JS&PAGE=reference&D=emed4&NEWS=N&AN=1999337759

Pallesen, J., Murin, C. D., De Val, N., Cottrell, C. A., Hastie, K. M., Turner, H. L., Fusco, M. L., Flyak, A. I., Zeitlin, L., Crowe, J. E., Andersen, K. G., Saphire, E. O., & Ward, A. B. (2016). Structures of Ebola virus GP and sGP in complex with therapeutic antibodies. *Nature Microbiology*, *1*(1), 139–148. https://doi.org/10.1038/nmicrobiol.2016.128

Pappalardo, M., Julia, M., Howard, M. J., Rossman, J. S., Michaelis, M., & Wass, M. N. (2016). Conserved differences in protein sequence determine the human pathogenicity of Ebolaviruses. *Scientific Reports*, *6*(March). https://doi.org/10.1038/srep23743

Park, D. J., Dudas, G., Wohl, S., Goba, A., Whitmer, S. L. M., Andersen, K. G., Sealfon, R. S., Ladner, J. T., Kugelman, J. R., Matranga, C. B., Winnicki, S. M., Qu, J., Gire, S. K., Gladden-Young, A., Jalloh, S., Nosamiefan, D., Yozwiak, N. L., Moses, L. M., Jiang, P. P., … Sabeti, P. C. (2015). Ebola Virus Epidemiology, Transmission, and Evolution during Seven Months in Sierra Leone. *Cell*, *161*(7), 1516–1526. https://doi.org/10.1016/j.cell.2015.06.007

Patrick Reid, S., Shurtleff, A. C., Costantino, J. A., Tritsch, S. R., Retterer, C., Spurgers, K. B., & Bavari, S. (2014). HSPA5 is an essential host factor for Ebola virus infection. *Antiviral Research*, *109*(1), 171–174. https://doi.org/10.1016/j.antiviral.2014.07.004

Peñas, J. A., Miranda, M. E., de Los Reyes, V. C., Sucaldito, M. N. L., & Magpantay, R. L. (2019). Risk assessment of Ebola Reston virus in humans in the Philippines. *Western Pacific Surveillance and Response Journal : WPSAR*, *10*(3), 1–8. https://doi.org/10.5365/wpsar.2017.3.004

Penny, C. J., Vassileva, K., Jha, A., Yuan, Y., Chee, X., Yates, E., Mazzon, M., Kilpatrick, B. S., Muallem, S., Marsh, M., Rahman, T., & Patel, S. (2019). Mining of Ebola virus entry inhibitors identifies approved drugs as two-pore channel pore blockers. *Biochimica et Biophysica Acta - Molecular Cell Research*, *1866*(7), 1151–1161. https://doi.org/10.1016/j.bbamcr.2018.10.022

Perkins, M. D., & Kessel, M. (2015). What Ebola tells us about outbreak diagnostic readiness. In *Nature Biotechnology* (Vol. 33, Issue 5, pp. 464–469). https://doi.org/10.1038/nbt.3215

Piot, P., & Spencer, J. (2018). From 1976 to 2018: Reflections on early investigations into the Ebola virus. In *Transactions of the Royal Society of Tropical Medicine and Hygiene* (Vol. 112, Issue 12, pp. 527–528). Oxford University Press. https://doi.org/10.1093/trstmh/try088

Prescott, J., Bushmaker, T., Fischer, R., Miazgowicz, K., Judson, S., & Munster, V. J. (2015). Postmortem stability of Ebola virus. *Emerging Infectious Diseases*, *21*(5), 856–859. https://doi.org/10.3201/eid2105.150041

Prins, K. C., Cárdenas, W. B., & Basler, C. F. (2009). Ebola Virus Protein VP35 Impairs the Function of Interferon Regulatory Factor-Activating Kinases IKKε and TBK-1. *Journal of Virology*, *83*(7), 3069–3077. https://doi.org/10.1128/jvi.01875-08

Raab, M., Roth, E., Nguyen, V. K., & Froeschl, G. (2021). The 2021 ebola virus outbreak in guinea: Mistrust and the shortcomings of outbreak surveillance. *PLoS Neglected Tropical Diseases*, *15*(6). https://doi.org/10.1371/journal.pntd.0009487

Radoshitzky, S. R., Warfield, K. L., Chi, X., Dong, L., Kota, K., Bradfute, S. B., Gearhart, J. D., Retterer, C., Kranzusch, P. J., Misasi, J. N., Hogenbirk, M. A., Wahl-jensen, V., Volchkov, V. E., Cunningham, J. M., Jahrling, P. B., Aman, M. J., Bavari, S., Farzan, M., Kuhn, J. H., … Universite, C. B. (2011). *Ebolavirus ◌-Peptide Immunoadhesins Inhibit Marburgvirus and Ebolavirus Cell Entry □*. *85*(17), 8502–8513. https://doi.org/10.1128/JVI.02600-10

Rashighi, M., & Harris, J. E. (2017). Ebola RNA Persistence in Semen of Ebola Virus Disease Survivors. *Physiology & Behavior*, *176*(3), 139–148. https://doi.org/10.1053/j.gastro.2016.08.014.CagY

Rasmussen, A. L. (2016). Host Factors in Ebola Infection. In *Annual Review of Genomics and Human Genetics* (Vol. 17, pp. 333–351). Annual Reviews Inc. https://doi.org/10.1146/annurev-genom-083115-022446

Rey, F. (2021). Structure-function relations of the sars-cov-2 spike protein and impact of mutations in the variants of concern. *Comptes Rendus - Biologies*, *344*(1), 77–110. https://doi.org/10.5802/CRBIOL.53

Reynard, O., Borowiak, M., Volchkova, V. A., Delpeut, S., Mateo, M., & Volchkov, V. E. (2009a). Ebolavirus Glycoprotein GP Masks both Its Own Epitopes and the Presence of Cellular Surface Proteins. *Journal of Virology*, *83*(18), 9596–9601. https://doi.org/10.1128/jvi.00784-09

Reynard, O., Borowiak, M., Volchkova, V. A., Delpeut, S., Mateo, M., & Volchkov, V. E. (2009b). *Ebolavirus Glycoprotein GP Masks both Its Own Epitopes and the Presence of Cellular Surface Proteins □*. *83*(18), 9596–9601. https://doi.org/10.1128/JVI.00784-09

Reynard, O., & Volchkov, V. E. (2015). Entry of Ebola Virus is an Asynchronous Process. *Journal of Infectious Diseases*, *212*, S199–S203. https://doi.org/10.1093/infdis/jiv189

Reynolds, P., & Marzi, A. (2017). Ebola and Marburg virus vaccines. In *Virus Genes* (Vol. 53, Issue 4, pp. 501–515). Springer New York LLC. https://doi.org/10.1007/s11262-017-1455-x

Rivera, A., & Messaoudi, I. (2015). *Pathophysiology of Ebola Virus Infection: Current Challenges and Future Hopes*. https://doi.org/10.1021/id5000426

Rivera, A., & Messaoudi, I. (2016). Molecular mechanisms of Ebola pathogenesis. *Journal of Leukocyte Biology*, *100*(5), 889–904. https://doi.org/10.1189/jlb.4ri0316-099rr

Rodriguez, L. L., Roo, A. De, Guimard, Y., Trappier, S. G., Sanchez, A., Bressler, D., Williams, A. J., Rowe, A. K., Bertolli, J., Khan, A. S., Ksiazek, T. G., Peters, C. J., & Nichol, S. T. (1995). *Persistence and Genetic Stability of Ebola Virus during the Outbreak in Kikwit , Democratic Republic of the Congo , 1995*. 170–176.

Rollin, P. E., Bausch, D. G., & Sanchez, A. (2007). Blood chemistry measurements and D-dimer levels associated with fatal and nonfatal outcomes in humans infected with Sudan Ebola virus. *Journal of Infectious Diseases*, *196*(SUPPL. 2). https://doi.org/10.1086/520613

Saeed, M. F., Kolokoltsov, A. A., Albrecht, T., & Davey, R. A. (2010). Cellular entry of ebola virus involves uptake by a macropinocytosis-like mechanism and subsequent trafficking through early and late endosomes. *PLoS Pathogens*, *6*(9). https://doi.org/10.1371/journal.ppat.1001110

Saijo, M., Niikura, M., Ikegami, T., Kurane, I., Kurata, T., & Morikawa, S. (2006). Laboratory diagnostic systems for Ebola and Marburg hemorrhagic fevers developed with recombinant proteins. In *Clinical and Vaccine Immunology* (Vol. 13, Issue 4, pp. 444–451). https://doi.org/10.1128/CVI.13.4.444-451.2006

Sanchez, A. (2007). Analysis of filovirus entry into vero E6 cells, using inhibitors of endocytosis, endosomal acidification, structural integrity, and cathepsin (B and L) activity. *Journal of Infectious Diseases*, *196*(SUPPL. 2), 251–258. https://doi.org/10.1086/520597

Sanchez, A. (2014). Ebola virus. *Centers for Disease Control and Prevention*, *17*(4), 242–247. https://doi.org/10.1684/mtp.2014.0537

Sanchez, A., Kiley, M. P., Kienk, H., & Feldmann, H. (1992). *Sequence analysis of the Marburg virus*

nucleoprotein gene : comparison to Ebola virus and other non-segmented negative-strand RNA viruses. *3*, 347–357.

Sanchez, A., Lukwiya, M., Bausch, D., Mahanty, S., Sanchez, A. J., Wagoner, K. D., & Rollin, P. E. (2004). Analysis of Human Peripheral Blood Samples from Fatal and Nonfatal Cases of Ebola (Sudan) Hemorrhagic Fever: Cellular Responses, Virus Load, and Nitric Oxide Levels. *Journal of Virology*, *78*(19), 10370–10377. https://doi.org/10.1128/jvi.78.19.10370-10377.2004

Sanchez, A., Trappier, S. G., Mahy, B. W. J., Peters, C. J., & Nichol, S. T. (1996). The virion glycoproteins of Ebola viruses are encoded in two reading frames and are expressed through transcriptional editing. *Proceedings of the National Academy of Sciences of the United States of America*, *93*(8), 3602–3607. https://doi.org/10.1073/pnas.93.8.3602

Sanchez, A., Yang, Z.-Y., Xu, L., Nabel, G. J., Crews, T., & Peters, C. J. (1998). Biochemical Analysis of the Secreted and Virion Glycoproteins of Ebola Virus. *Journal of Virology*, *72*(8), 6442–6447. https://doi.org/10.1128/jvi.72.8.6442-6447.1998

Santoro, F., Donato, A., Lucchesi, S., Sorgi, S., Gerlini, A., Haks, M. C., Ottenhoff, T. H. M., Gonzalez-Dias, P., Nakaya, H. I., Huttner, A., Siegrist, C. A., Medaglini, D., & Pozzi, G. (2021). Human transcriptomic response to the VSV-vectored ebola vaccine. *Vaccines*, *9*(2), 1–15. https://doi.org/10.3390/vaccines9020067

Schickli, J. H., Kaur, J., Ulbrandt, N., Spaete, R. R., & Tang, R. S. (2005). An S101P Substitution in the Putative Cleavage Motif of the Human Metapneumovirus Fusion Protein Is a Major Determinant for Trypsin-Independent Growth in Vero Cells and Does Not Alter Tissue Tropism in Hamsters. *Journal of Virology*, *79*(16), 10678–10689. https://doi.org/10.1128/jvi.79.16.10678-10689.2005

Schieffelin, J. S., Shaffer, J. G., Goba, A., Gbakie, M., Gire, S. K., Colubri, A., Sealfon, R. S. G., Kanneh, L., Moigboi, A., Momoh, M., Fullah, M., Moses, L. M., Brown, B. L., Andersen, K. G., Winnicki, S., Schaffner, S. F., Park, D. J., Yozwiak, N. L., Jiang, P.-P., … Garry, R. F. (2014). Clinical Illness and Outcomes in Patients with Ebola in Sierra Leone. *New England Journal of Medicine*, *371*(22), 2092–2100. https://doi.org/10.1056/nejmoa1411680

Schlereth, J., Grünweller, A., Biedenkopf, N., Becker, S., & Hartmann, R. K. (2016). RNA binding specificity of Ebola virus transcription factor VP30. *RNA Biology*, *13*(9), 783–798. https://doi.org/10.1080/15476286.2016.1194160

Schmidt, M. L., & Hoenen, T. (2017). Characterization of the catalytic center of the Ebola virus L polymerase. *PLoS Neglected Tropical Diseases*, *11*(10), 1–14. https://doi.org/10.1371/journal.pntd.0005996

Schnell, M. J., Buonocore, L., Whitt, M. A., & Rose, J. K. (1996). *The Minimal Conserved Transcription Stop-Start Signal Promotes Stable Expression of a Foreign Gene in Vesicular Stomatitis Virus*. *70*(4), 2318–2323.

Schudt, G., Dolnik, O., Kolesnikova, L., Biedenkopf, N., Herwig, A., & Becker, S. (2015). Transport of Ebolavirus Nucleocapsids Is Dependent on Actin Polymerization: Live-Cell Imaging Analysis of Ebolavirus-Infected Cells. *Journal of Infectious Diseases*, *212*(Suppl 2), S160–S166. https://doi.org/10.1093/infdis/jiv083

Schümann, M., Gantke, T., & Mühlberger, E. (2009). Ebola Virus VP35 Antagonizes PKR Activity through Its C-Terminal Interferon Inhibitory Domain. *Journal of Virology*, *83*(17), 8993–8997. https://doi.org/10.1128/jvi.00523-09

Shabman, R. S., Hoenen, T., Groseth, A., Jabado, O., Binning, J. M., Amarasinghe, G. K., Feldmann, H., & Basler, C. F. (2013). *An Upstream Open Reading Frame Modulates Ebola Virus Polymerase Translation and Virus Replication*. *9*(1). https://doi.org/10.1371/journal.ppat.1003147

Shabman, R. S., Jabado, O. J., Mire, C. E., Stockwell, T. B., Edwards, M., Mahajan, M., Geisbert, T. W., & Basler, F. (2014). *Deep Sequencing Identifies Noncanonical Editing of Ebola and Marburg Virus RNAs in Infected Cells*. *5*(6), 1–11. https://doi.org/10.1128/mBio.02011-14.Editor

Shabman, R. S., Leung, D. W., Johnson, J., Glennon, N., Gulcicek, E. E., Stone, K. L., Leung, L., Hensley, L., Amarasinghe, G. K., & Basler, C. F. (2011). DRBP76 associates with Ebola virus VP35 and suppresses viral polymerase function. *Journal of Infectious Diseases*, *204*(SUPPL. 3), 911–918. https://doi.org/10.1093/infdis/jir343

Shorten, R. J., Brown, C. S., Jacobs, M., Rattenbury, S., Simpson, A. J., & Mepham, S. (2016). Diagnostics in Ebola Virus Disease in Resource-Rich and Resource-Limited Settings. In *PLoS Neglected Tropical Diseases* (Vol. 10, Issue 10). Public Library of Science.

https://doi.org/10.1371/journal.pntd.0004948
Simmons, G., Wool-Lewis, R. J., Baribaud, F., Netter, R. C., & Bates, P. (2002). Ebola Virus Glycoproteins Induce Global Surface Protein Down-Modulation and Loss of Cell Adherence. *Journal of Virology*, *76*(5), 2518–2528. https://doi.org/10.1128/jvi.76.5.2518-2528.2002
Simon, H. (2000). *Role of reactive oxygen species (ROS).pdf* (pp. 415–418).
Soni, S. P., Adu-Gyamfi, E., Yong, S. S., Jee, C. S., & Stahelin, R. V. (2013). The Ebola virus matrix protein deeply penetrates the plasma membrane: An important step in viral egress. *Biophysical Journal*, *104*(9), 1940–1949. https://doi.org/10.1016/j.bpj.2013.03.021
Spengler, J. R., Prescott, J., Feldmann, H., & Spiropoulou, C. F. (2017). Human immune system mouse models of Ebola virus infection. In *Current Opinion in Virology* (Vol. 25, pp. 90–96). Elsevier B.V. https://doi.org/10.1016/j.coviro.2017.07.028
Srinivas, V., Yadav, P., Mittal, V., Chaubal, G., Chhabra, M., Mattoo, S., Rai, A., & Mourya, D. T. (2016). Follow-up of Ebola Patient, 2014–2015. *Emerging Infectious Diseases*, *83*(4), 748–750. https://doi.org/10.4269/ajtmh.2010.10-0237
St Claire, M. C., Ragland, D. R., Bollinger, L., & Jahrling, P. B. (2017). Animal models of Ebolavirus infection. In *Comparative Medicine* (Vol. 67, Issue 3, pp. 253–262).
Stahelin, R. V. (2014). *Membrane binding and bending in Ebola VP40 assembly and egress*. *5*(June), 1–12. https://doi.org/10.3389/fmicb.2014.00300
Stoop, N., Desbureaux, S., Kaota, A., Lunanga, E., & Verpoorten, M. (2021). Covid-19 vs. Ebola: Impact on households and small businesses in North Kivu, Democratic Republic of Congo. *World Development*, *140*, 105352. https://doi.org/10.1016/j.worlddev.2020.105352
Sui, J., & Marasco, W. A. (2002). *Evidence against Ebola Virus sGP Binding to Human Neutrophils by a Specific Receptor*. *14*, 9–14. https://doi.org/10.1006/viro.2002.1715
Sullivan, N. J., Peterson, M., Yang, Z., Kong, W., Duckers, H., Nabel, E., & Nabel, G. J. (2005). Ebola Virus Glycoprotein Toxicity Is Mediated by a Dynamin-Dependent Protein-Trafficking Pathway. *Journal of Virology*, *79*(1), 547–553. https://doi.org/10.1128/jvi.79.1.547-553.2005
Sztuba-solinska, J., Diaz, L., Kumar, M. R., Wiley, M. R., Jozwick, L., Kuhn, J. H., Palacios, G., Radoshitzky, S. R., Le, S. F. J., & Johnson, R. F. (2016). *A small stem-loop structure of the Ebola virus trailer is essential for replication and interacts with heat-shock protein A8*. *44*(20), 9831–9846. https://doi.org/10.1093/nar/gkw825
Tai, C. J., Li, C. L., Tai, C. J., Wang, C. K., & Lin, L. T. (2015). Early viral entry assays for the identification and evaluation of antiviral compounds. *Journal of Visualized Experiments*, *2015*(104), 1–8. https://doi.org/10.3791/53124
Takada, A., Fujioka, K., Tsuiji, M., Morikawa, A., Higashi, N., Ebihara, H., Kobasa, D., Feldmann, H., Irimura, T., & Kawaoka, Y. (2004). Human Macrophage C-Type Lectin Specific for Galactose and N -Acetylgalactosamine Promotes Filovirus Entry . *Journal of Virology*, *78*(6), 2943–2947. https://doi.org/10.1128/jvi.78.6.2943-2947.2004
Takada, A., Watanabe, S., Ito, H., Okazaki, K., Kida, H., & Kawaoka, Y. (2000). Downregulation of β1 integrins by Ebola virus glycoprotein: Implication for virus entry. *Virology*, *278*(1), 20–26. https://doi.org/10.1006/viro.2000.0601
Takahashi, K., Halfmann, P., Oyama, M., Kozuka-Hata, H., Noda, T., & Kawaoka, Y. (2013). DNA Topoisomerase 1 Facilitates the Transcription and Replication of the Ebola Virus Genome. *Journal of Virology*, *87*(16), 8862–8869. https://doi.org/10.1128/jvi.03544-12
Tao, W., Xu, C., Ding, Q., Li, R., Xiang, Y., Chung, J., & Zhong, J. (2009). A single point mutation in E2 enhances hepatitis C virus infectivity and alters lipoprotein association of viral particles. *Virology*, *395*(1), 67–76. https://doi.org/10.1016/j.virol.2009.09.006
Taylor, J., Toh, C. H., Hoots, W. K., Wada, H., & Levi, M. (2001). Towards definition, clinical and laboratory criteria, and a scoring system for disseminated intravascular coagulation: On behalf of the scientific subcommittee on Disseminated Intravascular Coagulation (DIC) of the International Society on Thrombosis and . In *Thrombosis and Haemostasis* (Vol. 86, Issue 5, pp. 1327–1330). https://doi.org/10.1055/s-0037-1616068
Tchesnokov, E. P., Raeisimakiani, P., Ngure, M., Marchant, D., & Götte, M. (2018). Recombinant RNA-Dependent RNA Polymerase Complex of Ebola Virus. *Scientific Reports*, *8*(1), 1–9. https://doi.org/10.1038/s41598-018-22328-3
Thi, E. P., Mire, C. E., Lee, A. C. H., Geisbert, J. B., Zhou, J. Z., Agans, K. N., Snead, N. M., Deer, D.

J., Barnard, T. R., Fenton, K. A., Maclachlan, I., & Geisbert, T. W. (2015). Lipid nanoparticle siRNA treatment of Ebola-virus-Makona-infected nonhuman primates. *Nature*, *521*(7552), 362–365. https://doi.org/10.1038/nature14442

Torres, M., Hansen, K. N., & Jerrard, D. (2015). A Review for Emergency Providers. In *Emergency Medicine Clinics of North America* (Vol. 33, Issue 2, pp. e1–e18). W.B. Saunders. https://doi.org/10.1016/j.emc.2014.12.001

Tran, E. E. H., Simmons, J. A., Bartesaghi, A., Shoemaker, C. J., Nelson, E., White, J. M., & Subramaniam, S. (2014). Spatial Localization of the Ebola Virus Glycoprotein Mucin-Like Domain Determined by Cryo-Electron Tomography. *Journal of Virology*, *88*(18), 10958–10962. https://doi.org/10.1128/jvi.00870-14

Trommer, S., Funke, C., Volchkov, V., Klenk, H., & Becker, S. (1996). *SHORT COMMUNICATION Termini of All mRNA Species of Marburg Virus : Sequence and Secondary Structure*. *380*, 376–380.

Urbanowicz, R. A., McClure, C. P., Sakuntabhai, A., Sall, A. A., Kobinger, G., Müller, M. A., Holmes, E. C., Rey, F. A., Simon-Loriere, E., & Ball, J. K. (2016). Human Adaptation of Ebola Virus during the West African Outbreak. *Cell*, *167*(4), 1079-1087.e5. https://doi.org/10.1016/j.cell.2016.10.013

Valerdi, K. M., Hage, A., van Tol, S., Rajsbaum, R., & Giraldo, M. I. (2021). The role of the host ubiquitin system in promoting replication of emergent viruses. *Viruses*, *13*(3), 1–15. https://doi.org/10.3390/v13030369

Vande Burgt, N. H., Kaletsky, R. L., & Bates, P. (2015). Requirements within the Ebola viral glycoprotein for tetherin antagonism. *Viruses*, *7*(10), 5587–5602. https://doi.org/10.3390/v7102888

Varkey, J. B., Shantha, J. G., Crozier, I., Kraft, C. S., Lyon, G. M., Mehta, A. K., Kumar, G., Smith, J. R., Kainulainen, M. H., Whitmer, S., Ströher, U., Uyeki, T. M., Ribner, B. S., & Yeh, S. (2015). Persistence of Ebola Virus in Ocular Fluid during Convalescence. *New England Journal of Medicine*, *372*(25), 2423–2427. https://doi.org/10.1056/nejmoa1500306

Vega, M. D. La, Caleo, G., Audet, J., Qiu, X., Kozak, R. A., Brooks, J. I., Kern, S., Wolz, A., Sprecher, A., Greig, J., Lokuge, K., Kargbo, D. K., Kargbo, B., Caro, A. Di, Grolla, A., Kobasa, D., Strong, J. E., Ippolito, G., Herp, M. Van, & Kobinger, G. P. (2015). *Ebola viral load at diagnosis associates with patient outcome and outbreak evolution*. *125*(12), 4421–4428. https://doi.org/10.1172/JCI83162DS1

Volchkov, V. E., Chepurnov, A. A., Volchkova, V. A., Ternovoj, V. A., & Klenk, H. D. (2000). Molecular characterization of guinea pig-adapted variants of Ebola virus. *Virology*, *277*(1), 147–155. https://doi.org/10.1006/viro.2000.0572

Volchkov, V. E., Feldmann, H., Volchkova, V. A., & Klenk, H. D. (1998). Processing of the Ebola virus glycoprotein by the proprotein convertase furin. *Proceedings of the National Academy of Sciences of the United States of America*, *95*(10), 5762–5767. https://doi.org/10.1073/pnas.95.10.5762

Volchkov, V. E., Mu, E., Kolesnikova, L. V, & Weik, M. (2001). *Editing of the GP Gene and Viral Cytotoxicity Recovery of Infectious Ebola Virus from Complementary DNA : RNA Editing of the GP Gene and Viral Cytotoxicity*. *1965*(2001). https://doi.org/10.1126/science.1057269

Volchkov, V. E., Volchkova, V. A., Chepurnov, A. A., Blinov, V. M., Dolnik, O., Netesov, S. V., & Feldmann, H. (1999). Characterization of the L gene and 5' trailer region of Ebola virus. *Journal of General Virology*, *80*(2), 355–362. https://doi.org/10.1099/0022-1317-80-2-355

Volchkova, V. A., Dolnik, O., Martinez, M. J., Reynard, O., & Volchkov, V. E. (2011). Genomic RNA editing and its impact on Ebola virus adaptation during serial passages in cell culture and infection of guinea pigs. *Journal of Infectious Diseases*, *204*(SUPPL. 3), 941–946. https://doi.org/10.1093/infdis/jir321

Volchkova, V. A., Dolnik, O., Martinez, M. J., Reynard, O., & Volchkov, V. E. (2015). RNA Editing of the GP Gene of Ebola Virus is an Important Pathogenicity Factor. *Journal of Infectious Diseases*, *212*, S226–S233. https://doi.org/10.1093/infdis/jiv309

Volchkova, V. A., Klenk, H. D., & Volchkov, V. E. (1999). Delta-peptide is the carboxy-terminal cleavage fragment of the nonstructural small glycoprotein sGP of Ebola virus. *Virology*, *265*(1), 164–171. https://doi.org/10.1006/viro.1999.0034

Wahl-Jensen, V., Bollinger, L., Safronetz, D., De Kok-Mercado, F., Scott, D. P., & Ebihara, H. (2012).

Use of the syrian hamster as a new model of ebola virus disease and other viral hemorrhagic fevers. In *Viruses* (Vol. 4, Issue 12, pp. 3754–3784). https://doi.org/10.3390/v4123754

Walldorf, J. A., Cloessner, E. A., Hyde, T. B., MacNeil, A., Bennett, S. D., Carter, R. J., Redd, J. T., & Marston, B. J. (2019). Considerations for use of Ebola vaccine during an emergency response. In *Vaccine* (Vol. 37, Issue 48, pp. 7190–7200). Elsevier Ltd. https://doi.org/10.1016/j.vaccine.2017.08.058

Wang, J., Manicassamy, B., Caffrey, M., & Rong, L. (2011). Characterization of the receptor-binding domain of ebola glycoprotein in viral entry. *Virologica Sinica*, *26*(3), 156–170. https://doi.org/10.1007/s12250-011-3194-9

Watanabe, S., Noda, T., & Kawaoka, Y. (2006). Functional Mapping of the Nucleoprotein of Ebola Virus. *Journal of Virology*, *80*(8), 3743–3751. https://doi.org/10.1128/jvi.80.8.3743-3751.2006

Watson, R. J., Tree, J., Fotheringham, S. A., Hall, Y., Dong, X., Steeds, K., Gouriet, J., Salguero, F. J., Burton, C., Pitman, J., Easterbrook, L., Richards, K. S., Burton, J., Bewley, K., Bruce, C., Hiscox, J. A., Carroll, M. W., & Funnell, S. G. P. (2021). *Dose-Dependent Response to Infection with Ebola Virus in the Ferret Model and Evidence of Viral Evolution in the Eye*. https://doi.org/10

Weidmann, M., Sall, A. A., Manuguerra, J. C., Koivogui, L., Adjami, A., Traoré, F. F., Hedlund, K. O., Lindegren, G., & Mirazimi, A. (2011). Quantitative analysis of particles, genomes and infectious particles in supernatants of haemorrhagic fever virus cell cultures. *Virology Journal*, *8*, 2–7. https://doi.org/10.1186/1743-422X-8-81

Weik, M., Enterlein, S., Schlenz, K., & Mühlberger, E. (2005). The Ebola Virus Genomic Replication Promoter Is Bipartite and Follows the Rule of Six. *Journal of Virology*, *79*(16), 10660–10671. https://doi.org/10.1128/jvi.79.16.10660-10671.2005

Weir, M. R., & Weir, T. E. (2002). Marburg and ebola hemorrhagic fevers. *Mucocutaneous Manifestations of Viral Diseases*, 421–428. https://doi.org/10.1201/b14016-19

Wendt, L., Brandt, J., Bodmer, B. S., Reiche, S., Schmidt, M. L., Traeger, S., & Hoenen, T. (2020). The Ebola Virus Nucleoprotein Recruits the Nuclear RNA Export Factor NXF1 into Inclusion Bodies to Facilitate Viral Protein Expression. *Cells*, *9*(1). https://doi.org/10.3390/cells9010187

Whelan, S. P. J., Barr, J. N., & Wertz, G. W. (2004). Transcription and replication of nonsegmented negative-strand RNA viruses. *Current Topics in Microbiology and Immunology*, *283*, 61–119. https://doi.org/10.1007/978-3-662-06099-5_3

WHO. (2020). *Technical information note: WHO recommended criteria for declaring the end of the Ebola virus disease outbreak*. *March*. https://www.who.int/who-documents-detail/who-recommended-criteria-for-declaring-the-end-of-the-ebola-virus-disease-outbreak

WHO. (2022). Ebola Virus Disease Republic of Uganda. *2018*, *November*, 1–5. http://library.health.go.ug/publications/statistics/uganda-bureau-statistics-statistical-abstract-2018

Wong, G., Gao, G. F., & Qiu, X. (2016). Can Ebola virus become endemic in the human population? *Protein and Cell*, *7*(1), 4–6. https://doi.org/10.1007/s13238-015-0231-8

Wong, G., & Qiu, X. (2016). Designing efficacious vesicular stomatitis virus-vectored vaccines against Ebola virus. *Methods in Molecular Biology*, *1403*, 245–257. https://doi.org/10.1007/978-1-4939-3387-7_12

Wool-Lewis, R. J., & Bates, P. (1998). Characterization of Ebola Virus Entry by Using Pseudotyped Viruses: Identification of Receptor-Deficient Cell Lines. *Journal of Virology*, *72*(4), 3155–3160. https://doi.org/10.1128/jvi.72.4.3155-3160.1998

Yamaoka, S., & Ebihara, H. (2021). Pathogenicity and Virulence of Ebolaviruses with Species- and Variant-specificity. In *Virulence* (Vol. 12, Issue 1, pp. 885–901). Bellwether Publishing, Ltd. https://doi.org/10.1080/21505594.2021.1898169

Yamayoshi, S., Noda, T., Ebihara, H., & Goto, H. (2008). Ebola Virus Matrix VP40 Protein Uses the COPII Transport System for Its Intracellular Transport. *Cell Host Microbe*, *23*(1), 1–7. https://www.ncbi.nlm.nih.gov/pmc/articles/PMC2688697/pdf/nihms-110443.pdf

Yang, Z., Duckers, H., Sullivan, N., Abel, E. L. G. N., & Abel, G. A. R. Y. J. N. (2000). Identification of the Ebola virus glycoprotein as the main viral determinant of vascular cell cytotoxicity and injury. *Nature Medicine*, *6*(8), 6–9. http://www.nature.com/nm/journal/v6/n8/abs/nm0800_886.html

Yu, D. S., Weng, T. H., Wu, X. X., Wang, F. X. C., Lu, X. Y., Wu, H. B., Wu, N. P., Li, L. J., & Yao, H. P. (2017). The lifecycle of the Ebola virus in host cells. In *Oncotarget* (Vol. 8, Issue 33, pp.

55750–55759). https://doi.org/10.18632/oncotarget.18498

Zaki, S. R., Shieh, W. J., Greer, P. W., Goldsmith, C. S., Ferebee, T., Katshitshi, J., Tshioko, F. K., Bwaka, M. A., Swanepoel, R., Calain, P., Khan, A. S., Lloyd, E., Rollin, P. E., Ksiazek, T. G., & Peters, C. J. (1999). A novel immunohistochemical assay for the detection of Ebola virus in skin: Implications for diagnosis, spread, and surveillance of Ebola hemorrhagic fever. *Journal of Infectious Diseases*, *179*(SUPPL. 1), 36–47. https://doi.org/10.1086/514319

Zampieri, C. A., Fortin, J.-F., Nolan, G. P., & Nabel, G. J. (2007). The ERK Mitogen-Activated Protein Kinase Pathway Contributes to Ebola Virus Glycoprotein-Induced Cytotoxicity. *Journal of Virology*, *81*(3), 1230–1240. https://doi.org/10.1128/jvi.01586-06

Zaneveld, L. J. D., Waller, D. P., Anderson, R. A., Chany, C., Rencher, W. F., Feathergill, K., Diao, X. H., Doncel, G. F., Herold, B., & Cooper, M. (2002). Efficacy and safety of a new vaginal contraceptive antimicrobial formulation containing high molecular weight poly(sodium 4-styrenesulfonate). *Biology of Reproduction*, *66*(4), 886–894. https://doi.org/10.1095/biolreprod66.4.886

Zhou, Yang, & Wang. (2020). Distinct conformational states of SARS-CoV-2 spike protein. *File:///C:/Users/VERA/Downloads/ASKEP_AGREGAT_ANAK_and_REMAJA_PRINT.Docx*, *21*(1), 1–9.

Zhu, W., Banadyga, L., Emeterio, K., Wong, G., & Qiu, X. (2019). The Roles of Ebola Virus Soluble Glycoprotein in Replication, Pathogenesis, and Countermeasure Development. *Viruses*, *11*(11). https://doi.org/10.3390/v11110999